ALGINATE BASED ADVANCED WOUND CARE BIOMATERIAL FOR DIABETIC WOUND MANAGEMENT

RAJALEKSHMY G.P.

PhD THESIS

2023

SREE CHITRA TIRUNAL INSTITUTE FOR MEDICAL SCIENCES AND

TECHNOLOGY, TRIVANDRUM

An Institution of National Importance established by an Act of the Indian Parliament
(Act No.52 of 1980)

Dept. of Science and Technology, Govt. of India
www.sctimst.ac.in

ALGINATE BASED ADVANCED WOUND CARE BIOMATERIAL FOR DIABETIC WOUND MANAGEMENT

A THESIS SUBMITTED BY

RAJALEKSHMY G.P.

TO

SREE CHITRA TIRUNAL INSTITUTE FOR MEDICAL SCIENCES AND TECHNOLOGY, TRIVANDRUM.

IN PARTIAL FULFILMENT OF THE REQUIREMENTS

FOR THE AWARD OF

DOCTOR OF PHILOSOPHY

2023

DECLARATION

I, Rajalekshmy G.P., hereby certify that I had personally carried out the work depicted in the thesis titled, ***"Alginate based advanced wound care biomaterial for diabetic wound management"***, except where due acknowledgement has been made in the text. No part of this thesis has been submitted for the award of any other degree or diploma prior to this date.

Signature

Rajalekshmy G.P.

Reg No. 2017/PHD/06

Date 30/06/2023

श्री चित्रा तिरुनाल आयुर्विज्ञान एवं प्रौद्योगिकी संस्थान, त्रिवेंद्रम, जैवचिकित्सकीय प्रौद्योगिकी स्कंध
पूजप्पुरा, तिरुवनन्तपुरम - 695 012, केरल, भारत
SREE CHITRA TIRUNAL INSTITUTE FOR MEDICAL SCIENCES AND TECHNOLOGY, TRIVANDRUM
BIO MEDICAL TECHNOLOGY WING
POOJAPPURA, THIRUVANANTHAPURAM - 695 012, KERALA, INDIA
(एक राष्ट्रीय महत्व का संस्थान, विज्ञान एवं प्रौद्योगिकी विभाग, भारत सरकार)
An Institution of National Importance, Department of Science & Technology, Government of India)
टेलीफॉन नं./Telephone No: 0471-2340801/2520450, फैक्स/Fax: 0471-2341814
ई-मेल/E-mail:sct@sctimst.ac.in वेबसाइट/Website : www.sctimst.ac.in

CERTIFICATE BY THE RESEARCH GUIDE

Name of the Guide: **Dr. Rekha M.R.**

Division/Department: **Division of Biosurface Technology**

This is to certify that **Rajalekshmy G.P.**, department/division of Division of Biosurface Technology of this institute has fulfilled the requirements prescribed for the Ph.D. degree of the Sree Chitra Tirunal Institute for Medical Sciences and Technology, Trivandrum.

The thesis entitled, ***"Alginate based advanced wound care biomaterial for diabetic wound management"*** was carried out under my direct supervision. No part of the thesis was submitted for the award of any degree or diploma prior to this date.

*Clearance was obtained from the Institutional Animal Ethics Committee for carrying out the study.

Signature

Name of the Guide
Dr. Rekha M.R.

Date: 30/06/2023

APPROVAL OF THE THESIS

The thesis entitled

ALGINATE BASED ADVANCED WOUND CARE BIOMATERIAL FOR DIABETIC WOUND MANAGEMENT

Submitted by

RAJALEKSHMY G.P.

for the degree of

Doctor of Philosophy

of

SREE CHITRA TIRUNAL INSTITUTE FOR MEDICAL SCIENCES AND TECHNOLOGY, TRIVANDRUM

is evaluated and approved by

.....

Dr. Rekha M.R.
Scientist G, Div. of Biosurface Technology
SCTIMST, Trivandrum, Kerala.

(Name & Signature of the Guide)

Sourabh Ghosh
.....

Dr. Sourabh Ghosh
Professor, Dept. of Textile & Fibre Engineering
Indian Institute of Technology, Delhi.

(Name & Signature of thesis examiner)

Dedicated to my family, teachers & friends……

ACKNOWLEDGEMENTS

It is my pleasure to express my sincere gratitude to all the individuals, whose support during the PhD work allowed me to complete this thesis.

First of all, I would like to express my sincere gratitude to my research guide, Dr. Rekha M.R. for her guidance and continuous encouragement during the entire course of this work. I earnestly thank her for the innovative ideas, critical discussions and personal support.

I convey my sincere gratitude to the Director, SCTIMST and the Head, BMT Wing, SCTIMST for all the facilities provided during the course of my work.

I am extremely grateful to my Doctoral Advisory Committee members, Dr. Roy Joseph, Dr. A. Maya Nandkumar and Dr. T.V. Anilkumar for their valuable time, suggestions and support right from the beginning of the work.

I am greatly indebted the Council of Scientific & Industrial Research, Delhi for the PhD fellowship and providing the financial assistance during the course of the work.

I am very much thankful to all staffs of the Academic division for conducting the timely evaluation and all the academic assistance in this venture.

I express my gratitude to Dr. Manoj Komath, Head of the Department, Department of Biomaterial Science and Technology, for providing me permission to access the facilities of the Department. I am very thankful to Dr. Suresh Babu, Dr. Remya and Dr. Adarsh for helping me in FTIR and ICP analysis. I wish to thank Mr. Nishad for helping in the SEM analysis. I would like to extend my gratitude to Dr. Jayasree R.S. the Head of Division of Biophotonics and Imaging for providing me permission for fluorescent microscopy.

I thank Ms. Jasmin Joseph for helping me in mechanical testing and lyophilization. I am thankful to Dr. Renjith, Dr. Radha kumari and Mr. Willi Paul of

Central analytical facility for HPLC, thermogravimtrey and confocal microscopy analysis. I express my sincere gratitude to Dr. Lynda V. Thomas for granting permission to access FTIR, contact angle analysis and RT PCR. I am very much thankful to Dr. Amrita, Ms. Jijo Wilson and Ms. Anjitha for helping me with RTPCR analysis. I thank Dr. Anugya Bhatt for providing facilities for microscopy and Mr. Renjith Kartha for helping me in flow cytometry analysis. I thank Dr. Anil Kumar P.R. and Dr. Naresh Kasoju for providing the cell lines for in vitro analysis. I thank Dr.Deepu and Dr. Vibha for helping in the Micro CT analysis.

I am extremely thankful to Dr. Harikrishnan V.S., Division of Laboratory animal science and all staffs Mr. Manoj, Mr. Sunil, Mr. Sajeev, Mr. Prasanth and Mr. Sarath for providing me with animals for the in vivo studies and helping me through the experiments. I express my sincere gratitude to Dr. Sachin J. Shenoy for performing all the animal surgeries. His patience and dedication was a great inspiration for me.

I am extremely thankful to the members of Division of Experimental Pathology for helping me in the animal experiments. I express my sincere gratitude to Dr. T.V. Anilkumar for providing me permission to access their facilities for cell culture studies, molecular analysis as well as histopathological evaluations. I am very much thankful to Dr. Geetha, and Mr. Pratheesh for training me in the histopathological evaluations. I wish to thank Dr. Reshma, Dr. Manjula, Dr. Resmi and Dr. Poornima for their love and support.

I express my whole hearted gratitude to the Director, NIIST for providing me permission to access their facilities. I am grateful to Dr. Luxmi Verma for NMR analysis, Dr. Saju Pillai for XPS analysis and Dr. Praveen for the circular dichroism analysis. I am extremely thankful to the Director, RGCB for permitting me to avail confocal microscopy facility and I thank Mr. Prakash for providing the cell lines.

I am thankful to all the staffs of the accounts, library, computer division, Stores and purchase of the BMT wing for their help.

I am really thankful to the past and present lab members of the Division of Biosurface Technology for providing a cordial environment to work. I thank the former

lab members Dr. Priya, Dr. Caroline, Ms. Linsha, Ms. Annie, Ms. Rajapriya, Ms. Anaga, Ms. Aswathy, Ms. Nayana, Ms. Sunitha, Mr. Riyas, Mr. Rashad, Ms. Gopika, Ms. Anjana, Ms. Krishnapriya and the present lab members Dr. Dharavath Ravi, Ms. Linju, Ms. Divya and Ms. Ancy for their love and support.

Thanks to all my friends inside and outside SCTIMST for their help and friendship. Special mention to my batchmates Ms. Gopika Ramesh, Ms. Gopika Gopan, Ms. Dhanya, Ms. Swathi, Mr. Amal and Ms. Bridget for their support.

I express my sincere gratitude to my family for their support over the years. I thank my parents and in-laws for their genuine love and prayers. I extend my sincere thanks to my beloved husband Mr. Sreelal for his love, understanding and support. I greatly value his constant encouragement throughout my PhD career, which helped me for the successful completion of this work. My acknowledgement would be incomplete without thanking my little son, Adhrith, who always made me cheerful.

Above all, I bow before Almighty God for giving me strength, health and opportunity to undertake this research and complete it successfully.

Rajalekshmy G.P.

TABLE OF CONTENTS

LIST OF FIGURES

LIST OF TABLES

LIST OF ABBREVIATIONS

S No	Abbreviation	Full Form
1	ADPMS	Alginate diamine PEG-g-poly(PEGMA)
2	AGE	Advanced glycation end products
3	AGMS	Alginate-g-poly(methacrylic acid)
4	AGPMS	Alginate-g-poly(PEGMA)
5	Akt	Ak strain transforming
6	AMP	Antimicrobial peptide
7	APC	Allophycocyanin
8	APS	Ammonium persulphate
9	ATR	Attenuated total reflection
10	BSA	Bovine serum albumin
11	CD	Circular dichroism
12	DAPI	4',6-diamidino-2-phenylindole
13	DCFDA	2'-7'-Dichlorodihydrofluorescein diacetate
14	DFU	Diabetic foot ulcer
15	DMSO	Dimethyl sulfoxide
16	ECM	Extracellular matrix
17	ELISA	Enzyme linked immunosorbent assay
18	ERK	Extracellular signal regulated kinase
19	FBS	Fetal bovine serum
20	FGF	Fibroblast growth factor
21	FITC	Fluorescein isothiocyanate
22	FTIR	Fourier transform infrared spectrophotometry
23	GAPDH	Glyceraldehyde 3-phosphate dehydrogenase
24	GH	Growth factor
25	GO	Glucose oxidase
26	GPC	Gel permeation chromatography
27	H_2O_2	Hydrogen peroxide

28	HBOT	Hyperbaric oxygen therapy
29	HIF	Hypoxia inducible factor
30	HPLC	High-performance liquid chromatography
31	ICP OES	Inductively coupled plasma - optical emission spectrometry
32	IGF	Insulin growth factor
33	IL-6	Interleukin-6
34	IR	Insulin receptor
35	LDA	Live dead assay
36	LPS	Lipopolysaccharide
37	MEM	Minimum essential medium
38	MMP	Matrix metalloproteinases
39	MTT	3-(4,5-dimethylthiazol-2-yl)-2,5-diphenyltetrazolium bromide
40	NMR	Nuclear magnetic resonance
41	NSAID	Non-steroidal anti-inflammatory drugs
42	P13K/Akt	Phosphoinositide 3-kinase
43	PBS	Phosphate buffered saline
44	PDGF	Platelet derived growth factor
45	PEG	Poly ethylene glycol
46	PEGMA	Poly (ethylene glycol) methacrylate
47	POD	peroxidase
48	ROS	Reactive oxygen species
49	RT PCR	Reverse transcription polymerase chain reaction
50	SEM	Scanning electron microscopy
51	SIM	Simvastatin
52	TEMED	Tetramethylethylenediamine
53	TGF	Tumour growth factor
54	TIMP	Tissue inhibitors of metalloproteinases
55	TNF	Tumour necrotic factor
56	VEGF	Vascular endothelial growth factor
57	WVTR	Water vapor transmission rate
58	XPS	X-ray photoelectron spectroscopy

SYNOPSIS

Wounds are defined as the discontinuity of the skin layers caused by physical or thermal injury or by underlying diseases. Wound healing is a highly complex, dynamic process with highly coordinated cellular events. Wound that fails to heal through the natural phases of wound healing in an orderly and timely manner are referred to be chronic. Chronic wounds are associated with diabetes, vascular diseases, poor circulation, neuropathy and the patient population is generally adults' especially geriatric people. Chronic wounds takes prolonged time for healing and can recur, which in turn affects the quality of life adversely and causes morbidity or even mortality. Chronic wounds create a number of challenges in the health care system, which accounts for spending billions of dollars worldwide every year. It has been estimated that in developed countries, 1 to 2% of the population will experience a chronic wound during their lifetime and the rate is increasing year after year. Thus chronic non-healing wounds represent an economic burden for health care systems. Chronic wounds are more prevalent in patients with diabetes mellitus due to the impairment in the healing process. The treatment strategies adopted for diabetic wound management is still inadequate. Diabetic wounds are caused by multiple factors, among which neuropathy and peripheral artery disease are the major triggers. The continuing trauma, infection, altered cellular function and signalling and patient related other factors may predispose to delayed wound healing.

Understanding and addressing the challenges in the treatment of chronic wounds leads to better clinical outcomes with faster wound closure, resulting in improved patient quality of life and reduced health care costs. Most of the ulcers do

not heal with standard treatment, so additional treatment modalities are required. Currently the diabetic foot ulcer treatment include the use of antibiotics to treat infection and revascularization therapy for peripheral artery disease. The use of advanced wound care therapies such as growth factors, engineered skin and extracellular matrices and negative pressure wound care therapy creates a socio economic burden to the whole health care system.

The advanced wound care market is growing at a compound annual growth rate of 6.4%. The market is mainly driven by technological advances, ageing population, problems associated with ineffective treatment methods for chronic wound healing and need for safer and effective treatment for chronic wounds. The recent researches on treatment for diabetic foot ulcers suggest that there is no particular treatment or dressing products of sufficient efficacy to recommend. The high incidence of new ulceration after healing is the main reason which makes the selection of an appropriate dressing difficult. Among different advanced wound care products, alginate dressings are designed for treating moderately or highly exudating wound types. While considering the dressing cost and wound management properties, alginate is the better choice of dressing. But its poor mechanical stability and degradability prevents it from wide clinical use. The removal of alginate dressing from the wound bed through saline irrigation disturbs the underlying tissues as well as the deposition of alginate fibre debris over the wound bed creates foreign body reaction. So alginate dressing with good stability has high demand in this clinical scenario.

The spatiotemporal delivery of biomolecule is very critical for healing to proceed. Topical delivery using biomaterial has increased demand in advanced

therapies because of its high versatility and ease of use. Since the chronic wound surface is highly unfavorable for healing to proceed, the biomaterial should be effective in altering the adverse condition and make it favorable for the biomolecule to act. However critical *in vitro* and *in vivo* evaluations are needed before clinical usage.

Here in this study, our goal was to develop an alginate based wound care biomaterial for diabetic wound management. It was aimed to develop alginate based material with better mechanical strength that will not disintegrate in chronic wound exudates and also can aid in healing process. It was also aimed to deliver multiple biomolecules to the wound surface in a spatio-temporal manner using this alginate based matrix. The complete work is discussed in five chapters. The first chapter deals with the introduction about the research of area of interest and the current scenario. Based on the research problem and the literature survey carried out, it was hypothesized that grafting will improve the mechanical stability of alginate and biomolecule loaded graft-alginate based hydrogels can be used as an advanced wound care material for diabetic wound management. To prove the hypothesis, the objectives were formulated as follows;

- To develop anionic polysaccharide based wound dressing with main emphasis on alginate & its derivatives.
- Characterization of derived wound dressing material.
- Incorporation of various bioactive molecules such as anti-inflammatory drugs, enzymes, or hormones targeting diabetic wounds.
- To analyze the release profile of bioactive molecules loaded onto dressing material.

- *In vitro* evaluations with cell types of skin.
- Analysis of healing potential efficacy by *in vivo* evaluation.

The second chapter is on the review of literature, in which the relevance of advanced wound care products in diabetic wound management is discussed. This chapter also details the wound healing bioactive molecules selected for this study and the development of bioactive dressings intended for topical biomolecule delivery. The biomolecules selected for this study includes insulin, simvastatin and glucose-oxidase peroxidase system. The effect of topical delivery of these biomolecules on modulating different phases of wound healing and the current advancements in this field of bioactive dressing is also discussed.

The methodologies adopted for carrying out the experiments are discussed in the third chapter. This chapter is divided into four sections. The first section describes the methods used for the grafting of alginate with different methacrylate monomers and synthesis of xerogels. Different physico-chemical characterization techniques were used for the optimization of the xerogels. After characterizing the alginate, three different xerogels were synthesized by grafting with different monomers. In the first system, alginate was grafted with poly (methacrylic acid) followed by chemical and ionic cross-linking. The second xerogel was synthesized by grafting with poly (PEGMA) chains and xerogels were obtained with crosslinking. In the third system, alginate was conjugated with diamine PEG and grafted with poly (PEGMA) chains. Optimized monomer concentration was selected by analysing grafting parameters such as grafting yield, grafting efficiency and total conversion to homopolymer formation. Based on percentage swelling, water vapour transmission rate, porosity and degradation studies, suitable batch of xerogels were selected from each systems such

as AGM2S3, AGPM2S2 and ADPM2S2. The detailed characterization was performed to optimize the selected xerogels. Spectroscopic techniques such as FTIR, NMR and XPS, contact angle, mechanical testing, thermogravimetry, scanning electron microscopy and micro computed tomography were used for characterization. Further, the effect of released strontium ions from the hydrogel on various parameters was analysed by haemostatic activity, collagenase inhibitory activity and wound closure by scratch wound assay. The optimized xerogels were compared with the commercial alginate wound dressings.

In the second section, the methods followed for the efficacy evaluation of the xerogels for biomolecule delivery is described. The selected biomolecules viz., insulin, simvastatin and glucose oxidase were loaded within the xerogel by diffusion filling method. Further the release profile was analysed and, quantified by HPLC and ELISA techniques and the structural analysis was performed by circular dichroism. The material which showed controlled release for all the selected biomolecules and where the biological activity of biomolecules remained intact was selected for the *in vitro* cell based studies. The methodologies for evaluating the *in vitro* wound healing effects of the biomolecule loaded hydrogels are detailed in the third section. The optimized concentration of the biomolecules were identified and loaded within the hydrogel. The *in vitro* wound healing effects were studied using various types of skin cells such as L929 fibroblast cells, HaCaT keratinocyte and RAW 264.7 macrophages under hyperglycemic conditions. The role of biomolecules in wound healing was determined using scratch wound assay for cellular migration, actin filament staining using rhodamine-phalloidin staining and gene expression by RT PCR analysis. The effect of insulin in healing process was further studied by cellular apoptosis by flow

cytometry using Annexin-PI staining and the expression of phospho Akt by immunostaining. The anti-inflammatory activity of simvastatin was assessed by quantifying TNFα by ELISA and macrophage polarization by flow cytometry. The role of GO-POD system in regulating the reactive oxygen species was assessed by the DCFDA assay.

The last section deals with the *in vivo* efficacy evaluation of the optimized xerogel loaded with selected biomolecule in the diabetic rat model. The diabetic rat model was created by single intra peritoneal injection of streptozotocin in Sprague Dawley rats and the stable hyperglycemic rats were selected for the experiment. The experiment consist of four test groups and one control group. Full thickness wounds of size 2 x 2 cm were created on the dorsal surface of the rat and covered with the wound dressing materials. The tissue sections were collected for the histopathology evaluation at predetermined time intervals such as 7, 14 and 21 days. The rate of re-epithelialization was determined by Haematoxylin and Eosin staining. The effect of topical delivery of insulin was further assessed by the expression of phospho Akt by immunohistochemistry.

The fourth chapter deals with the results and discussions. Alginate based advanced wound dressings were developed by grafting with methacrylic acid monomers and dual cross-linked with methylene bisacrylamide and strontium ions. After determining the optimized formulation, three xerogels were synthesized. Alginate-g-methacrylic acid (AGM2S3) xerogels showed excellent water absorption and less bioadhesive nature, but showed limited mechanical strength. Alginate-g-poly (PEGMA) xerogels (AGPM2S2) showed improved flexibility and mechanical

stability, but higher concentration of PEGMA used for grafting showed cytotoxic effect as well as increase in bioadhesive nature. Alginate diamine PEG-g-poly (PEGMA) xerogels (ADPM2S2) showed good mechanical strength, less bioadhesive nature and increased cell viability. While analysing the efficacy of the materials for the controlled delivery of loaded biomolecules, AGM2S3 hydrogels ensures controlled delivery of insulin and glucose oxidase, but burst release was observed with simvastatin. Structural variation was observed with insulin and GO loaded within AGPM2S2 hydrogels. The ADPM2S2 hydrogels was able to maintain the controlled delivery of biomolecules without any structural variation. So biomolecules loaded within ADPM2S2 hydrogels were selected for *in vitro* evaluations. Insulin loaded hydrogels showed good cellular migration and proliferation. Insulin also helps in the actin filament organization and favours collagen deposition. Good anti-inflammatory activity was observed with simvastatin loaded system, but disruption in the actin filament organization was observed. The GO-POD loaded hydrogels could effectively regulate the local glucose and ROS level, which favours wound healing process. Due to the improved wound healing effect compared to the other biomolecules, insulin loaded system has been selected for *in vivo* evaluation. A significant improvement in wound closure was observed with insulin loaded ADPM2S2 compared to the insulin alone treatment. ADPM2S2 hydrogel showed significant improvement in wound closure within 14 days compared to commercial alginate wound dressings.

The fifth chapter describes the summary, conclusions and future research. Alginate based wound care biomaterials were successfully developed with good mechanical strength. The in-house developed xerogels have better performance as wound care material compared to commercial alginate based dressings. Among which,

ADPM2S2 hydrogels showed controlled release for all the selected biomolecules and more importantly the biological activity of biomolecules remained intact. The *in vitro* studies on various skin cells were performed with ADPM2S2 loaded with different biomolecules. Among which insulin shows good cellular migration and collagen deposition. So the insulin loaded ADPM2S2 hydrogel was further selected for *in vivo* evaluation on diabetic rat models which showed accelerated wound closure. Hence it is concluded that the alginate based ADPM2S2 xerogels could be used as an advanced wound care material for diabetic wound management and insulin loaded hydrogels could be a promising therapeutic strategy.

CHAPTER 1

INTRODUCTION

1.1 Skin: Structure and physiology

The skin is the highly adaptive and multifunctional organ that protects the body from the environmental challenges. Skin act as the primary defense barrier and perform homeostatic functions such as regulation of body temperature, sensory reception, water balance, synthesis of vitamins and hormones, and absorption of material. The three layers of skin such as epidermis, dermis and hypodermis, act as an effective barrier to external environment and allow the transmission of sensory information. The outer most is the impermeable epidermal layer with sebaceous glands, sweat glands and hair follicles. The epidermis is composed of specific cells known as keratinocytes, which synthesize the protective protein keratin. The epidermis is the continuously renewing layer and the 80% of the layer is composed of keratinocytes. The differentiation of the cells occur when it migrate from basal layer to the surface of the skin resulting in keratinization. The mitotically active cells in the basal layer give rise to the outer epidermal layer. The cornified layer provide mechanical support to the underlying epidermis and prevent water loss and invasion of foreign substances (Kolarsick et al., 2011). The epidermis also contains the melanocytes, which produce the melanin pigment and Merkel cells, acting as mechano-receptor.

The dermis layer is enriched with extracellular matrix, vasculature and mechanoreceptors, which provides the skin strength and immunity. The dermis is

fundamentally composed of the fibrillar structural protein known as collagen, act as the major stress resistant material of the skin. Collagen accounts for 70% of the skin's dry weight and it exist in a constant state of flux, being degraded by the proteolytic enzyme collagenase and replacing with the new fibers. On the other hand, the elasticity of the skin is provided by the elastin fibers. The dermis lies on the subcutaneous tissue, which contains small lobes of fat cell called lipocytes. The subcutaneous adipose tissue acts as the energy reserve and also provide the body with buoyancy. The thickness of these layers varies depending on the anatomy of the body. (Wilkinson and Hardman, 2020). The loss of continuity of the skin epithelia by external agents result in skin injury. Skin itself has the innate ability to repair, which allows healing efficiently and quickly and the whole process is collectively known as wound healing response. During the healing process, the multiple cell types residing in these different layers coordinate in a precise manner to bring about healing. Skin repair is the most complex process in the human body (Tottoli et al., 2020).

1.2 Wound healing: cellular mechanisms

Wound healing is highly organized dynamic process including cellular, humoral and molecular mechanisms. It consists of overlapping phases of inflammation, proliferation and remodeling (figure I). Wound healing can be primary or secondary healing. Primary healing is uncomplicated, non-infected with well approximated wound. Secondary healing occurs when wound is disrupted by infection, hypoxia or underlying diseases. During secondary healing granulation tissue formation and epithelialization over the new tissue takes place. There are specific cells, growth

factors and cytokines involved in the complete closure of wound. The cells like platelets, neutrophils, fibroblasts, keratinocytes, endothelial cells, macrophage, monocytes and T lymphocytes appear at the wound site and play critical role in the wound healing.

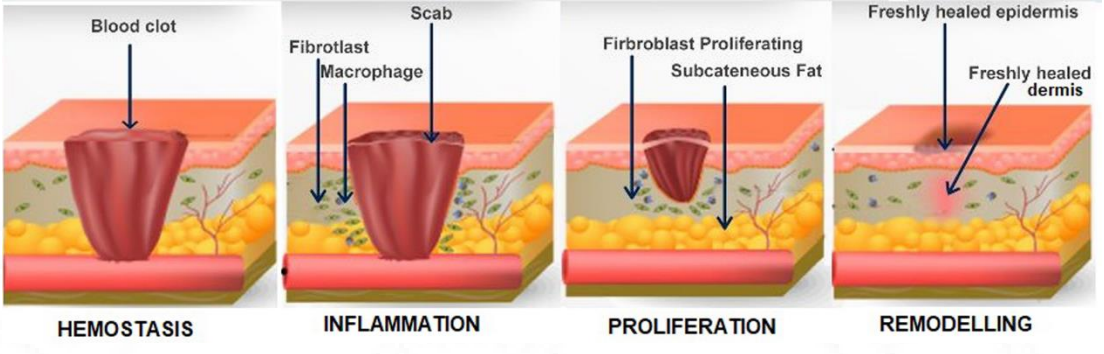

Figure I: Different stages of wound healing (Wallace et al., 2021).

During vascular haemostasis, blood leaked from the damaged blood vessel coagulates to limit further loss and maintain the integrity. The coagulation consists of thrombocytes and platelet aggregation in fibrin network to re-establish the hemostasis to prevent microorganism invasion. Fibrin acts as a temporary matrix for cell migration and maintains the skin integrity. During inflammatory phase the increasing gradient of chemokine favours the trans-migration of leucocytes to the wound surface. Inflammatory cells help to release lysosomal enzymes and reactive oxygen species that would facilitate the clean-up of various cell debris. The secretion of pro inflammatory cytokines from neutrophils elicit inflammatory phase. Within 48 hours after onset of lesion, the monocytes from the blood vessels infiltrate into the site and differentiate into macrophages. Based on the gene expression, macrophage can be M1

proinflammatory or M2 anti-inflammatory type. Macrophage plays significant role in the transition from inflammatory phase to the proliferative stage. Macrophages help in the phagocytosis and release of proangiogenic, fibrinogenic and inflammatory factors to the wound area. The release of cytokines favours the granulation tissue formation (Gonzalez et al., 2016).

The proliferative phase re-establishes the epithelial barrier which includes angiogenesis, fibroplasia and re-epithelialization. Angiogenesis involves endothelial cell proliferation, rearrangement of basal membrane and recruitment of perivascular structures. This supplies adequate nutrients, oxygen as well as immune competent cells. Granulation tissue formation begins four days after the formation of lesion. Epidermal cells at the wound edge migrate and undergo cycles of polarized extension and contraction of actin cytoskeleton. Fibroplasia begins with formation of granulation tissue. During fibroplasia, fibroblasts proliferate and deposit extracellular matrix. The formation of ECM is important for cell adhesion and regulates growth, movement and differentiation of cells. Fibroblast response to cytokines and growth factors helps in proliferation and response to metallo-proteases and their inhibitors. Deposition of collagen can replace the fibrin provisional matrix. Activated fibroblast then differentiate into myofibroblast, which are rich in alpha smooth muscle actin and initiate wound contraction. The deposition of collagen results in the formation of avascular and acellular scar organised by 80-90% type I collagen and rest by type II collagen. The synthesis of collagen occurs throughout the healing process, while

proliferation of fibroblast declines to adjust the balance between synthesis and degradation of the ECM.

Remodelling is the last phase of wound healing and it occurs from 21st day and lasts up to one year after injury. Granulation tissue formation gets reduced by apoptosis of the cells. The structural and hydration role provided by proteoglycans and glycosaminoglycan also gets diminished. In the mature wound, collagen III is replaced by the stronger collagen I, which is rearranged into parallel fibrils forming low cellularity scars. Further angiogenic process declines and metabolic activity slows down and finally stops.

1.3 Wounds: classification

The wounds are defined as the damage to the integrity of biological tissue, including skin, mucous membranes, and organ tissues caused by various types of trauma. There are no specific standards for the classification of wounds. Wounds are classified in different ways which helps in the proper management of the wound. The important factors are the nature of the injury, time frame for healing and the depth of the wound, which decide whether wound needs any surgical intervention for healing. Centers for disease control and prevention, US (CDC) has developed wound classification system (table I) based on cleanliness and wound condition (Herman and Bordoni, 2021) .

Type of wound	Characteristics
Class 1 wounds	Clean uninfected wounds without any inflammation. The wounds are primarily closed and do not enter respiratory, alimentary, genital or urinary tract.
Class 2 wounds	Clean contaminated wounds and can enter respiratory, alimentary, genital or urinary tract
Class 3 wounds	Contaminated and open wounds result from insult to the sterile technique
Class 4 wounds	Dirty infected wounds result from the improper care to the traumatic wounds

Table I: Wound classification system based on cleanliness and wound condition developed by CDC, US (Onyekwelu et al., 2017).

Wounds can be further classified depending on the extent of injury into the tissue layers. It can be partial thickness due to loss of epidermal or superficial dermal layers or can be full thickness due to penetration into the deeper dermis layers along with epidermal layers. Superficial wounds heal by epithelialization without significant scar formation. If wound environment is maintained appropriately it can heal within 10 days. But in the case of partial thickness wounds, healing is by re-epithelialization followed by wound contraction and scar formation. It usually takes about 10-21 days to heal (Percival, 2002).

Depending on onset and duration of the wounds it can be classified as acute or chronic. Accidents, trauma, burns and surgical wounds are considered as acute wounds. Acute wound occur suddenly rather than over time and repair more rapidly resulting in durable closure. But chronic wounds fail to proceed to the normal repair process in timely manner. The entire process is prolonged and the quality of the tissue is poor. So the functional wound closure may not be complete in chronic wounds and

there is a chance of reoccurrence. This causes serious concerns about the patient's health and the quality of life (Whitney, 2005).

1.4 Chronic non-healing wounds

The magnitude and the incidence of non-healing wounds are increasing due to aging population and associated health conditions. A wound that does not decrease in size by 30% within 3 weeks or 50% within 4-5 weeks is considered as chronic. Based on the aetiology, the wound healing society classifies chronic wounds into different categories such as venous ulcers, pressure ulcers and neuropathic/diabetic ulcers and arterial insufficiency ulcers, among which venous ulcers and diabetic ulcers are more prevalent. The statistics of chronic wounds may vary, though it is estimated that, 1-2% of the population experience chronic wounds in developed countries. Among which the prevalence of venous ulcers is 0.2 to 1%, pressure ulcers is 0.5% and 5 to 10% of people with diabetes suffer from neuropathic ulcers (Järbrink et al., 2016). Chronic wounds are characterized by raised, hyper proliferative and non-advancing wound margins. The wound area remains inflamed which impede healing process. The factors that make wounds chronic includes the increased pressure and trauma, increased bacterial load, presence of excessive proteases that degrade growth factors and cell surface structures, increased senescent cell population with impaired proliferative and secretory capacities and inappropriate treatment (Widgerow, 2012). These factors affect the functionality of cells such as migration, proliferation, angiogenic response, collagen accumulation and granulation tissue formation.

Venous ulcers primarily occur in the legs caused by poor blood circulation due to dysfunctional blood valves and obstructed veins, while pressure ulcers affect bed ridden patients having limited mobility. Constant pressure affects the blood flow in the capillaries and the areas at greatest risk are sacrum, shoulder blades and heels. However, in diabetic patients, diabetic ulcers frequently begin as minor scratches and go undetected because of nerve loss and restricted sensitivity. Chronic wounds affect the quality of patient life causing pain, depression, loss of function along with prolonged hospitalization. So the proper identification of the cause of chronic wound is critical for successful treatment (Whitney, 2005).

The non-healing wound fails to proceed through normal healing process and remains in chronic inflammatory state. This can result in hypertrophic or keloid scars. Keloids are characterized by thick collagen fibers, whereas as hypertrophic scars contain fibers as nodules. The continuous growth of granulation tissue results in excessive scar formation. There will be excessive secretion of growth factors and lack of molecules promoting apoptosis and ECM remodelling. Hypertrophic scars contain excessive micro vessels which get occluded by over-proliferation and functional regression of endothelial cells. There is myofibroblast hyperactivity and excessive collagen production. The change in ECM and mechanical irritation results in excessive scarring.

1.5 Diabetic wounds

1.5.1 Social impact

Diabetic foot ulcers describe the break in the skin of the foot of a diabetic patient, which do not heal promptly. Despite of the advancement in the last 25 years of wound care, diabetic wounds still remains as a health care burden. The global cost of diabetic wound treatment estimated to be $1.3 trillion dollars, among which one third expenditure is on lower limb amputation. There are several factors which impede prompt healing. The dominant factors include loss of sensory function, peripheral artery disease and infection (Patel et al., 2019). Hyperglycemia causes oxidative stress on nerve cells leading to neuropathy. The glycosylation of nerve proteins results in nerve dysfunction and further ischemia. Motor, autonomic and sensory neurons are involved in neuropathic ulcers. Impaired motor nerve function result in loss of foot musculature which leads to an imbalance of flexors and extensors leading to anatomic deformities and eventual skin ulceration. The clinician should be aware of the cause of DFU to decide effective treatment. Impaired sensory neurons cause loss of peripheral sensation, so that the patient may not notice foot wounds. Hyperglycemia can also induce vascular changes in the peripheral arteries of foot. Due to dysfunction of endothelial cells the levels of vasodilator decreases resulting in vasoconstriction and plasma hyper coagulation resulting in ischemic injury. Immune changes such as increased apoptosis of T lymphocytes can reduce diabetic wound healing (Aumiller and Dollahite, 2015).

1.5.2 Classification

Diabetic wounds are classified and scored for the ease of communication between healthcare professionals and for deciding the clinical outcome. A system was developed by Jordan University hospital in 2004 for scoring ulcers depending on depth, extend of bacterial colonization, phase of healing and associated aetiology. Out of many classification systems, the Meggitt-Wagner classification is the most cited one. The diabetic wound are graded into categories ranging from grade zero to grade five, depending on the depth of the skin lesion and presence or absence of gangrene. This system allows the monitoring of bidirectional progression from grade zero to grade four and regression from grade four to grade zero. So this system can be used as diagnostic tool (Santema et al., 2015).

1.5.3 Pathophysiology and molecular basis

The healing processes in diabetic patients get stalled and the alterations in the normal healing phases results in non-healing wounds (figure II). During hemostasis phase, hypercoagulability and decrease in fibrinolysis have been observed in diabetic patients than normal subjects. The prolonged inflammatory phase is another observation, which results in delayed healing response. The neutrophils in the diabetic wound bed have altered cytokine release pattern with reduced functionality. This enhances the susceptibility to wound infection. The hyperglycaemia causes reduced proliferation and migration of fibroblast and keratinocytes, resulting in delayed wound closure. The impairment in the angiogenic response causes reduced blood flow to the

wound area. Due to the functionally altered fibroblast, there will be reduction in collagen deposition leading to defective ECM formation.

Diabetic wounds are characterized by oxidative stress. Advanced glycation end products (AGE) accumulation is one of the reasons for oxidative damage. AGEs are large molecular protein with longer half-life than collagen. The accumulation of AGE over the skin collagen leads to the formation of glycosylated collagen, having altered function. Increased exposure to reactive oxygen species lead to cellular dysfunction by destruction of intracellular proteins and lipids. Reduced level of extracellular dismutase was observed with non-healing wounds. These are one of the prime enzymes for the elimination of ROS. Long term hyperglycaemia can produce large number of AGE in the body leading to chronic wounds. AGE accumulation activate NF-kB pathway in keratinocytes which inhibit the transition from S to G2/M phase. AGE deposition in nerve tissue can damage axial plasma transport and affect intracellular signal transduction and protein phosphorylation result in axonal degeneration (Huijberts et al., 2008). Tennenberg et al studied that in diabetic patients, hyperglycaemia induce apoptosis of neutrophils, which contribute to the susceptibility of infection in diabetic patients (Tennenberg et al., 1999).

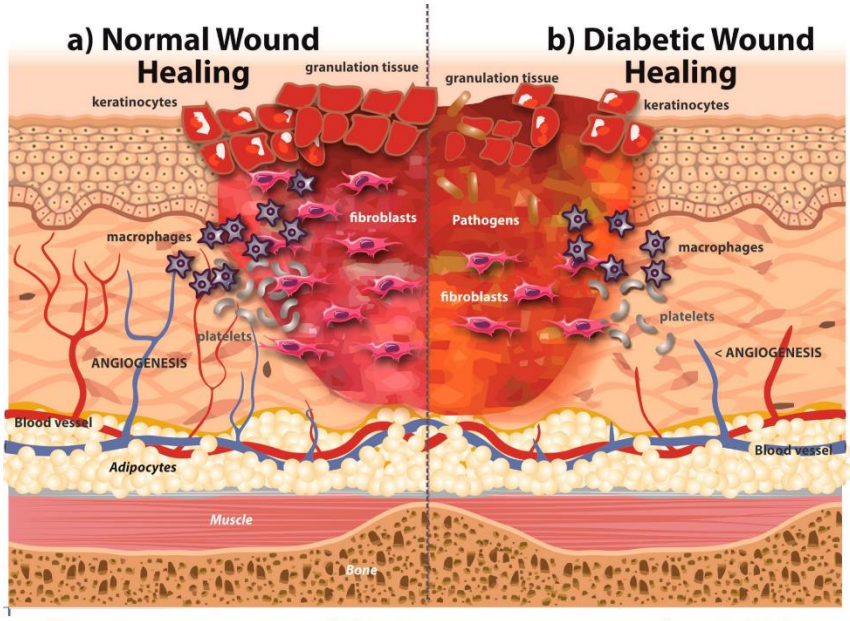

Figure II: Comparison of wound healing process in normal health condition and in diabetic condition (Perez-Favila et al., 2019).

In diabetic patients, functions of macrophages are impaired with imbalanced M1/M2 ratio. High glucose level augments macrophage activity and produces more reactive oxygen species, which causes cellular damage. AGE accumulation induces the production of TNF alpha from macrophages which impairs epithelialization and cause non-healing wound. Increased oxidative stress in endothelial cells reduces blood supply to the wound area. Human diabetic fibroblasts show severe impairment in VEGF production with increased degradative pathway due to high expression of MMP 9. The increased protease activity can lead to tissue destruction and inhibit repair process. Hyperglycaemia increases the expression of MMPs and decrease expression of TIMPs. Dysregulation of T cells, B cells and monocytes results in the inhibition of diabetic host immunity. Wagner et al reported that reduced number of T cells and its receptors in diabetic patients favours accumulation of pathogenic effector T cells,

which lead to elevated level of TNF alpha and IL-6 (Wagner, 2011). Defective production of growth factor receptor and its rapid degradation also occur in diabetic wound environment.

1.5.4 Challenges in treating diabetic wounds

The management of chronic wounds is often challenging. A thorough assessment of the patient and the wound is needed. The cost of diabetic wound management creates a major economic burden to the healthcare system. It is reported that the individuals with diabetic foot ulcers who progressed from Wagner grades 1 to 2 to the higher grades, utilized resources incrementally leading to higher expenditure (Driver et al., 2010). Early detection and prevention of diabetic foot have received a lot of attention. A systematic approach to both assessment and treatment is needed to get a favorable outcome. A multidisciplinary approach is highly recommended for the management of chronic wounds. The designing of treatment strategies for stalled wound should be based on considering the physiological factors along with biological alterations. The common wound care principles include sharp debridement, moisture control, appropriate dressing selection, control of underlying disease and nutrition at systemic level. There should be control of host factors like diabetes, hypertension, drugs, smoking and nutrition (Widgerow, 2012).

Different studies have shown that there is no sufficient superiority to recommend a particular treatment for diabetic wound management. Another critical aspect of diabetic ulcers is the emergence of new ulcer after healing. It has been reported that about 40% of people have a new ulcer whether at the same site or another

within 12 months (Huang et al., 2019). After four weeks of routine treatment, a wound's ability to heal enough should be assessed again, and the necessity for advanced therapeutic agents should be taken into account. But choosing the right therapy is frequently not based on evidence. So the targeted education is another essential part of preventing secondary ulcer formation (Jeffcoate et al., 2018). The sensory loss in diabetic neuropathic patients increases the incidence of lower extremity amputation. It has been reported that the use of multi-disciplinary teams including the relevant specialties such as nursing, orthopedics, plastic surgery, nutrition, endocrinology and vascular surgery in diabetic wound management could effectively reduce the risk of DFU related amputation by 80-85%.

It is necessary to understand the micro environment of DFU to decide the optimum therapy. To effectively manage diabetes, a supportive microenvironment must be established. The development of ulcers and the eventual onset of diabetic foot are both impacted by changes in the local microenvironment, which also affects some cellular components and other elements in the local necrotic tissue. Wound healing can be accelerated by controlling the microenvironment and reducing inflammation. The developments in the wound dressing materials are useful for changing the local wound environment. The type of wound dressing material can simply shift the wound healing cascade (Li et al., 2023). So the adequate care of the diabetic wounds helps to lower the cost, hospitalization and improves the quality of life.

1.5.5 Current diabetic wound care strategies

With the advent of technology, more treatments for DFUs have been introduced, including the manufacture of skin replacements, negative pressure wound therapy, hyperbaric oxygen therapy, novel wound dressings containing growth factors, and the use of tissue engineered constructs. These treatments encourage the development of neuroprotective, pro-angiogenic, and anti-inflammatory substances, which are beneficial for the proper wound care. The use of mesenchymal stem cells (MSC) derived from adipose tissue is now being investigated as a possible therapy for diabetic neuropathy. Negative pressure wound therapy (NPWT), which is most frequently administered with the vacuum assisted closure device employing a sealed open-pore sponge or gauze. This technique can be used as an adjunct to surgical debridement for treating chronic contaminated wounds. This technique can also be used to support skin graft and protect wounds at high risk of breakdown (Putnis et al., 2014). Another treatment strategy is the hyperbaric oxygen treatment (HBOT). The hypoxic tissues in chronic wounds prevent ulcer repair and oxygen is crucial to the healing process to proceed. For a better clinical outcome during HBOT, the patient is maintained in a room with 100% oxygen saturation and an atmospheric pressure 1.4 atmospheres absolute (Sharma et al., 2021). Therapy with hyperbaric oxygen encourages fibroblast growth, strengthens the immune system, and accelerates angiogenesis. The treatment of diabetic wound ulcers with hyperbaric oxygen has been recommended and practiced. However, there is little scientific evidence to support the efficacy or safety of this method (Zhang et al., 2022).

Growth factor based therapy is another approach for DFU management. Several growth factors such as platelet-derived growth factor (PDGF), fibroblast growth factor (FGF), epidermal growth factor (EGF), transforming growth factor (TGF β) and vascular endothelial cell growth factor (VEGF) have shown potentials in promoting wound healing. Growth factors participate in the biological events such as chemotaxis, cell proliferation, extracellular matrix deposition, angiogenesis, and tissue reconstruction. The sustained and dose dependent delivery of growth factors towards the wound site is very critical, since its uncontrolled release may result in tumorigenic activity. Beclapermin (recombinant PDGF) have shown therapeutic efficacy in randomized controlled trials of significant numbers of patients. But the cost of the growth factor based treatment is high and also has inconsistent performance in trials. Hence it is critical that a careful evaluation by clinical trials is needed before therapeutic application (Bennett et al., 2003).

The use of skin equivalents that incorporate growth factors, cells, and/or biomaterials has received a lot of attention in DFU management. Dermagraf® is a product that works because of its bio absorbable synthetic scaffold, metabolically active fibroblasts, and ECM components. Apligraf® promotes the generation of cytokines and growth factors that are comparable to those found in healthy human skin. AlloDerm®, which is composed of a structured acellular dermal matrix of healthy collagen promotes neovascularization and fresh skin regrowth in humans. Economic analysis by Ontario health, stated that the use of skin substitutes for the treatment of non-healing diabetic foot ulcers are much expensive and effective than

conventional wound care. For the treatment of difficult-to-heal diabetic foot ulcers and venous leg ulcers, skin replacements were both highly effective and expensive than conventional care alone. The incremental cost-effectiveness ratio (ICER) of skin substitutes with standard therapy in comparison to standard care alone for diabetic foot ulcers was found to be $48,242. The high cost as well as the lack of knowledge about the skin substitutes are the main barriers for the clinical use in patients with diabetic wounds (Ontario Health (Quality), 2021).

1.6 Wound dressings for diabetic wound management

To develop an ideal wound dressing material for diabetic wound management, the concepts of wound healing must be incorporated into desirable wound dressing properties. A moist wound environment has been identified as ideal condition for healing. Modern wound dressings were produced during late 20th century. The first modern dressing was synthesised during mid-1980s, which was occlusive type dressing for providing moist environment and aiding faster re-epithelialization of wounds (Queen et al., 2004). The selection of wound dressing is based on the type, location, extend and depth of the wound and amount of the exudate. An ideal wound dressing should have high absorption capacity, avoid pain on removal, allow visualization of wound, should not induce any allergic response. It should offer mechanical protection of the wound from the external environment and also from the hazardous components present in the wound exudate. The dressing should keep optimum moisture and pH level at the wound surface. It should allow gas exchange with the environment for optimum cellular activities and should not release any non-

biodegradable particles or fibres into the wound surface. The material should be cytocompatible and free from toxic or irritant chemicals that leach out from the dressing. The material should also be easily removable from the wound without disturbing the underlying tissues and should be affordable to majority.

1.6.1 Conventional wound care products

The conventional wound care products include gauze, lint, plasters, bandages and cotton wool. They are used as a primary or secondary dressing to protect the wound from contamination. Gauze dressings composed of cotton, rayon, polyester woven and nonwoven fibers offer some amount of defense against bacterial infection. With the aid of their fibers some sterile gauze pads can be utilized to collect liquids and exudates from an open wound. Regular change of these dressings is necessary to prevent the maceration of healthy tissues (Shi et al., 2020). Gauze bandages are less economical. Excessive wound drainage causes dressings to get wet and have a tendency to stick to the site, making removal uncomfortable as well as damaging to the healing wound. Different functions are carried out by synthetic bandages consisting of polyamide polymers, cellulose, and natural cotton wool. Tulle dressings appropriate for superficial clean wounds are available commercially as impregnated dressings with paraffin. Traditional dressings should typically be used as a secondary dressing or for clean, dry wounds with low exudate levels. Modern dressings with more sophisticated formulations have taken the place of conventional dressings because the former cannot offer a moist environment for the wound (Rezvani Ghomi et al., 2019).

1.6.2 Advanced wound care products

Instead of only covering the wound, modern wound dressings have been devised to help it heal. The main goals of these dressings are to prevent dehydration of the wound and to encourage healing. The market offers a wide variety of products depending on the type and origin of the wound, making the selection very challenging. Modern bandages for wounds are often made of synthetic polymers and fall under the categories of passive, interactive, and bioactive products. Gauze and tulle dressings are examples of passive materials that are non-occlusive and used to cover a wound so that its internal functionality can be recovered. The interactive dressings are available in different forms such as films, foam, hydrogel, and hydrocolloids. Each type of dressings have its own advantages for making them ideal for treating specific type of wound (Medikabazaar, 2022). The advantages and disadvantages of different types of wound dressings are summarized in the table II.

Type of wound care material	**Advantages**	**Disadvantages**
Gauze dressing	Remove exudate from the wound	Cause dehydration of the wound Disturbs new epithelium formation
Tulle dressing	Aid in healing but not absorb wound exudate	Cause allergic responses
Semi permeable film dressing	Allow moisture to evaporate Reduces pain Act as barrier to prevent environmental contamination	Require secondary dressing to hold the dressing in place

Hydrogels	Provide moist environment and reduce wound temperature Promote granulation tissue formation	Accumulation of exudate causes maceration of the tissue Exudate accumulation lead to bacterial proliferation and foul smell in wounds
Hydrocolloids	Easy to use and moderately absorptive Stimulate autolytic debridement process	The gel formed over the wound surface can be thick, yellow or malodorous. Sometimes adhere to the wound surface and difficult to remove
Foam dressings	Protect the wound and keep the wound moist Used with moderately exudating wound	Can adhere to wounds if exudate dries
Hydrofibers	Highly absorbent No need to be changed frequently Available in sheets or ribbon	Not used with dry eschar and non-exudating wounds Need of secondary dressing

Table II: Advantages and disadvantages of different types of wound dressings (Pilehvar-Soltanahmadi et al., 2018).

Despite these well stated goals for different types of advanced wound care products, it is difficult to suggest an ideal wound dressing for diabetic wound management. This is mainly due to the heterogeneous nature of the diabetic wounds as well as the lack of research based supportive evidence to suggest a particular dressing over another. Patients with diabetic wounds are usually excluded from the randomized clinical trials of wound dressings, due to different underlying pathologies. So more research need to be focused on developing advanced wound care material for diabetic wound management. In this scenario, to develop new formulations for treating diabetic wounds, natural polymers especially polysaccharides have been given more attention. The use of polysaccharides as wound care material is highly promising due

to their excellent biocompatibility, ability to promote cell growth and regenerative capacity.

1.7 Polysaccharides as wound dressing materials

Polysaccharides are considered as stereo regular polymers of monosaccharides extracted from plants, animals, fungi, algae or obtained via fermentation. These are considered as unique raw material for various applications such as texture modifiers, gelling agents, thickeners, emulsifiers, stabilizers, coating agents, dietary fibers and as packaging films (Zied et al., 2012). Polysaccharide based wound dressing are now becoming popular due to their non-toxic, non-immunogenic and highly absorptive nature. They are naturally derived, highly abundant and inexpensive in nature, which enables the large scale production of wound care materials. Polysaccharides vary in terms of molecular weight, charge, structure and chemical properties, which favour the fabrication of wound dressing specific to the wound aetiology. Various chemical and biological properties such as non-toxicity, biocompatibility, biodegradability, chelation, poly functionality, high chemical reactivity and absorption capacity support their application as healing agent. The high hydrophilicity, presence of different functional groups and flexible polymer chains provide them excellent absorption behaviour. The excellent hydrophilic nature and the ease of chemical modification enable formation of hydrogels.

Polysaccharides can be fabricated into membranes, gels or hydrogels for different applications. They can be also modified into biomimetic platforms for bioactive molecule release. Their application as wound care material depends on the

characteristic features such as biomolecule immobilization and its controlled release. Polysaccharide formulations can also act as transdermal delivery systems for controlled release of active ingredients. Bioactive materials can target inflammatory, proliferative or remodelling phase of healing by direct cell interaction or by extracellular matrix mediation. They modulate the signalling pathways of various cells involved in wound healing such as fibroblasts, keratinocytes, endothelial cells and macrophages (Al-Jabri, 2021). The wound treatment strategy based on inducing fibroblast proliferation, ECM restoration and keratinocyte migration plays significant role in healing process.

Carbohydrate polymers from natural sources has been studied extensively and utilized in pharmaceutical and industrial applications for many years. Polysaccharides can be neutral (cellulose, dextran, pullulan, galactomannan, glucuronan), cationic (chitosan), acidic (alginate, pectin, hyaluronan, gellan, xanthan) or with sulphate groups (carrageenan, heparin, fucoidan) (Zied et al., 2012). Anionic polysaccharides composed of carboxylated sugars, which are specific reactive groups can be easily functionalized to develop structures with appropriate biomedical applications. The industrially used anionic polysaccharides include carboxy methyl cellulose (Balonose, Kelcol) and carboxy methyl starch (Explotab, Primoyab). The anionic character of the polysaccharides depends on the ionic strength and pH. Anionic polysaccharide can form gels in the presence of divalent cations (Tai et al., 2019). The presence of anionic groups makes the hydrogels pH sensitive and the hydroxyl and carboxyl groups permits the crosslinking with tunable mechanical and swelling properties.

Glycosaminoglycans are linear anionic polysaccharides expressed on the cell surface and in the extracellular matrix. Glycosaminoglycans play significant role in wound healing process through re-epithelialization and increased vascularization. Cell differentiation, cell adhesion, cell signalling and cellular-matrix interactions are also mediated by glycosaminoglycans. Skin contain hyaluronic acid, which is a glycosaminoglycan. Hyaluronan has been extensively studied for tissue repair due to its physico-chemical properties and specific interaction with the cells. Different studies showed that the properties of hyaluronan depend on its molecular weight. High molecular weight HA has anti-inflammatory and immunosuppressive activity, whereas low molecular weight displays pro-inflammatory actvity (Litwiniuk et al., 2016).

Another anionic macromolecular polysaccharide is xanthan, produced from sugar cane and corn and other derivatives by *Xanthomonas campestris* in aerobic conditions. The current potential application of xanthan gum is in pharmaceutics especially in tablets to yield a sustained release of drugs. It can be used as appropriate vehicle for antimicrobial peptide in a retention increasing formulation. Jinjian Huang et al, developed silver nano particle incorporated xanthan gum film, blocks the biofilm formation in acute wounds. The composite were able to alleviate the inflammation at the injury site and promote angiogenesis and granulation tissue formation (Jinjian Huang et al, 2017). Gellan is another water-soluble anionic polysaccharide produced by the bacterium *Sphingomonas elodea*. It consists of repeating unit of tetrasaccharide units of two residues of D-glucose and one of each residues of L-rhamnose and D-glucuronic acid. Nor Jannah et al, developed gellan gum hydrogel with ibuprofen for

transdermal application. The slow release of ibuprofen from the gel, together with excellent mechanical properties, antibacterial action and biocompatibility makes it good choice for slow and moderately exudating wounds (Nor Jannah Mohd et al, 2016).

Although polysaccharides have many advantages, some of its disadvantages such as poor mechanical strength, faster disintegration etc limits its application as a biomaterial. The chemical modification of polysaccharides helps to overcome such problems. The presence of several features in the polymer backbone enables the modification of polysaccharide chains into desired characteristics. It can be fabricated into porous tissue regeneration structures, into micro particles, hydrogels or other three dimensional scaffolds.

1.7.1 Alginate in wound care

Alginate is one of an extensively researched polysaccharide to develop various biomaterials and clinically relevant products. They are anionic and hydrophilic polysaccharides derived from brown seaweeds and bacteria. Alginate is usually extracted from brown algae *(Phaeophyceae), Ascophyllum nodosum, Laminaria hyperborea, Laminaria japonica, Macrocystis pyrifera, and Laminaria digitate.* The monomer units of alginate are β-D-mannuronic acid (M) and α-L-guluronic acid (G), linked through 1,4 glycosidic linkage (Figure III). The G and M blocks of alginate are responsible for the gelation and viscosity. The blocks can be consecutive G residues (G block), M residues (M block) or alternating M and G residues (MG block). The physical properties of the alginate is determined by the ratio of M and G blocks

(Aderibigbe and Buyana, 2018). Alginate is biocompatible, non-toxic and does not elicit any immune response. It is very essential to ensure that alginate is free of impurities after purification process. Alginate based systems are one of the promising materials in the field of drug delivery, wound healing, tissue engineering, cell encapsulation and biosensing. Alginate is highly versatile molecule and can be fabricated into different forms such as foams, hydrogels, aerogels, nanocomposites, microspheres, scaffolds, and sponges (Hegde et al., 2022). By derivatization, favorable properties can be imparted onto alginate for various applications. The therapeutic efficacy of alginate based products is influenced by the ratio of other polymers used in combination with alginate, nature and time of cross-linking, nature of excipients and the nature of incorporated biomolecule. Alginate dressing are usually prepared by ionic cross-linking with different divalent ions to form gels or further processed to from freeze dried porous sheets. Alginate based nanofibers synthesized by electrospinning are potential wound dressing materials. The nanofibers enhance the proliferation of epithelial cells and promote ECM formation (Liu et al., 2021).

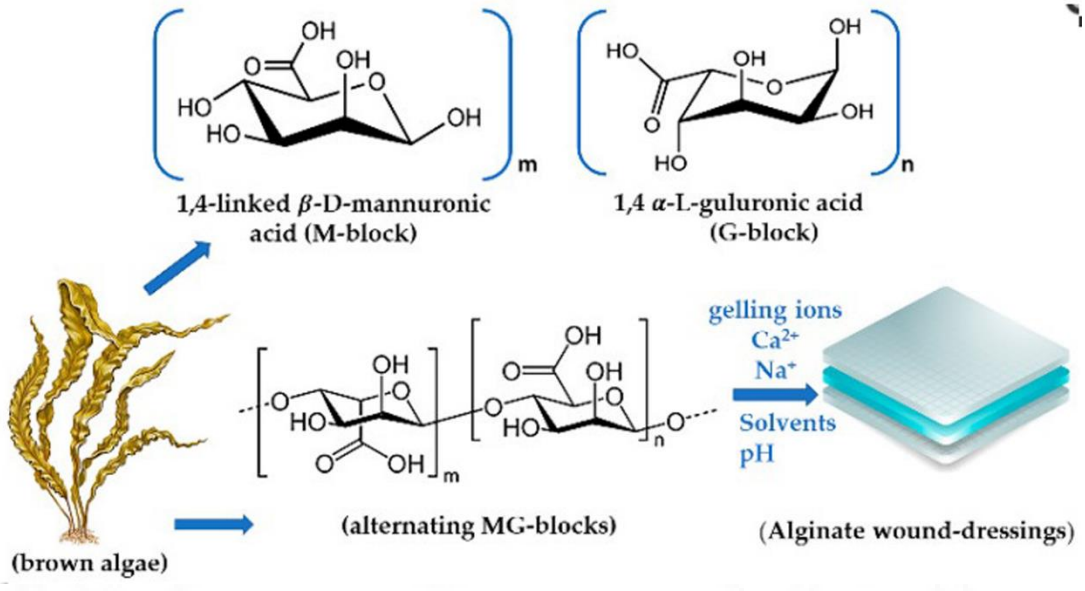

Figure III: Structure of alginate chains with different blocks and synthesis of alginate based wound dressing material (Barbu et al., 2021).

Hydrogel based wound care materials play a significant role in wound management over the years. Hydrogel dressing possess soft-tissue like water content with adequate flexibility and highly sensitive to physiological environment. Alginate hydrogels can be synthesized by covalent or non-covalent cross-linking methods. Ionically cross-linked alginate hydrogels are usually used in the wound care. The co-operative binding of divalent ions occurs with G blocks of two polymer chains on opposite sides, resulting in diamond shaped hole contacting a hydrophilic cavity. This configuration is known as the egg box model (Lee and Mooney, 2012). The use of stimuli-responsive hydrogels, also referred to as "smart hydrogels," for the treatment of diabetic wounds has received a lot of focus recently. The basic feature of this system is its ability to modify mechanical properties, swelling ability, hydrophilicity and permeability of biologically active molecules in response to a variety of stimuli,

including temperature, hydrogen potential (pH), protease, and other biological factors (Zhang et al., 2023).

1.7.2 Commercial alginate based dressings

Alginate has been used in many industries since 1930s. It was known as 'mariners cure' since it has been used by sailors centuries ago to heal wounds. In 1881, alginic acid was first extracted by the British chemist, Stanford. The key market players in the alginate wound care market are 3M, Essity AB (BSN Medical, Smith & Nephew PLC, ConvaTec Group plc and Coloplast A/S. The market leaders are taking efforts to add advanced functionalities to the wound dressing to increase consumer convenience. The commercially available alginate dressings are summarized in the given table III.

Name of the dressing	**Composition**	**Study effects**
Sorbsan	Mannuronate-rich calcium alginate dressing	• Forms a soft fragile gel • Disintegrates rapidly compared with other alginates
Tegagel	Mannuronate-rich calcium alginate dressing	• High degree of wet integrity • Fibers are closely compressed, fluid diffusion is more difficult than in other alginates
kaltostat	Guluronate-rich calcium alginate dressing	• Ensure a moist environment • Applied to bleeding wounds due to its hemostatic properties • Suitable for moderate to high exuding wounds • Necessitates more frequent change • Requires a secondary dressing to hold it in place

Algiderm	Guluronate-rich calcium alginate dressing	• Induces a strong gel formation • Excellent dressing integrity • Can absorb 20 times its weight in exudate
Saf-gel	Carbomer propylene glycol sodium—Ca ALG	• Used for Abrasions, cuts, sloughy and necrotic wounds • Surface moisturizer
Silvercell	36% Ca ALG with high G—6% CMC—28% A Calcium alginate with carboxy methyl cellulose	• Antibacterial effect due to release of silver ion
Medihoney®	Calcium alginate – Manuka honey	• Antibacterial effect
Flaminal gel	ALG—PEG matrix—notatin—lactoperoxidase—guaiacol	• Antimicrobial effect • Wound surface moisturizer exudate absorber • Debrides necrotic tissue
Fibracol plus dressing	Calcium alginate – collagen	• Promote ECM formation

Table III: Commercial alginate based wound care materials

1.8. Scaffold mediated delivery of therapeutic molecules to the wound site- Bioactive wound dressings

Bioactive wound dressing are defined as the material which promote the wound healing process, either being constructed from materials having endogenous activity or serve as support for the delivery of bioactive compounds. Biomolecule based strategy has been used for wound healing in recent years. Bioactive molecules can regulate wound healing process by controlling cellular processes. The use of biomaterials in wound healing and tissue regeneration is well established as a promising therapeutic approach. The bioactivity can be introduced through the

incorporation of adhesion factors, cleavage sites for enzyme activity and addition of poly anionic sites which mimic the electrostatic interaction of biological regulatory polysaccharides. Among different biomaterials, hydrogels play a significant role in wound healing, since their characteristics are similar to the ECM. Due to its highly porous structure, high biocompatibility and fast functionalization, hydrogels are the promising biomaterial for biomedical applications. They can be modulated as environmentally sensitive hydrogels according to the wound micro environment.

Bioactive molecules are cell-permeable and non-immunogenic that can selectively modulate the intracellular processes. So they are considered as the next generation of regenerative medicine. The bioactive molecules include small or large molecular weight proteins, nucleic acids or monoclonal antibodies. The Food and Drug Administration (FDA) has approved over 150 recombinant biopharmaceuticals, and the number of applications and approvals are continuously expanding. The biomolecules used for wound healing applications include growth factors, antimicrobials, natural plant extracts, immune-modulatory proteins such as cytokines, hormones, inorganic ions, anti-inflammatory molecules, enzymes etc. The same biomolecules can send various messages to different kinds of cells at different healing phases. So the controlled spatiotemporal delivery of biomolecules is essential for successful wound healing process. The incorporation of bioactive molecules in wound care products has been adapted as the first line of treatment in wound management which considerably reduces the total therapy costs.

1.9 Gap area

Even though bioactive molecule based treatment is an attractive alternative for treatment of skin wounds, there still exist some challenges in using biomolecules for wound healing applications. The selection of suitable biomaterial for developing bioactive wound dressing is a major challenge. Alginate has become one of the top choices for developing bioactive wound care materials, because it can act as a carrier for bio-active compounds and maintain the sustained delivery for promoting wound healing. However, most of the alginate based dressings are ionically crosslinked structures which easily disintegrate in the wound site, especially exudating wounds and the remnants can get lodged in the wound site. Histopathological evaluation revealed the presence of foreign body reaction by the incorporation of alginate fibres surrounded by a giant cell, resulting in prolonged tissue edema (Morgan, 1997). Another major issue is the removal of alginate dressing from the wound bed. Usually, irrigation with normal saline (Sorbsan) or removal with pair of forceps (kaltostat) needed, which disturbs the underlying tissues. So there is a need of mechanically stable alginate as a wound dressing and also as a carrier for localized biomolecule delivery.

The screening of suitable bioactive molecule for skin repair is also a challenge. The in vitro results of the bioactive molecules may not reflect with the in vivo regenerative results. Hence appropriate in vitro as well as in vivo models need to be optimized. The delivery of biomolecules through systemic circulation could be ineffective for chronic wound management due to the poor circulation in the necrotic wound bed, which leads to poor bioavailability. The topical formulations such as

creams, ointments or gels create practical difficulty due to their inconsistent effect. It is difficult to maintain the concentration at the wound surface due to normal movement or during dressing changes. The increased concentration of free radicals at the wound surface creates oxidative stress that interferes with the cellular processes. The wound exudate enriched with proteases causes the degradation of bioactive molecules especially growth factors. The reduced availability of oxygen is another challenge which delays the cellular functions. The presence of necrotic tissue is another issue which lack the ability to heal and is also prone to infection (Whittam et al., 2016).

The treatment strategies of diabetic wound should aim to treat from cellular or molecular level. Hence appropriate biomolecules should be selected for promoting healing process in stalled diabetic wounds. The biomolecule of interest should able to control the prolonged inflammatory phase, promote cell proliferation and migration, reduce reactive oxygen stress in the wound bed and promote collagen deposition. Currently available alginate wound care materials are not appropriate for diabetic wound management. As mentioned above, its dissolution in wound exudates and poor mechanical strength makes it unsuitable for chronic wound management. Besides, alginate materials as such are unsuitable for biomolecule delivery as it cannot maintain a sustained delivery owing to dissolution in the wound exudates. So it is essential to develop mechanically stable alginate based wound care material without compromising its hydrophilicity and biocompatibility.

1.10. Hypothesis

Grafting will improve the mechanical stability of alginate and biomolecule loaded graft-alginate based hydrogels can be used as an advanced wound care material for diabetic wound management

1.11. Aim and objectives

Based on the research problem, we aimed to develop an alginate based wound material with good mechanical strength, which can deliver selected biomolecules in a controlled way for diabetic wound management. To prove the hypothesis, the objectives were formulated as follows;

- To develop anionic polysaccharide based wound dressing with main emphasis on alginate & its derivatives.
- Characterization of derived wound dressing material.
- Incorporation of various bioactive molecules such as anti-inflammatory drugs, enzymes, or hormones targeting diabetic wounds.
- To analyze the release profile of bioactive molecules loaded onto dressing material.
- *In vitro* evaluations with cell types of skin.
- Analysis of healing potential efficacy by *in vivo* evaluation.

CHAPTER 2

REVIEW OF LITERATURE

2.1 Biomolecule assisted wound healing

Biomolecule assisted therapy can reprogram the endogenous repairing potential of the cells. This technique is one of the promising strategies to achieve in situ skin regeneration. Skin regeneration can be achieved by either replenishing the skin surface with sufficient number of repairing cells or by activating endogenous repair potential. Skin grafts and tissue engineered skin substitutes are used for this purpose. Stem cell therapy is a promising approach in the field of regenerative medicine. However there still exist some challenges for using stem cells for regenerative wound healing. This includes, determination of ideal source of stem cells, method of administration and defining the role of stem cells in real clinical situation (Nourian Dehkordi et al., 2019).

Studies show that genetic approaches can be used for cellular reprogramming, but it has low efficiency and integration risk. Compared to genetic manipulations, biomolecule activated reprogramming of cells provides highest efficiency and improved quality. Recent studies shows that biomaterials loaded with bioactive molecules promote vascularization, cell migration and proliferation through regulation of signaling pathways. The therapeutic potential of bioactive molecules may represent the next generation of regenerative medicine. The bioactive molecules can be large natural molecules such as proteins, cytokines, or lipids or it can be small molecules that regulate specific signaling pathways for cell reprogramming and repair. The

molecules are stable, cost effective, non-immunogenic, cell permeable and are safe for administration. Bioactive molecules can modulate intracellular events with their cell specific targets. They can also activate the local repair process (Oliva and Almquist, 2020). Recent studies shows that bioactive molecules can replace the transcription factors and helps in direct reprogramming of cells, which is promising method for getting unlimited supply of cells for developing tissue engineered skin and for cellular transplantation. The skin repair cells can be obtained through biomolecule induced differentiation and promote endogenous stem cell proliferation and homing. They also stimulate the somatic cell proliferation and reprogram into repairing cells. They modulate the wound micro environment by reducing inflammation, regulate wound pH and promote angiogenesis. Recent studies show that bioactive molecules can reduce scar formation during remodelling phase. Tissue regeneration now focuses on the direct application of bioactive molecules to the target site. This new field emerging recently is called in situ regeneration (Dias et al., 2020).

2.2 Role of bioactive molecules in wound healing

Different classes of biomolecules show significant improvement in wound healing activities. Among which, important molecules are growth factors, which are able to regulate the activities such as cell division, differentiation, migration or gene expression. Depending on the target receptors, growth factors can act in autocrine, paracrine or endocrine fashions. The action of growth factors are usually short lived, upon binding with receptors, it may get degraded by the proteolytic enzymes. Even though, growth factor incorporated materials are clinically available in market, the

issues regarding its safety and cost in the clinical settings are not properly addressed (Briquez et al., 2015). The high cost of the production of purified growth factors prevents their integration into wound dressings and most of the time, the use of single growth factor may not be sufficient for optimum wound healing. It is necessary to study the safety and the pharmacokinetics of the growth factors using non-clinical models before clinical trials (Greenhalgh, 1996).

The bioactive components extracted from the natural sources also play significant role in wound healing. Herbal medicines plays significant role in disinfection, debridement and provision of favorable environment for wound healing. But proper clinical evaluation and optimum therapeutic dose need to be validated before clinical applications. The infections associated with wounds are responsible for the high rate of morbidity and mortality. To address the infection associated with the wounds, the antimicrobial agents are developed comprises of antibiotics, nanoparticles and natural products. The antibiotics can alter the bacterial structure and function by interfering with different molecular pathways (Simões et al., 2018). The increased use of antimicrobials leads to the emergence of multidrug resistant bacteria against natural and synthetic antibiotics.

New therapeutic approaches like nanomedicine are introduced in the antimicrobial therapy. Some of the nanoparticles possess bactericidal effect through the release of toxic metal ions or through the generation of reactive oxygen species. Among different nanoparticles, silver ion based particles are widely used in the development of antimicrobial wound dressing. Silver nanoparticles can inhibit the activity of

mitochondrial respiratory chain complexes I, II, III, and IV as well as inhibit the replication and transcription processes. Another molecule of interest, having anti-microbial activity is honey. It has been used as a natural healing agent since ancient times. Honey also takes part in debridement activity, granulation, wound contraction and epithelialization (Simões et al., 2018). The role of antimicrobial peptides (AMP) in treating wound infection has been recognized very recently. AMPs are considered as the natural antibiotics with great potential in effectively killing the bacteria with minimum risk of resistance (Nasseri and Sharifi, 2022). Different AMPs are involved in wound healing process, among which defensins and cathelicidin LL-37 helps to control the skin infection and promote reestablishment of the skin tissue (Thapa et al., 2020).

In this work, we are focusing on the delivery of other classes of bioactive molecules such as inorganic ions, hormones, anti-inflammatory drugs or enzymes that plays important role in wound healing process.

2.3.1 Inorganic ions in wound healing

Inorganic ions are ubiquitous in the environment and some of them play significant role in homeostasis and regulatory functions in the body. Studies have shown that inorganic ions can penetrate the skin and induce local effects. They act as messengers, carriers or cofactors of enzymes and stabilizers for proteins and lipids. Inorganic ions are used for curing skin diseases by local administration. The transport of ions across the skin is compromised by the outermost layer *stratum corneum*. The passive diffusion of ions across *stratum corneum* is possible through intracellular

routes by lipid core via polar head group pathways. Sometimes protein channels or receptors allow the specific transport of ions across the skin, which needs energy expenditure. Inorganic ions play significant role in wound healing process. Recent studies show that the introduction of inorganic ions through biomaterials could improve neo tissue formation and vascularization.

Calcium is one of the inorganic ions which have been studied extensively in wound healing. Calcium ion plays significant role in intracellular signaling by acting as secondary messenger. Apart from being critical coagulation factor for maintaining homeostasis, they act as fundamental cue for regulating cellular function during wound healing. The extracellular calcium concentration increases upon injury, persist through out inflammatory and proliferative phases and decline during remodelling phase. Several calcium containing dressings are developed to facilitate wound healing. Calcium alginate dressings are commercially available which enhance wound healing by upregulating collagen production (Subramaniam et al., 2021). The antibacterial effect of silver has been used for developing antimicrobial wound dressings. Silver ions also has anti-inflammatory role in wound healing. (Graham, 2005). Silver can be incorporated within the dressings in either form such as ionic silver or as metallic silver. Newer dressing contains silver in the nanocrystalline form and it gets eluted to the wound area in a sustained fashion. Silver has toxic systemic as well as local effects if used in high concentration. (Khansa et al., 2019).

Zinc ions are involved in the regulation of enzymatic activity. Being the co-factor of MMP molecules, Zn ions play significant role in the digestion of ECM

components during healing process. The keratinocyte proliferation and differentiation is also controlled by zinc. Iron, another inorganic ion, have regulatory role in inflammatory phase during wound healing. Since iron is the active centre of pro-collagen lysyl hydroxylases, it is involved in maturation of pro-collagen and stabilized collagen triple helix. The role of magnesium ions in various cell behavior like cell proliferation, differentiation and migration has been reported in various studies. Magnesium ions also have significant role in collagen and fibronectin deposition. Copper ions are another intracellular regulator of cell metabolism during wound healing. Copper ions induce angiogenesis by inducing the expression of hypoxia induced factor - 1 (HIF-1) and increase the transcription of VEGF (Coger et al., 2019). Copper ions can modulate the activity of proteins involved in wound healing and the control of copper homeostasis might be a target for therapeutic intervention for wound healing (Kornblatt et al., 2016).

The biological role of strontium ions are well known in the ortho-dental fields. Strontium ions are one of the essential trace elements in the human body, plays significant role in the bone metabolism. Strontium ions shows dual regulatory activity by activating bone osteoblast for increasing bone metabolism and mineralization, at the same time, it suppresses the osteoclast activity to reduce bone resorption (You et al., 2022).. Numerous studies have suggested that the Sr doped biomaterials shows significant improvement in the bone formation around the bone defect. Strontium renelate is successfully used in the clinical practice for the treatment of osteoporosis. Strontium ions also promote the fibroblast and keratinocyte migration and

proliferation (Alsharif et al., 2023).. Strontium and calciums ions are chemically similar and exhibit similar physiological functions. Strontium ions can bind with the calcium ion receptor on the cell membrane and can activate Wnt pathway. During skin injury, the Wnt pathway get activated, which has significant role in controlling inflammation and programmed cell death (Yu et al., 2021). As shown in the figure IV, Sr ions activate Wnt pathway through calcineurin-activated T nuclear factor signalling resulting in cell replication. The binding of strontium ions can activate the CaSR/P13K/Akt pathway leading to inhibition of GSK3, β-catenin nuclear translocation and transcription, which results in the increased cell proliferation and migration (Saidak and Marie, 2012). Some of the studies related with wound healing effects of strontium ions has been summarized in the table IV.

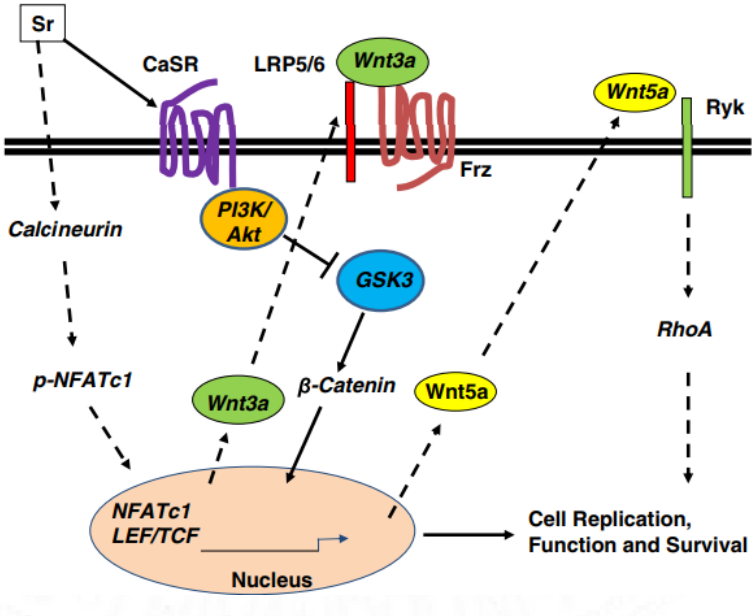

Figure IV: The interaction of strontium ions with the cell membrane, leading to the activation of Wnt pathway and CaSR/P13K/Akt pathway (Saidak and Marie, 2012).

Material composition	***In vitro/ in vivo* wound healing model**	**Effects strontium ion in wound healing**
Strontium loaded Silk fibroin/Sodium alginate (SF/SA) blend films (S. Li et al., 2017)	*In vitro* assessment of VEGF and bFGF protein levels	• Potential ability to induce angiogenesis
Strontium-contained bioactive glasses microspheres (SrBGM) (Zhao et al., 2018)	Full thickness wounds in mice	• Promote early vascularization • Induce macrophage to polarize M2 phenotype at the implantation site
Sodium alginate/ chitosan blended membrane (Li et al., 2020)	full-thickness skin defect model in rabbits	• Shows a better epithelialization • Upregulate the expression of main growth factors such as EGF, bFGF, VEGF, and TGF-β
Strontium ion cross-linked starch hydrogel (Mao et al., 2020)	Cell migration studies with fibroblasts and endothelial cells	• High potential to promote angiogenesis • Significant inhibitory effect on the growth of *S.aureus*
Sr loaded sodium alginate/polyethyleneimine hydrogels (Lu et al., 2020)	Full thickness skin defects in rat	• Adheres to the tissue • Self-healing abilities • Rapid angiogenesis of skin tissue and accelerated the repair of defects.

Table IV: Studies related to the wound healing effect of strontium ions

. These studies demonstrate that the inorganic ion incorporated wound dressings could be a cost effective therapeutic strategy for wound healing applications.

2.2.2 Hormones in wound healing

The balance between anabolic and catabolic hormones affects the overall process of wound healing. During injury, a stress response is created, which decrease normal anabolic hormone activity and increase the catabolic hormonal activity. These imbalances affect the overall protein synthesis and thus delay the healing process. So the hormonal environment is critical for wound healing, which can be beneficially modified. The exogenous delivery of anabolic hormone has been developed to improve the overall protein synthesis. The four major anabolic hormones that affect healing process includes, human growth hormone, insulin like growth factor, insulin, testosterone and estrogen. Each hormone has a specific mode of action and there is some considerable inter-relationship between them.

Human growth hormone is a potent anabolic hormone produced from pituitary gland. Growth hormone increases the cellular uptake of amino acids and thus increases protein synthesis. The skin contains HGH receptors on the surface of epidermal cells and the exogenously administered GH increases the thickness of the skin. It is used for the treatment of severe burns at the donor site with skin graft to improve the rate of re-epithelialization. The other wound healing effects of GH are; it increases wound collagen content, improve wound tensile strength and increase the local production of IGF-1 by fibroblasts. Kim et al studied the effect of topically delivered recombinant growth hormone in full thickness wound created in pig models and observed accelerated wound healing rate (Kim et al., 2009). Even then, there are reports of serious complication that exist with the use of GH therapy.

Insulin like growth factor-1 (IGF-1) is a poly peptide hormone produced by various wound cells such as fibroblasts and platelets. IGF-1 increases wound epithelialization and angiogenesis. The adenovirus mediated gene transfer of IGF -1 in diabetic impaired murine wound models enhanced wound healing and angiogenesis through VEGF dependent pathway (Balaji et al., 2014). Recently, the effect of female sex hormone estrogen on wound healing has been studied. Estrogen reduces the inflammatory response by suppressing excessive neutrophils to the wound area and reduce the expression of TNF-α from macrophages (Mukai et al., 2019). Rittie et al demonstrated the topical delivery of estradiol induced pro collagen I and III mRNA level in post-menopausal women and promote cutaneous wound healing (Rittié et al., 2008). However more clinical trials are needed to establish the wound healing effects of these hormones.

There are extensive studies and clinical trials that demonstrate the efficacy of insulin in wound healing. Insulin stimulates the growth and development of various skin cells and affects cell proliferation, migration and secretion by keratinocytes, endothelial cells and fibroblasts. Insulin shows cell protective anabolic effects and metabolic effects which make insulin an ideal therapeutic agent for wound healing. Since it is cheaper than growth factors, insulin therapy is very cost effective treatment for acute and chronic wounds. Being an FDA approved molecule, insulin is in clinical use for several decades, economically viable and available in huge volumes.. Insulin can be locally delivered as local injection, spray, creams or through dressing system. Different studies shows that topically delivered insulin accelerate healing by various

mechanisms without causing any side effects. In certain population of diabetic patients the wound closure is delayed. It is reported that the controlled delivery of insulin towards the wound site helps to accelerate the wound closure in diabetic patients. As shown in the figure V, the canonical signaling pathways such as IR/SHC/ERK and IR/IRS/PI3K/AKT pathways are activated by insulin, which enhance the cellular functions like migration, proliferation, angiogenesis, morphogenesis and cellular survival.

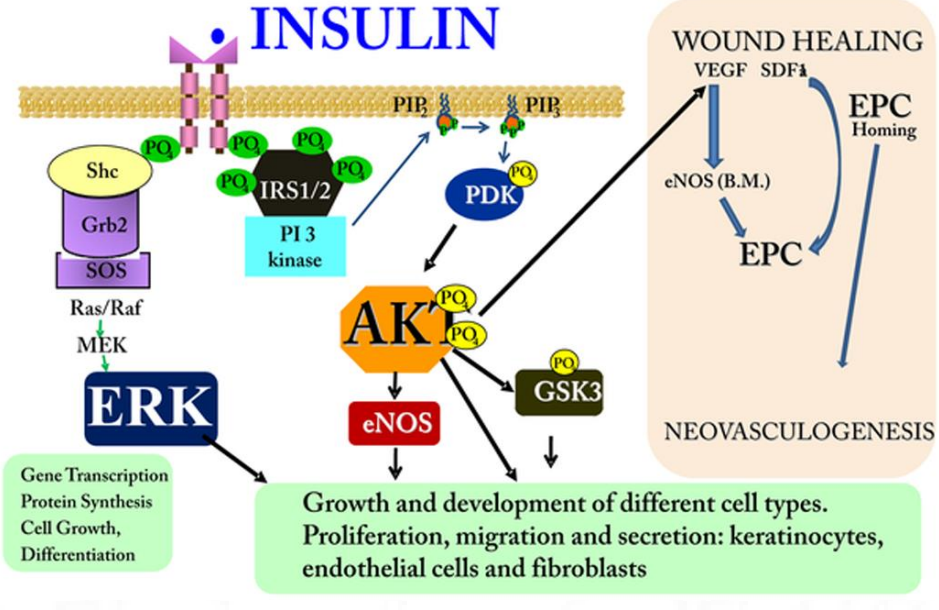

Figure V: Effect of insulin on cellular and molecular mechanisms of wound healing in diabetes (Lima et al., 2012).

The topically delivered insulin has been appreciated in the field of wound healing and further studies are needed to improve understanding of the role of insulin in various phases of healing. The studies related to the topical delivery of insulin are summarized in the table V.

Material composition	***In vitro/ in vivo* wound healing models**	**Effect of insulin in wound healing**
Insulin loaded poly(d,l-lactide-co-glycolide) microspheres (Hrynyk et al., 2010)	Scratch wound assay on keratinocytes	• Slow release of bioactive insulin upto 25 days • Increased keratinocyte migration • Increase in the expression of phospho Akt
Insulin-loaded poly(d,l-lactide-co-glycolide) (PLGA) microparticles loaded within alginate sponge dressings (Hrynyk et al., 2012)	Human keratinocyte migration assay	• Bioactive insulin released up to 10 days • Promote keratinocyte migration in vitro
Insulin-loaded nanoparticles embedded in poly(vinyl alcohol)-borate hydrogels (Abdelkader et al., 2018)	Diabetic rat models	• Sustained release of insulin • Accelerated wound closure
Silver nanoparticles (AgNPs) with insulin (Kaur et al., 2019)	Diabetic rat models with 15 mm diameter full thickness wounds	• Regulation of the balance between pro (IL-6, TNFα) and anti-inflammatory cytokines (IL-10) at the wound site to promote faster wound remodeling.
Insulin-loaded silk fibroin microparticles (Yang et al., 2020)	Full thickness wound on diabetic rat models	• Insulin promote HIF-1α target gene expression and its downstream biological effect like angiogenesis and wound extracellular matrix deposition

polycaprolactone and polyethylene oxide electron spun fibers (Walther et al., 2023)	*Ex vivo* human skin wounds	• Fibers favor surface guided cell migration • Increase in wound healing biomarkers

Table V: Studies on topical delivery of insulin for wound healing applications

The effectiveness of topical delivery of insulin is hampered by various environment factors in the wound bed and also its poor retention. So it is necessary to develop wound dressings which can deliver the molecules in a controlled manner. So this study focus on the spatio-temporal delivery of bioactive insulin loaded with advanced wound care material.

2.2.3 Anti-inflammatory drugs in wound healing

The inflammatory phase during wound healing is highly organized process and the level of inflammation can reveal the healing time and the quality of repair. But the prolonged inflammation may result in deregulated wound healing process with excessive scarring. The extended inflammatory phase in chronic wounds causes imbalanced growth factors, increased proteolytic activity, high bacterial load, increased inflammatory mediators leading to enhanced tissue destruction (Xu et al., 2021). Non-steroidal anti-inflammatory drugs (NSAIDs) are widely used in the clinics for controlling the inflammation. These drugs inhibit the enzyme cyclooxygenases 1 and 2 (COX-1 and COX-2) and exhibit anti-inflammatory, antipyretic, analgesics and thrombotic properties. Several studies reported that the use of NSAIDs have negative impact on wound healing process by decreasing keratinization, angiogenesis, granulation and epithelialization. To overcome this issue, numerous COX inhibitors

has been developed, among which the prominent COX-2 inhibitor approved by FDA is Celecoxib. A perfect balance between pro and anti-inflammatory mediators need to be maintained for proper tissue homeostasis (Krischak et al., 2007).

Statins are a class of lipid lowering medications. They lower the cholesterol level in the body by inhibiting the 3-hydroxy-3-methyl-glutaryl-coenzymeA (HMG-CoA) reductase that catalyzes the conversion of HMG-CoA to mevalonate, which is a primary rate-limiting step in cholesterol biosynthesis. Statins show various pleotropic effects and are now considered as the new therapeutic modality for different pathologic conditions (Zhang et al., 2020). Recently, the wound healing effect of statins has been identified. Statins block the synthesis of farnesyl pyrophosphate, which is one of a potent inhibitor of keratinocyte migration. Statins can also promote wound healing by acting as an anti-inflammatory agent, by inhibiting the activity of NF-κβ, which is one of an important transcription regulatory protein involved in inflammatory response (Figure VI). Statins promote the aggregation of inflammatory cells, increase the secretion of cellular factors and nitric oxide production and protect endothelial cell function (Fitzmaurice et al., 2014).

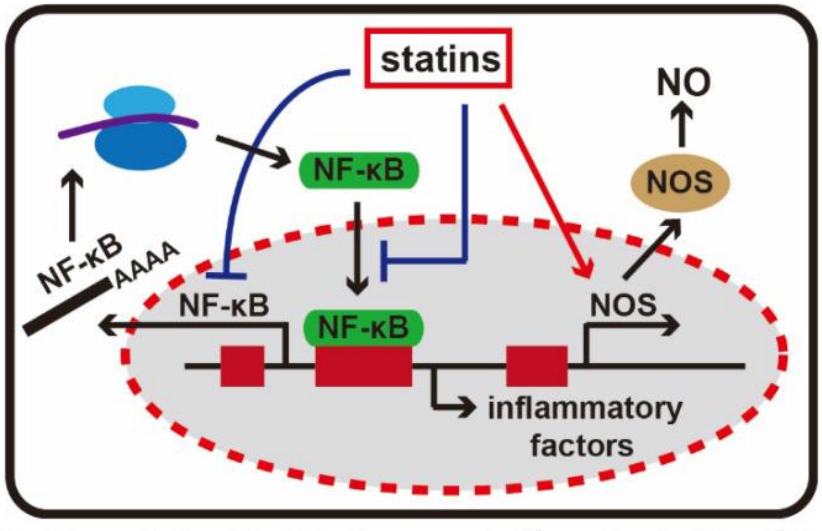

Figure VI: Molecular mechanism of anti-inflammatory action of statin drugs (Zhang et al., 2020).

Among different statins, the wound healing effect of simvastatin is extensively studied. The topical administration of simvastatin resulted in the accelerated wound recovery with significant improvement in angiogenesis and lymphangiogenesis (Asai et al., 2012). Simvastatin promote the macrophage infiltration, which increased the concentration of vascular endothelial growth factor in granulation tissue. The immunomodulatory effect of simvastatin provides anti-inflammatory activity, by lowering the expression of TNFα and IL-1β and reduce leucocyte infiltration (Buabeid et al., 2022). So the topical application of statins is a promising approach for wound care, but its formulation and application methods need to be optimized for maximizing its potential beneficial effects. Some of the studies related with the topical delivery of simvastatin is given in the table VI.

Material composition	***In vitro/ in vivo* wound healing models**	**Effect on wound healing**
Simvastatin microemulsion (Rego et al., 2007)	Full thickness excision wounds ($1cm^2$) on Wistar rat models	• Significant reduction in leucocyte infiltration • Reduce inflammatory response • Showed anti-bacterial effect
Simvastatin mixed with petroleum jelly (Asai et al., 2012)	Full thickness excision wounds (8mm) on murine models	• Increases in both angiogenesis and lymphangiogenesis • Promotes capillary morphogenesis • Antiapoptotic effect on lymphatic endothelial cells.
Simvastatin mixed with 2% carboxy methyl cellulose solution (Khoshneviszadeh et al., 2014)	1 cm^2 circular full-thickness wound on Sprague Dawley rats	• Induction of fibroblast proliferation and collagen bundle synthesis • Anti-inflammatory activity and epithelialization induction
Simvastatin-incorporated mesoporous hydroxyapatite microspheres loaded in alginate hydrogel (Yu et al., 2016)	Full-thickness skin defects measuring 18 mm in diameter in Sprague Dawley rat	• Increased angiogenesis by the up-regulation of the expression of hypoxia-inducible factor-1α (HIF-1α) and vascular endothelial growth factor (VEGF) • Accelerated re-epithelialization
Simvastatin (SIM) loaded elastic provesicular systems made by Span 80, Tween 80 and sodium cholate (Abd El-Alim et al., 2020)	Full-thickness, skin excision round wounds of 5 mm diameter on Wistar albino rats	• Significant reduction in wound size in rats, fourteen days post-wounding • Significant increase in expression of • Vascular endothelial growth factor and collagen type I compared to the free drug
Simvastatin dissolved in paraffin oil and mixed with petroleum jelly (Ramhormozi et al., 2021)	Second degree deep burn wound model in rats	• Activate Akt/mTOR signaling and improve burn wound healing • Increased expression of CD31, VEGF, and α-SMA protein

Simvastatin loaded alginate – pectin hydrogel (Rezvanian et al., 2021)	Full thickness wounds on diabetic rat model (8mm dia)	• Enhanced re-epithelialization and collagen deposition • Showed pro-angiogenic effect • Accelerated diabetic wound healing

Table VI: Studies related topical delivery of simvastatin for wound healing application

2.2.4 Enzymes incorporated wound dressings

Among the numerous proteins involved in wound healing various enzymes also have an important role to play. Different enzyme classes such as redox sensitive enzymes, proteases or enzymes with anti-microbial properties are used for wound healing applications. Singh et al loaded serratiopeptidase into poly (vinyl) alcohol-gelatin hydrogels and observed accelerated re-epithelialization in *in vivo* model. Serratiopeptidases are powerful treatment modality for the treatment of pain, inflammation and is used in wound debridement. The moist environment provided by the hydrogel promote granulation tissue formation and serratiopeptidase remove the layer of dead and necrotic tissues.(Singh and Singh, 2012). Parnell et al reported that the endopeptidase loaded glycerine contacting hydrogels are effective in the management of stage II and stage III pressure ulcers (Parnell et al., 2005). Nitric oxide releasing poly(ε-caprolactone)/chitosan wound dressing was developed by Zhou et al which accelerated the wound healing process by enhancing granulation tissue formation. Histopathological evaluation showed improved organization of regenerated tissues with enhanced collagen synthesis and pro-angiogenesis. So this could be a potential candidate for chronic ischemic wounds (Zhou et al., 2017).

The accumulation of free radicals is one of the reasons for delayed wound healing in chronic wounds. The incorporation of anti-oxidant system in wound dressing could effectively remove reactive oxygen generated at the wound bed and promote healing process. Superoxide dismutase is an antioxidant enzyme which catalyses the decomposition of superoxide radical into H_2O_2. A composite hydrogel of chitosan/heparin/poly (γ-glutamic acid) loaded, loaded with superoxide dismutase for wound healing applications (Zhang et al., 2018). The dressing proved to accelerate wound healing by promoting wound closure and collagen deposition in diabetic rat models Glucose oxidase is another endogenous oxidoreductase, which catalyzes the oxidation of glucose into gluconic acid and hydrogen peroxide. The topical delivery of glucose oxidase helps to reduce the local glucose concentration in diabetic wounds and the release of H_2O_2 promote leucocyte recruitment, release of vascular endothelial growth factor and improve blood flow towards the wound site (Shi et al., 2022). Glucose oxidase molecules are now widely used in the biomedical field and its topical delivery could be beneficial for wound management.

2.3 Biomaterial based topical delivery of biomolecules

The topical delivery of biomolecules either through direct application or by intradermal injection results in the exposure to high amount of drug in a limited period of time. This may not produce desired therapeutic effect. Hence various biomaterials are used for the protected spatio-temporal delivery of biomolecules. Biomaterials such as scaffold, hydrogel or nanoparticles exert great impact on healing rather than free molecules (Pop and Almquist, 2017). The biomaterial selected for localized delivery should be biocompatible or bioresorbable. Ideally, the biomaterials should mimic the

skin structure, so that the material itself can contribute directly towards the healing process.. The surface porosity, topography and texture of biomaterials can be easily modified for required applications. The texture provides the cues for the cellular guidance, while the porosity enables the rapid cell infiltration and matrix deposition. The molecular structure of the biomaterial should be elucidated for the controlled delivery of molecules. By analyzing the structural patterns, tunable bioactivity and degradability can be incorporated.

The topical administration of biomolecules can be achieved by two approaches. The first is to directly incorporate the molecules into the biodegradable scaffold, so that as the material degrades, molecules can be released by the controlled degradation process. The second approach is to incorporate nano or micro spheres or carriers with biomolecules. The release of molecules is possible through the controlled degradation of the carriers. The incorporation of biological cues into the scaffolds can further control the release pattern according to the wound microenvironment.

2.4. Wound healing biomaterials

Biomaterials are designed and developed as per the clinical need to meet the clinical requirements for treating a particular disease or condition. Biomaterials are developed from nontoxic, non-immunogenic materials and it requires to be haemo and biocompatible. Biomaterials come in contact with the cells/tissue and the resulting interactions are known to modulate the cell microenvironment and thereby it influences the cell phenotype and cellular responses. Wound healing biomaterials are developed to stimulate the healing process by its endogenous activity or through the

delivery of biomolecules. Hence, recently bioactive and biomimetic scaffolds are widely explored for wound healing applications. The scaffolds can be fabricated into different forms depending on the desired properties. The polymeric biomaterials serve as a barrier and also provide moist environment for the healing to proceed. Natural and synthetic polymers are used for developing wound dressings. Some of the natural polymers include chitosan, collagen, alginate, hyaluronan etc. The synthetic polymers used in the wound care market are polycaprolactone (PCL), polylactide-co-glycolide (PLGA), polyethylene glycol (PEG), polyurethane (PU), hydrocolloids etc.

2.4.1. Synthetic polymers

Wound dressing made with polyurethane found to exhibit good mechanical as well as biological properties. Polyurethane is synthesized by the condensation reaction of polyols with isocyanate to generate urethane bond. The well-ordered hard segments formed by hydrogen bonds within the polyurethane structure provide high elasticity and strength. By varying monomer ratio, desired mechanical properties can be achieved. The combination of PEG and PCL during the synthesis of polyurethane improved the biological properties of the polyurethane dressings. Currently, the major concern of the poly urethane dressing is the use of monomers from petrochemical source and the use of isocyanate shown to be carcinogenic (Morales-González et al., 2022). Poly (lactide-co-glycolide (PLGA) is another synthetic polymer used for the development of wound care material. These are biodegradable polymers, consisting of poly lactic acid and poly glycolic acid residues. (Chereddy et al., 2016). The wound healing scaffolds loaded with PLGA microspheres are promising carriers for the

sustained delivery of drug towards wound bed. Cheng et al reported the that PLGA microspheres loaded with anti-microbial peptide OP-145, showed sustained release up to 28 days and significantly reduced the biofilm formation and inflammatory response (Cheng et al., 2022).

Recently electrospun poly(ε-caprolactone) (PCL) scaffolds are gaining wide attention as matrices for skin tissue engineering and for wound healing applications. The degradation rate of PCL is slow compared to other synthetic polymers. These scaffolds encapsulate and deliver substances active in wound healing. Fahimirad et al developed electrospun poly(ε-caprolactone) (PCL)/Chitosan (CS)/curcumin (CUR) nanofiber loaded with curcumin nanoparticles and observed significant improvement in wound healing of MRSA (Methicillin-resistant *Staphylococcus aureus*) infected wounds (Fahimirad et al., 2021). Poly ethylene glycol is another important polymer for wound healing applications. It is used as a biodegradable and cytocompatible bioadhesive hydrogel for controlled delivery of therapeutics. Ouyang et al developed a MMP-sensitive PEG hydrogel modified with RGD sequence for the encapsulation of different growth factors and cells. This system showed the controlled release of biomolecules and could be used a cell transplantation vector and as a release system (Ouyang et al., 2019).

2.4.2. Natural polymers

Among different natural polymers, alginate, chitosan, collagen, hyaluronic acid and silk fibroin are extensively used in wound management due to their biocompatibility, biodegradability and structural similarity with ECM molecules.

Chitosan is one of the most promising biolpolymer that is widely investigated for wound healing applications and is obtained by the deacetylation of chitin. Due to their rigid structure and insoluble nature in water at neutral pH, the derivatives of chitosan are prepared by introducing appropriate functional groups into their structure. Chitosan and its derivatives have significant role in hemostasis, antimicrobial activity and promote neovascularization. A novel bionic hydrogel of chitosan was synthesized by Han et al, by grafting with methacrylate, N-hydroxymethyl acrylamide and dopamine. The hydrogel showed excellent hemostatic activity in mouse liver hemorrhage models (Han et al., 2020). Guo et al developed reactive oxygen species scavenging injectable quaternary ammonium chitosan (QCS)/tannic acid (TA) hydrogel for wound healing applications. This hydrogel offers a promising network as wound dressing material and promote healing in full thickness skin wound model (Guo et al., 2022).

Collagen is the key component in the ECM and plays critical role in the regulation different phases of healing. The tensile strength of the healed skin tissue is determined by the type, amount and the organization of the collagen. Collagen based matrices are mainly used for skin and soft tissue repair. Collagen based wound dressing are a combination of collagen with other natural or synthetic polymers or it can be used as amorphous gels, powder forms or as sheets. the coating of collagen on the surface of matrices help to improve moisture retention as well as promote cell adhesion (Mathew-Steiner et al., 2021). The use of chitosan- collagen hydrogel material in a randomized clinical trial for treating neuropathic diabetic foot ulcers, showed

significant reduction in healing time with lower number of dressing changes (Djavid et al., 2020).

2.5. Alginate based biomaterials for various biomedical applications

Alginate is another promising biomaterial in the wound care market. Alginate has great potential in biomedical application due to its biodegradability and biocompatibility. The abundance of GM block and their interaction in the alginate chain provide them excellent swelling characteristics. Alginate can form different cross-linked structures with metallic ions or other molecules via ionic, electrostatic and covalent linkages. It can be transformed into biofilms, hydrogels, wafers, fibers, sheets or foams to maintain moist environment (Lee and Mooney, 2012). Due to its biocompatibility with the human tissue, alginate based scaffolds are widely used in the tissue regeneration. In the food industry, alginate has wide applications such as gelling, thickening, stabilizing or emulsifying agent and also used to coat fruits and vegetables to prevent microbial invasion. About 11.9% of the advanced wound care market is occupied with alginate based wound care materials. (Mollah et al., 2021).

2.5.1. Alginate based drug delivery systems

Alginate gels are widely investigated for the release of low molecular weight drugs. Alginate based nanoporous gels of pore size ~5 nm are utilized for the continuous and instantaneous release of drugs. The partially oxidized and ionically cross-linked alginate gels could release flurbiprofen almost completey within 1.5h, indicating its potential application in oral delivery (Maiti et al., 2009). The simultaneous or sequential delivery of multiple drugs is possible through alginate gels

depending on the mode of incorporation and chemical structure of the drug. Biuhadir et al developed chemically modified alginate hydrogel using low molecular oligomers and cross-linked with spacer molecule adipic dihydrazide and loaded with different antineoplastic drugs. Methotrexate was non-intearctive with alginate and got rapidly released, while doxorubicin covalently attached with polymer backbone and released via chemical hydrolysis of the linker. Mitoxantrone was ionically cross-linked with the gel and released only after the dissociation of the gel (Bouhadir et al., 2001). Alginate is an excellent candidate for protein delivery also, since it protects the native structure of the protein from denaturation. The extended delivery of high isoelectric pH (pI) proteins such as chymotrypsin and lysozyme was observed with alginate based microspheres, which enables the site specific long-term delivery (Wells and Sheardown, 2007).

2.5.2. Alginate based tissue engineering scaffolds

The various applications of alginate gels have been exploited in the field of tissue engineering and regeneration. Alginate gels can be readily adapted for developing 2D or 3D cell culture systems for regeneration. Since alginate lacks the receptors for mammalian cells and shows minimum protein adsorption, different synthetic peptides and cellular adhesion receptors can be readily incorporated into alginate gels. The RGD (arginine-glycine-aspartate) modified alginate gels are more frequently used in cell culture studies. The presence of RGD peptides enhances the cellular adhesion and proliferation, and also control the phenotype of the growing cells (Neves et al., 2020).

Alginate hydrogels can be incorporated with other cell specific instructive cues, which enable the lineage specific commitment of entrapped stem cells. Osteoinductive peptide incorporated alginate hydrogel was developed by Maia et al for site specific delivery of mesenchymal stem cells (Maia et al., 2014). The hydrogel mechanical properties can be modulated to guide the cellular response via mechanotransduction. The incorporation of photosensitive groups allows the in situ cross-linking under light exposure in the presence of photoinitiator (Chou and Nicoll, 2009). The cross-linking of alginate hydrogels can also be driven by temperature sensitive approach. Wang et al developed glycidyl methacrylate groups incorporated alginate macromonomers, which forms an in situ hydrogel at 37°C in the presence of a thermal initiator (Wang et al., 2015). Nowadays, the alginate hydrogels has been explored to create the 4D culture systems, which enables the cells to respond to an applied stimulus for a long time in a predictable manner.

2.5.3. Alginate as wound healing biomaterials

Alginate based wound care materials play very significant role in the management of both acute and chronic wounds. Alginate wound care materials are typically produced as the calcium cross-linked gel, followed freeze drying to produce porous sheet in the form of fibrous non-woven dressings. The dressings absorb wound fluid and re-gel to create moist environment to promote granulation tissue formation and rapid epithelialization. Commercially alginate is available in varying compositions in terms of molecular weight and viscosity, due to the variation in the distribution pattern of M-block and G-block. It is necessary to ensure that alginate should be

properly purified and free of impurities, because the presence of impurities can stimulate the immunogenic response (Aderibigbe and Buyana, 2018).

The excellent biocompatibility, high water content, permeability to water makes the alginate an ideal candidate for developing wound care material. Due to the highly porous structure and ability to deliver biomolecules towards wound microenvironment, alginate based hydrogels are more suitable for chronic wound management. In spite of these advantages, alginate wound dressing suffer from a few limitations such as poor mechanical strength and easily dissolution. Many approaches have been taken to improve the mechanical strength of alginate based hydrogels. The combination of alginate with other natural polymers or synthetic polymers could improve its mechanical strength. The different approaches selected for the synthesis of alginate hydrogels include ionic cross-linking, covalent cross-linking, thermal gelation, and free radical polymerization (Lee and Mooney, 2012). Ionically cross-linked alginate hydrogels are not stable under the physiological pH due to the exchange of divalent ions. Chemical modification of alginate by conjugation and covalent cross-linkng will improve its structural stability as well as mechanical properties. However the swelling property is significantly controlled by the nature of the cross-linking molecule used. So the use of hydrophilic cross-linking molecules such as PEG compensates for the reduction of the hydrophilic nature. In alginate covalent hydrogels, there is possibility of non-covalent crosslinking, such dual crosslinking approaches can further enhance the mechanical stability (Mollah et al., 2021).

The free radical polymerization enables the transformation of the linear polymer chains into 3D networks that could be achieved at the temperature and physiological pH in the presence of some initiators and catalysts. The mechanical properties of alginate can be further improved by grafting of different monomers to alginate backbone. Alginate grafted methacrylate monomers shows good mechanical stability than ionically cross-linked hydrogels. Shah et al developed chondroitin sulphate grafted alginate based thermoreversible hydrogel showed improvement in mechanical properties and could be used as a suitable candidate for encapsulation of cells for promoting wound healing phases (Shah et al., 2021). So the strategies to promote the mechanical strength of alginate gel could be beneficial for managing highly exudating wounds and also the spatiotemporal delivery of biomolecule.

2.4 Alginate based advanced wound care materials

The research on alginate dressing for chronic wound management has increased in recent years. Due to its hydrophilic nature, biocompatibility and versatility, alginate is widely used in the wound care market. An increased rate of progress is being made in the development of alginate-based biomaterials for wound healing due to its biocompatibility and promising results from both *in vivo* and *in vitro* trials. Since the chronic wound bed is highly unstable for the spatiotemporal delivery of biomolecules, there is a need of effective biomaterial, which is able to alter the adverse condition and make it favorable for the biomolecule to act. Some of the approaches using alginate based wound care materials for diabetic wound management are given in the table.

Material composition	Biomolecule delivered	Main results
Alginate – heparin hydrogel (Tanihara et al., 2001)	Basic fibroblast growth factor (bFGF)	• Sustained release of bFGF over one month resulted in increased cellular infiltration and angiogenesis.
Alginate hydrogel/ composite bandage (Mohandas et al., 2015)	zinc oxide nanoparticles (nZnO)	• Excellent anti-bacterial activity • Increased keratinocyte infiltration towards wound area
Calcium alginate hydrogel (Catanzano et al., 2015)	Tea tree micro oil emulsion	• Antibacterial activity
calcium alginate hydrogel (He et al., 2019)	Rubidium ions	• Anti – inflammatory effect • Enhancement in angiogenesis and re-epithelialization
Calcium alginate-hyaluronan hydrogel (Wang et al., 2019)	Protamine nanoparticles	• pH responsive release • increased expression of VEGF • anti-bacterial activity
Alginate hydrogel (Ilmi et al., 2020)	Extract from Okra fruit	• Anti-oxidant activity • Reduce local glucose level • Accelerated wound healing
Quaternized chitosan/Mg/alginate dressing (Wang et al., 2021)	Magnesium ions	• Promote angiogenesis • Anti-bacterial effect
Calcium alginate films (Ahmed et al., 2021)	Ciprofloxacin and fluconazole	• Effective in the treatment of infection associated with DFU

Table VII: Alginate based bioactive dressing for wound healing application

The topical delivery enables the convenient self-administration for patients and also avoids the issues of gastrointestinal tract absorption and first pass metabolism in liver during oral administration, thus improve the bioavailability. For successful

topical delivery of biomolecules, different challenges associated with the wounds need to be addressed. It is necessary to have better understanding of the detailed mechanisms and regulatory network of the skin development and its spatial and temporal changes. This helps in developing combinations of proregenerative bioactive molecules for promoting wound healing. Another challenge is the development of safe and effective delivery system for bio active molecules towards the targeted site. Scaffolds, hydrogels or other forms of biomaterials can be used as delivery vehicle for controlled release. This helps to reduce the off targeted effects and tumerogenic effects during clinical application. Alginate based topical delivery could be a promising therapeutic approach for diabetic wound management. As of now no alginate based products are available which is meant for topical delivery of therapeutic molecules, as per need, to the wound site. Hence more research is needed for the development of mechanically stable alginate material which can be used for managing chronic wounds and also can deliver biomolecule to the wound site.

CHAPTER 3

MATERIALS AND METHODS

This chapter describes the various synthesis and characterization methods adopted for achieving the objectives of the work. The first section describes the methods for modification of alginate with different monomer units and the corresponding xerogel synthesis. By using various physico-chemical characterization techniques, three xerogels were optimized and compared with commercial alginate based products. The second section describes the methodologies used for the efficacy evaluation of the xerogels for biomolecule delivery. The methodology for evaluating the *in vitro* wound healing effects of the selected xerogels and the biomolecule loaded xerogels are discussed in the third section. The last section deals with the *in vivo* efficacy evaluation of the optimized xerogel loaded with selected biomolecule in the diabetic rat model.

3.1 Synthesis and characterization of alginate-based xerogels

Alginate was modified by grafting with different monomers methacrylic acid and PEGMA. In another modification, prior to grafting, conjugation with diamine PEG was performed. The grafted co-polymers of alginate were coded as alginate-g-poly (methacrylic acid), alginate-g-poly (PEGMA) and alginate diamine PEG-g-poly (PEGMA). The optimized formulation was identified for xerogel synthesis and different xerogels were synthesized by varying the concentration of strontium ion cross-linking. Based on the percentage of swelling, dissolution, porosity and water vapor transmission rate, an appropriate cross-linking concentration for each batch was

selected. Finally three xerogels were selected namely, AGM2S3, AGPM2S2 and ADPM2S2 and further characterized by various physico-chemical techniques. To evaluate the physical properties of the xerogels as an advanced wound care material, a comparison with commercial alginate based wound care materials were also performed.

3.1.1 Materials

Sodium alginate, methacrylic acid (99% MW: 86.09 Da) and Poly (ethylene glycol) methacrylate (Mn 360Da), Diamine poly ethylene glycol (O,O′-Bis(2-aminopropyl) polypropylene glycol-block-polyethylene glycol-block-polypropylene glycol/Jeffamine, MW 600Da),-Ethyl-3-[3-dimethyl aminopropyl carbodiimide hydrochloride (EDC), Minimum essential medium (MEM), 0.25% Trypsin –EDTA and 3-(4, 5-dimethylthiazol-2-yl)-2, 5-diphenyl tetrazolium bromide (MTT), Collagen from bovine achilles tendon and collagenase from *Clostridium histolyticum* (824 units/mg collagen) were purchased from Sigma Aldrich, US. N, N - Methylene Bisacrylamide, Ammonium persulphate (APS), N, N, N', N' – Tetramethyl ethylene diamine (TEMED) and Strontium chloride hexahydrate ($SrCl_2.6H_2O$) from SRL, India. Foetal bovine serum (FBS) from GIBCO (US). LIVE/DEAD™ Viability/Cytotoxicity Kit, for mammalian cells, was purchased from Invitrogen, Thermo Scientific, US. All other reagents were of analytical grade and were purchased from SRL, Merck India and SD Fine Ltd., India.

3.1.2 Characterization of alginate

3.1.2.1 Alginate molecular weight determination

a) Gel permeation chromatography

The chromatographic column was filled with Sephadex G-200 (pore size 50µm) with phosphate buffer (pH 7.4) as the mobile phase. The column was calibrated using potassium dichromate and blue dextran, and Kav (distribution coefficient) was calculated from the obtained total volume and void volume. A calibration curve was plotted with Kav against log (M.W.) using dextran standards. The eluted fractions of the sample loaded were collected and the presence of alginate was analyzed by the phenol sulphuric acid method. The molecular weight was determined from the calibration curve.

b) Ubbelohde viscometer

The molecular weight of the sodium alginate was further confirmed with an Ubbelohde viscometer. The flow time of different concentrations of alginate solution through the viscometer was measured and relative, specific, reduced and intrinsic viscosity was calculated and graphs were plotted with the concentration of solution against reduced viscosity and intrinsic viscosity. The molecular weight was calculated using the Mark Houwink equation,

$$\eta_{inh} = K\, m^{a}$$

Where η_{inh} is inherent viscosity, m is the molecular weight and K and a are the constants. The values of K and a selected for the calculation were 0.0123 and 0.960 respectively (Mouseli et al, 2014).

3.1.2.2 Mannuronic acid/Guluronic acid ratio (M/G ratio)

The M/G ratio of alginate was assessed via partial hydrolysis, as previously described (Haug et al., 1974). Alginate (100mg) was dissolved in 10ml of 0.3M HCl and partially hydrolyzed at 100°C. After cooling and centrifuging the solution, the quantity of the soluble component was calculated using the phenol-sulfuric acid technique. This is equivalent to the alginate MG block. The residue was carefully neutralised with 0.2M NaOH while suspended in 0.1M NaCl. Using 0.1 M HCl, the pH was brought down to 2.8 - 3.0. After centrifugation, the precipitate was recovered, suspended in water, and neutralised to make it soluble. The phenol-sulphuric acid technique was then used to calculate the quantity of carbohydrates. The quantity of residue that dissolves at pH 2.85 corresponds to the MM block of the alginate chain, whereas the amount that precipitates at pH 2.85 corresponds to the GG block. The following equation was used to compute the M/G ratio:

$$\mathrm{M/G\ ratio} = \frac{\mathrm{MM\ x\ 2\ + MG}}{\mathrm{GG\ x\ 2 + MG}}$$

Where MM, MG and GG are the percentages of MM, MG and GG blocks respectively. FTIR analysis of polyguluronic acid and polymannuronic acid were also done (Bruker Alpha Opus, UK).

3.1.3 Synthesis of alginate-based xerogels

3.1.3.1 Synthesis of alginate-g-poly (methacrylic acid)

Different formulations of alginate-g-poly (methacrylic acid) were synthesized by free radical polymerization initiated by ammonium persulphate and catalysed by

tetramethyl ethylene diamine. A 0.6% alginate solution was mixed with increasing concentrations of methacrylic acid and different grafts were produced (AGM1, AGM2, AGM3 and AGM4) as given in table 1. After 3 hours of polymerization reaction at 60°C, the graft copolymer was precipitated with acetone, weighed and then extracted with methanol for 24h to remove the homopolymer of poly (methacrylic acid). The pure graft copolymer was then dried at 60°C to a constant weight.

Formulations	SA (%)	MAA (M)	APS (mM)	TEMED (mM)
AGM1	0.6	1.2		
AGM2	0.6	1.3	8.7	11.5
AGM3	0.6	1.4		
AGM3	0.6	1.5		

Table 1: Formulations of alginate-g-poly (methacrylic acid) by varying monomer concentration.

3.1.3.2 Synthesis of alginate-g-poly (PEGMA)

A 0.6 % solution of sodium alginate was prepared and mixed with the required amount of PEGMA. Different formulations (AGPM1, AGPM2, AGPM3 and AGPM4) were prepared by free radical polymerization initiated by ammonium persulphate and catalysed by TEMED (table 2). After 3h of polymerization reaction at 60°C, the graft copolymer was precipitated with methanol, weighed and then extracted with acetone for 24h to remove the homopolymer of poly (PEGMA). After the complete removal of the homopolymer, the pure graft copolymer was dried at 60°C to a constant weight.

Formulations	SA (%)	PEGMA (M)	APS (mM)	TEMED (mM)
AGPM1	0.6	1.2	8.7	11.5
AGPM2	0.6	1.3		
AGPM3	0.6	1.4		
AGPM4	0.6	1.5		

Table 2: Formulations of alginate-g-poly (PEGMA) by varying monomer concentration.

3.1.3.3 Synthesis of Alginate Diamine PEG-g-poly (PEGMA)

Another approach for the synthesis of the alginate graft copolymer was using diamine PEG molecule. Alginate was conjugated with diamine PEG molecule before grafting with poly (PEGMA). Alginate solution (1.7%) was treated with EDC (56mM, H_2O) for 30 minutes to activate the carboxyl groups of alginate, followed by the addition of diamine PEG (100mM) drop by drop and stirred for 16 hours (Scheme 1). The reaction was maintained at a pH of 4.5. The purification of the reaction mixture was carried out by dialysis against distilled water using a cellulose ester membrane (MWCO: 14000 Da) for 2 days to remove any unreacted molecules. After confirmation of conjugation by FTIR and NMR analysis, alginate-diamine PEG conjugate (ADPEG) was grafted with poly (PEGMA) chains by free radical polymerization initiated by APS and catalysed by TEMED. By varying monomer concentrations, different formulations were prepared (ADPM1, ADPM2, ADPM3, and ADPM4) as shown in table 3. After 3h of polymerization reaction at 60°C, the graft copolymer was precipitated with methanol, weighed and then extracted with acetone for 24h to remove the homopolymer of poly (PEGMA). After the complete

removal of the homopolymer, the pure graft copolymer was dried at 60°C to a constant weight.

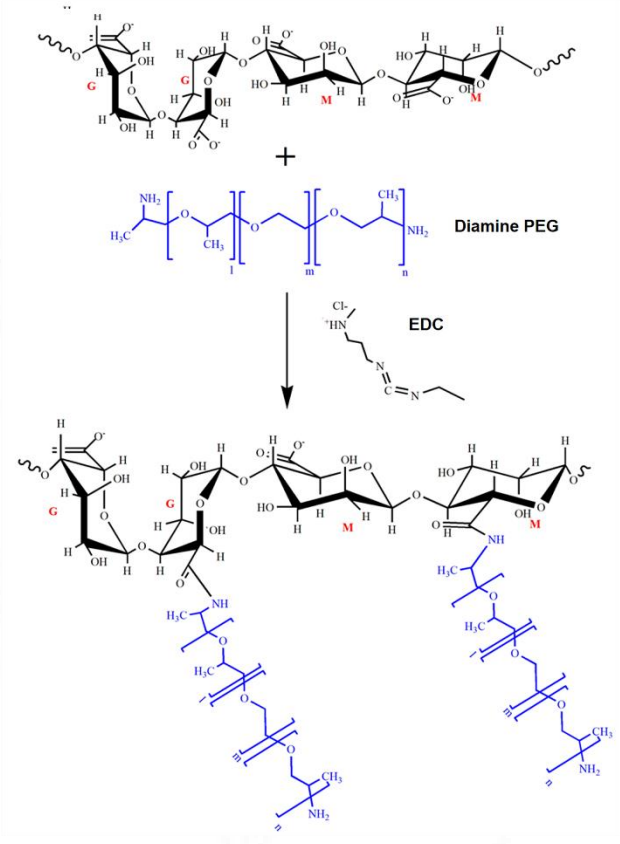

Scheme 1: Synthesis of alginate diamine PEG conjugate by EDC coupled reaction

Formulations	SA (%)	PEGMA (M)	APS (mM)	TEMED (mM)
ADPM1	0.6	1.10	8.7	11.5
ADPM2	0.6	1.15		
ADPM3	0.6	1.20		
ADPM4	0.6	1.25		

Table 3: Formulations of alginate diamine-g-poly (PEGMA) by varying monomer concentration.

3.1.3.4 Characterisation of alginate graft copolymers

3.1.3.4.1 Analysis of grafting efficiency

The grafting yield and grafting efficiency of different formulations were calculated by the following equations;

$$\text{GY } \% = \left[\frac{\text{Wg} - \text{Wo}}{\text{Wo}}\right] \text{x } 100$$

$$\text{TC } \% = \left[\frac{\text{Wh}}{\text{Wm}}\right] \text{x } 100$$

$$\text{GE } \% = \frac{(\text{Wg} - \text{Wo})}{(\text{Wg} - \text{Wo}) + \text{Wh}} \text{ x } 100$$

Where GY %, GE % and TC % are the percentages of grafting yield, grafting efficiency and total conversion to homopolymer respectively and also W_o, W_g, W_h and W_m denote the weight of the original (ungrafted) NaAlg, grafted NaAlg, homopolymer and monomer respectively.

3.1.3.4.2 Spectroscopic analysis

FTIR studies of sodium alginate, grafted polymers such as alginate-g-poly(methacrylic acid) (AGM2), alginate-g-poly(PEGMA) (AGPM2), alginate diamine conjugate (ADPEG) and alginate diamine PEG-g-poly(PEGMA) (ADPM2) were carried out using Thermo Nicolet 5700 spectrophotometer. The samples were analysed by ATR method (Attenuated Total Reflection) over the scan range 500 – 4000 cm^{-1} (Thermo Nicolet 5700 spectrophotometer, Australia). The proton NMR (^1H NMR) analysis of sodium alginate and its grafted polymers such as AGM2, AGPM2 and ADPM2 as well as ADPEG were carried out by dissolving them in deuterium

oxide and recorded using 500MHz spectrometer (BrukerAvance300 NMR Spectrometer, UK).

3.1.3.4.3 Zeta potential analysis

The zeta potential of the native alginate and the graft co-polymers were analysed using Zetasizer Nano ZS (Malvern Instruments Ltd., UK) at 25°C.

3.1.3.4.4 Quantification of carboxyl groups

The grafting of monomer chains of poly (methacrylic acid) to the alginate chains was confirmed by the quantification of free carboxyl groups using the toluidine blue assay. The dye binds with the anionic sites to form a dye-polymer complex, which results in the colour change from blue to red-violet (MacIntosh, 1941). The final coloured complex was extracted into the hexane layer and the reduction in the blue colour was measured at 630nm.

3.1.3.4.5 Quantification of amino groups

The amino groups introduced after conjugation of alginate with diamine PEG molecule (ADPEG) were quantified by TNBS (trinitro benzene sulphonic acid) assay. 2, 4, 6-trinitro benzene sulphonic acid reacts with free amino groups containing compounds to produce orange coloured derivative and its absorbance was measured at 410nm. The change in the percentage of amino groups after grafting of ADPEG with poly (PEGMA) was also quantified.

3.1.3.4.6 Gel permeation chromatography

The molecular weight of the selected formulations after grafting was analysed by GPC (G 200 Sephadex column, pore size 40-120 μm) using dextran standard and 0.1M phosphate buffer (pH 7.2) as the mobile phase.

Based on the results obtained by these characterisations optimum formulations were identified. The optimised formulations are AGM2, AGPM2 and ADPM2.

3.1.3.5 Synthesis of xerogels using optimized formulations

Different xerogels of each optimized formulation were synthesized by free radical polymerization reaction as a single-step reaction. For the synthesis of xerogels, methylene bisacrylamide (13mM) was added as the chemical cross-linker to the optimized formulation. The solution was kept at 60°C for hydrogel formation. The gel was then subjected to washing and followed by ionic cross-linking with strontium ions with varying concentrations such as 50mM, 100 mM, 150 mM and 200 mM. The unreacted monomers were removed by washing them in distilled water for 24h. After freezing, the gel was subjected to lyophilisation to obtain the xerogel and kept in a desiccator for 24h and then stored at room temperature. The xerogels were coded as given in table 4. The scheme of synthesis of the xerogels alginate-g-poly(methacrylic acid), alginate-g-poly(PEGMA) and alginate diamine PEG-g-poly(PEGMA) are depicted in scheme 2, scheme 3 and scheme 4 respectively.

Conc. of Strontium ions (mM)	Alginate-g-poly(methacrylic acid) xerogels	Alginate-g-poly(PEGMA) xerogels	Alginate diamine PEG-g-poly(PEGMA) xerogels
50 mM	AGM2S1	AGPM2S1	ADPM2S1
100 mM	AGM2S2	AGPM2S2	ADPM2S2
150 mM	AGM2S3	AGPM2S3	ADPM2S3
200 mM	AGM2S4	AGPM2S4	ADPM2S4

Table 4: Different xerogels prepared by varying cross-linking concentrations of strontium ions

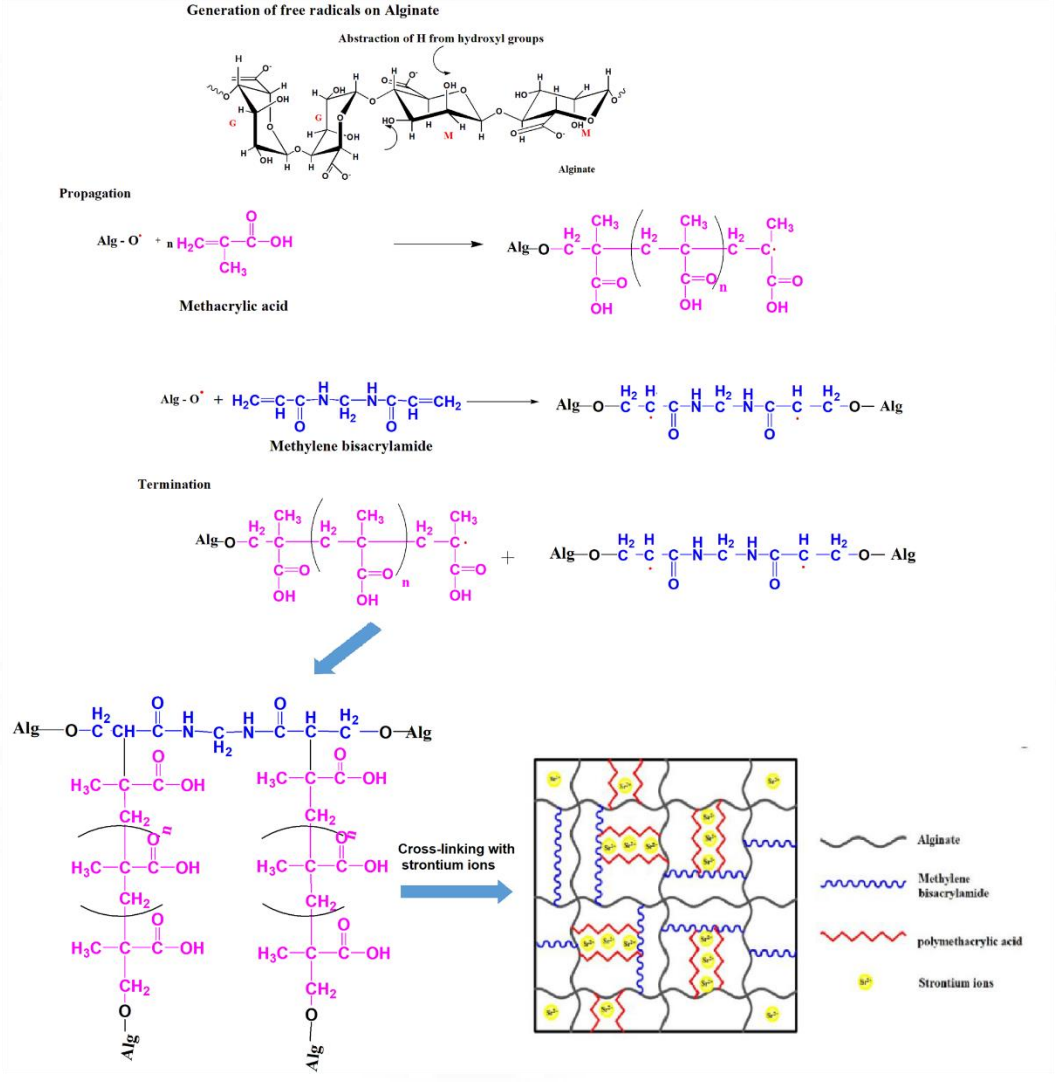

Scheme 2: Schematic representation of the synthesis of alginate-g-poly (methacrylic acid) xerogel

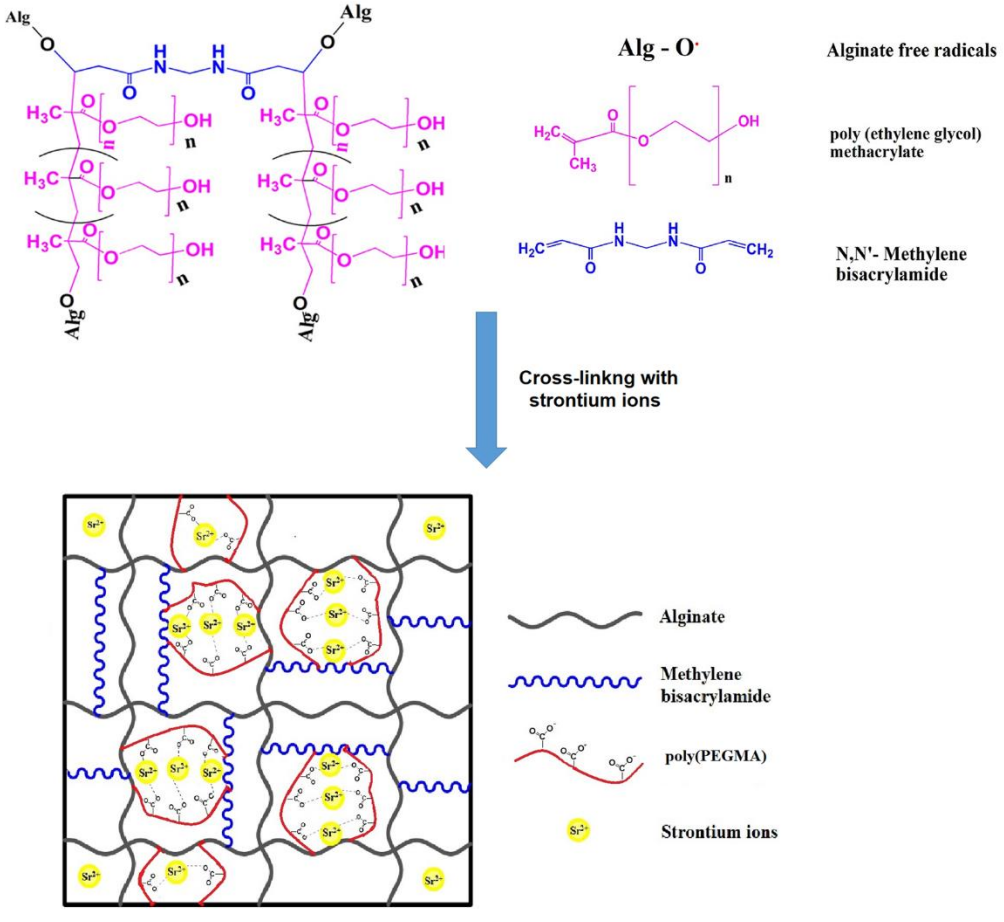

Scheme 3: Schematic representation of the synthesis of alginate-g-poly (PEGMA) xerogels

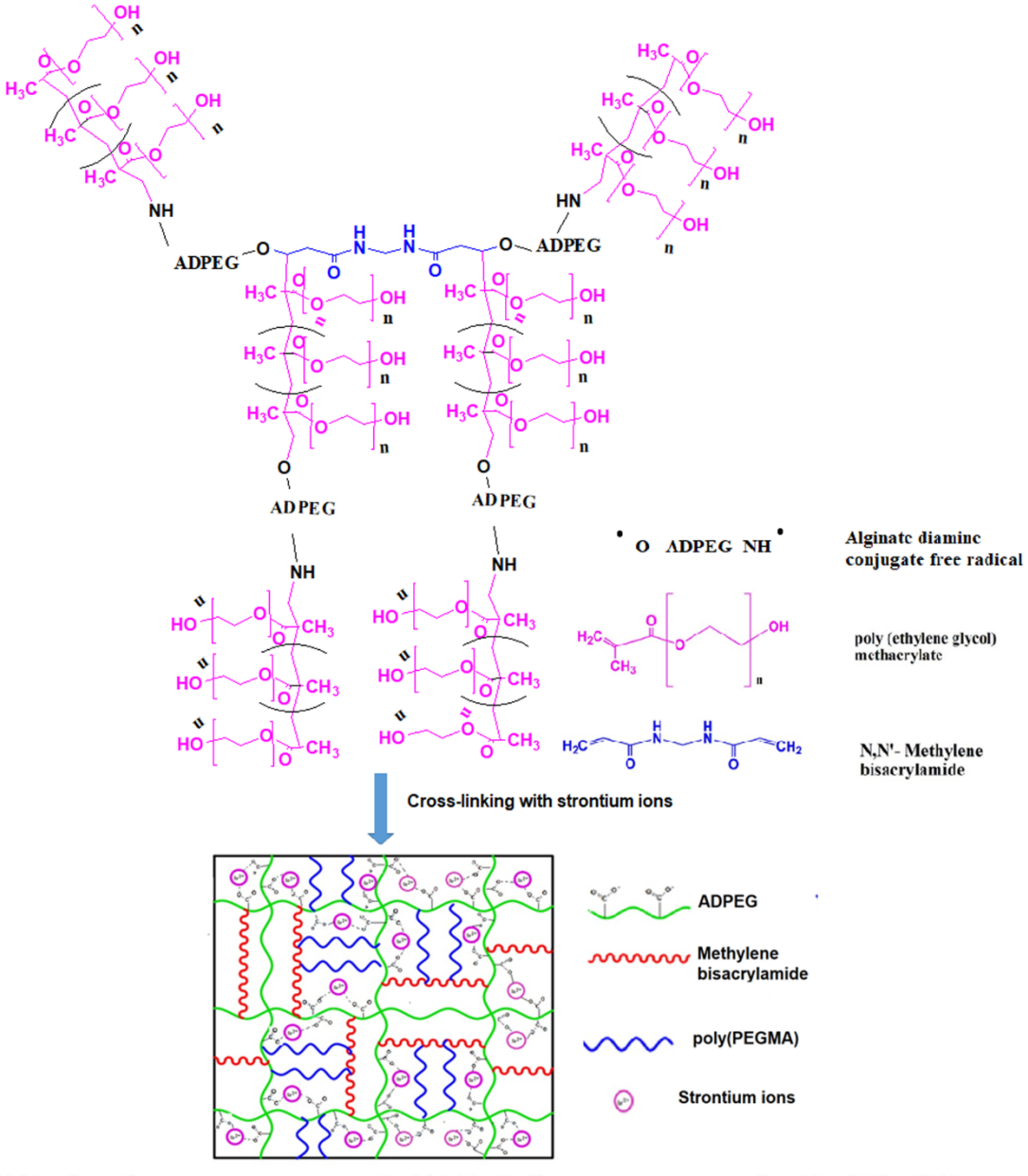

Scheme 4: Schematic representation of synthesis of alginate diamine PEG-g-poly (PEGMA) xerogels

3.1.4 Selection of xerogels based on varying cross-linking density

Physico-chemical characterization of xerogels was performed to evaluate the xerogels for further analysis as wound healing material.

3.1.4.1 Swelling studies

The percentage swelling of the xerogels was analysed in phosphate buffer at different pH. A preweighed amount of the xerogel was kept in 10ml phosphate buffered solution of different pH 5.8, 6.8, 7.4 and 8 in triplicate. The swollen gel was removed at specific time intervals and the surface of the gel was wiped out to remove excess water. The hydrogel was weighed and returned to the same medium until a constant weight was obtained.

The percentage swelling was calculated by the following equation.

$$\% \text{ of swelling at time t} = \frac{(Wt - Wo)}{Wo} \times 100$$

Where W_o is the initial weight of the xerogel and W_t denotes the weight of the xerogel after time t.

3.1.4.2 Water Vapour Transmission rate

The water vapour transmission rate of materials was analysed by ASTM standards E96/E96M-16. Test vials were filled with an equal volume of distilled water to a level 3⁄4 inch from the specimen. The xerogels were attached to the mouth of the vial using Teflon tape and the vials were kept at 37℃. Analysis was carried out with 6 replicas for each xerogel. The vials were weighed from day 0 to day 5 and a graph was plotted with the change in weight against time. Water vapour transmission was calculated using the given equation and it is expressed as $g/m^2/day$.

$$WVTR = (G/t)/A$$

Where, G is the change in weight of the dish after time t and A is the surface area of the mouth of the test dish.

3.1.4.3 Percentage porosity

Using the ethanol displacement technique, the % porosity of the xerogels was determined. A preweighed sample of the xerogel was submerged in a graduated cylinder holding a known volume of ethanol (90%). A series of short depressurizations and pressurizations were used to drive ethanol into the pores of the xerogel until no air bubbles were visible coming from the material. The volume of ethanol with and without the ethanol-impregnated sample was noted. The % porosity and the density of the material are calculated as given below;

$$\% \text{ porosity } = \frac{V1 - V3}{V2 - V3} \text{ x } 100$$

$$\text{Density (g/cm}^3\text{)} = \frac{W}{V2 - V3}$$

Where, V_1, V_2 and V_3 are the volume of initial ethanol taken in the cylinder, total ethanol with ethanol-impregnated sample and the residual ethanol after removal of the sample respectively.

3.1.4.4 Dissolution studies

The weight loss of the xerogel by dissolution was determined by immersing it in pseudo extracellular fluid at pH 7.4 for 72h. Pseudo extracellular fluid was prepared by dissolving 0.68g of sodium chloride, 0.22 g of potassium chloride, 2.5g of sodium bicarbonate, and 0.35g of sodium dihydrogen phosphate in 100ml distilled water (El-Wakil et al., 2019). At predetermined time intervals, samples were taken out and

washed to remove salt adsorbed on the surface. Then the samples were dried by lyophilisation and weighed to determine the weight loss using the equation,

$$\text{weight loss } \% = \left(\frac{\text{Wt} - \text{Wo}}{\text{Wo}}\right) \text{X } 100$$

Where W_t is the weight of the xerogel at time t and W_o is the initial weight of the xerogel.

Based on the above mentioned characterisation studies the following xerogels were identified for further studies. The optimized xerogels are AGM2S3, AGPM2S2 and ADPM2S2.

3.1.5 Characterization of the optimized xerogels

The optimized xerogels from each batch were further characterized by various techniques. The wound healing effects of the xerogels were also analysed by *in vitro* studies.

3.1.5.1 Fourier Transform Infrared Spectroscopy

FTIR studies of the xerogels AGM2S3, AGPM2S2 and ADPM2S2 were carried out using Thermo Nicolet 5700 spectrophotometer. The samples were analysed by ATR method (Attenuated Total Reflection) over the scan range 500 – 4000 cm^{-1} (Thermo Nicolet 5700 spectrophotometer, Australia).

3.1.5.2 Thermogravimetry

The thermal stability of ungrafted alginate and the optimized xerogels were analysed using thermogravimetry SDT-Q600 Simultaneous DTA-TGA, TA Instruments Inc, USA). The samples were heated from room temperature to 1000 °C, at a heating rate of 10 °C/min under inert conditions.

3.1.5.3 Contact angle measurement

The water contact angle approach was used to assess the hydrophobicity and hydrophilicity of these xerogels. Water in air contact angle of the xerogels was measured by the sessile drop method by employing a video-based contact angle measurement equipment (DataPhysics OCA15 plus, Germany) and image software (SCA20 software, Germany). Within 5 seconds after the introduction of a water droplet, the contact angle of the xerogels was determined at 23°C. The average was calculated using values from four separate measurements made at different locations.

3.1.5.4 Scanning electron microscopy (SEM)

The microstructure of the surface of the xerogels was characterized by scanning electron microscopy. The surface of the xerogels was analysed and compared with strontium cross-linked alginate xerogels (ALGS) as the control. The dried samples were sputter coated with gold (Hitachi E1010, Japan) and analysed with SEM (Hitachi S2400, Japan).

3.1.5.5 Micro Computed Tomography

The three-dimensional pore size distribution of the xerogels was analysed using micro-computed tomography (Scanco Medical, Switzerland) and compared with alginate control.

3.1.5.6 Tensile strength

The xerogels were subjected to mechanical testing and compared with strontium cross-linked alginate controls. The tensile properties were analysed using the Universal Testing Machine (Instron, USA) using a 100 N load cell and cross-head

speed of 5 mm/min. The testing was performed at 24℃ and 50% humid conditions. The tensile strength was analysed in both dry and wet states and compared with strontium cross-linked alginate controls.

3.1.5.7 Bioadhesiveness

The bioadhesive properties were evaluated using a TA.HD plus Texture Analyzer (Stable Micro Systems, Surrey, UK). Double-sided adhesive tape was used to secure the sample disc (10 mm in diameter) to the circular probe (10 mm), which was subsequently lowered onto the rat skin surface (mounted to a mucus rig) while exerting a downward force of 100 g for a predetermined period. The probe was removed at a set speed of 5 mm/s after 2sec contact duration. The amount of force needed to separate the sample disc from the tissue's surface was calculated. The region under the peak is the work of adhesion, and the mean maximum force is the force of detachment or bioadhesive force. Subsequently, the experiment was further performed on the wounded skin surface to analyse the adhesiveness.

3.1.5.8 Strontium ion loading and release

The amount of strontium ions involved in crosslinking during xerogel synthesis was determined by quantifying the strontium ions remaining in the solution after cross-linking. The following equation was used for calculation.

$$\begin{aligned}&\text{Amount of strontium ions involved in crosslinking}\\&= \text{concentration of strontium ions in solution before crosslinking}\\&- (\text{the concentration of strontium ions in solution after crosslinking}\\&+ \text{concentration of strontium ions in 24h wash solution})\end{aligned}$$

The amount of Sr^{2+} engaged in cross-linking was quantified by the O-cresolphthalein complexone (OCPC) method (Pollard and Martin, 1956). Strontium reacts with O-cresolphthalein complexone in an alkaline solution to produce a violet-coloured complex, and the complex gives an absorbance at 577nm. The preweighed samples of all batches were immersed in 5ml phosphate buffer (pH 7.4) to assess the release of strontium from the xerogels. At intervals of 0, 8, 24, 48, and 72 h, 100µl samples were taken, and the released strontium ions were measured using the O-cresolphthalein technique.

3.1.5.9 X-ray Photoelectron spectroscopy (XPS)

Using X-ray photoelectron spectroscopy (XPS) instrument PHI 5000 Versa Probe II (ULVAC-PHI Inc., USA) equipped with micro-focused (200µm, 15KV) monochromatic Al-Kα X-Ray source (hν =1486.6eV), the chemical states of strontium ions were investigated. Using the survey scan of the xerogel, elemental composition and binding energy were calculated.

3.1.5.10 Optical Emission Spectroscopy with inductively coupled plasma (ICP-OES)

The elemental composition of strontium and sodium ions was identified by ICP-OES analysis. The xerogels of known quantity were digested in an acid mixture, then diluted to the required volume and analysed as per the ICP-OES protocol (Perkin Elmer, model: 5300DV, USA).

3.1.5.11 Hemostatic activity

To assess the hemostatic activity, the xerogels were cut into equal pieces (dimension 10x10x2mm) and soaked in 100µl of citrated rabbit whole blood

containing 3.8% (w/v) sodium citrate at a ratio of 9:1 and kept for 5 min. To begin the coagulation process, a 10µl of 0.2M $CaCl_2$ was added slowly and incubated at 37°C. The samples were taken out at specific time points, such as 2, 5, 8 and 10 min and added 3ml deionized water. The red blood cells outside the clot get lysed by the addition of water. The absorbance of the released haemoglobin solution was measured at 540nm. The absorbance of haemoglobin from 100µl citrated whole blood lysed with 3ml distilled water was used as the reference. The blood clotting index (BCI) was calculated as follows;

$$BCI = \left(1 - \frac{As}{Aw}\right) X\ 100\ \%$$

Where Aw is the absorbance of whole blood treated with deionized water and As is the absorbance of the sample. The BCI values were plotted against the corresponding time points.

3.1.5.12 Collagenase inhibitory activity

The role of strontium ions in preventing the degradation of collagen by inhibiting the activity of the collagenase enzyme was analysed by the Sirius red assay. By the inhibition of collagenase activity, the undegraded collagen substrate gives a coloured product with Sirius red. A known weight of the xerogel was mixed with equal volumes of collagen substrate (1mg/ml) and collagenase (50IU) and then incubated at 37°C for 30 minutes. A 100µl of the reaction mixture was then treated with Sirius red reagent and incubated for 1h under mild shaking. After washing in 5% acetic acid several times until the yellow colour was removed, the precipitate dissolved in 0.1N

NaOH and absorbance was measured at 550nm. Strontium ion (3mM) was used as the positive control and the reaction without any inhibitor was treated as negative control.

3.1.6. Cell culture studies

3.1.6.1. Cytocompatibility studies – test on extract

Cytocompatibility of the xerogels was analysed by test on extract studies on L929 fibroblast cells and HaCaT keratinocytes. The cells were trypsinized using 0.25% trypsin-EDTA and seeded at a density of 1x 10^4 cells/well in 96 well plate and incubated for 24h in an incubator at 37°C under a 5% CO_2 atmosphere. For the test on extract studies, the samples were placed in a phosphate buffer with pH 7.4 for 24, 48 and 72h at 37°C. The cells were exposed to the extract and incubated for 24h at 37°C in a 5% CO_2 atmosphere. Positive (0.1% Triton X100) and negative controls (growth medium) were maintained under same conditions. After incubation, the samples were removed and 100µl MTT reagent was added (0.5 mg/ml) to each well and incubated for 3h. The reagent was then removed and 200µl of dimethyl sulphoxide was added to dissolve the formazan crystals. The absorbance was measured at 570nm using a microplate reader (Tecan Infinite F50, Switzerland). The cell viability was calculated using the equation,

$$\text{Percentage cell viability} = \frac{\text{As}}{\text{Ac}} \times 100$$

Where As is the absorbance of the sample and Ac is the absorbance of the control (untreated cells).

3.1.6.2. Direct contact assay

To assess cell viability in presence of the xerogels, direct contact assay was performed on L929 cells. The cells were seeded in 4 well plates at a density of 1 $x10^4$ cells/well and after attaining 80% confluency, the EtO sterilized test samples were placed on the cell layer on replicate wells in such a way that the specimen covers approximately one-tenth of the cell layer surface. The cells were then incubated for 24 h and 48h at 37°C under 5% CO_2 atmosphere and images were taken using an inverted microscope (DM IL inverted microscope, Leica Microsystems, Germany) at 20x magnification. The control cells were treated with poly (vinyl chloride) stabilized with organo-tin (PVC-Sn) as the positive control and ultra-high molecular weight polyethylene (UHMWPE) as the negative control.

3.1.6.3. Live dead assay

Toxicity was further assessed by live dead assay. Fibroblast cells were seeded in 4 well plates at a density of $1x10^4$ cells/well. The cells were exposed to the extract of the xerogels for 24h and 48h. After incubating for 24h, the media was removed and washed thoroughly with PBS. The cells were then treated with LDA stain containing 2 µM calcein AM and 4 µM EtBr and incubated for 20 minutes at room temperature. The cells were again washed with PBS and fixed using 1% formaldehyde solution. It was then visualized using fluorescence microscope (Olympus IX83, Japan) and images were taken at 20x magnification.

3.1.6.4. Scratch wound assay

The *in vitro* wound healing activity of xerogels was studied by the scratch wound assay. HaCaT keratinocyte cells were seeded at a density of 1x 10^4 cells/well in 4 well plates and incubated for 24 h at 37°C under 5% CO_2 atmosphere. After 24h, the medium was removed and the monolayer was scratched with a 200µl pipette tip across the centre of the well. The wells were gently washed twice with PBS to remove the detached cells. To this cell layer, 24h extracts from the hydrogels were added. Strontium ion (3mM) was taken as the positive control and media alone as the negative control. The cell migration was analysed at different time points such as 4h, 24h and 48h, stained with live dead staining and visualized under a fluorescent microscope (Olympus IX83, Japan). The images were taken at 10x magnification. The percentage of wound closure was calculated by Image J analysis at different time points.

3.1.7 Comparison of the xerogels with commercial alginate-based wound dressings

The in-house developed xerogels were compared with the commercial alginate-based wound care products. The commercial materials selected for our study include two different alginate wound dressing for moderate to heavily draining wounds, which was denoted as P1 and P2.

3.1.7.1 Swelling studies

The percentage swelling of P1 and P2 was analysed in phosphate buffer at different pH. A preweighed amount of the products were placed in 10ml phosphate buffer of different pH 5.8, 6.8, 7.4 and 8 in triplicate. At predetermined time, the swollen gel was removed and the surface of the gel was wiped out to remove excess

water. The gel was weighed and returned to the same buffer until a constant weight was obtained.

The percentage swelling was calculated by the following equation.

$$\% \text{ of swelling at time t} = \frac{(Wt - Wo)}{Wo} \times 100$$

Where W_o is the initial weight of the material and W_t denotes the weight after time t.

3.1.7.2 Water Vapour Transmission rate

To determine the water vapour transmission rate of the materials, ASTM standards E96/E96M-16 were followed. Test vials were filled with an equal volume of distilled water to a level 3⁄4 inch from the specimen. The materials were attached to the mouth of the vial using Teflon tape and the vials were kept at 37°C. Analysis was carried out with 6 replicas for each material. The vials were weighed from day 0 to day 5 and a graph was plotted with the change in weight against time. Water vapour transmission was calculated using the given equation and it is expressed as $g/m^2/day$.

$$WVTR = (G/t)/A$$

Where, G is the change in weight of the dish after time t and A is the surface area of the mouth of the test dish.

3.1.7.3 Dissolution studies

The weight loss of the products in pseudo extracellular fluid was analysed at pH 7.4 for 72h. At predetermined time intervals, samples were taken out and washed to remove salt adsorbed on the surface. Then the samples were dried by lyophilisation and weighed to determine the weight loss at different pH using the equation,

$$\text{weight loss } \% = \left(\frac{\text{Wt}}{\text{Wo}}\right) \text{ X } 100$$

Where W_t is the weight of the xerogel at time t and W_o is the initial weight of the xerogel.

3.1.7.4 Cytotoxicity – direct contact assay

The cytotoxicity of the selected products was analyzed by direct contact assay on fibroblast cells. The cells were seeded in 4 well plates at a density of 1 $x10^4$ cells/well and after attaining 80% confluency, the test samples were placed on the cell layer on replicate wells in such a way that the specimen covers approximately one-tenth of the cell layer surface. The cells were then incubated for 24 h and 48h at 37°C under 5% CO_2 atmosphere and images were taken using 20x objective using an inverted microscope (DM IL inverted microscope, Leica Microsystems, Germany). The control cells were treated with poly(vinyl chloride) stabilized with organo-tin (PVC-Sn) as positive control and ultra-high molecular weight polyethylene (UHMWPE) as a negative control.

3.2 Evaluation of the efficacy of xerogels for biomolecule delivery

The efficacy of the developed xerogels for biomolecule delivery was evaluated by various techniques. The biomolecules selected for the study includes insulin, simvastatin and glucose oxidase-peroxidase. The controlled delivery of biomolecule towards the wound site is essential for promoting wound healing activity. There are different studies which reported the wound healing effects of these biomolecules, but there is lack of a good delivery system to release the biomolecules in a controlled manner. The wound healing effect of insulin has been already established. Through

this study, the effect of controlled release of insulin towards the chronic wound site has been studied. Apart from the anti-inflammatory effect of simvastatin, the other wound healing effects are explored here. There are few studies reported the wound healing effect of glucose oxidase and peroxidase. So here the effect of controlled delivery of GO-POD in wound healing was analyzed under hyperglycemic conditions.

3.2.1 Materials

Huminsulin 100IU/mL, regular, recombinant DNA origin, Eli Lilly & Company, India. Simvastatin (≥97% HPLC, solid, MW 418 Da) was purchased from Sigma Aldrich, USA. Glucose oxidase and recombinant peroxidase (r-POD, 10 K.units) were purchased from SRL, India.

3.2.2 Delivery of insulin through xerogels

3.2.2.1 In vitro release of insulin

The xerogels were loaded with insulin at a concentration of 1 IU/10mg of material by diffusion filling method. The release of insulin was studied in phosphate buffer at pH 7.4 as two different release systems - immersed release system and membrane-based release system. In immersed system, the loaded hydrogels were placed directly into 3ml buffered solution and 100µl of the released solution was withdrawn at predetermined time intervals and replaced with the buffer to maintain the solution volume. While in the case of membrane-based system, insulin-loaded material was placed onto the membrane of a cell culture insert (polycarbonate membrane, Dia: 12mm, Pore size: 0.4µm, Millipore, USA) and kept in contact with the buffer solution in a 12 well plate. A 50µl of released medium withdrew and

replaced with an equal volume of buffer solution. The periodic release of insulin was analyzed by Lowry's method. The insulin release experiments were performed in triplicates and the percentage release of insulin at different time intervals was calculated.

3.2.2.2 Insulin analysis by high performance liquid chromatography (HPLC)

The insulin released from the xerogels by 24h was quantified by the HPLC method. Insulin was loaded at a concentration of 1IU/10mg of xerogel and placed in 10 ml PBS (pH 7.4) at 37℃. HPLC was performed using Waters system 600 series pump, RP18 column 4.6 x 150 mm. Gradient elution was carried out at a flow rate of 1 ml/min with a mobile phase consisting of eluent A- 0.1% trifluoro acetic acid (TFA) in acetonitrile/water (20/80) and eluent B-0.1% TFA in acetonitrile/water (50/50). The elution profile was monitored using Waters UV detector at 220nm. Insulin (Huminsulin R, 1IU/mL) was taken as standard for quantification.

3.2.2.3 Insulin analysis by enzyme linked immunosorbent assay (ELISA)

The activity of released insulin from the xerogels was further confirmed by ELISA (Mercodia Insulin ELISA kit, Sweden). The preweighed xerogels were loaded with insulin (1IU/10mg of xerogel) and placed in 10 ml PBS (pH 7.4) at 37℃. The 24h and 48h extracts were collected and performed ELISA for detecting the released insulin. It is a solid phase two-site immune assay, based on the direct sandwiching of the insulin molecule between two monoclonal antibodies directed against two separate antigenic determinants of the insulin. Anti-insulin antibodies attached to microplate wells and peroxidase-conjugated anti-insulin antibodies interact with the insulin

present within the sample during incubation. The unbound enzyme-labelled antibody is easily removed by washing and the bound conjugates were identified by the reaction with 3, 3', 5, 5'-tetramethylbenzidine to produce a coloured complex. The reaction was stopped by adding acid and the endpoint was measured using plate reader.

3.2.2.4 Circular dichroism (CD)

Circular dichroism (CD) measurements were performed on CD spectrometer (JASCO 810 spectrometer, Japan) equipped with Peltier thermostatic cell holder. CD spectra were recorded as θ in millidegrees in the far UV region. The conformational structures of insulin released from the xerogels (1IU loaded within 10mg of xerogel) after 24 and 48h were analysed in phosphate buffer (pH 7.4) and compared with the insulin standard.

3.2.3 Delivery of simvastatin through xerogels

3.2.3.1 In vitro release of Simvastatin

Simvastatin was dissolved in the DMSO-water mixture (1:1). The drug was then loaded onto the hydrogels at a concentration of 6µM/mg material by diffusion filling method (200µL was loaded from the stock solution (60µM) onto 10 mg xerogel). The release of simvastatin (SIM) from the hydrogel was assessed in phosphate buffer at pH 7.4. The release was analysed using immersed release system (by directly placing the SIM-loaded hydrogel into the buffer) and using membrane-based release (by placing the loaded gel onto the membrane of cell culture insert-polycarbonate membrane, Dia: 12mm, Pore size: 0.4µm). To study the release profile, a predetermined volume of released SIM withdrew at specific time intervals and

replaced with buffer to maintain the solution volume. The periodic release of SIM was analysed by absorbance at 238nm. The experiments were performed in triplicates and calculated the percentage of release at different time intervals.

3.2.3.2 Simvastatin quantification by high performance liquid chromatography (HPLC)

The amount of simvastatin released from the xerogel was quantified by HPLC analysis. Simvastatin was loaded at a concentration of 60µM/10mg of xerogel and placed in 10 ml PBS (pH 7.4) at 37℃. HPLC was performed using Waters HPLC/GPC system with 600E series. Purospher STAR RP-18e (5µm) column was selected as the stationary phase and a mixture of ammonium acetate buffer (pH 8) and acetonitrile in the ratio 35:65 v/v was used as mobile phase. The flow rate was set at 1ml/min and the samples were analyzed using Waters 2487 UV detector at 240 nm. The released SIM after 24h was then quantified using calibration with the SIM standard.

3.2.4 Delivery of glucose oxidase-peroxidase through xerogels

3.2.4.1 In vitro release of glucose oxidase (GO) and peroxidase (POD)

The UV absorption spectra of glucose oxidase (GO) and peroxidase (POD) were taken using spectrophotometer (Varian Cary 50 UV-vis Spectrophotometer, USA). By diffusion filling method, glucose oxidase was loaded at a concentration of 1.5IU/10mg of material and the release was assessed in phosphate buffer (pH 7.4). The GO-loaded hydrogels were placed onto the membrane of the cell culture insert (polycarbonate membrane, Dia: 12mm, Pore size: 0.4µm) and kept in contact with the buffer solutions in a 12-well plate. The predetermined volumes of released GO

withdrew at specific time intervals and replaced with buffer solution to maintain the volume. The periodic release of GO was analysed by UV spectroscopy at 210nm. The release experiment was performed in triplicates. Similarly, peroxidase was loaded into the different hydrogels (15 IU/10mg material) and the release was analysed for up to 24h by UV spectroscopy at 408nm.

3.2.4.2 Effect of GO-POD loaded hydrogel on high glucose medium – evaluation of glucose and hydrogen peroxide levels

The xerogels were loaded with a combination of GO-POD (GO: 1.5 IU, POD: 15IU per 10mg sample) and placed in high glucose media (25mM glucose). The periodic reduction in glucose concentration was analyzed by the O-toluidine method of glucose estimation. Glucose condenses with O-toluidine reagent in acetic acid to form a blue-green N-glycosylamine and its absorbance was measured at 623nm. Similarly, the amount of H_2O_2 produced by GO-POD catalyzed reaction was also monitored. The released H_2O_2 reacts with potassium iodide and liberates iodine, which in turn bleaches the colour of toluidine blue to leuco form. The periodic reduction in glucose and H_2O_2 was monitored for 8h.

3.2.4.3 Circular dichroism (CD)

Circular dichroism (CD) measurements were performed on CD spectrometer (JASCO 810 spectrometer, Japan) equipped with Peltier thermostatic cell holder. CD spectra were recorded as θ in mill degrees in the far UV region. The conformational structures of glucose oxidase released from the xerogels (1.5IU loaded within 10mg

of xerogel) after 8h and 24h were analyzed in phosphate buffer (pH 7.4) and compared with GO standard.

3.3 In vitro wound healing studies with biomolecules using optimized xerogel under hyperglycemic conditions

Based on the efficiency of the xerogels for biomolecule delivery, the optimized xerogel ADPM2S2 was selected for further *in vitro* wound healing studies. The wound healing effects of ADPM2S2 loaded with insulin, simvastatin and glucose oxidase-peroxidase were performed under high glucose conditions (Dulbecco's Modified Eagle Medium with high glucose of 25mM). Fibroblasts (L929), keratinocytes (HaCaT) and macrophages (RAW 264.7) cell lines used for this study. The growth medium for L929 was minimal essential medium with normal glucose (5mM). For HaCaT and RAW 264.7 cells, RPMI 1640 with low glucose (11.1mM) was used as the growth medium. Since all the experiments were performed under high glucose conditions, initially the cells were acclimatised with the high glucose condition by gradient increase in glucose concentration in the growth medium. The experiments were performed with the cells conditioned in DMEM high glucose medium (25mM).

3.3.1 Materials

Minimum essential medium (MEM), 0.25% Trypsin –EDTA, 3-(4, 5-dimethylthiazol-2-yl)-2, 5-diphenyl tetrazolium bromide (MTT), Lipopolysaccharides (LPSs) from *Escherichia coli* O111:B4 and 2′, 7′-Dichlorodihydrofluorescein diacetate were purchased from Sigma Aldrich, US. Foetal bovine serum (FBS) and Dulbecco's Modified Eagle Medium with high glucose from GIBCO (US). Phalloidin-

tetramethylrhodamine B isothiocyanate for actin filament staining was purchased from Santa Cruz Biotechnology, US. Phospho AkT1 (Ser 473) Monoclonal antibody (14-6), rabbit anti-mouse IgG (H+L, FITC tagged) secondary antibody, Mouse TNFα ELISA kit, FITC-tagged CD86 (B7-2) Monoclonal Antibody (24F) and APC-tagged CD163 Monoclonal Antibody (eBioGHI/61 (GHI/61)) were purchased from Invitrogen™, Thermofisher Scientific, US. For qPCR studies, High capacity cDNA synthesis kit and PowerUp SYBR Green Master Mix were purchased from Applied Biosystems, Thermofisher Scientific, US and the primers for gene expression analysis from Integrated DNA Technologies, US.

3.3.2 Effect of insulin on wound healing

3.3.2.1 Cytotoxicity evaluation

Cytocompatibility of the insulin loaded xerogels was analysed by test on extract studies on L929 fibroblast cells and HaCaT keratinocytes. The cells grown to about 80% confluency were trypsinized, seeded at a density of 1x 10^4 cells/well in 96 well-plate and incubated in CO_2 incubator at 37°C under 5% CO_2 for 24 h. The cells were then incubated with the extracts of insulin-loaded xerogel (100mIU/10mg xerogel) taken at different time points (24, 48 and 72h) for the next 24h. The untreated cells and 1x Triton X-100 were the negative and positive controls respectively. After incubation, the media was removed and 100µL of MTT reagent was added (0.5 mg/ml) and incubated for 3h. The resulting formazan crystals were dissolved in 200µL of dimethyl sulfoxide (DMSO) and the absorbance was measured at 570nm in an automated microplate reader (Tecan Infinite F50, Switzerland).

Cell viability was expressed as the mean percentage of sample absorbance relative to untreated cells.

Percentage cell viability = $\frac{As}{Ac} \times 100$

Where As is the absorbance of sample and Ac is the absorbance of control (untreated cells). The cell viability with varying concentrations of insulin was also analysed by MTT assay.

3.3.2.2 Scratch wound assay

In vitro wound healing activity of released insulin was analyzed by scratch wound assay on keratinocytes and fibroblast cells. The cells were seeded at a density of $2x10^4$ cells/well in 4 well plates and incubated for 24h at 37°C under 5% CO_2 conditions. After 24h, the medium was removed and the monolayer was scratched with a 200µl pipette tip across the centre of the well. The wells were gently washed twice with PBS to remove the detached cells. The insulin-loaded hydrogel (100 mIU insulin/10mg xerogel) and hydrogel alone were placed within the cell culture insert (pore size: 0.4µm, dia 12mm) and kept directly over the cell surface. The cell migration across the wound area was observed at 4, 8 and 24h under high glucose conditions by live dead staining. The cells were visualised under fluorescence microscope (Olympus IX83, Japan) at 0, 4, 8 and 24 h. The percentage of wound closure was calculated by Image J analysis.

3.3.2.3 Collagen deposition

To study the effect of insulin on collagen synthesis by fibroblast cells, the Sirius red assay was performed. Cells were seeded on 24 well-plate and incubated

overnight at 37℃ and 5% CO_2 atmosphere. After incubation with 24h extracts of insulin-loaded hydrogel (100 mIU insulin/10mg xerogel), hydrogel alone and insulin (100mIU) were added to the cells and incubated for 24h under hyperglycemic conditions. The cells were fixed with 1% formaldehyde solution, after which it was removed and the plate was air dried. To this, 150µL Sirius red reagent was added and kept for 1h under mild shaking. The stain was removed and the cell layer was washed with 5% acetic acid until the yellow colour was removed, the red-coloured precipitate was then dissolved in 0.2ml sodium hydroxide (0.1 N NaOH) and the obtained solution was read at 550 nm. Stained untreated cells were used to evaluate the collagen deposition levels in the treated cells.

3.3.2.4 Cell migration-Actin staining

The migration of the fibroblast cells was analyzed by actin staining. Actin filaments play a crucial role in cellular migration during wound healing process. Here the effect of insulin in actin filament organization in L929 cells was analyzed. L929 cells were treated with 24h extracts of insulin-loaded hydrogel (100 mIU insulin/10mg xerogel), hydrogel alone and insulin (100mIU). After 24 h, the nuclear stain was done with Hoechst stain for 30min. The cells were then fixed in 1% formaldehyde solution for 20min. After PBS wash, cells were permeabilized using 0.2% Triton X100 in 1% BSA in PBS for 20min, washed twice with PBS and then blocked with 1% BSA in PBS for 30 min. After removing the blocking solution, cells were incubated with Rhodamine Phalloidin solution (0.2µg/mL) for 20 min. After PBS washing, visualized with fluorescent microscope (Leica DM IRB, Germany).

3.3.2.5 Expression of Phospho AKT

L929 cells were seeded in 4 well plates at a density of $1x10^4$ cells/well. After attaining 80% confluency, cells were treated with the 24h extracts of hydrogel alone, insulin-loaded hydrogel (100 mIU insulin/10mg xerogel) and insulin (100mIU) and incubated at 37℃ and 5% CO_2 atmosphere for 24h under high glucose conditions. Cells were then fixed with 1% formaldehyde for 20 min and permeabilized with 0.2% Triton X in 1% BSA in PBS for 20 min. After PBS wash, the cells were treated with 2% BSA in PBS for 60 min. Cells were then treated with primary antibody (0.5mg/ml, dilution 1:100) and kept at 4℃ overnight. After PBS wash, the cells were stained with secondary antibody (1.5mg/ml, dilution 1:100) for 45 min and the nuclear stain was done with DAPI for 2-3min. The cells were visualized under fluorescent microscope (Leica DM IRB, Germany).

3.3.2.6 Annexin-PI assay for cellular apoptosis

The role of insulin in preventing the programmed cell death during the hyperglycemic condition was analyzed by Annexin V FLUOS – PI staining. During apoptosis, the phosphatidyl serine of the plasma membrane gets exposed to the outer leaflet, which has a higher affinity for the protein annexin V. So that the apoptotic cells can be detected using FITC-conjugated annexin V by flow cytometry, while propidium iodide (PI) bind with the necrotic or late apoptotic cells, characterized by the loss of the integrity of the plasma and nuclear membranes. L929 cells were seeded in 24 well plates at a cell density of $2x10^4$ cells/well. After reaching 80% confluency, cells were treated with the extracts of hydrogel (100 mIU insulin/10mg xerogel),

insulin-loaded hydrogel and insulin (100 mIU/ml) and incubated for 24h. After 24h, cells were washed with PBS, trypsinized to detach the cells and resuspended in 500µl media. The cells were pelleted by centrifugation at 500 rpm for 10 min at 4℃ and washed with PBS. Then treated with 100µl annexin V Fluos-PI solution and kept in dark for 15 min. The cells were finally suspended in 400µl of incubation buffer. The single cell suspension was then analysed using flow cytometry ((Cytoflex, Beckman coulter, USA). The results were compared with different controls such as untreated unstained cells, untreated FITC stained cells and untreated PI stained cells.

3.3.2.7 Gene expression studies

The expression level of various genes involved in wound healing was analyzed by qPCR analysis. The genes selected for the analysis include COL1A1 and TGF-β1 expression from L929, keratin 16 and GLUT1 expression from HaCaT and IL-6, TNFα, CD86 and CD163 from RAW 264.7 cells. The cells were seeded in 12 well-plate at a density of $2x10^6$ cells/well. After reaching 80% confluency, the cells were treated with 24h extract of insulin-loaded hydrogel, hydrogel alone (100 mIU insulin/10mg xerogel) and insulin (100mIU) for 24h. Using the Trizol method of RNA extraction, RNA from the cells was extracted and its purity was evaluated using Nanodrop spectroscopy (Nanodrop 2000c, Thermofisher Scientific, US). A260/280 ratio of 1.8-2.0 was selected for further analysis. Using 750ng of RNA, cDNA was constructed and real-time PCR was performed. GAPDH was used as the house-keeping gene and gene expression was reported as fold change using the equation given below;

$$\triangle \text{Ct} = \text{Ct (gene of interest)} - \text{Ct (housekeeping gene)}$$

$$\triangle\triangle \text{Ct} = \triangle \text{Ct (sample)} - \triangle \text{Ct (control average)}$$

$$Fold\ gene\ expression = 2\text{^}(-\triangle\triangle \text{Ct})$$

Where, Ct is the cycle threshold value.

3.3.3 Effect of simvastatin in wound healing

3.3.3.1 Cytotoxicity evaluation

The cytotoxic response of the simvastatin-loaded xerogel was analysed by test on extract studies on L929 cells and HaCaT cells. After attaining 80% confluency, cells were treated with the extracts of SIM-loaded hydrogel (60µM/10mg of xerogel) and hydrogel alone at different time points such as 24, 48 and 72h and incubated for 24h at 37°C under 5% CO_2 atmosphere. The untreated cells and 1x Triton X-100 were the negative and positive controls respectively. After incubation, the medium containing samples was removed and 100µl of MTT was added (0.5 mg/ml) and incubated for 3h. MTT solution was then removed and the formazan crystals formed were dissolved in 200µl of dimethyl sulfoxide (DMSO). The absorbance was then measured at 570nm in an automated microplate reader (Tecan Infinite F50, Switzerland).

Cell viability was expressed as the mean percentage of sample absorbance relative to untreated cells.

Percentage cell viability = $\frac{\text{As}}{\text{Ac}} \times 100$

Where As is the absorbance of sample and Ac is the absorbance of control (untreated cells). Similarly, the cell viability in presence of varying concentrations of simvastatin was analysed by MTT assay.

3.3.3.2 Scratch wound assay

In vitro wound healing activity of released simvastatin was analyzed by scratch wound assay on fibroblasts and keratinocytes. L929 cells were seeded at a density of $2x10^4$ cells/ well in 4 well plates. After 24h, media was removed and the monolayer was scratched with a 200µl pipette tip across the centre of the well. The detached cells were washed with PBS and SIM-loaded hydrogel (60µM/10mg of xerogel) and hydrogel alone placed within the cell culture insert (pore size: 0.4µm, dia 12mm) were kept over the scratch for 24h under hyperglycemic conditions. Control cells were treated with SIM (60µM) and high glucose media alone. The cell migration across the wound area was observed at 4,8 and 24h after staining with live dead assay kit and visualised under fluorescence microscope (Olympus IX83, Japan). The percentage of wound closure was calculated by Image J analysis.

3.3.3.3 Collagen deposition

The effect of simvastatin on collagen synthesis was analysed by the Sirius red assay on L929 cells. Cells were seeded in 24 well plates ($1x10^4$ cells/well) incubated overnight at 37°C and 5% CO_2 atmosphere. After incubation, cells were treated with the 24h extracts of SIM-loaded hydrogel (60µM/10mg of xerogel), hydrogel alone and SIM (60µM) under high glucose conditions. After 24h of incubation, cells were fixed with 1% formaldehyde solution. The cells were then treated with 150ul Sirius red

reagent and kept for 1h under mild shaking. The stain was removed and the cell layer was washed with 5% acetic acid and dissolved the red precipitate in 0.1N NaOH solution. The absorbance was measured at 550 nm with untreated cells as the control.

3.3.3.4 Cell migration - Actin staining

The migration of cells in presence of simvastatin was analyzed by actin staining. L929 fibroblast cells were seeded in 4 well plates ($1x10^4$ cells/well). After attaining 80% confluency, cells were treated with the 24h extracts of hydrogel alone, SIM-loaded hydrogel (60µM/10mg of xerogel) and SIM (60µM) under hyperglycemic conditions. After 24h incubation, media was removed, cells were washed with PBS and nuclear staining was done with Hoechst for 30min. The cells were then fixed in 1% formaldehyde solution and permeabilized using 0.2% Triton X100 in 1% BSA in PBS for 20min. The permeabilized cells were then washed twice with PBS and blocked with 1% BSA in PBS for 30 min. After removing the blocking solution, incubated with rhodamine phalloidin solution (0.2µg/ml) for 20 min. After PBS washing, cells were visualized with fluorescent microscope (Leica DM IRB, Germany).

3.3.3.5 Anti-inflammatory activity

The anti-inflammatory activity of simvastatin was analyzed with RAW 264.7 macrophage cells. , The inflammatory response was stimulated by treating cells with 1 ng/ml LPS (lipopolysaccharide from *E.coli* O111:B4 strain) for 5 hours. Then cells were incubated with the sample solution of 24h extracts of hydrogel alone, SIM-loaded hydrogel (60µM/10mg of xerogel) and SIM (60µM) under hyperglycemic conditions.

After 24h of incubation, the culture extracts were collected and the amount of TNF-α produced was quantified by ELISA (Mouse TNF-α ELISA, Thermofisher scientific).

3.3.3.6 Macrophage polarization - Flow cytometry analysis

The effect of simvastatin on macrophage polarization was analyzed by flow cytometry. RAW 264.7 macrophage cells were seeded in 12 well plates ($2x10^5$ cells/well) and after obtaining 80% confluency, cells were stimulated with LPS (1ng/ml) for 5h. Then the cells were incubated with the 24h extracts of hydrogel alone, SIM-loaded hydrogel (60µM/10mg of xerogel) and SIM (60µM) under hyperglycemic conditions. After 24h of incubation, cells were trypsinized and centrifuged at 5000 rpm for 10 min. After PBS wash, the non-specific sites were blocked with 1% BSA for 10 min. After centrifugation, supernatant was removed carefully and cells were treated with antibodies specific for M1 and M2 macrophages, FITC-tagged CD86 (B7-2) Monoclonal Antibody (1µl (0.5µg/test)) and APC-tagged CD163 Monoclonal Antibody (5µl (0.5µg/test)) and kept at 4°C for 30 min. Then the cells were centrifuged, washed and resuspended in PBS for flow cytometry analysis (Cytoflex, Beckman coulter, USA).

3.3.3.7 Gene expression studies

The effect of simvastatin on the expression of various genes involved in wound healing was analyzed by qPCR analysis. The genes selected for the analysis include COL1A1 and TGF-β1 expression from L929, keratin 16 and GLUT1 expression from HaCaT and IL-6, TNFα, CD86 and CD163 from RAW 264.7 cells. The cells were seeded in 12 well-plate at a density of $2x10^6$ cells/well. After reaching 80%

confluency, the cells were treated with 24h extract of SIM-loaded hydrogel (60µM/10mg of xerogel), hydrogel alone and SIM (60µM) for 24h. RNA was extracted by Trizol method and its purity was evaluated using Nanodrop spectroscopy (Nanodrop 2000c, Thermofisher Scientific, US). A260/280 ratio of 1.8-2.0 was selected for further analysis. Using 750ng of RNA, cDNA was constructed and real-time PCR was performed. GADPH was used as the house-keeping gene and gene expression was reported as fold change using the equation given below;

$$\triangle \text{Ct} = \text{Ct (gene of interest)} - \text{Ct (housekeeping gene)}$$

$$\triangle\triangle \text{Ct} = \triangle \text{Ct (sample)} - \triangle \text{Ct (control average)}$$

$$Fold\ gene\ expression = 2\text{^}(-\triangle\triangle \text{Ct})$$

Where, Ct is the cycle threshold value.

3.3.4 Effect of Glucose oxidase-peroxidase in diabetic wound healing

3.3.4.1 Cytotoxicity evaluation

Cytocompatibility of the xerogels loaded with GO-POD was analysed by test on extract studies on L929 fibroblast cells and HaCaT keratinocytes. The cell viability with different concentrations of GO was analyzed by MTT assay on both fibroblast and keratinocyte cell lines. The cells grown to about 80% confluency were seeded at a density of 1x 10^4 cells/well in 96 wells plate and incubated at 37°C under 5% CO_2 atmosphere for 24h. The medium was removed and treated with 24h extracts of GO-loaded hydrogel (150mIU/10mg xerogel), GO-POD-loaded hydrogel (GO: 150mIU, POD: 1.5 IU/10mg xerogel), hydrogel alone and GO-POD (GO: 150Miu/mL, POD: 1.5 IU/mL). The untreated cells and 1x Triton X-100 treated cells were the negative

and positive controls respectively. After incubation, 100µl of MTT was added (0.5 mg/ml) and incubated for 3h. MTT solution was then removed and the formazan crystals formed were dissolved in 200µL of dimethyl sulfoxide (DMSO). The absorbance was then measured at 570nm in an automated microplate reader (Tecan Infinite F50, Switzerland). Cell viability was expressed as the mean percentage of sample absorbance relative to untreated cells.

$$\%\ cell\ viability = \frac{As}{Ac} x\ 100$$

Where, As is the absorbance of sample and Ac is the absorbance of control (untreated cells).

3.3.4.2 Scratch wound assay

To assess the *in vitro* wound healing effect of GO-POD loaded hydrogels, the scratch wound assay was performed on fibroblast and keratinocytes. Cells were seeded at a density of $2x10^4$ cells/well in 4 well plates and incubated for 24 h at 37°C under a 5% CO_2 atmosphere. After attaining 80% confluency, a scratch was created with a 200µl pipette tip across the centre of the well and PBS wash was given to remove detached cells. Then the cell culture insert (pore size: 0.4µm, dia: 12mm) with hydrogel loaded with GO (150mIU/10mg xerogel), GO-POD (GO: 150mIU/10mg, POD: 1.5 IU/10mg xerogel), hydrogel alone and GO-POD (GO: 150mIU/mL, POD: 1.5 IU/mL) was kept directly over the cell surface under high glucose conditions. The wound area was observed and images were taken at predetermined time intervals (0h, 4h, 8h and 24h) after staining with the live-dead assay kit. The cells were visualised

under fluorescence microscope (Leica DM IRB, Germany) and the percentage of wound closure was calculated by Image J analysis.

3.3.4.3 Collagen deposition

The role of GO and POD in promoting *in vitro* collagen production was analyzed by the Sirius red assay. L929 cells were seeded on 24 well-plate and after attaining 80% confluency, cells were treated with 24h extracts of GO-loaded hydrogel (150mIU/10mg xerogel), GO POD-loaded hydrogel (GO: 150mIU/10mg xerogel, POD: 1.5 IU/10mg xerogel), hydrogel alone and GO-POD (GO: 150mIU/mL, POD: 1.5 IU/mL) for 24h under high glucose conditions. The cells were then fixed with 1% formaldehyde solution, after which it was removed and the plate was air dried. To this 150µL Sirius red reagent was added and kept for 1h under mild shaking. The stain was removed and the cell layer was washed with 5% acetic acid until the yellow colour got removed. The red-coloured precipitate was then dissolved in 0.2 ml 0.1N NaOH and the absorbance was taken at 550 nm. Stained untreated cells were used to compare the results.

3.3.4.4 Cell migration-Actin staining

The migration of cells, grown under high glucose medium, in presence of GO-POD enzymes was analyzed by actin staining. L929 fibroblast cells were seeded on 4 well-plates and after attaining 80% confluency, treated with the 24h extracts of GO-loaded hydrogel (150mIU/10mg xerogel), GO-POD-loaded hydrogel (GO: 150mIU, POD: 1.5 IU/10mg xerogel), hydrogel alone and GO-POD (GO: 150mIU/mL, POD: 1.5 IU/mL). After 24h of incubation, the nuclear stain was done with Hoechst for

30min. The cells were then fixed in 1% formaldehyde solution and washed with PBS. Cells were permeabilized using 0.2% Triton X100 in 1% BSA in PBS for 20min, followed by washing twice with PBS and blocked with 1% BSA in PBS for 30 min. After removing the blocking solution, incubated with Rhodamine Phalloidin solution (0.2µg/ml) for 20 min. and the cells were visualized with fluorescent microscope (Leica DM IRB, Germany).

3.3.4.5 In vitro reactive oxygen species (ROS) production

Glucose oxidase is an oxidoreducatse enzyme that converts glucose to glucono-lactone and generate hydrogen peroxide during the process. To evaluate the hydrogen peroxide formation in presence of glucose oxidase and also the effect of peroxidase, DCFDA (2′, 7′-Dichlorodihydrofluorescein diacetate) was used. By the DCFDA assay, the ROS production within the cells was detected. L929 cells were seeded at a density of $1x10^4$ cells/well in 4 well-plate and incubated for 24h at 37°C under 5% CO_2 atmosphere. After reaching 80% confluency, cells were treated with the 24h extracts of GO-loaded hydrogel (150mIU/10mg xerogel), GO-POD-loaded hydrogel (GO: 150mIU, POD: 1.5 IU/10mg xerogel), hydrogel alone and GO-POD (GO: 150mIU/mL, POD: 1.5 IU/mL) under high glucose conditions for 24h. Media alone was treated as the negative control and 2mM H_2O_2 as the positive control. After 24h of incubation, the cells were treated with DCFDA stain and images were taken with fluorescent microscopy (Olympus IX83, Japan). The cell-permeant DCFDA can diffuse into the cell and get deacetylated by cellular esterases to a non-fluorescent

compound, which is later getting oxidised by the intracellular ROS into highly fluorescent 2', 7' –dichlorofluorescein (DCF).

3.3.4.6 Gene expression studies

The effect of these enzymes on the expression of various genes involved in wound healing was analyzed by qPCR analysis. The genes selected for the analysis include COL1A1 and TGF-β1 expression from L929, keratin 16 and GLUT1 expression from HaCaT and IL-6, TNFα, C86 and CD163 from RAW 264.7 cells. The cells were seeded in 12 well-plate at a density of $2x10^6$ cells/well. After reaching 80% confluency, the cells were treated with 24h extract of GO-loaded hydrogel (150mIU/10mg xerogel), GO-POD-loaded hydrogel (GO: 150mIU, POD: 1.5 IU/10mg xerogel), hydrogel alone and GO-POD (GO: 150mIU/mL, POD: 1.5 IU/mL) for 24h under high glucose conditions. RNA was extracted with the Trizol method and its purity was evaluated using Nanodrop spectroscopy (Nanodrop 2000c, Thermofisher Scientific, US). A260/280 ratio of 1.8-2.0 was selected for further analysis. Using 750ng of RNA, cDNA was constructed and real-time PCR was performed. GADPH was used as the house-keeping gene and gene expression was reported as fold change using the equation given below;

$$\triangle \text{Ct} = \text{Ct (gene of interest)} - \text{Ct (housekeeping gene)}$$

$$\triangle\triangle \text{Ct} = \triangle \text{Ct (sample)} - \triangle \text{Ct (control average)}$$

$$Fold\ gene\ expression = 2\text{^}(-\triangle\triangle \text{Ct})$$

Where, Ct is the cycle threshold value.

3.4 Evaluation of wound healing efficacy by in vivo animal models

From the *in vitro* experiments, the biomolecule having excellent wound healing activity was selected for further *in vivo* evaluation. The topical delivery and the wound healing efficacy of insulin loaded within ADPM2S2 xerogel was analyzed in diabetic rat models.

3.4.1 Materials

Sprague Dawley rats were obtained from the Division of Small animal Facility, SCTIMST, Trivandrum. Streptozotocin, Harris's haematoxylin and Phospho AkT1 (Ser 473) Monoclonal antibody (14-6) were purchased from Sigma Aldrich, US. Ketamine hydrochloride and isoflurane were procured from Neon Laboratories, India and Xylazine hydrochloride from Pharmika India Pvt Ltd, India. For Histopathology analysis, Formalin from Molychem, India, Disodium hydrogen phosphate and Sodium dihydrogen phosphate from SRL, India, Eosin, Glacial acetic acid, 2-propanol, Xylene, Ammonia, Hydrochloric acid purchased from Merck, US, Mounting media and Paraffin wax from Leica, Germany. For Immunohistochemistry analysis, Supersensitive polymeric-HRP detection system purchased from BioGenex Laboratories, USA and all other reagents were of analytical grade and were purchased from SRL, Merck India and SD Fine Ltd., India.

3.4.2 *In vivo* wound healing experiment on diabetic rat models

3.4.2.1 Diabetic rat model

In vivo animal experiments were performed with the approval of the Institutional Animal Ethics Committee (B form No. SCT/IAEC-435/JANUARY/2022/112 dated

21/02/2022). Ninety Sprague Dawley rats having 300±30g weight were maintained under standard laboratory conditions with a 12h day/night cycle and maintained at a controlled environment with a temperature of 22±3°C and humidity of 30-70%. Feed and water were given ad libitum. Diabetes mellitus was induced in rats under fasting via a single intraperitoneal injection with streptozotocin (60 mg/kg) freshly prepared in 0.1M sodium citrate buffer (pH 4.5). Then animals were subjected to fasting for approximately 7h with only water provided ad libitum. 1hour after injection, feed and glucose water (10%) given. After 24h, blood glucose level will be analyzed with glucometer to confirm the development of hyperglycemia.

Three days after injection, blood glucose levels were analyzed with a glucometer to confirm the development of hyperglycemia. The blood glucose level was monitored daily for 2 weeks and animals showing blood glucose levels ≥250 mg/dl were considered diabetic and stable diabetic rats were taken for the studies. A total of 60 diabetic rats were randomly selected for the wound healing study.

3.4.2.2 Treatment with alginate-based xerogels

The rats were divided into five groups, four test groups and one control group (n=4). Three time points were selected (7, 14 and 21 days). Animals were anaesthetized with ketamine (90 mg/kg) and xylazine (5 mg/kg) intramuscularly. The dorsal fur of the animals was clipped with an electrical trimmer and disinfected with betadine solution. A single full-thickness excision wound of size 2 x 2 cm was created on the dorsal side of the rat by scalpel blade. The test groups were treated with hydrogel alone, insulin-loaded hydrogel (200mIU insulin loaded within 4cm^2 xerogel), insulin

alone (200mIU/mL) and commercial alginate wound dressing. The materials were placed over the wound by covering them in burn mesh and attached with a bandage without disturbing the wound area. The diabetic rats with untreated wounds were kept as the control. The animals were housed in individual cages. The wounds were cleaned and dressing changes were given every 48h. The area of wound closure was calculated by planimetry and morphometric analysis. After the completion of the experiment, the rats were euthanized on particular days (7, 14 and 21 days) by CO_2 inhalation. The wound area with normal skin was explanted for histological evaluation.

3.4.2.3 Planimetry

The percentage of wound closure was calculated by planimetry. The digital photos of the wounds were taken (Nikon D3500) on day 0 and at the time of sampling using a photographic stand which helps to take the photo from a uniform distance. The area of the wound was traced on paper on alternative days and the % reduction in wound area was calculated using the following equation;

$$\%\ wound\ closure = \frac{wound\ area\ day\ 0 - wound\ area\ day\ (n)}{(wound\ area\ day\ 0)}\ x\ 100$$

Where n is the number of days of wound healing.

3.4.3 Histopathology evaluation

The explanted sections were fixed in 10% buffered formalin for 24h and sampled the desired wound area. The tissue cassettes containing the samples were treated with grades of alcohol (50% alcohol for 3h and 70% alcohol for 2h) and kept in an automatic tissue processor for 12h (Leica TP1020, Germany). The tissue sample

will undergo dehydration, clearing and embedding in paraffin wax. The samples were blocked in paraffin wax and sectioned into 4µm thickness using microtome (Leica RM2255, Germany).

3.4.3.1 Haematoxylin & Eosin Staining

To evaluate the re-epithelialization rate during the wound healing process, the paraffin sections were stained with Haematoxylin & Eosin. The sections were deparaffinized in xylene and hydrated to water through descending grades of alcohol. The nuclear staining was performed with Harris Haematoxylin for 30 min, followed by differentiation in acid alcohol and bluing in ammonia water. The cytoplasm was stained with Eosin for 2 min, washed in water and dehydrated through ascending grades of alcohol. The stained sections were then cleared in xylene and mounted for microscopic evaluation (BX51 microscope, Olympus Corporation, Japan).

3.4.3.2 Immunohistochemistry

Immunohistochemistry was performed to evaluate the expression of proliferative marker phoshoAkt during the healing process. The expression of the marker was analysed in test groups treated with insulin loaded hydrogel, hydrogel alone and compared with untreated controls at different time points. The paraffin sections were deparaffinised and hydrated to water through descending grades of alcohol. Antigen retrieval was performed in citrate buffer (pH 6.8) at 92℃ for 20min and cooled for 30min. The endogenous peroxidase activity was stopped with 10% H_2O_2 and non-specific binding was blocked with 1%BSA. Sections were then treated with phospho Akt primary antibody (0.5mg/mL, 1:100) dilution for 1h and washed in

wash buffer, followed by treatment with super-enhancer and HRP-labelled secondary antibody for 20 min and 30 min respectively. After proper washing, sections were treated with the substrate 3, 3′-Diaminobenzidine (DAB) and counterstained with Haematoxylin. Finally, sections were dehydrated through ascending grades of alcohol, cleared in xylene and mounted for microscopic evaluation (BX51 microscope, Olympus Corporation, Japan). The images were captured by a DP71 camera loaded onto a BX51 microscope (Olympus Corporation, Japan) and quantified using Image Pro version 3DS6.1 software (Media Cybernetics, Silver Spring, MD).

3.5 Statistical analysis

All the data are represented as mean ± standard deviation. The statistical analysis was performed by unpaired Student's t-test using MS excel. The significant difference between groups was defined at p-value <0.05.

CHAPTER 4

RESULTS & DISCUSSIONS

4.1 Synthesis and characterization of alginate-based xerogels

4.1.1 Characterization of alginate

Alginate with medium viscosity was selected for xerogel synthesis. The molecular weight by GPC analysis was found to be $1.82x10^5$ Da. By the Ubbelohde viscometer analysis, the calculated molecular weight was $2.2x10^5$ Da. The reported viscosity of alginate was ≥2,000 cP, 2% (25°C)(lit.). Alginate was spectroscopically characterized by FTIR and NMR analysis (figure 1A-B). The characteristic absorption peak of hydroxyl group was obtained at 3265 cm^{-1}. The stretching vibration of –CH group and the C-O-C group of saccharide units were observed at 2925cm^{-1} and 1030 cm^{-1} respectively. The symmetric and asymmetric stretching of carboxylate group was observed at 1593cm^{-1} and 1407cm^{-1} respectively. Due to the presence of sodium salt, the peak corresponding to carboxylate group was shifted to 1593cm^{-1}. This indicates the solubility of alginate in water and also showed the conversion of carbonyl group to carboxylate anion (Varaprasad et al., 2020). In the ^1H NMR spectra, alginate showed a shift at 3.7 to 4.5 ppm due to the mannuronate and guluronate residues of the alginate. The distribution pattern of M-block and G-block is another important parameter for determining the physico-chemical properties of alginate. The calculated M/G ratio was 1.57. In the FTIR spectra (figure 1C) of polyguluronic acid and polymannuronic acid, the fingerprint region of carbohydrate was observed within the range of 950-750 cm^{-1}, which corresponds to the C-O stretching vibration of the uronic

acid residues. The mannuronic acid and the guluronic acid residues were assigned at 820 cm^{-1} and 787 cm^{-1} respectively (Leal et al., 2008). The peak at 1125 cm^{-1} was assigned to the C-O and C-C stretching of the pyranose ring and the peak at 1030 cm^{-1} showed C-O stretching vibrations (M P Filippov, 1974). Using A_{1125}/A_{1030} ratio M/G ratio can be calculated and it was found to be 1.52. Form these results, it was observed that the alginate used in this study with guluronic acid content at the lower side and had higher polyM content.

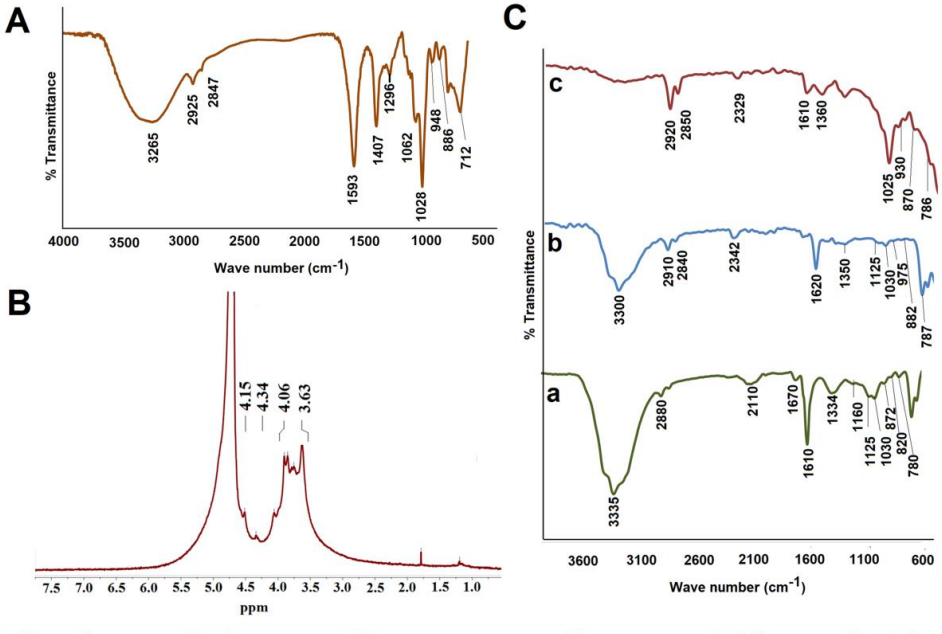

Figure 1: A) FTIR spectra and B) ^{1}H NMR spectra of sodium alginate. C) FTIR spectra of different fractions of sodium alginate a) GG block b) MM block and c) MG block.

4.1.2 Synthesis of alginate-based xerogels

4.1.2.1 Synthesis of alginate-g-poly (methacrylic acid) xerogels

Alginate-g-poly (methacrylic acid) xerogels were synthesized by grafting poly (methacrylic acid) chains by free radical polymerization. Prior to xerogel synthesis, appropriate ratio of alginate: monomer was found out by analyzing grafting yield,

grafting efficiency and total conversion to homopolymer chains (figure 2 A). The percentage grafting yield was >70% for AGM1, AGM2 and AGM3, among which AGM2 showed higher % GY of 86%. But the % grafting efficiency was higher for AGM1 and AGM2 compared to AGM3. The homopolymer chain formation for AGM1 was 18%, while that of AGM2 was 11%. AGM3 and AGM4 showed homopolymer formation of >20% and reduced grafting yield and efficiency, so these formulations were not taken for xerogel synthesis. Due to the significant reduction in the homopolymer chain formation and higher grafting yield along with grafting efficiency AGM2 formulation was selected. The determination of grafting yield and efficiency helps to ensure the appropriate grafting of poly (methacrylic acid) chains to the alginate backbone. The chances of formation of homopolymer chains were higher with increase in monomer concentration.

Further, zeta potential and free carboxyl groups of the formulations were analyzed (figure 2B) and AGM2 showed a zeta potential of -62 ± 1.3 mV and % free carboxyl group content was 88%, which further confirmed the effective grafting of homopolymer chains of poly (methacrylic acid). The increase in the negative charge of AGM2 compared to alginate was due to the grafting of poly (methacrylic acid) chains to alginate backbone. The free carboxyl group content also increased by 15%. The molecular weight of AGM2 was 1.87×10^5 Da and that of native alginate was 1.82×10^5 Da. The increase of molecular weight by 4000-5000 Da confirmed the successful grafting reaction. The alginate content of the formulation AGM2 was 30±2.3%, as analyzed by the phenol sulphuric acid method.

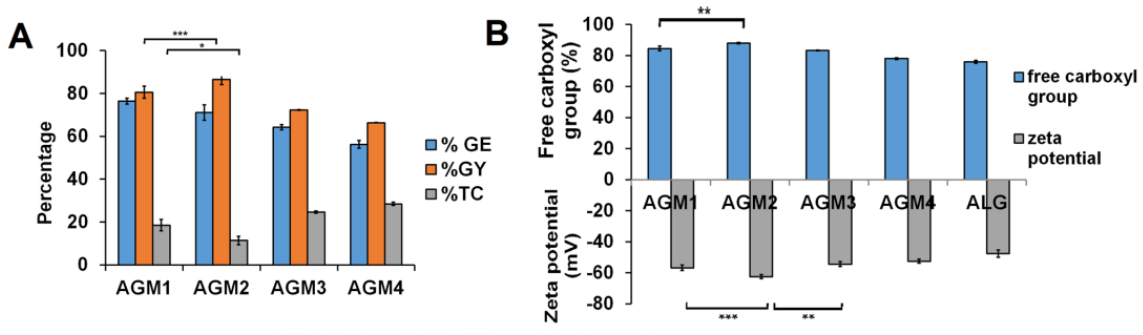

Figure 2: A) grafting parameters of different formulations of Alg-g-poly (methacrylic acid), % GE- % grafting efficiency, %GY - % grafting yield, % TC - % conversion into homopolymer of poly (methacrylic acid). The difference in grafting yield between AGM1 and AGM2 is significant at **p< 0.001. Formation of homopolymer in comparison with AGM1 and AGM2 is significant at *p<0.05) B) The extent of grafting of poly (methacrylic acid) chains to alginate analyzed by estimating % free carboxyl groups and zeta potential, compared with ungrafted alginate as control.(**p<0.01, ***p<0.001).

The xerogels were prepared by using AGM2 formulation. The proposed reaction for xerogel synthesis comprises of a single step reaction involving alginate, monomer, cross-linker, initiator and catalyst, which were added subsequently. Poly (methacrylic acid) chains were grafted to alginate by free radical polymerization reaction initiated by ammonium persulphate and catalyzed by TEMED. The initiator, ammonium persulphate decomposed on heating and form anion free radicals, which extract hydrogen from the second and third hydroxyl groups of alginate generating alginate macro radicals. These free radicals of alginate randomly react with either poly (methacrylic acid) or bisacrylamide and further generate macrmolecular free radicals. Interlinked structures of polymer chains were formed by these two species of macromolecular free radicals. The bisacrylamide have two free radical regenerated ends, so that it can bind with alginate-methacrylic acid at both the ends.

The hydrogel of alginate-g-poly (methacrylic acid) was formed within 30 minutes at 60°C with chemical cross-linking with bisacrylamide. The formation of permanent cross-linking structures with these irreversible chemical linkages allows more absorption of water and biomolecules. But it was observed that the hydrogel formed by covalent cross-linking alone was not strong enough and the leachants of alginate was confirmed in the medium by the phenol sulphuric acid method. This indicates the need of dual cross-linking with cations to enhance its integrity. By exposing the alginate-methacrylic acid gel to the strontium ions, the gel become stronger in appearance. The gel was slightly milky white in appearance and become further opaque after cross-linking with strontium ions. The carboxylate groups of alginate and methacrylic acids were ionically linked with strontium ions, which reduced the leaching out of alginate from the xerogels. The dissolution of alginate chains was 30.4% before ionic cross-linking, whereas it was only 20% after ionic cross-linking. So the strontium ion mediated physical cross-linking makes the gel stronger in addition to the existing covalent cross-linking.

The covalent cross-linking present in a hydrogels are irreversible chemical links, which forms permanent network structure. These linkages allow the absorption of water or bioactive compounds and permit its release by diffusion. While the ionically cross-linked hydrogels are formed by reversible linkages, which forms non-permanent network structure. Ionically cross-linked hydrogels are generally considered as bio-compatible and well-tolerated, which exhibits higher swelling and pH sensitivity, compared to covalent cross-linked hydrogel (Berger et al., 2004). So

this dual cross-linking approach would be beneficial for improving the mechanical stability as well as promoting the biomolecule delivery.

Different batches of xerogels (AGM2S1, AGM2S2, AGM2S3 and AGM2S4) were synthesized by varying the strontium ion concentration. After proper washing and freeze drying, the xerogels were obtained by lyophilization. The white opaque xerogels were converted to transparent hydrogel on contact with water or PBS (figure 3). AGM2S1 xerogels showed surface cracks upon lyophilization and AGM2S4 xerogel was very hard and brittle in nature. AGM2S2 and AGM2S3 showed good flexibility and was chosen for further optimization.

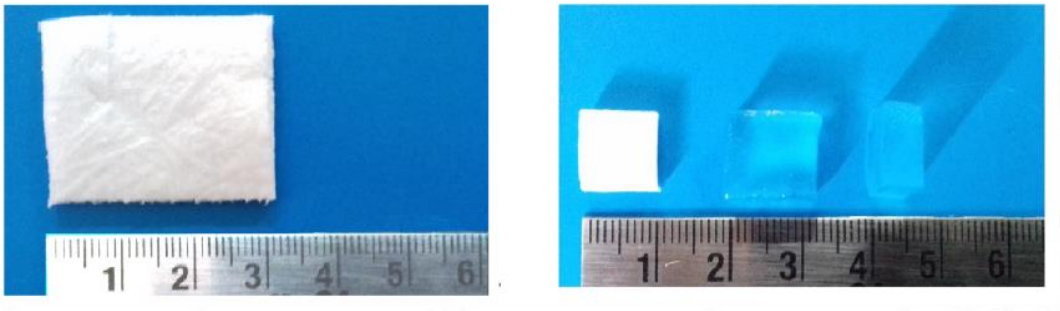

Figure 3: Alginate-g-poly (methacrylic acid) xerogel is a white opaque matrix and on contact with water or PBS gets converted to transparent hydrogel.

4.1.2.1.1 Chemical characterization

Chemical characterization of the xerogels were performed by FTIR and NMR spectroscopic analysis (figure 4 A-B). The grafting was confirmed by the characteristic peak at 1720 cm^{-1} of the carboxyl group of methacrylic acid. Khasana et al reported that, during polymerization reaction, the IR spectra of methacrylic acid showed the disappearance of characteristic C=C bond at 1540 cm^{-1} due to the formation of poly (MAA) chains. (Khasana et al, 2010). The effective cross linking with methylene

bisacrylamide was confirmed by the presence of peaks at 1256 cm^{-1} and 1534 cm^{-1} for CN bond and deformation of (N-H) moiety (amide II band) respectively. Further NMR analysis confirmed the grafting of poly (MAA) chains. As seen in figure 4B the shift corresponding to methylene and methyl groups was observed at 6.5-6.7 and 2.1 ppm respectively.

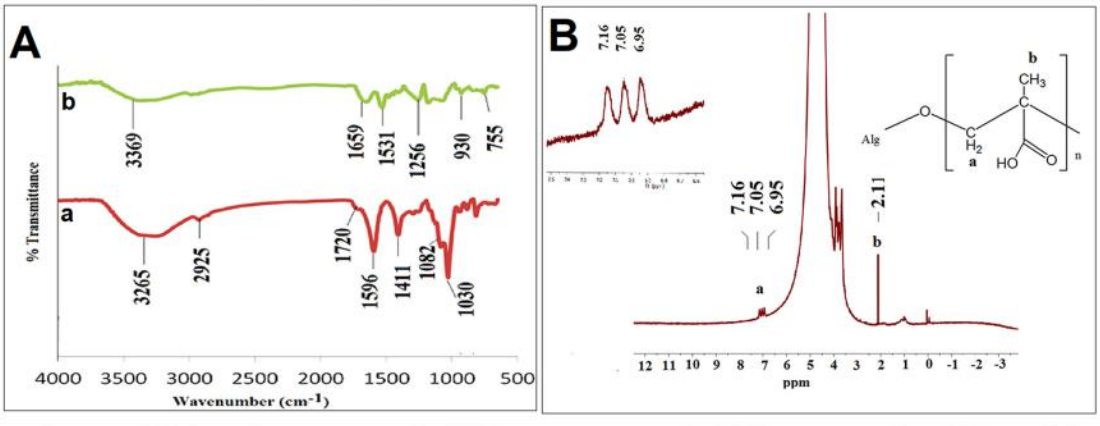

Figure 4: A) FTIR spectra of a) alginate-g-poly (methacrylic acid) copolymer and b) alginate-g-poly (methacrylic acid) xerogel obtained after cross-linking. B) ^{1}H NMR spectra of alginate-g-poly (methacrylic acid) copolymer.

4.1.2.1.2 Physical characterization

The swelling kinetics of the hydrogels AGM2S2 and AGM2S3 was analyzed at different pH for a time period of 48h (figure 5 A-B). AGM2S2 had higher % swelling at all pH compared to AGM2S3. Overall a fivefold increase in volume was observed. But the swelling pattern of AGM2S2 showed a reduction after 6h. However a stable swelling pattern was observed with AGM2S3. The percentage swelling was higher at pH 7.4, a swelling of 3789±67% and 3124±45% for AGM2S2 and AGM2S3 respectively after 48h. Both hydrogels showed a lower % swelling at pH 5.8 and higher swelling at pH 8. While considering the pKa of alginate (3.2), the carboxylic groups

of alginate exist as $–COO^-$ groups at pH above pKa, which results in the expansion of the hydrogel due to the electrostatic repulsion of $–COO^-$ groups (Liu et al., 2016). This was followed by the ionization of methacrylic acid groups. The pKa of methacrylic acid monomer is 4.7 and after polymerization to poly(methacrylic acid), a shift in pKa towards 6 to 7 is observed (Guo and Hu, 2007). So the ionization of poly (methacrylic acid) chains occurs in the basic medium. Hence this resulted in the higher swelling of alginate-g-poly (methacrylic acid) hydrogels at pH above 7.

The swelling behavior of the cross-linked polymers is dependent on both penetrant diffusion and polymer relaxation. The repulsion of carboxyl groups at pH above 5 leads to the chain expansion and relaxation. So at higher pH (>5), the swelling of the gel occurs by the relaxation-controlled mechanism, whereas at acidic pH or pH less than pKa, the ionization will be minimal resulting in lower swelling (Kim et al., 2003). The hydrophilic molecule present within the xerogel causes the migration of water molecule resulting in swelling. This absorbed water is regarded as the primary bound water. As the xerogel swells, the hydrophobic domains of poly (methacrylic acid) get exposed, which allows more inflow of water into the gel, contributing to the secondary bound water.

The incorporated acrylic groups can also regulate the pH along with functional groups of alginate (Koehler et al., 2017). During the progression of wound chronicity, the pH of the wound bed become alkaline, which reduces the oxygen availability and also the migration of the fibroblast resulting in impaired extra cellular matrix formation. As the wound become chronic, more amount of wound fluid is produced.

So the swelling of the xerogel at the pH 6.8, 7.4 and 8.0 are very critical. Hence the higher swelling % would help to manage the excess wound fluid without causing damage to the surrounding tissues. The higher swelling enhances the effective release of biomolecules as the wound become chronic. The pH 5.8 represents the pH of the unwounded skin, a lower swelling at this pH slows down the biomolecule delivery upon attaining the normal pH after healing achieved. This also prevents the dehydration of wound bed by excess fluid absorption.

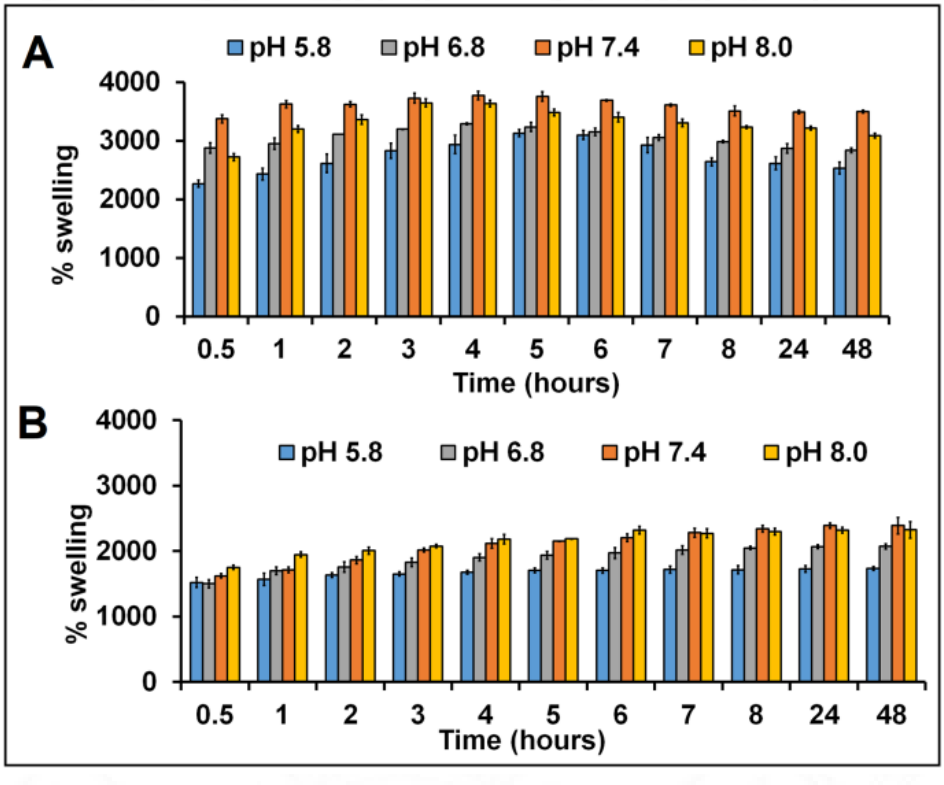

Figure 5: The percentage of swelling of alginate-g-poly (methacrylic acid) xerogels A) AGM2S2 and B) AGM2S3 at different pH such as 5.8, 6.8, 7.4 and 8.0.

Water vapor transmission rate is another important parameter which regulates the wound micro environment. An optimum moisture level should be maintained at the wound surface to promote healing process. A wound dressing with high WVTR

causes dehydration, whereas low WVTR causes accumulation of wound exudate leading to tissue maceration. Here the water vapor transmission rate for AGM2S2 was 1786±73g/m^2/24h, while that of AGM2S3 was 1879±75g/m^2/24h. Alginate control showed a higher WVTR of 2596±75g/m^2/24h (figure 6A). Studies reported that WVTR ranging from 2000-2500 g/m^2/24h would be beneficial for burn wound healing. (Queen et al., 1987). It has been suggested that, wound dressing should have a moderate WVTR of values preferably closer to the lower limit of this range. So the WVTR of the xerogel could be adequate for preventing dehydration form moderately exudating wounds.

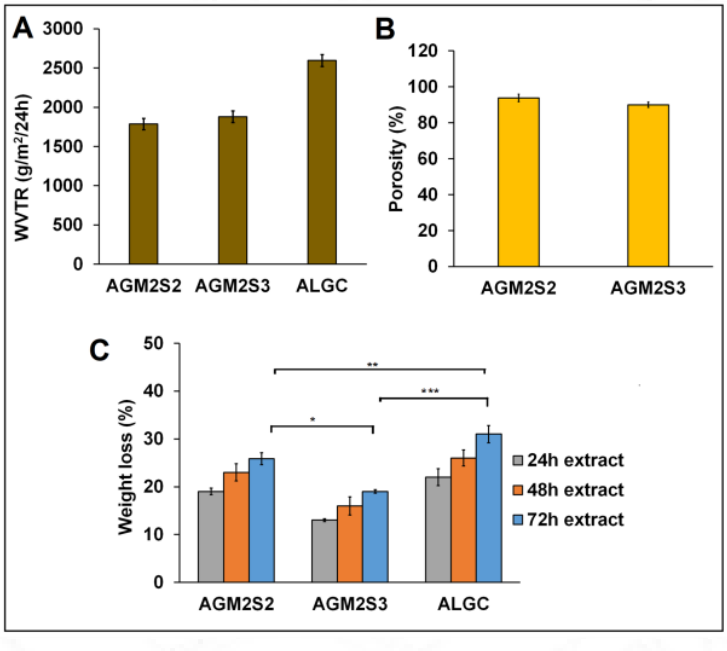

Figure 6: The comparison of different physical properties of alginate-g-poly(methacrylic acid) xerogels AGM2S2 and AGM2S3 based on the A) water vapor transmission rate B) percentage porosity and C) percentage weight loss in pseudo extra cellular fluid at pH 7.4 analyzed upto 72h (*p<0.05, **p<0.01, ***p<0.001).

The % porosity of the material analyzed by ethanol displacement method showed AGM2S2 with 94±1.5% and AGM2S3 with 90±2.1% porosity (figure 6B).

The physical stability of the material is another important factor for clinical application. The % weight loss of the material was analyzed in pseudo extracellular fluid at pH 7.4 for different time points (figure 6C). Compared to AGM2S2, degradation was lower for AGM2S3 xerogel. The percentage weight loss at 72h for AGM2S2, AGM2S3 and strontium cross-linked alginate controls (ALGS) were 25.8±3.7%, 19.5±1.7% and 31±2.5% respectively. Alginate controls without strontium cross-linking was highly unstable and >80% weight loss occurred within 4h. So strontium cross-linked alginate controls were used for comparison.

Based on these results, AGM2S3 was selected as the optimized xerogel and was taken for further studies.

4.1.2.1.3 Mechanical characterization

The mechanical strength of the xerogel AGM2S3 and strontium cross-linked alginate controls were analysed using the Universal testing machine both in dry and wet conditions (figure 7 A-B). Under dry condition AGM2S3 xerogel showed a tensile strength of 520±50 KPa in dry condition and 60±5.4 KPa in wet condition. For alginate controls, tensile strength in dry and wet conditions was 400±45 KPa and 27±2.3 KPa respectively. AGM2S3 showed higher Young's modulus of 15.3 ± 1.2 in dry condition and 9.9 ± 1.3 in wet condition. This showed the rigidity of the bulk polymer network of the xerogel with limited chain movement under dry condition. Even at wet state, the xerogel was able to retain its structural integrity and flexibility.

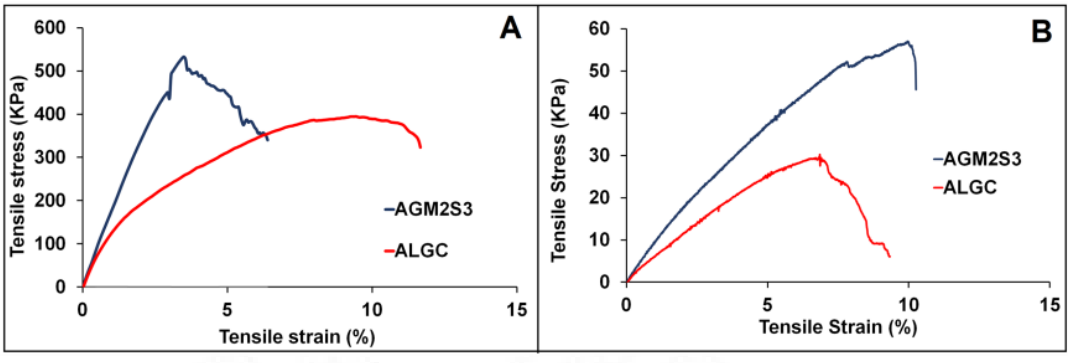

Figure 7: Tensile strength of AGM2S3 xerogel analysed in A) dry condition and B) wet condition and compared with alginate controls.

The adhesiveness of the material also influences the healing process. The bioadhesive properties were performed on rat skin and the quantitative evaluation was made by measuring the peak adhesion force and the work of adhesion. The adhesive force of the xerogel was 0.9 ± 0.14N/cm, whereas it was 1.28 ± 0.09N/cm for alginate controls. The bioadhesive force measured on wounded skin shows a peak adhesion force of 0.61 ± 0.06N/cm and 0.52 ± 0.05N/cm for the xerogel and alginate control respectively. The other mechanical parameters are mentioned in the table 1. For the treatment of chronic wounds, non-adhesive dressings are preferred. This ensures the removal of dressing without damaging the underlying granulating tissues and could reduce pain on removal. The graft modification of the alginate reduced the adhesiveness of the material.

Mechanical Characterization		AGM2S3	ALGC
Test condition	**parameters**		
Xerogel (dry condition)	Tensile strength (KPa) Modulus (MPa)	520 ± 50 15.3 ± 1.2	400 ± 45 9.9 ± 1.3
Hydrogel (wet condition)	Tensile strength (KPa) Modulus (MPa)	60 ± 5.4 9.9 ± 1.3	27 ± 2.3 0.18 ± 0.01
Normal rat skin	Bioadhesive force (N/cm) Work of adhesion (g.sec)	0.9 ± 0.14 2.3 ± 0.90	1.28 ± 0.09 1.9 ± 0.12
Wounded rat skin	Bioadhesive force (N/cm) Work of adhesion (g.sec)	0.61± 0.06 54 ± 28	0.52 ± 0.05 29 ± 14

Table 5: The comparison of mechanical parameters of AGM2S3 xerogel with alginate control.

4.1.2.1.4 Morphological characterization

The surface morphology was analyzed by micro CT as well as by SEM analysis. The pore size distribution by micro CT showed that, in AGM2S3 xerogel pore size ranged from 50 to 150µm, while that of alginate control was 100 to 250 µm (figure 8 A-D). A narrow distribution was observed with AGM2S3, but the control showed a broader pore size distribution. The pore structure was further analyzed by SEM (figure 9). The pore size of alginate control was 167 ± 54 µm, while that of AGM2S3 was 76 ± 23 µm as analyzed by SEM. The pore size and its distribution are very essential in determining the absorptive characteristics and the WVTR of the hydrogel. The highly cross-linked structures showed a heterogenous pattern of pore distribution. Due to a larger concentration of monomers during the initial polymerization phase, a microporous gel structure develops. A macroporous structure is produced as the reaction progresses because the monomer concentration is reduced.

This results in anisotropic distribution of pores within the material (Kast and Funke, 1979).

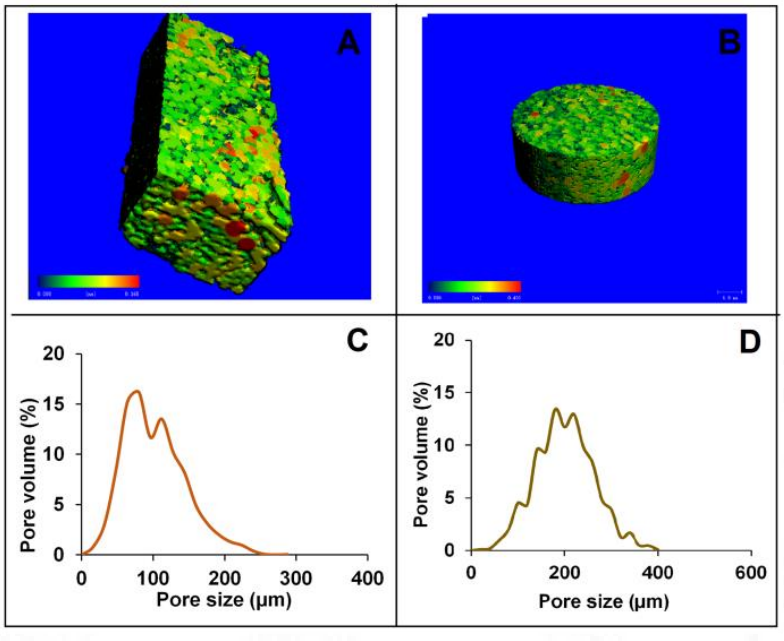

Figure 8: Micro computed tomography image of A) AGM2S3 xerogel and B) alginate control. The distribution of the pores in C) AGM2S3 xerogel and D) alginate control

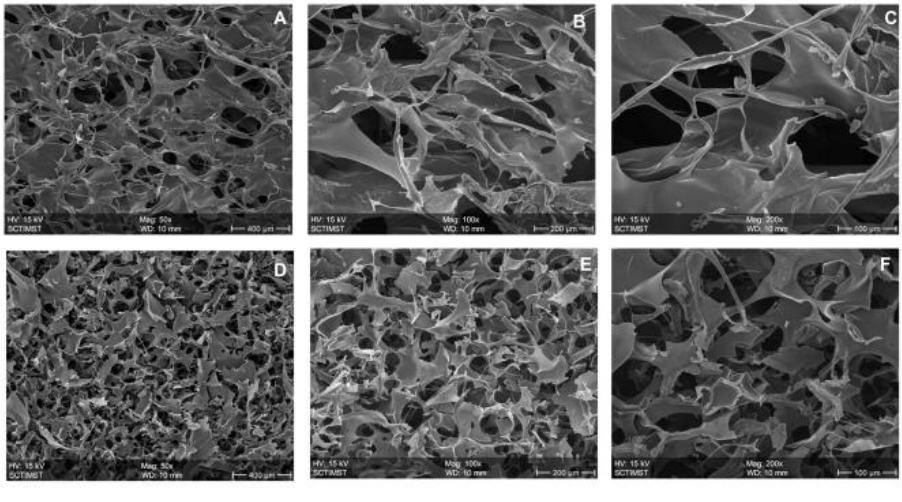

Figure 9: Scanning electron microscopy images of alginate control (A-C) and AGM2S3 xerogel (D-F) at different magnification (50x, 100x and 200x).

The surface characteristics were further analyzed by contact angle measurement (figure 10 A-B). The contact angle of alginate control and AGM2S3 was 52.05±3.74° and 66.3±2.28° respectively. Even though the hydrophilic nature of the alginate was maintained after the modification, a small increase in the hydrophobicity was observed due to the incorporation of poly (methacrylic acid) chains. The thermal characterization of the alginate and the AGM2S3 xerogel was performed by the thermogravimetric analysis (figure 10 C-D). The thermogram of sodium alginate showed weight loss in three stages such as, dehydration (28-186°C), pyrolysis (267°C) and destruction (514°C). There was 20.1% weight loss was observed as moisture during dehydration and 64.1% by carbonization. But with AGM2S3, the moisture loss was only 12.2% and decomposition loss was 60%. The 50% weight loss of pure alginate occurred at 255°C and that of AGM2S3 at 390.5°C. After complete thermal decomposition of the organic moieties in two or three steps, metal oxides will be formed as the final residue. Here xerogel showed residual amount of 7.8% due to strontium ion cross-linking. The native alginate also showed a residual amount of 8.4% due to the presence of sodium ions.

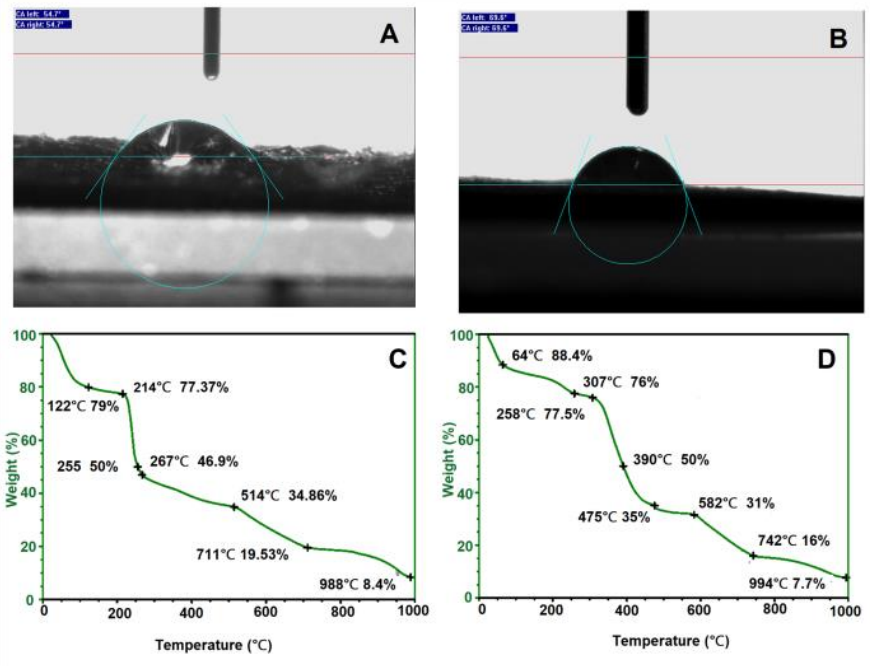

Figure 10: Contact angle measurement of A) alginate control and B) AGM2S3 xerogel by sessile drop method. Thermogram of C) Alginate control and D) AGM2S3 xerogel showing the temperature for different stages of degradation and the corresponding percentage weight.

4.1.2.1.5 Strontium ion quantification

To analyse the wound healing effect of strontium ions, it is important to quantify the strontium ion within the xerogel and released from the xerogel. The concentration of strontium ions involved in cross-linking reaction was found to be 58±4.4% for AGM2S3 xerogel. But the amount of strontium ions released from the xerogel was only <10% analyzed upto 72h (figure 11A), suggesting a strong binding of strontium ions within the xerogel. The ICP analysis showed that the xerogel contains 6.35mg/g strontium ions and 0.61mg/g sodium ions, whereas that of alginate control had 9.16 mg/g sodium ions with no traces of strontium ions (figure 11B). The concentration of strontium ion on the surface of the xerogel was further analysed by

XPS (figure 11 C-D) and it was 1% in Sr3d state and with a binding energy of 134 eV. The survey scan spectra showed the elemental composition of the xerogel as C1s-64.5%, O1s-34% and N1s-0.5%.

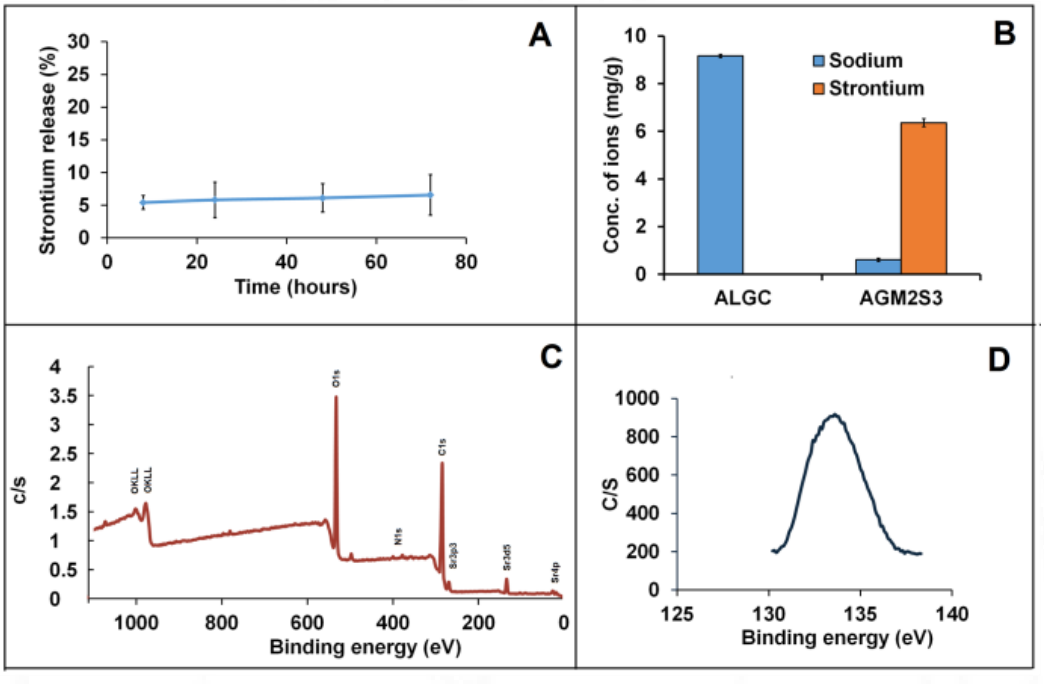

Figure 11: A) The percentage of strontium ions released from AGM2S3 xerogel placed in PBS (pH 7.4) analysed upto 72h. B) Strontium ion quantification by ICP analysis. C) Survey spectra of the xerogel by XPS analysis and D) Binding energy calculation of strontium ions within the xerogel by XPS analysis.

The role of strontium ions in hemostatic activity and collagenase inhibitory activity was analysed (figure 12 A-B). The AGM2S3 xerogels showed 82% hemostatic activity within 5 minutes compared to 6% by alginate controls. Hemostasis is a complex pathological process involving various activating and inhibitory molecules, among which calcium ions plays a significant role. Here strontium ions can substitute for the calcium ions but its effect is fundamentally different from that of calcium ions (Erik H. Mürer, 1981). The higher amount of cross-linked strontium ions results in

higher hemostatic activity. Strontium ions play a significant role in polyphosphoinositide metabolism by promoting the turnover of platelet phosphatidyl inositol pool. Phospholipids are involved in the cell activation and controlled release of granules for the platelet aggregation. Best, Bone and Russell reported that similar to calcium ions, strontium ions can also stimulate the secretion of 5-hydroxytryptamine in platelets which favours haemostatic activity (Best et al., 1981). But the collagenase inhibitory activity of the xerogel was lower (27%) compared to strontium ions (3mM). This can be attributed to the lower release as the strontium ions are tightly bound within the xerogel and resulting in decreased collagenase inhibitory activity.

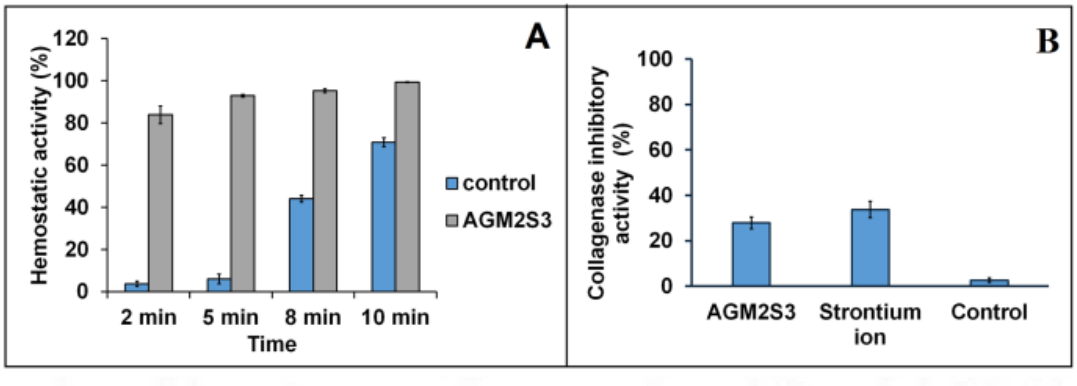

Figure 12: A) The percentage of haemostatic activity of the xerogel AGM2S3 and the alginate control analysed at different time points (2 min, 5min, 8min and 10min). B) Collagenase inhibitory activity of the xerogel compared with strontium ions (3mM) and alginate controls.

4.1.2.1.6 Cell culture studies

The cytotoxicity of the material was assessed by cell viability assays. MTT assay was performed on fibroblast cells and keratinocytes (figure 13 A-B). The test on extract studies showed that, >80% viability was obtained with L929 cells treated with

5mg/ml extract of the xerogel up to 72h, whereas HaCaT cells showed >80% viability up to 48h only. The cell viability was reduced to <70% by treating with 72h extract of 10mg/ml of xerogel. So the xerogel concentration up to 5mg/ml can be safely used with both cell lines. A similar result was obtained with direct contact assay (figure 13C) on L929 cells. More than 80% cells retained the morphology, which was further confirmed by the live dead assay (figure 13D). The percentage of dead cells analysed by live dead assay was 6% and 17% with the treatment of 24h and 48h extracts of the xerogels respectively. The biomaterial intended for application over the skin must be compatible with the skin cell types. The process of healing may be hampered by any leach outs from the substance when come in contact with the wound bed. The cytotoxicity of strontium ions were evaluated in fibroblast and keratinocytes and >75% viability was observed with strontium ion concentration upto 20 $mmol.L^{-1}$ with both the cell lines. Akyol et al studied the cytotoxic and proliferative effect of strontium ions on fibroblast cells and observed that cells were viable up to 2.5% of $SrCl_2$ and at 1.25% a higher cell proliferation was observed compared to controls (Akyol et al., 2013). Strontium ions have mitogenic effect on keratinocytes. Furukawa et al studied that keratinocytes stimulated with 1 to 3mM Sr^{2+} ions showed higher cell viability and the optimal addition of Sr ions doubled the number of keratinocytes. Sr^{2+} ions promote the G0/G1 transition very fast and increase the number of cells in S and G2/M phase. So with the treatment of optimal concentration of Sr^{2+} ions produces uniform population of proliferative but non differentiating cells (Furukawa et al., 1988).

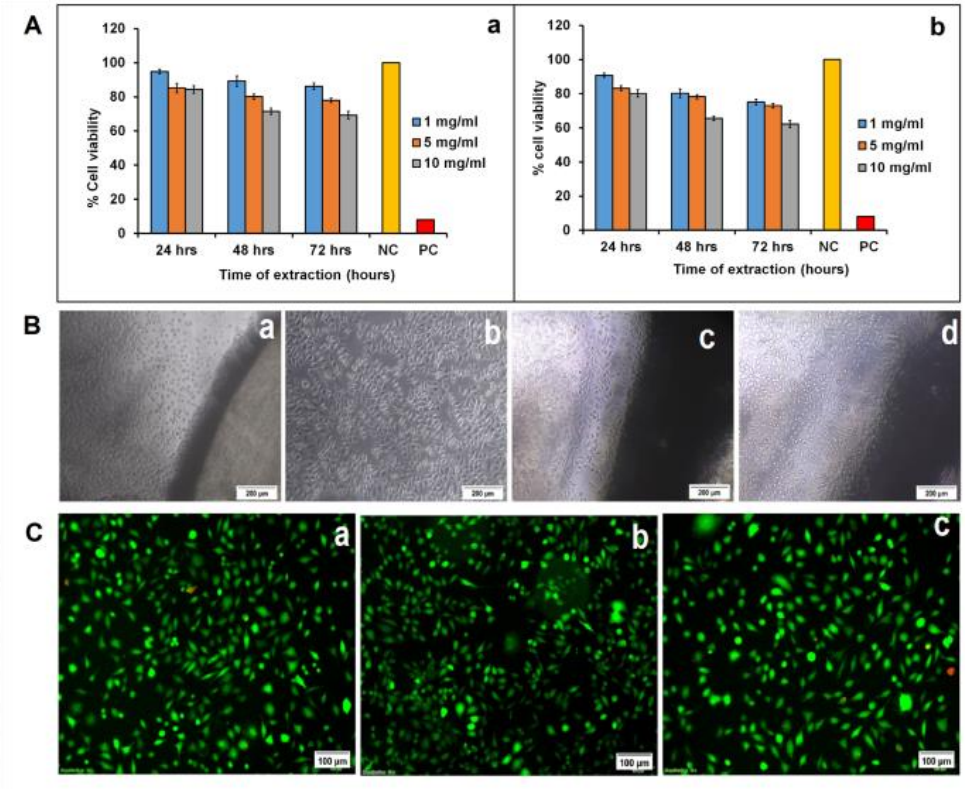

Figure 13: A) Test on extract study on a) L929 fibroblast and b) HaCaT keratinocytes treated with the extracts of the hydrogel at different time points (24h, 48h and 72h). B) Direct contact assay on L929 cells a) positive control b) negative control c) 24h and d) 48h contact of the AGM2S3. C) Live dead assay on L929 cells treated with a) media alone b) 24h extract and c) 48h extract of AGM2S3 hydrogel.

The *in vitro* wound healing effect of the xerogel AGM2S3 was analysed by scratch wound assay on HaCaT cells (figure 14). Cells treated with growth medium alone were taken as the negative control and strontium ions (3mM) as the positive control. At 4h, the % wound closure for AGM2S3, NC and PC were 20±3.3%, 34±4.7% and 43±6.4% respectively. After 48h, >90% wound closure was observed with AGM2S3 and PC.

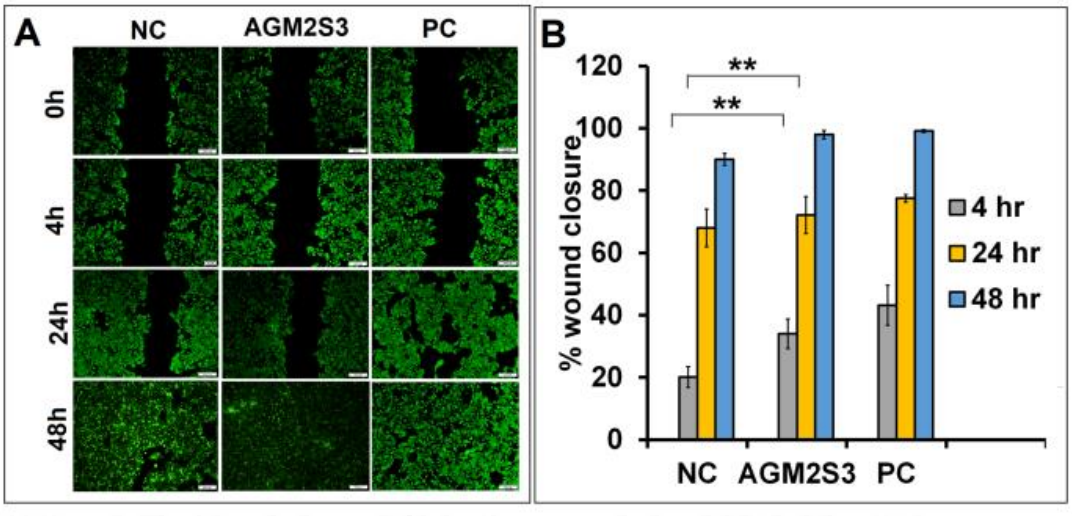

Figure 14: Scratch wound assay on HaCaT cells treated with extract of AGM2S3 hydrogel and compared with NC and PC (NC: negative control-media alone, PC: positive control-strontium ion (3mM) B) Percentage wound closure analyzed by ImageJ software upto 48h. (**p<0.01).

4.1.2.2 Synthesis of alginate-g-poly (PEGMA) xerogels

Alginate-g-poly (PEGMA) xerogels were synthesized by grafting poly (PEGMA) chains by free radical polymerization. Appropriate alginate: monomer ratio was identified before xerogel synthesis by evaluating the grafting yield, grafting efficiency and total conversion to homopolymer chains (figure 15A). A higher grafting yield and grafting efficiency was observed with AGPM1 and AGPM2. The formulations AGPM3 and AGPM4 was not taken for further studies due to higher hompolymer chain formation of >30%. A lower hompolymer chain formation was observed with AGPM2 of 16±3.53%. This formulation showed a grafting yield of 71±1.3% with an efficiency of 80±1.8%. AGPM2 showed a zeta potential of -41±1.4mV and free carboxyl groups of 46±2.3% (figure 15B). The molecular weight AGPM2 was $2.17x10^5$ Da as analysed by GPC studies. There was an increase of 34000Da than native alginate. The increase in MW signifies the successful grafting of

PEGMA to alginate chains. The percentage alginate content of AGPM2 was 35±1.5%. Based on the results, the formulation AGPM2 was selected for xerogel synthesis.

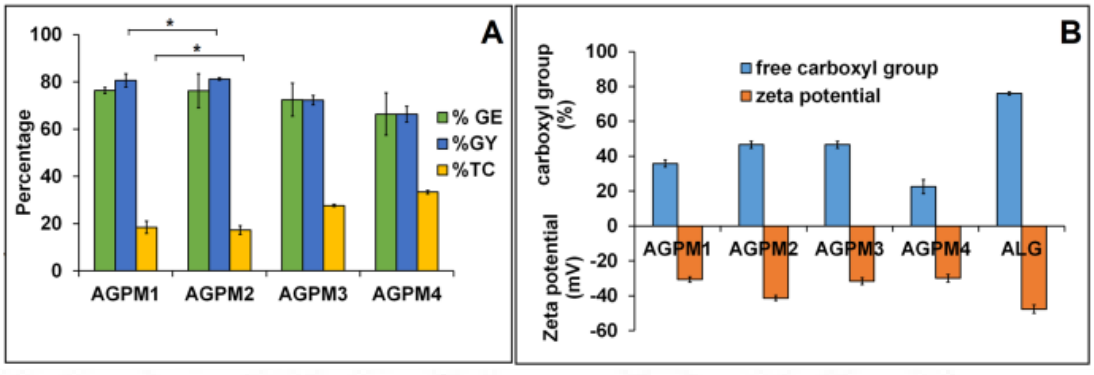

Figure 15: A) grafting parameters of different formulations of Alg-g-poly (PEGMA), % GE- % grafting efficiency, %GY - % grafting yield, % TC - % conversion into homopolymer of poly (PEGMA). The difference in grafting yield between AGPM1 and AGPM2 is significant at *$p < 0.05$. Formation of homopolymer in comparison with AGM1 and AGM2 is significant at *$p<0.05$ B) The extent of grafting of poly (PEGMA) chains to alginate analyzed by estimating % free carboxyl groups and zeta potential, compared with ungrafted alginate as control.

Hydrogels of alginate-g-poly (PEGMA) was synthesized by free radical polymerization reaction and chemical and ionic cross-linking with methylene bisacrylamide and strontium ions respectively. By increasing strontium ion concentration, different batches were synthesized namely, AGPM2S1, AGPM2S2, AGPM2S3 and AGPM2S4 as shown in the figure 16. The uniform uptake of strontium ions was ensured by immersing hydrogels in strontium ion solution, which help to overcome the diffusional barrier and exposes the hydrogels uniformly to strontium ions. A reduction in diameter of the xerogels was noticed with increase in cross-linking density. AGPM2S1 had a diameter about 9cm, while that of AGPM2S2 and AGPM2S3 ranges between 6 to 7 cm. AGPM2S4 with 200 mM crosslinking was the smallest xerogel. The thickness of the xerogel ranges from 2 to 3 mm. All batches

showed good flexibility and became transparent hydrogel on contact with water or buffer.

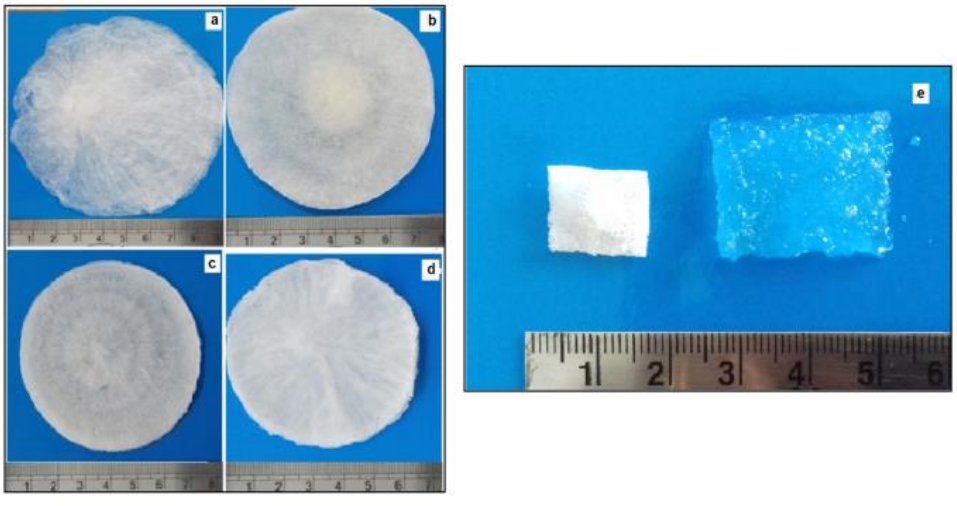

Figure 16: Different alginate-g-poly (PEGMA) xerogels and conversion into hydrogel on contact with water or buffer.

The surface of the xerogels AGPM2S3 and AGPM2S4 were found to be adhesive in nature. The M/G ratio of the alginate determines the cross-linking nature of the xerogels. Strontium ions have more affinity towards G blocks, however at high ionic concentration the complexation take place with M/G block also (Haug and Smidsrød, 1967; Montanucci et al., 2015). This results in the formation of MG/MG junctions with higher cross-linking density. Donati et al showed that the zipping of MG/MG junctions causes the release of water and leading to collapsed network (Donati et al., 2009). This could be the reason for the reduced diameter of the xerogels with increase in ionic concentration.

4.1.2.2.1 Chemical characterization

Chemical characterization of the xerogels was carried out by FTIR and NMR analysis to confirm grafting and crosslinking reactions (figure 17). Grafting with poly (PEGMA) showed the characteristic peak of carbonyl group at 1723 cm^{-1}.Both asymmetric and symmetric peaks of PEG molecules were observed at 1241 cm^{-1} and 1146 cm^{-1} respectively. Peak observed at 1095 cm^{-1} corresponds to the C-O-H alcoholic stretching of PEG molecule. The crosslinking with bisacrylamide was confirmed by the –NH bond at 1396 cm^{-1}. ^{1}H NMR spectra further confirmed effective grafting reaction. Poly (PEGMA) chains showed chemical shift around 2.87 to 3.59 ppm corresponding to methylene protons and shift around 1.82ppm indicates the methyl groups of poly (PEGMA). The peaks corresponding to vinyl groups of PEGMA were obtained at 5.70 and 6.10 ppm.

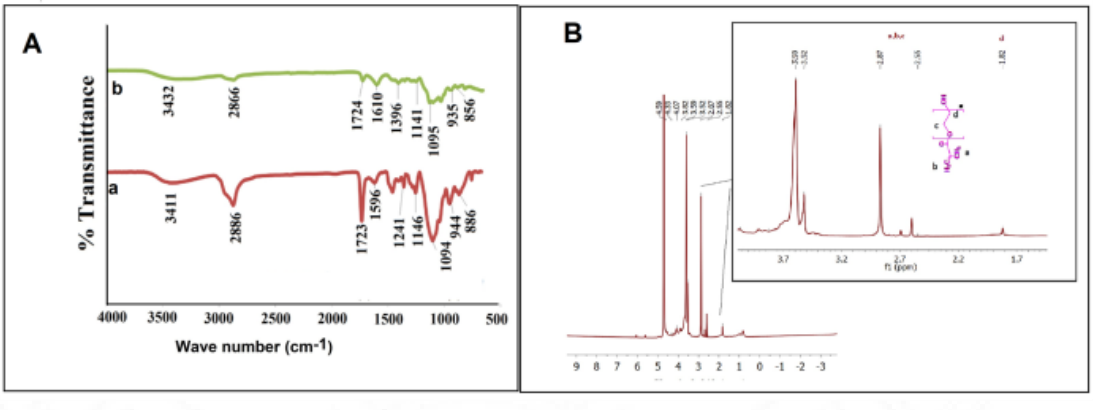

Figure 17: A) FTIR spectra of a) alginate-g-poly (PEGMA) (AGPM2) formulation and b) alginate-g-poly (PEGMA) xerogel. B) 1H NMR spectra of alginate-g-poly (PEGMA) (AGPM2) formulation.

4.1.2.2.3 Physical characterization

The % swelling of alginate-g-poly (PEGMA) xerogels were analyzed at various pH up to 48h (figure 18 A-D). A higher swelling of 2202±61% was obtained

with AGPM2S1 and lower swelling of 1226±32% for AGPM2S4 xerogel at pH 7.4. The overall swelling of AGPM2S2 at different pH corresponds to 2000%, while that of AGPM2S3 was 1500%. All xerogels reached equilibrium swelling within 3-5h and remained stable up to 48h. But a slight decrease in swelling was observed with AGPM2S3 after reaching equilibrium swelling. The M/G ratio of the alginate plays as significant role in swelling. PolyM blocks of alginate are more hydrate than the polyG blocks (Mørch et al., 2006). So the xerogels rich in polyM can absorb more exudate and form hydrogel rapidly (Brus et al., 2017). At lower concentration of strontium ions, the cross-linking density is low, resulting in high swelling. By increasing the ionic cross-linking, a reduction in swelling was observed. At higher ionic concentration, the cationic complexation occurs with MG blocks as well. So the number of junction zones will be lesser and decrease in chain flexibility will occur due to binding of multiple chains to the same element. This results in increased resistance to stretching leading to lower swelling (Davidovich-Pinhas and Bianco-Peled, 2010). The rate of diffusion of water into the xerogel depends on the cross-linking density. According to the distance from the ether oxygen atom of the PEG molecule, water molecules can occupy at different regions within the gel. The hydrogen bonding with water molecule decreases with increase in cross-linking concentration. The equilibrated water content of the gel determines the diffusion behaviour of the gel (Wu et al., 2009).

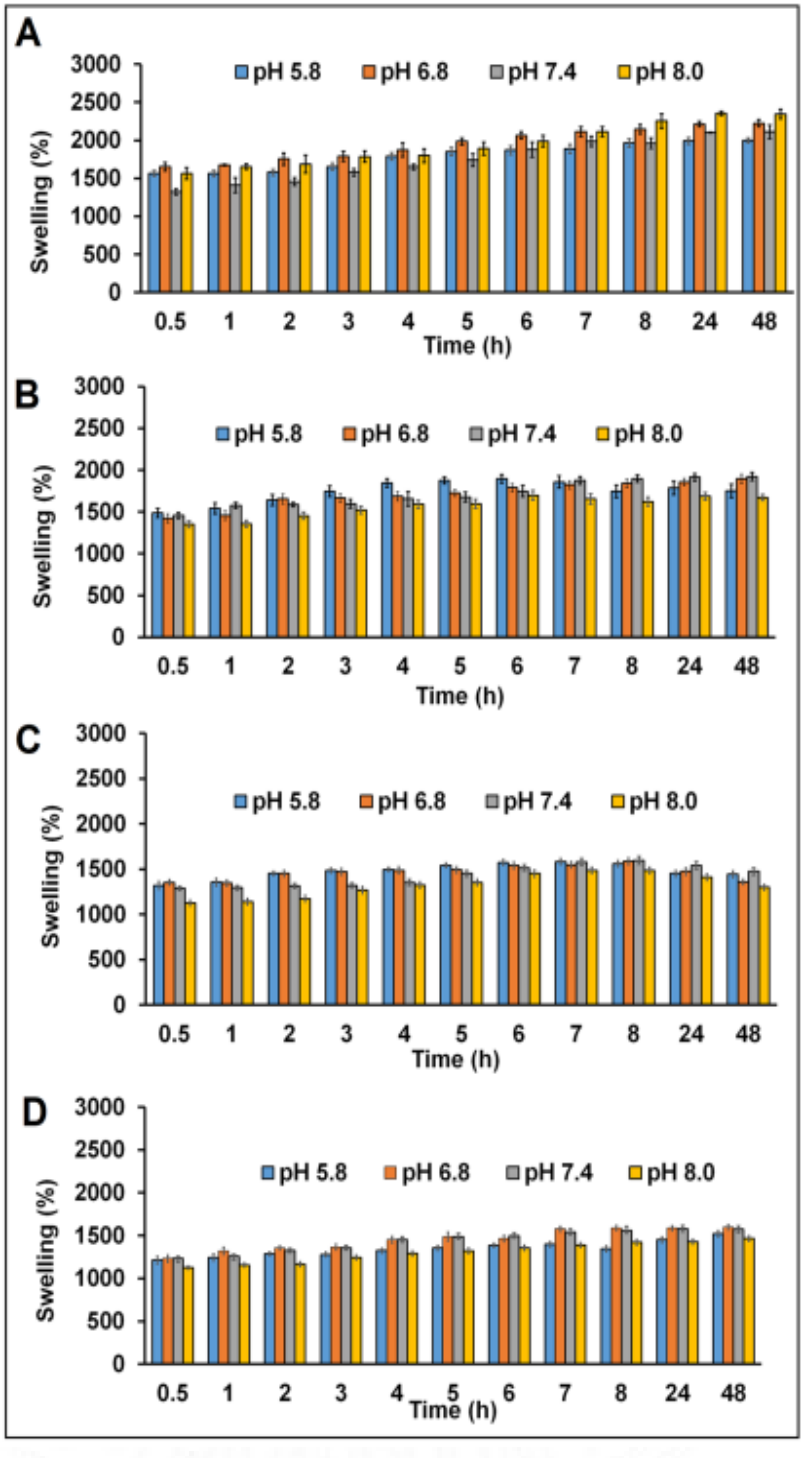

Figure 18: The percentage swelling of different alginate-g-poly (PEGMA) xerogels A) AGPM2S1 B) AGPM2S2 C) AGPM2S3 and D) AGPM2S4 at different pH (5.8, 6.8, 7.4 and 8.0) analysed upto 48h.

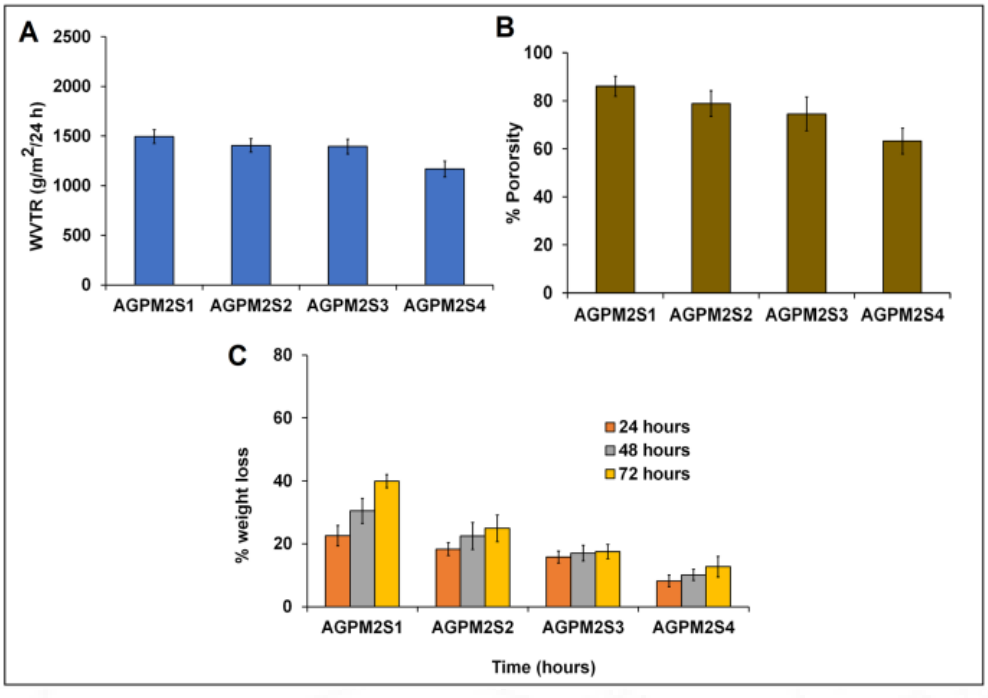

Figure 19: A) Water vapor transmission rate B) Percentage porosity and C) Percentage weight loss in pseudo extracellular fluid (pH 7.4) of different alginate-g-poly (PEGMA) xerogels.

The effect of increased strontium ion concentration was also reflected in WVTR. A reduction in WVTR was obtained with increased cross-linking (figure 19 A). A lower WVTR of 1150±75g/m^2/24h was obtained with AGPM2S4. The other xerogels AGPM2S1, AGPM2S2 and AGPM2S3 showed a WVTR ranging from 1300-1500g/m^2/24h. A reduction in porosity from 86% to 63% was also noticed with increase in strontium ion cross-linking (figure 19B). The reduction in pore size can be correlated with high M/G ratio. The divalent cation binding in alginate occurs by chelate bonding of two carboxyl groups at one chain and two vicinal hydroxyl groups form another chain (Schweiger, 1962). Cozzi et al reported that if the hydroxyl groups are modified, the selectivity of cation binding decreases. In the case of AGPMS

xerogels, the grafting occurs at hydroxyl groups. This lead to the improved binding of strontium ions at higher concentration (Cozzi et al., 1969).

The degradation studies of the xerogel were performed in pseudo extracellular fluid up to 48h (figure 19C). AGPM2S1 showed a higher weight loss of >35% within 48h. At pH 7.4, the % weight loss of the xerogels AGPM2S2, AGPM2S3 and AGPM2S4 were 22.4±2.7%, 17±1.7% and 10±2.6% respectively. At lower cross-linking concentration, a higher weight loss occurred due to the release of loosely bound alginate chains that were not involved in cross-linking. Usually, the ioincally cross-linked alginate hydrogels easily disintegrate due to the displacement of divalent cations with monovalent ions present in the phosphate buffer or physiological or tissue fluids. But here the xerogels attained the stability by grafting and chemical cross-linking, so the weight loss was minimal.

While comparing the xerogels, AGPM2S1 could not be selected due to its higher weight loss. The xerogel AGPM2S4 with higher cross-linking were also not suitable due to its lower WVTR and porosity. Among AGPM2S2 and AGPM2S3, a good % swelling and porosity was obtained with former.

So among different alginate-g-poly (PEGMA) xerogels, AGPM2S2 has been selected as the optimized xerogel for further analysis.

4.1.2.2.3 Mechanical characterization

The mechanical strength of the optimized xerogel in both dry and wet conditions were analysed (figure 20). The AGPM2S2 xerogel had a tensile strength of 433 ± 60 KPa in dry state and 148±17 KPa in wet condition. But in the case of alginate controls, tensile strength was found to be 400 ± 30 KPa in dry state and 27 ± 6 KPa in wet condition. As the figure indicates the xerogel showed increased tensile strength of 5.4 times in wet condition compared to alginate control. The material was not rigid and very flexible to handle and the reduced modulus of the xerogel also is indicative of the same.

Mechanical Characterization		**AGPM2S2**	**ALGC**
Test condition	**parameters**		
Xerogel (dry condition)	Tensile strength (KPa) Modulus (MPa)	433 ± 60 1.15±0.12	400 ± 30 9.9 ± 1.3
Hydrogel (wet condition)	Tensile strength (KPa) Modulus (MPa)	148±17 0.15±0.98	27 ± 6 0.18 ± 0.01
Normal rat skin	Bioadhesive force (N/cm) Work of adhesion (g.sec)	0.58 ± 0.01 15.6 ± 6.3	1.28 ± 0.09 1.9 ± 0.12
Wounded rat skin	Bioadhesive force (N/cm) Work of adhesion (g.sec)	0.62± 0.12 62 ± 25	0.52 ± 0.05 29 ± 14

Table 6: Comparison of mechanical characteristics of AGPM2S2 xerogel with alginate control

The bioadhesive force of the xerogel on normal rat skin was 0.58 ± 0.01N/cm, whereas it was 1.28 ± 0.09N/cm for alginate controls. The bioadesive force measured

on wounded skin shows a peak adhesion force of 0.62 ± 0.12N/cm and 0.52 ± 0.05N/cm for the xerogel and alginate control respectively. The other parameters are mentioned in the table 6. The increase in strain at break of the xerogel in both dry and wet condition can be attributed to the insertion of flexible PEGMA chains within alginate chains. The high M/G ratio also contribute to the increase in mechanical strength.

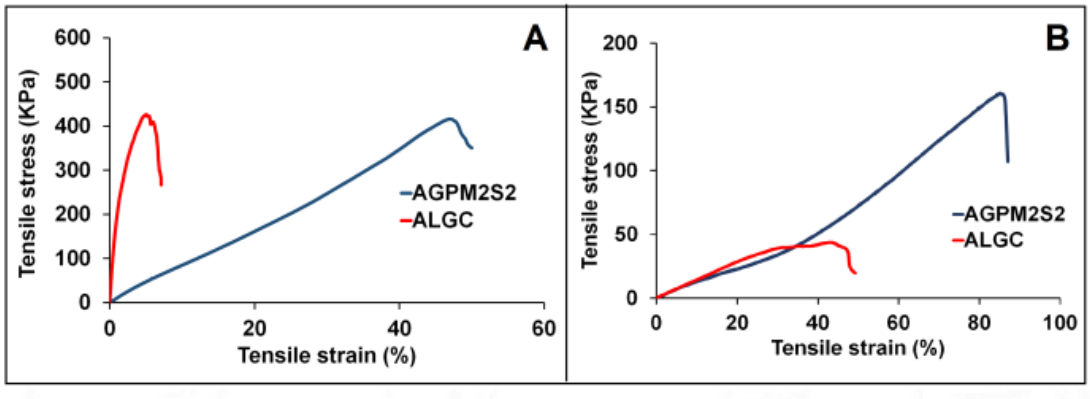

Figure 20: Tensile strength of AGPM2S2 xerogel analysed in A) dry condition and B) wet condition and compared with alginate controls.

4.1.2.2.4 Morphological characterization

The surface morphology of AGPM2S2 was analyzed by micro CT as well as by scanning electron microscopy analysis (figure 21). The pores of the xerogels showed a narrow distribution curve ranging from 80 -120µm in size. The SEM analysis showed that the pores have a smooth and firm topography. However some debris was noticed over the surface of the pores. The number of pores were lower compared to alginate controls, but it was good well-formed within the xerogel AGPM2S2. The pore size was found to be 80±37 µm for AGPM2S2 xerogel and 222 ± 68 µm for alginate controls. The network size of alginate gel depends on the length of the junctional

zones. As the M/G ratio increases, M block increases and the length of the junction zone decreases, resulting in decrease in network size (Yamagiwa et al., 1995). Martinsen et al reported the gels with high G content have bigger pore size than gels with high polyM content by SEM analysis (Martinsen et al., 1992).

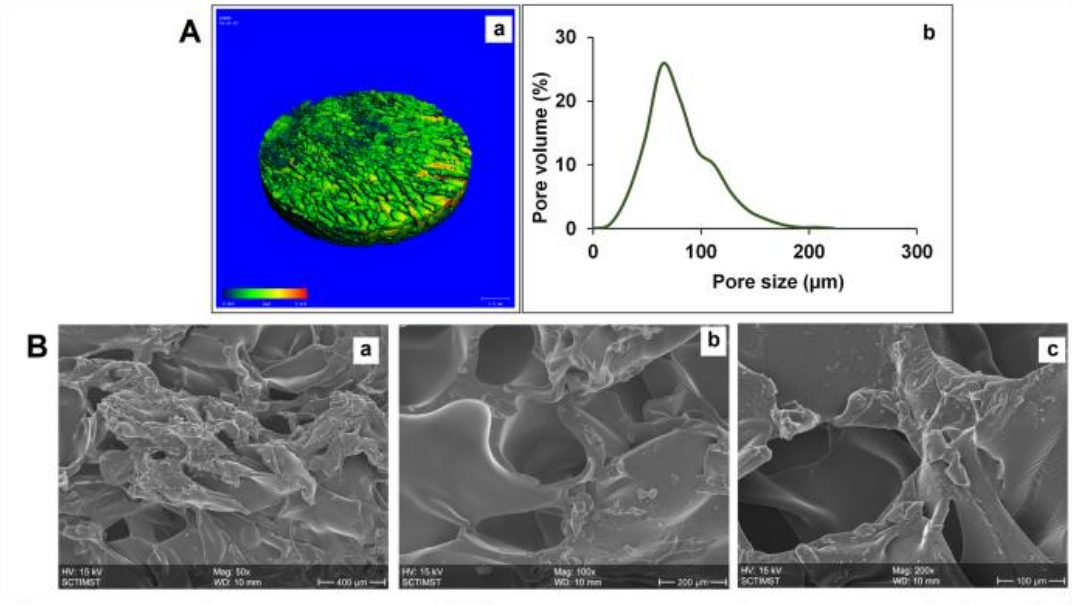

Figure 21: A) Micro computed tomography image and distribution of the pores in AGPM2S2 xerogel and B) Scanning electron microscopy images of AGPM2S2 xerogel (a-c) at different magnification (50x, 100x and 200x).

The thermogram of AGPM2S2 showed typical curve of PEGMA molecule (figure 22 A). The PEGMA molecules undergo degradation mainly in three stages. During stage1, moisture loss occurs at 100℃, with a mass loss of 1.1%, followed by 88% weight loss occurring at 238-415℃ and finally 8.75% weight loss occurs at 415-800℃. The calcination process or residue formation occurs at >800℃ (2.57%) (Savin et al., 2019). The xerogel showed 5% weight loss as moisture at 88℃, followed by 50% weight loss at 373℃. Finally, the residue formation occurred at 986℃ (10.17%), which corresponds to the metal oxides of strontium ions cross-linked within the

xerogel. The surface hydrophilicity was analyzed by the contact angle measurement. The AGPM2S2 xerogels showed a higher contact angle of 94°, but that of alginate control was 54.7° (figure 22 B). The grafting with poly (PEGMA) chains causes a reduction in the hydrophilic nature of the alginate.

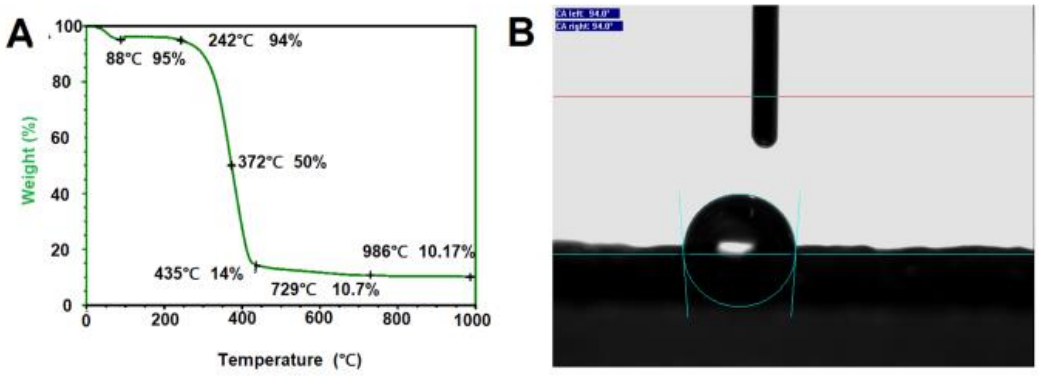

Figure 22: A) Thermogram of AGPM2S2 xerogel showing the temperature for different stages of degradation and the corresponding percentage weight B) Contact angle measurement of AGPM2S2 xerogel by sessile drop method.

4.1.2.1.5 Strontium ion quantification

The strontium ions present within the xerogel AGPM2S2 was analysed by various techniques. Only 12±3.4% of the strontium ions were present within the xerogel after the cross-linking reaction. But the release of strontium ions from the xerogel was found to be higher upto 42±4.3% within 72h (figure 23 A). Strontium ions have selective preference towards polyG block and have weaker interaction with polyM blocks. So the high polyM content is advantageous as the Sr binding affinity is weak and easily dissociate from the material. The release of strontium ions showed an initial burst release up to 8h followed by a slow phase. Place et al compared the release pattern of strontium ions form AlgG and AlgM, concluded that alginate rich in M block

released strontium very fast compared to G block rich alginate, because the selectivity in binding was absent with AlgM (Place et al., 2011). It is reported that a low quantity of strontium cannot influence cellular proliferation and also a high level of strontium can disrupt the cellular metabolic processes. Here a controlled release pattern was observed with high M alginate which is biologically significant and can be beneficial therapeutically.

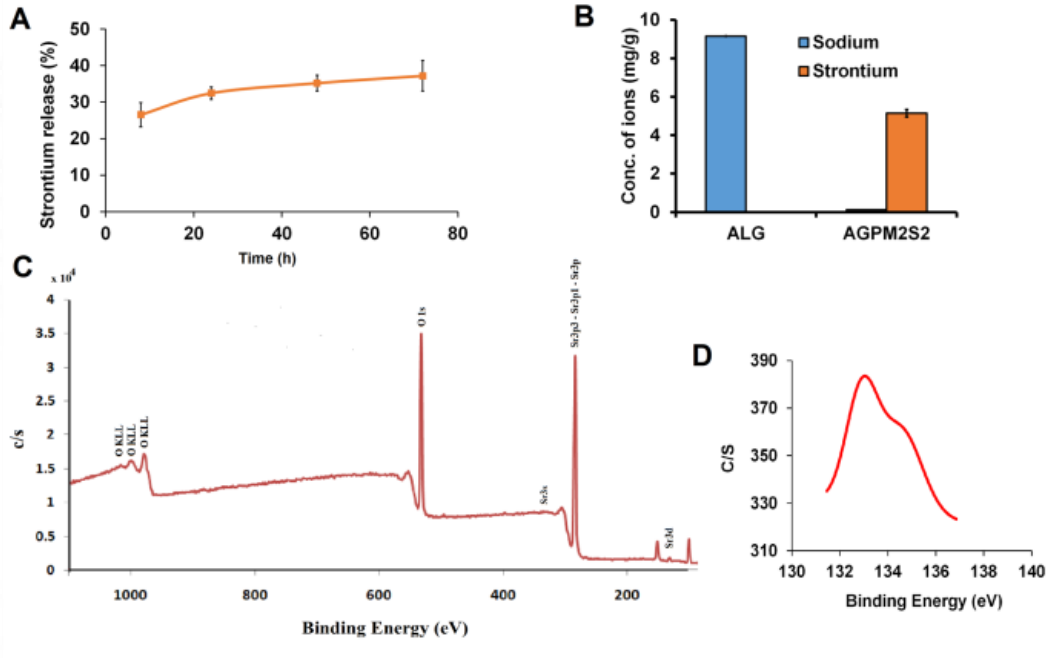

Figure 23: A) The percentage of strontium ions released from AGPM2S2 xerogel placed in PBS (pH 7.4) analysed upto 72h. B) Strontium ion quantification by ICP analysis. C) Survey spectra of the xerogel by XPS analysis and D) Binding energy calculation of strontium ions within the xerogel by XPS analysis.

The ICP results showed that the xerogel contain 5.1mg/g strontium ions and 0.11mg/g sodium ions, whereas that of alginate control had 9.16 mg/g sodium ions with no traces of strontium ions (figure 23 B). The concentration of strontium ion on the surface of the xerogel was further analysed by XPS, which measures the amount

of strontium ion present within 10nm from the surface (figure 23 C-D). From the figure it can be seen that the amount of strontium is 0.2% in Sr3d state and with a binding energy of 132.8 eV. The survey scan spectra showed the other elemental composition of the xerogel as C1s-69%, O1s-30.9% and N1s-0.6%. The deviation in binding energy compared to $SrCl_2$ standard (134 eV) was due to the physical interaction of strontium ions within the gel. Strontium ions are one of an alkaline earth metal having high water hydration energy that helps in swelling. On contact with water, more water bound to the coordination shell of Sr^{2+} at both internal and external region. More water get retained in the internal region due to smaller relaxation energy compared to outer surface. In this condition, a chemical shift was observed in Sr3d state upon changing the relative humidity (RH) from 0% to7%, which is observed as a change in the electrostatic energy as the result of swelling (Boucly et al., 2018).

The hemostatic activity and collagenase inhibitory activity of the xerogel was analysed. The role of strontium ions in hemostatic activity and collagenase inhibitory activity was analysed (figure 24 A-B). The AGPM2S2 xerogels showed 46% hemostatic activity within 5 minutes compared to 6% by alginate controls. The hemostatic activity further increased up to 75% and 84% for 8 min and 10 min respectively. The role of released strontium ions in the inhibition of collagenase activity was also analysed. The collagenase inhibitory activity of the xerogel was 36±2.3% compared to 33±3.1% of strontium ions (3mM). A significant increase in the collagenase inhibitory activity was observed with AGPM2S2 xerogel compared to controls. This was due to the increased release of strontium ions from the AGPM2S2

xerogel compared to the previous one. Braux et al studied the effect of strontium ions in MMP expression in bone cells. They observed that $SrCl_2$ showed a significant reduction in the expression of MMP1mRNA in bone cells compared to controls (Braux et al., 2011). So the localized delivery of strontium ions have a positive effect on MMP-TIMP balance, which is important for extracellular matrix formation.

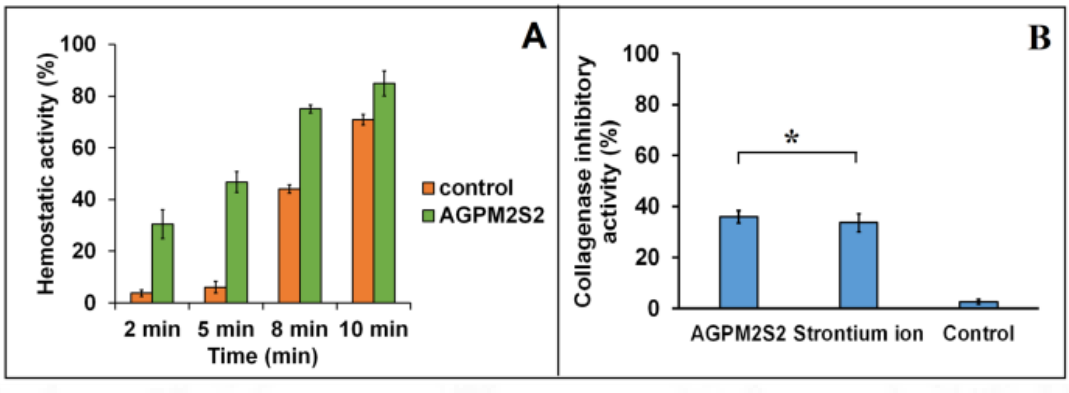

Figure 24: A) The percentage of haemostatic activity of the xerogel AGPM2S2 and the alginate control analysed at different time points (2 min, 5min, 8min and 10min). B) Collagenase inhibitory activity of the xerogel compared with strontium ions (3mM) and alginate controls (*p<0.05).

4.1.2.1.6 Cell culture studies

The cytotoxicity of the material AGPM2S2 was assessed by cell viability assays. MTT assay was performed on fibroblast cells and keratinocytes (figure 25 A). The test on extract studies on L929 cells showed >80% viability for cells treated with 1mg/ml and 5mg/ml extract of the xerogel up to 72h, whereas the extracts of 10mg/ml showed decrease in viability after 48h. Test on extract study on HaCaT cells showed >70% viability up to 48h with 5mg/ml extract. But the 10mg/ml extract of the xerogel was found to be cytotoxic on HaCaT cells. The direct contact (figure 25 B) of the xerogel AGPM2S2 over L929 cells for 24h showed that majority of the cells retained

the morphology. But after 48h contact, a change in cell morphology was noticed near the xerogel. This was further confirmed by live dead assay (figure 25 C). The percentage of dead cells analysed by live dead assay was 12% and 26% with the treatment of 24h and 48h extracts of the xerogels respectively. Some studies reported that the presence of PEG chains can impart cytotoxic effect. Liu et al demonstrated molecular weight dependant cytotoxicity by PEG on L929 cells with treatment of polyethylene glycol derivatives (Liu et al., 2017).

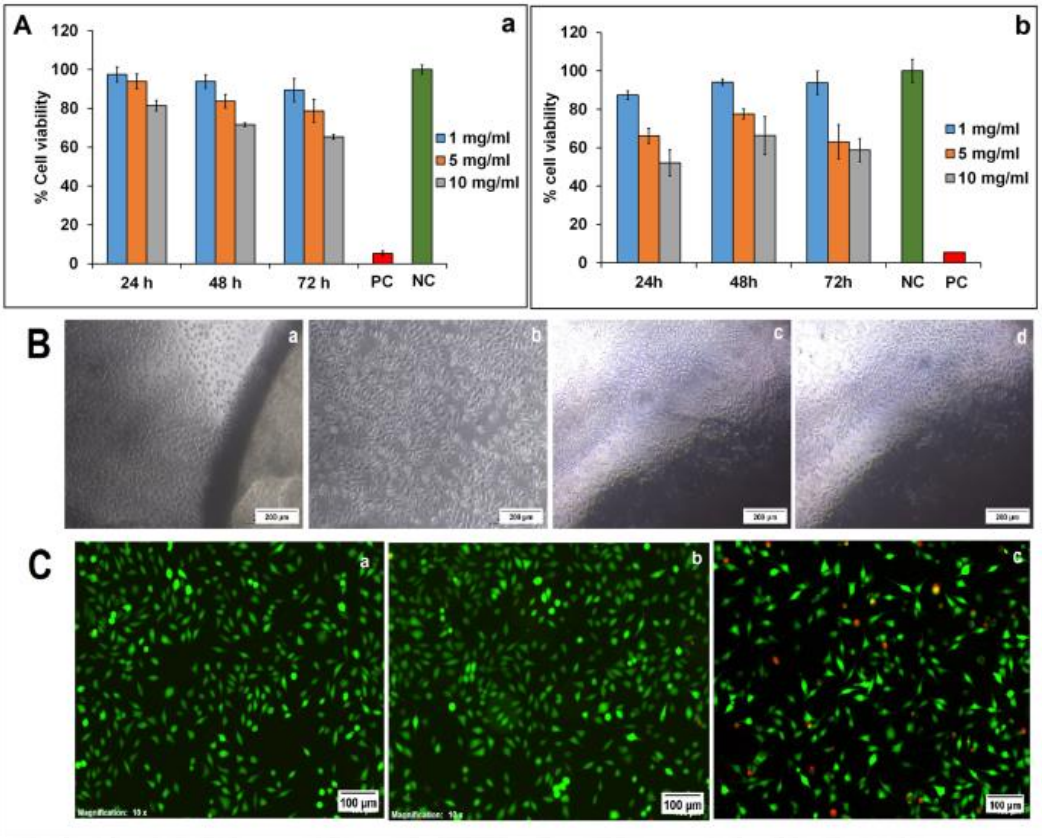

Figure 25: A) Test on extract study on a) L929 fibroblast and b) HaCaT keratinocytes treated with the extracts of the xerogel AGPM2S2 at different time points (24h, 48h and 72h). B) The direct contact assay on L929 cells a) positive control b) negative control c) 24h and d) 48h contact of AGPM2S2 hydrogel. C) Live dead assay on L929

cells treated with a) media alone b) 24h extract and c) 48h extract of AGPM2S2 hydrogel.

The *in vitro* wound healing effect of the xerogel AGPM2S2 was analysed by scratch wound assay on HaCaT cells (figure 26). Cells treated with growth medium alone were treated as the negative control and strontium ions (3mM) as the positive control. At 4h, the % wound closure for xerogel AGPM2S2, NC and PC were 34±2.7%, 20±2.6% and 59±6.4% respectively. After 48h, >90% wound closure was observed with AGPM2S2 and PC. The material showed a significant improvement in the wound closure compared to negative control. Strontium ions can substitute calcium ions almost quantitatively due to the similarity in their size. The radius of Ca^{2+} ions is 0.99 Å, while that Sr^{2+} ions is 1.12 Å. So Sr^{2+} ions can participate in the various cellular process mediated by Ca^{2+} ions. Cox et al reported the substitution of Sr^{2+} ions for Ca^{2+} ions in stimulating the thymidine incorporation and 2-deoxy glucose uptake (Cox et al., 2011). According to a study by Praeger et al., the cell yield achieved with 1.8 mmol.L-1 $SrCl_2$ treatment was consistently and statistically higher than those produced with any quantity of $CaCl_2$ (Praeger et al., 1987). Strontium ions have significant role in enhancing the fibronectin production form keratinocytes, which helps to improve cell matrix interaction and cell movement (Toda and Grinnell, 1987).

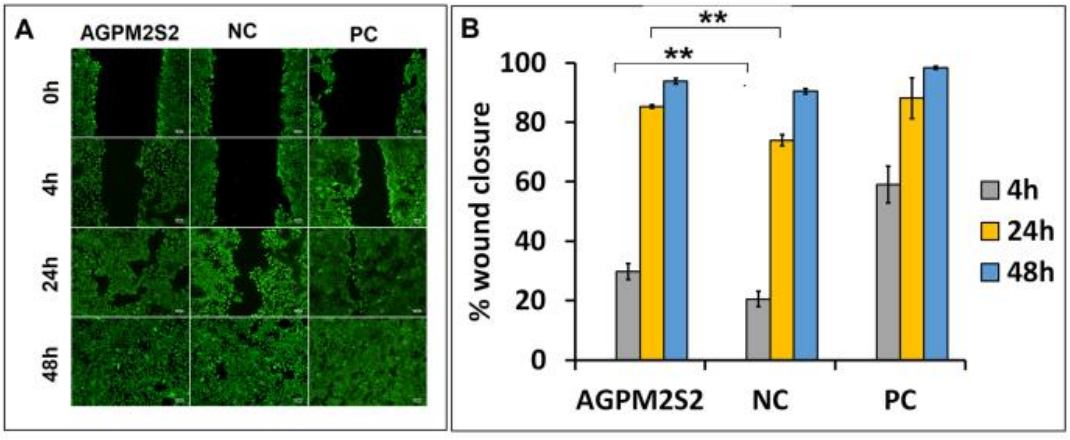

Figure 26: Scratch wound assay on HaCaT cells treated with extract of AGPM2S2 xerogel and compared with NC and PC (NC: negative control-media alone, PC: positive control-strontium ion (3mM) B) Percentage wound closure analyzed by ImageJ software up to 48h (**p<0.001).

4.1.2.3 Synthesis and characterization of alginate diamine PEG-g-poly(PEGMA) xerogels

Alginate diamine PEG conjugate (ADPEG) was synthesized by EDC reaction. After conjugation reaction, a change in zeta potential was noticed from -47.7 ± 2.4 mV that of native alginate to -30.1 ± 1.3 mV for the conjugate. The conjugate had 47±4% free carboxyl groups and 52±3% free amino groups. ADPEG was further grafted with poly (PEGMA) chains by free radical reaction and the grafting parameters were calculated (figure 27A). The grafting of poly (PEGMA) chains occurred by the extraction of hydrogen from 2^{nd} and 3^{rd} –OH groups of alginate and also from NH_2 group of diamine PEG molecule. The grafting efficiency and grafting yield determine how effectively PEGMA chains got grafted with alginate-diamine PEG. All formulations showed 80-90% grafting efficiency, but >80% grafting yield was obtained with ADPM1 and ADPM2. The homopolymer chain formation was also <20% for ADPM1 and ADPM2. A reduction in free amino groups was noticed (figure

27 B) with ADPM1 and ADPM2 to 19±4.6% and 20±3.8% respectively, which confirmed the conjugation reaction. The conjugation with diamine PEG molecule prior to grafting helps to reduce the PEGMA concentration, which further reduces the chance of homopolymer chain formation. ADPM2 showed a significant improvement in grafting efficiency and reduction in free amino group compared to ADPM1. An increase in molecular weight was noticed with GPC analysis. ADPM2 showed an increase in molecular weight of 57000Da from native alginate (ADPM2: $2.3x10^5$ Da, alginate: $1.8x10^5$ Da) by GPC analysis. The conjugation with bifunctional monomers such as diamine PEG (jeffamine) helps to tune the properties of hydrogel. Jeffamine can from network with lower cross-linking density, consequently with higher swelling ability. Studies showed that, jeffamine incorporated hydrogels have pH and thermoresponsive behaviour (Karakasyan et al., 2015). An injectable hydrogel of hyaluronic acid conjugated with jeffamine developed by Madau et al showed excellent rheological properties (Madau et al., 2021). Due to the stimuli responsive behaviour of jeffamine molecule, its incorporation within the hydrogel could be beneficial in biomolecule delivery towards the changing wound microenvironment.

Based on the results ADPM2 was selected as the optimized formulation for xerogel synthesis.

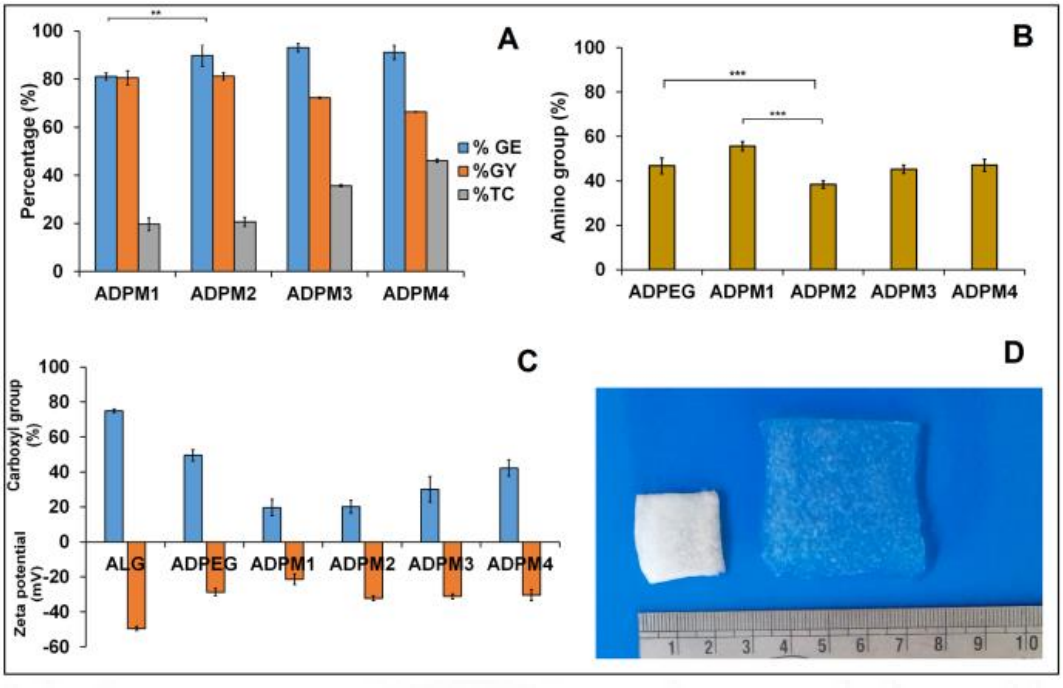

Figure 27: A) Grafting parameters of different formulations of Alginate diamine-g-poly (PEGMA), % GE- % grafting efficiency, %GY - % grafting yield, % TC - % conversion into homopolymer of poly (PEGMA). The difference in grafting efficiency between ADPM1 and ADPM2 is significant at **$p < 0.01$. B) Percentage of free amino groups of different formulations (***$p<0.001$) C) The extent of grafting of poly (PEGMA) chains to alginate analyzed by estimating % free carboxyl groups and zeta potential, compared with ungrafted alginate as control and D) Conversion xerogel into hydrogel on contact with water or buffer.

Xerogels of ADPMS were synthesized by crosslinking ADPM2 using varying concentration of strontium ion and thus obtained gels were subject to freeze drying. The obtained xerogels were as ADPM2S1, ADPM2S2, ADPM2S3 and ADPM2S4. A reduction in the diameter of the xerogel was noticed with increasing strontium ion concentration. On contact with water the xerogel got converted to hydrogel without compromising its mechanical stability (figure 27 D). All batches of xerogel showed good flexibility, both in dry and wet conditions. The adhesive nature was found to be

reduced compared to AGPMS xerogels due to reduced concentration of PEGMA used for xerogel synthesis.

4.1.2.3.1 Chemical characterization

The conjugation of alginate with diamine PEG and grafting with poly (PEGMA) chains were confirmed by FTIR and NMR analysis (figure 28). After diamine PEG conjugation, the characteristic –CH stretching of poly (ethylene glycol) was obtained at 2816 cm^{-1} and 2302 cm^{-1}. At 1583 $cm^{1,}$ the –NH bond (amide II) was observed, which confirmed the conjugation of diamine PEG molecule with alginate. ^{1}H NMR spectra showed protons of methyl and amino groups of PEG molecule at 1.1 to 1.4 ppm and 1.78 ppm respectively. After grafting with poly(PEGMA) chains, a chemical shift around 2.62 to 3.24 was observed which corresponds to the methylene protons of poly(PEGMA) and peak at 1.84 shows methyl groups of poly(PEGMA). Due to the conjugation with diamine PEG molecule, the vinyl protons of PEGMA at 5.70 and 6.10 has been shifted to 4.2 and 5.0 (Emaldi et al., 2017).

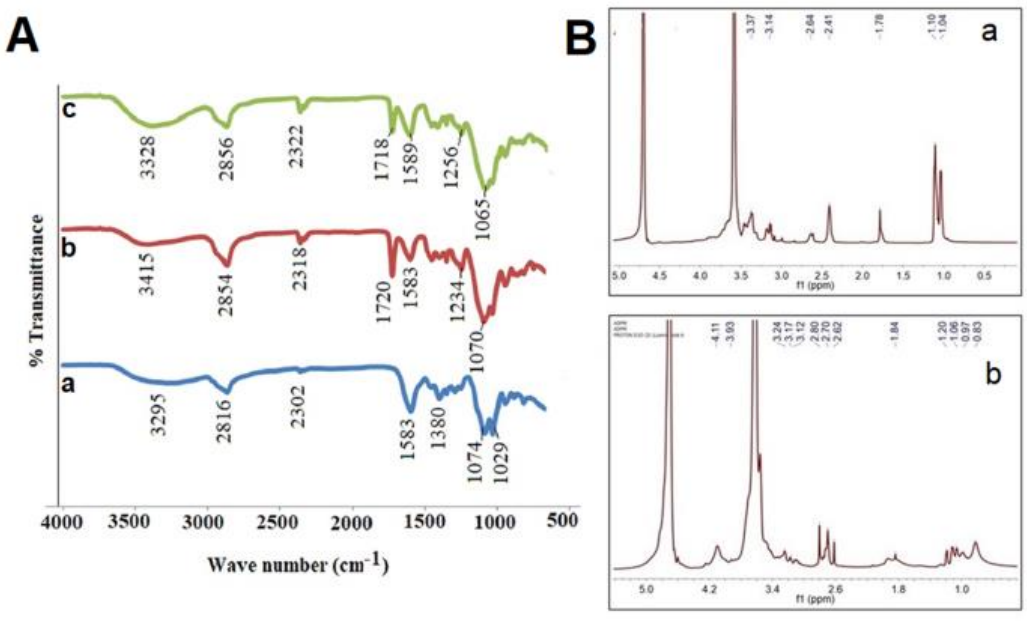

Figure 28: A) FTIR spectra of a) alginate diamine PEG (ADPEG) conjugate, b) alginate diamine-g-poly (PEGMA) (ADPM2) formulation and c) alginate diamine-g-poly (PEGMA) xerogel. B) ^{1}H NMR spectra of a) alginate diamine PEG (ADPEG) conjugate and b) alginate diamine-g-poly (PEGMA) (ADPM2) formulation.

4.1.2.3.2 Physical characterization

The percentage swelling of the xerogels was analyzed up to 48h at different pH (figure 29). Among which ADPM2S1 showed higher swelling of 2000% at all pH. Due to higher strontium ion crosslinking with ADPM2S4, the swelling reduced to half to 1000%. ADPM2S2 hydrogel showed a % swelling ranging from 1200 to 1600% at different pH over a period of 48h. The hydrophilic gels reaches equilibrium swelling as the hydration force get counter balanced by the cross-linking network. The swelling of ADPM2S2 at pH 6.8, 7.4 and 8 was similar, 1663±46%, 1564 ± 62% and 1564 ± 96% respectively. But at pH 5.8, swelling was reduced to 1230 ± 46%.

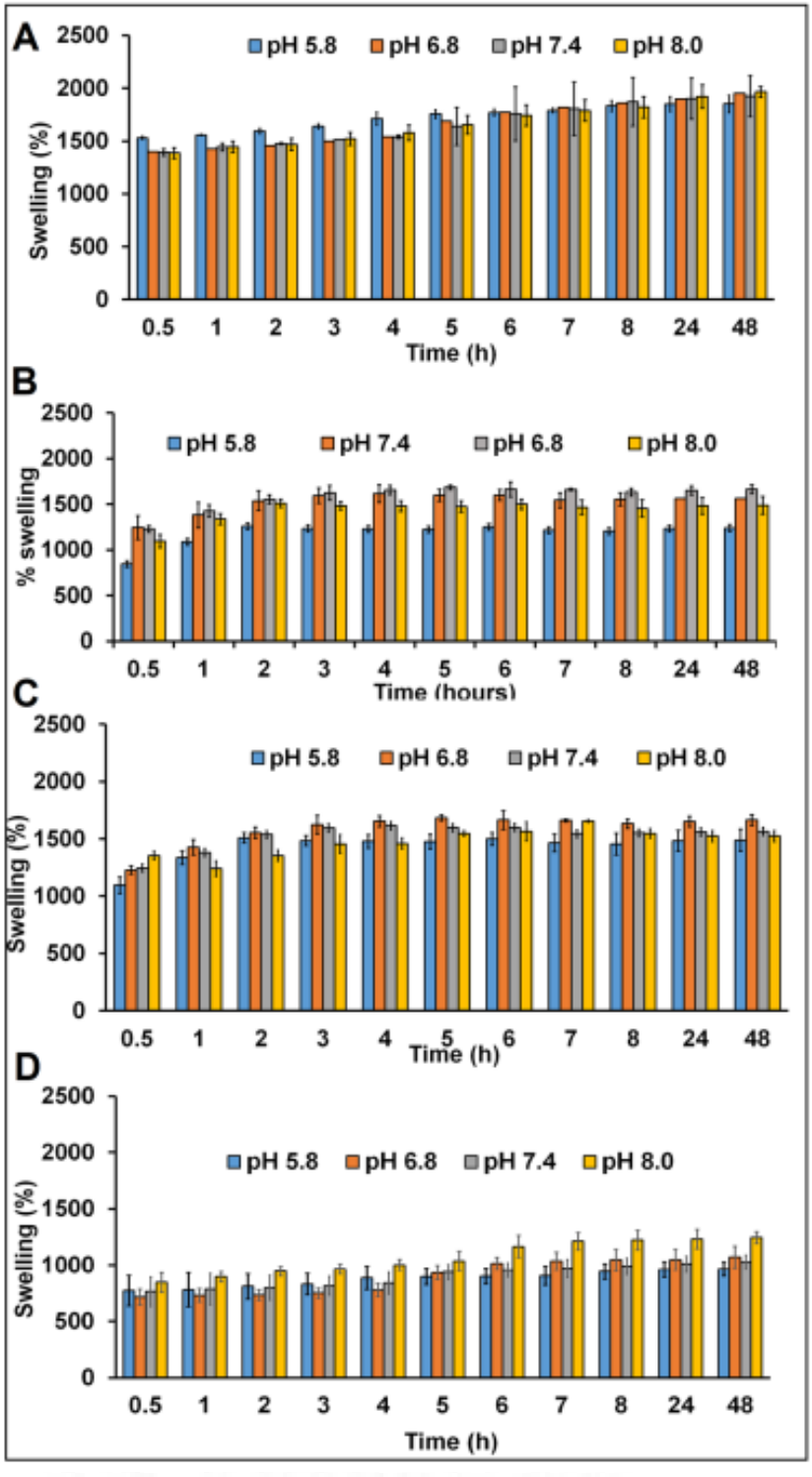

Figure 29: The percentage swelling of different alginate diamine-g-poly (PEGMA) xerogels A) ADPM2S1 B) ADPM2S2 C) ADPM2S3 and D) ADPM2S4 at different pH (5.8, 6.8, 7.4 and 8.0) analysed upto 48h.

The WVTR of the xerogels were ranging from 1400 -1500 g/m^2/24h at 37°C. The reduced swelling at acidic pH helps to control the unnecessary release of bioactive molecules loaded within the material as the wound heals. A reduction in percentage porosity was observed from 84% to 60% by increasing cross-linking concentration. The biodegradation studies were carried out in pseudo extracellular fluid at pH 7.4. All xerogels except ADPM2S1, showed <20% weight loss analyzed upto 72h. The xerogels ADPM2S1 and ADPM2S4 were omitted due to higher degradation and lower swelling respectively. Among ADPM2S2 and ADPM2S3, a stable swelling pattern was observed with ADPM2S2 and it has been further selected for characterization.

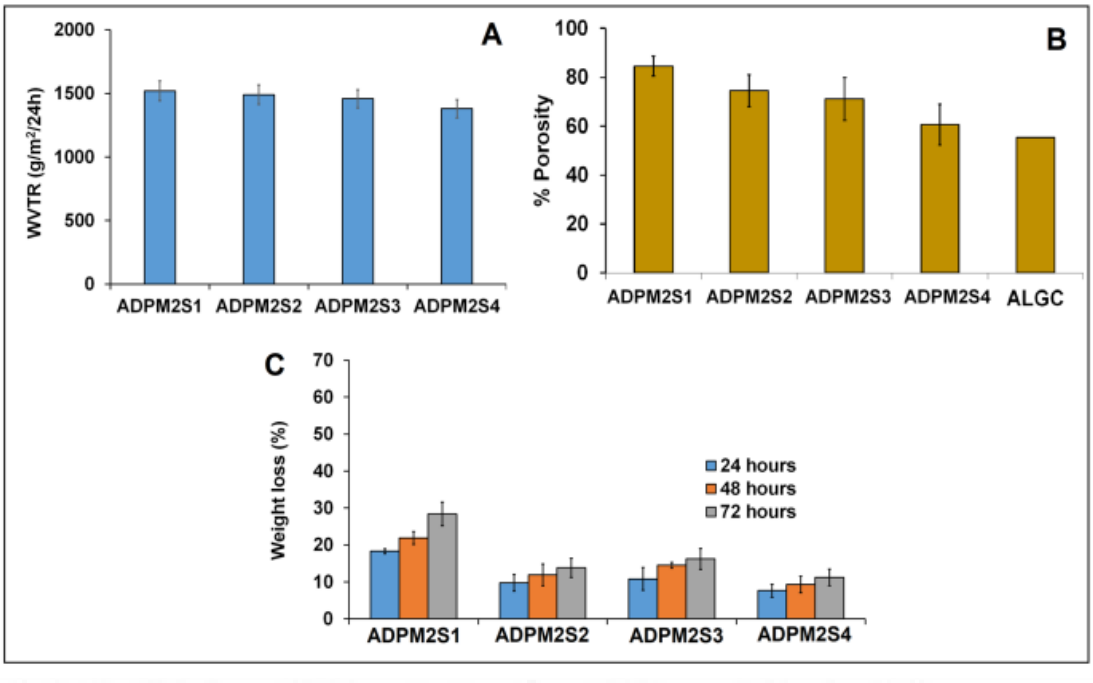

Figure 30: A) Water vapor transmission rate B) Percentage porosity and C) Percentage weight loss in pseudo extracellular fluid (pH 7.4) of different alginate diamine-g-poly (PEGMA) xerogels.

4.1.2.3.3 Mechanical characterization

The mechanical strength of the optimized xerogel in both dry and wet conditions were analysed (figure 31 A-B). The AGPM2S2 xerogel had a tensile strength of 435 ± 39KPa in dry state and 48±7KPa in wet condition. The modulus of the xerogel was 1.6±0.12MPa and 0.12±0.08 MPa in dry and wet conditions respectively. But in the case of alginate controls, tensile strength was found to be 400 ± 30 KPa in dry state and 27 ± 6 KPa in wet condition.

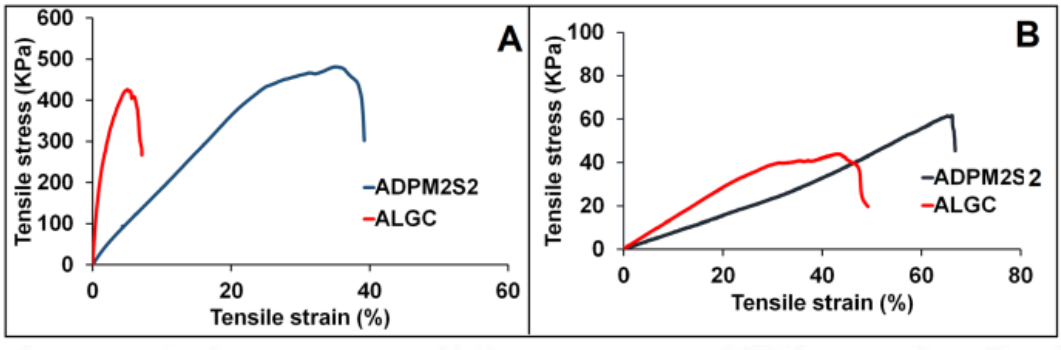

Figure 31: Tensile strength of ADPM2S2 xerogel analysed in A) dry condition and B) wet condition and compared with alginate controls.

Jeffamine based hydrogels have greater segmental flexibility, which provides better mechanical properties (Sharifi et al., 2014). The xerogel showed 2 fold increase in tensile strength in wet condition compared to alginate control. The bioadhesive force of the xerogel was 0.55 ± 0.07N/cm, whereas it was 1.28 ± 0.09N/cm for alginate controls. The bioadhesive force measured on wounded skin shows a peak adhesion force of 0.54 ± 0.08 N/cm and 0.52 ± 0.05N/cm for the xerogel and alginate control respectively. The low bioadhesive nature of the material enables the pain free removal from the wound surface. The other parameters are as mentioned in the table 7.

Mechanical Characterization		ADPM2S2	ALGC
Test condition	**parameters**		
Xerogel (dry condition)	Tensile strength (KPa) Modulus (MPa)	435 ± 39 1.6 ± 0.12	400 ± 30 9.9 ± 1.3
Hydrogel (wet condition)	Tensile strength (KPa) Modulus (MPa)	48 ± 7 0.12 ± 0.08	27 ± 6 0.18 ± 0.01
Normal rat skin	Bioadhesive force (N/cm) Work of adhesion (g.sec)	0.55 ± 0.07 17.6 ± 6.0	1.28 ± 0.09 1.9 ± 0.12
Wounded rat skin	Bioadhesive force (N/cm) Work of adhesion (g.sec)	0.54 ± 0.08 27 ± 10	0.52 ± 0.05 29 ± 14

Table 7: Comparison of mechanical properties of ADPM2S2 xerogel with alginate control.

4.1.2.1.4 Morphological characterization

The surface characteristics of the xerogel were analyzed by micro CT and SEM analysis. The micro CT data showed (figure 32 A) a narrow pore distribution with ADPM2S2 ranging from 70-100µm. The SEM analysis showed that (figure 32 B) the pores were well-formed, without any debri deposited over the surface of the xerogel. The pore size was found to be 76±24 µm for ADPM2S2 xerogel and 222 ± 68µm for alginate controls.

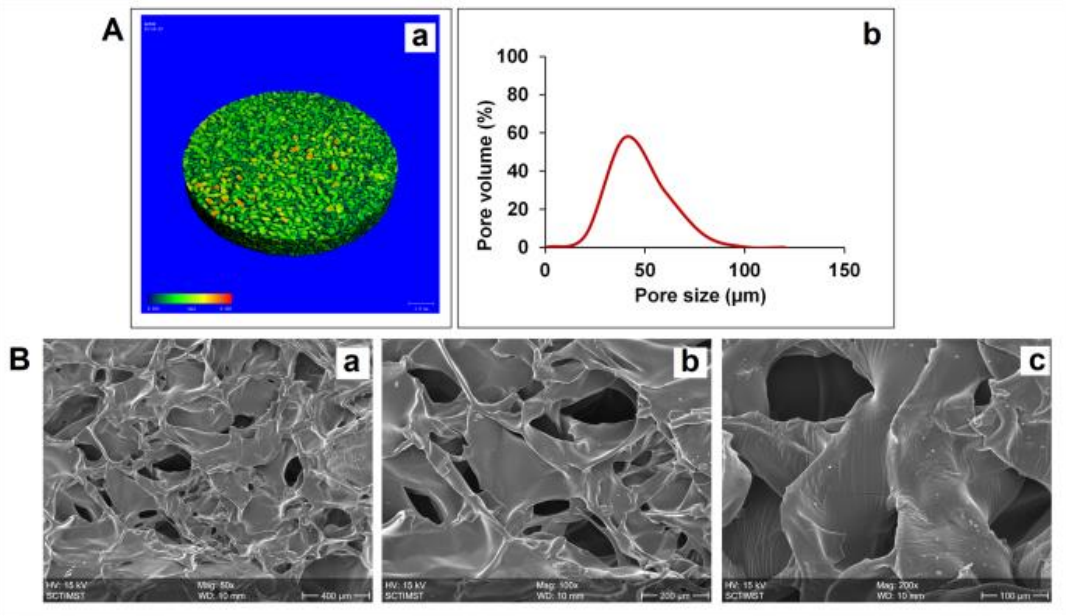

Figure 32: A) Micro computed tomography image and distribution of the pores in ADPM2S2 xerogel and B) Scanning electron microscopy images of ADPM2S2 xerogel (a-c) at different magnification (50x, 100x and 200x).

The thermogram (figure 33 A) of the ADPM2S2 xerogel showed typical degradation pattern of PEGMA monomers. The xerogel showed a 2.1% weight loss at nearly 100℃ which can be attributed to moisture content, followed by 50% weight loss at 370℃. Finally only residues remained at 789℃ (1.7%), which corresponds to the metal oxides of strontium ions cross-linked within the xerogel. The surface hydrophilicity was analyzed by the contact angle measurement. The ADPM2S2 xerogels showed a contact angle of 67.2°, while that of alginate control was 54.7° (figure 33 B). PEGMA grafting incorporates hydrophobicity to the xerogel surface. Upon contact with water, the minimum interfacial free energy of the hydrated poly(ethylene glycol) side chain, high surface mobility and steric repulsion effect contribute to the hydrophobic nature (Stadler et al., 2008). The high density of network

formed by the alginate gel limits the cell growth and cell anchorage. The protein absorption to the biomaterial surface is necessary to promote cell anchorage. But the hydrophilic nature of the alginate gels limits the protein absorption. The grafting of PEG molecules imparts hydrophobic nature to the alginate matrix, which promotes protein absorption and consequently cell anchorage. The hydrophobized derivatives of alginate has various applications, such as enzyme immobilization (Laurienzo et al., 2005). Since the concentration of PEGMA was reduced compared to the AGPM2S2 xerogel, the hydrophilic nature of the ADPM2S2 xerogel was greater than AGPM2S2.

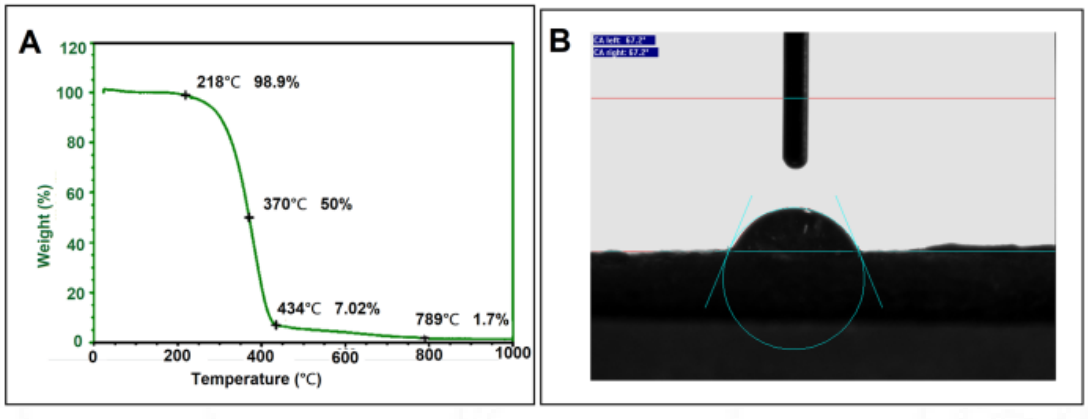

Figure 33: A) Thermogram of ADPM2S2 xerogel showing the temperature for different stages of degradation and the corresponding percentage weight B) Contact angle measurement of ADPM2S2 xerogel by sessile drop method.

4.1.2.1.5 Strontium ion quantification

The concentration of strontium ion present within the xerogel was quantified by various techniques. The amount of strontium ions involved in cross-linking was found to be 17±2.6% among which 42±4.1% released at pH 7.4 within 72h (figure 34 A). The ICP analysis revealed that the xerogel possess 5.52mg/g strontium ions and 0.038mg/g sodium ions, whereas that of alginate control had 9.16 mg/g sodium ions with no traces of strontium ions (figure 34 B). The XPS analysis (figure 34 C-D)

showed that, there was 0.3% strontium ions within 10nm from the xerogel surface in Sr3d state, with a binding energy of 135.2eV. The survey scan spectra showed the other elemental composition of the xerogel as C1s-76.4%, O1s-23% and N1s-0.3%.

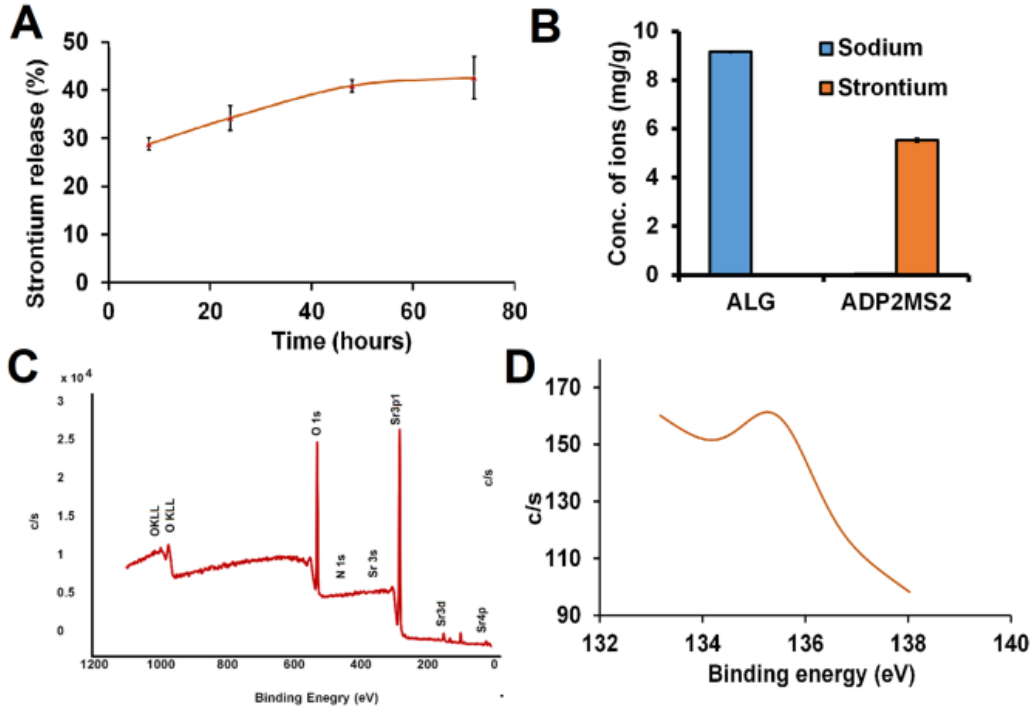

Figure 34: A) The percentage of strontium ions released from ADPM2S2 xerogel placed in PBS (pH 7.4) analysed upto 72h. B) Strontium ion quantification by ICP analysis. C) Survey spectra of the xerogel by XPS analysis and D) Binding energy calculation of strontium ions within the xerogel by XPS analysis.

The role of strontium ions in hemostatic activity and collagenase inhibitory activity was analysed (figure 35 A-B). The ADPM2S2 xerogels showed 59% hemostatic activity within 5 minutes compared to 6% by alginate controls. An increase in hemostatic activity noticed after 8 min (78%) and 10 min (84%). The collagenase inhibitory activity of the xerogel was 39±2.1% compared to 33±3.1% of strontium ions (3mM) treated as positive control. A significant improvement in the collagenase inhibitory activity was noticed with ADPM2S2 xerogel compared to positive control.

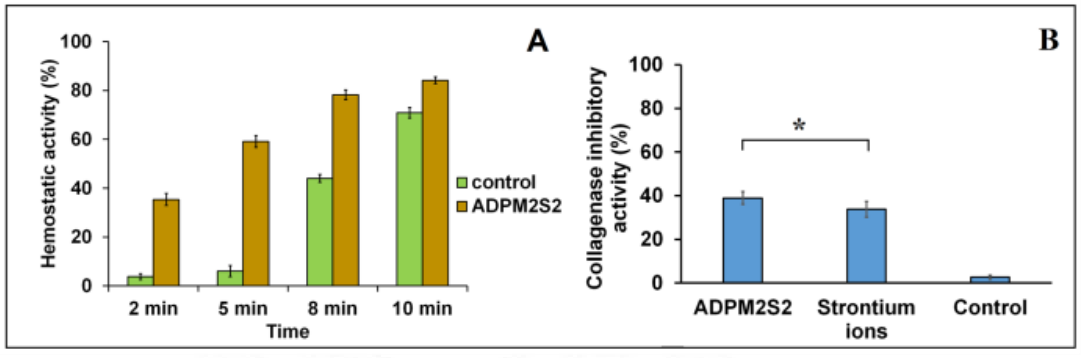

Figure 35: A) The percentage of haemostatic activity of the xerogel ADPM2S2 and the alginate control analysed at different time points (2 min, 5min, 8min and 10min). B) Collagenase inhibitory activity of the xerogel compared with strontium ions (3mM) and alginate controls (*p<0.05).

4.1.2.1.6 Cell culture studies

The cytotoxicity of the xerogel ADPM2S2 was assessed by cell viability assays. MTT assay was performed on fibroblast cells and keratinocytes (figure 36 A). The test on extract studies on L929 cells showed >80% viability for cells treated with 1mg/ml and 5mg/ml extract of the xerogel up to 72h, whereas the extracts of 10mg/ml showed decrease in viability after 48h. Test on extract study on HaCaT cells showed >75% viability upto 48h with 10mg/ml extract. The 1mg/ml extract and 5mg/ml extracts were non-cytotoxic to HaCaT cells upto 48h. The direct contact (figure 36 B) of the xerogel ADPM2S2 over L929 cells showed that more than 80% of the cells retained the morphology even after 48h of contact. This was further confirmed by live dead assay (figure 36 C). The percentage of dead cells analysed by live dead assay was <5 with the treatment of 24h and 48h extracts of the ADPM2S2 xerogels. Compared to AGPM2S2 xerogels, improved cell viability was observed with ADPM2S2 xerogels, due to the reduced concentration of PEGMA used for grafting.

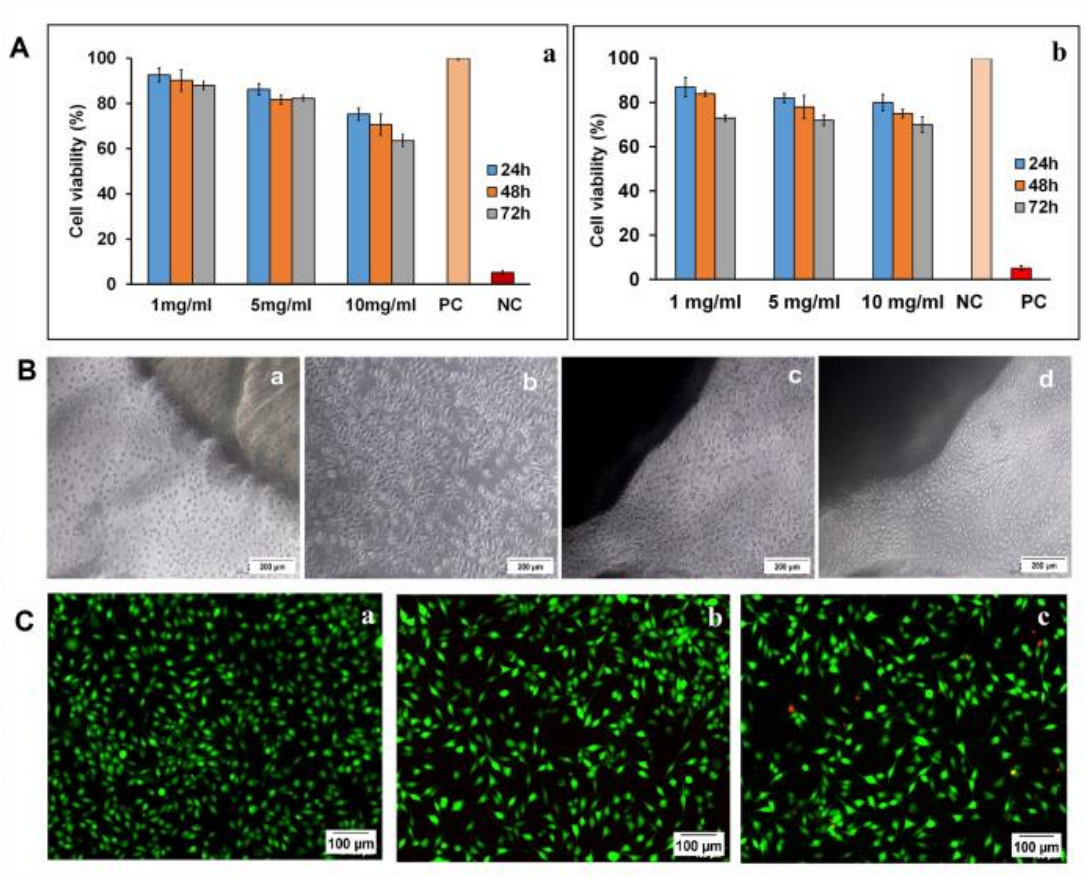

Figure 36: A) Test on extract study on a) L929 fibroblast and b) HaCaT keratinocytes treated with the extracts of the xerogel ADPM2S2 at different time points (24h, 48h and 72h). B) The direct contact assay on L929 cells a) positive control b) negative control c) 24h and d) 48h contact of ADPM2S2 hydrogel. C) Live dead assay on L929 cells treated with a) media alone b) 24h extract and c) 48h extract of ADPM2S2 hydrogel.

The *in vitro* wound healing effect of the xerogel ADPM2S2 was analysed by scratch wound assay on HaCaT cells (figure 37 A-B). Cells treated with growth medium alone were the negative control and strontium ions (3mM) were the positive control. At 4h, the % wound closure for xerogel ADPM2S2, NC and PC were 31±2.5%, 22±2.6% and 61±4.4% respectively. After 24h, >80% wound closure obtained with the xerogel and PC. The wound closure was complete within 48h. The

material ADPM2S2 showed a significant improvement in the wound closure compared to the negative control.

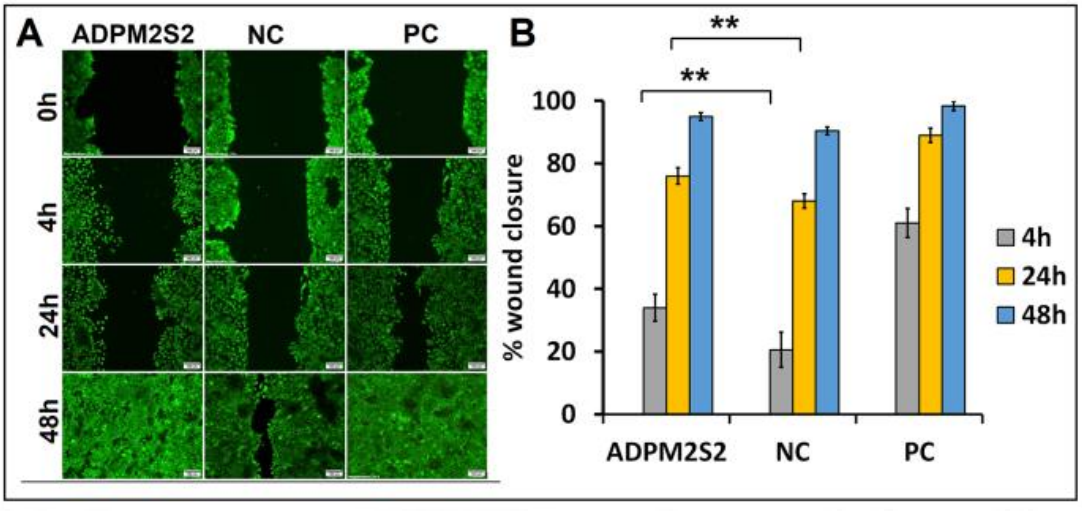

Figure 37: Scratch wound assay on HaCaT cells treated with extract of ADPM2S2 xerogel and compared with NC and PC (NC: negative control-media alone, PC: positive control-strontium ion (3mM) B) Percentage wound closure analyzed by ImageJ software up to 48h (**p<0.001).

4.1.3 Comparison of the xerogels with commercial alginate-based wound dressings

The physical properties of the xerogels were compared with the commercial alginate based wound care material. Two alginate wound dressings were selected for this study and they were coded P1 and P2. The materials were obtained as the sheets of alginate in different dimensions; P1 (10cm x 20cm) and P2 (10cm x 10cm). The percentage swelling, water vapour transmission rate and rate of dissolution were analysed. As shown in the figure 38 A-B, both the materials had a similar pattern of swelling. At pH 5.8 and 6.8, the materials showed a stable swelling upto 48h. The percentage swelling of P1 at pH 5.8 and 6.8 were 1351±87% and 1396±96% respectively. While that of P2 were 1276±74% and 1280±64% at pH 5.8 and 6.8 respectively. But both the products were found to be unstable at pH 7.4 and 8.0. After

24h, the materials got disintegrated in the buffer and observed as deposits of alginate fibres. The WVTR of the products P1 and P2 were 2500±76g/m^2/24h and 2476±74g/m^2/24h respectively (figure 38 C). The stability of the products in pseudo extracellular fluid was evaluated at pH 7.4 (figure 38 D) and the percentage weight loss of P1 was 44±4.2% after 24h and 65±4.3% at 48h. A higher % weight loss was observed with P2, 65±1.2% at 24h and 73±1.5% at 48h. After 72h both the products showed >80% weight loss. By the direct contact assay (figure 39), it was observed that, only 60% of the cells retained the morphology with the contact of the material P1 for 24h. The cell morphology was changing towards round shape within 48h. More number of cells were getting rounded with P2 compared to P1. The fibres of alginate were visible over the cell surface with both the materials and this deposited alginate fibres impart the cytotoxic effect.

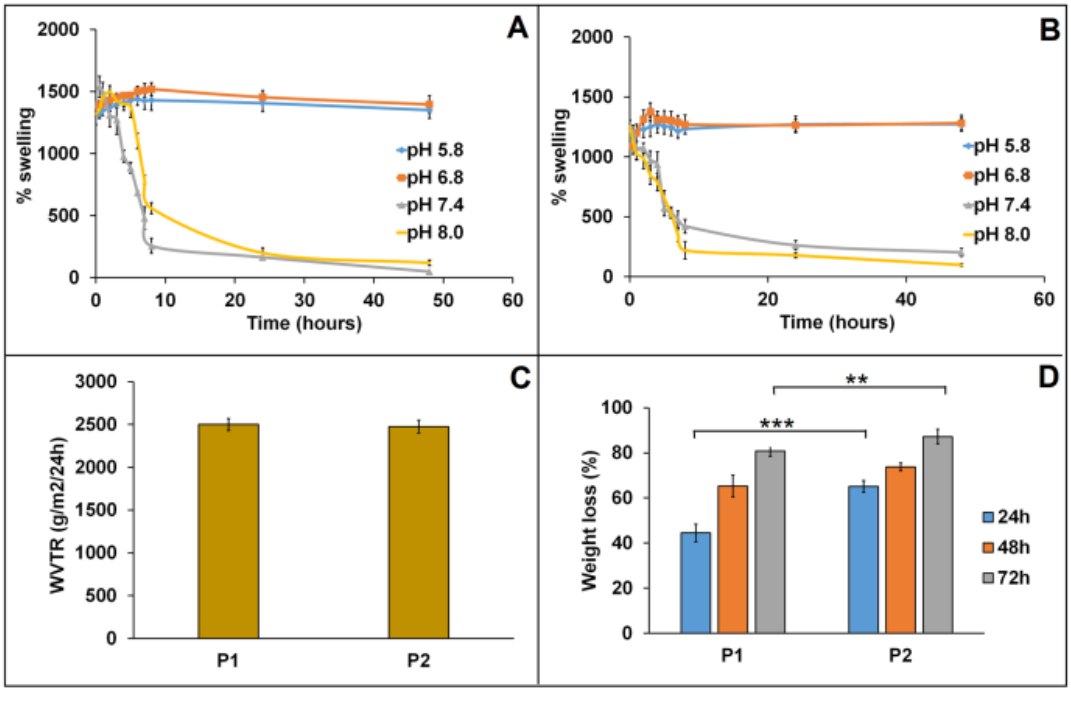

Figure 38: Percentage swelling of A) P1 and B) P2 at different pH (5.8, 6.8, 7.4 and 8.0) C) The comparison of water vapour transmission rate and D) percentage of dissolution in pseudo extracellular fluid (pH 7.4) of the materials P1 and P2 (**p<0.01, ***p<0.001).

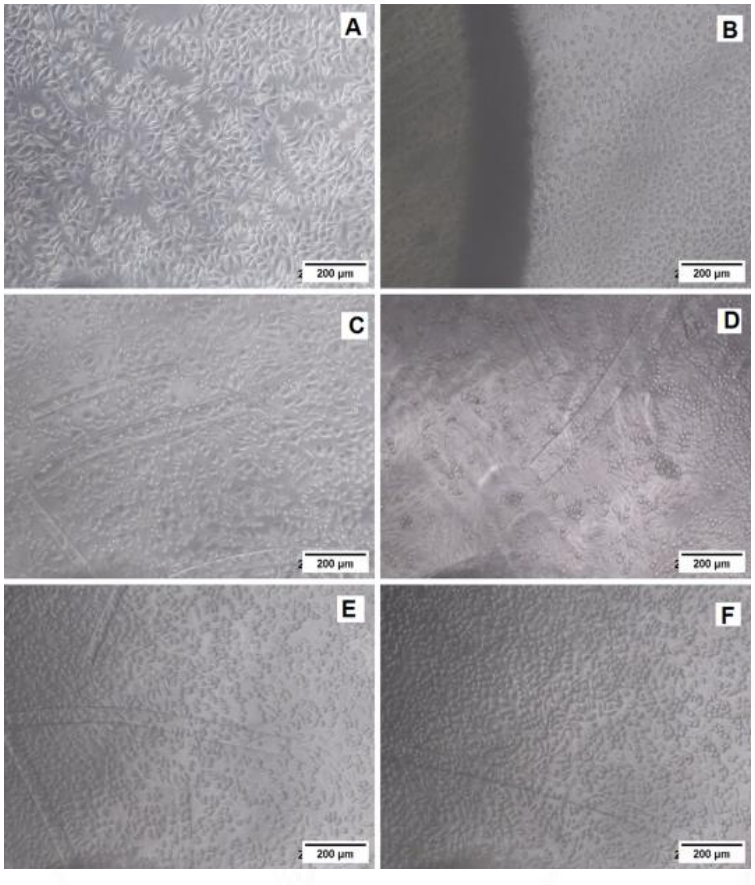

Figure 39: Direct contact assay on L929 cells treated with the materials P1 (C-D) and P2 (E-F) for 24h and 48h and compared with the controls A) NC and B) PC.

While comparing the physical properties of the in-house developed xerogel with the commercial alginate based products, the xerogels showed stable pattern of swelling at different pH (figure 40 A). But the commercial products were unstable at pH above 7. A high rate of dissolution was observed with the commercial products, >80% dispersed into fibres within 72h. But all the xerogels showed very lower rate of dissolution <20% within 72h (figure 40 B). The WVTR of commercial products ranges were 2596±76 g/m^2/24h and 2547±78 g/m^2/24h respectively (figure 40C). As

discussed before, the studies reported that WVTR ranging from 2000-2500 g/m^2/24h would be beneficial for burn wound healing (Queen et al., 1987). It has been suggested that, wound dressing should have a moderate WVTR of values preferably closer to the lower limit of this range. So the WVTR of the xerogel could be adequate for preventing dehydration from moderately exudating wounds. The deposition of alginate fibres had cytotoxic effect on L929 cells with the commercial products. But the xerogels were cytocompatible with the fibroblast cells up to 48h. So while comparing with the commercial alginate based dressings, the developed xerogels possess excellent physical properties as a wound care material.

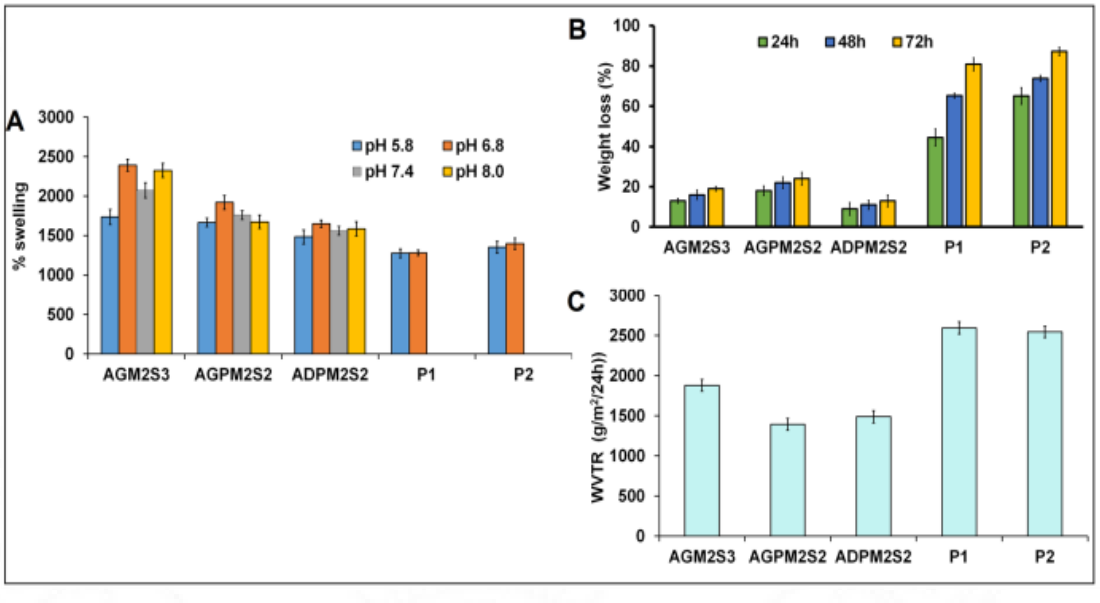

Figure 40: The comparison of xerogels AGM2S3, AGPM2S2 and ADPM2S2 with the commercial alginate wound care materials P1 and P2 for A) percentage swelling B) percentage weight loss and C) water vapour transmission rate.

4.2 Evaluation of the efficacy of xerogels for biomolecule delivery

4.2.1 Delivery of biomolecules through Alginate-g-poly (methacrylic acid) xerogel (AGM2S3)

4.2.1.1 Insulin delivery

The release of insulin from AGM2S3 hydrogel was analyzed for 48h in phosphate buffer at pH 7.4. Insulin was loaded by diffusion filling method by ensuring homogenous dispersion and also that the loading was within the holding capacity of the xerogel. A stable hydrogel of AGM2S3 was formed while loading, which held the entire insulin solution without exuding out. The insulin release was analyzed in both immersed and membrane based release systems (figure 41 A). With immersed release system, a burst release of insulin was observed, i.e. 25% release within one hour, reached up to 80% by 3h and 90% of the loaded insulin got released within 6h. The initial burst release of biomolecules occur from the low density macroporous region within the matrix and the sustained release occurs from the high density microporous regions (Patil et al., 1996). In the case of membrane based release system, initially a slow release was observed, followed by a steady state from 4th hour with 70% release and continued up to 48h. With membrane systems, the release of the biomolecule was possible only through the lower surface of the hydrogel through passive diffusion, where the gel had contact with the buffer through the membrane. To an extent, such a system can mimic the localized drug delivery towards the wound site in practice. The biomolecule release is by swelling and diffusion. The release kinetics showed that this system follows Korsemeyer Peppas model of release kinetics (table 8). The grafting of alginate and both covalent and ionic cross-linking aids in controlled release of

biomolecules from this matrix. The copolymerization of alginate with poly (methacrylic acid) imparts a slight hydrophobicity which also influences the release characteristics of the matrix. Unlike calcium cross-linked alginate hydrogel, the dual cross-linked hydrogels had low disintegration at physiological pH and promotes controlled delivery. Along with dual cross-linking, M/G ratio also plays a significant role in release pattern. In a study by Holte et al they compared the diffusion of different molecules through alginate gel matrices (Holte et al., 2006). It was observed that the diffusion of small molecule was faster in alginate gels with high G content and high concentration of calcium ions. The diffusion rate is dependent on the presence of free alginate molecules within the gel which is not engaged in calcium cross-linking. As the cross-linking concentration increases, the concentration of unbound alginate reduces, which helps in the free movement of molecules. From their study, they deduced that, G rich alginate helps in the faster release of molecule compared to M rich alginate gels due to increased porosity. In our study, alginate is of high M content and the grafting and dual cross-linking helps to improve the porosity of the gel. The introduction of methacrylic acid groups in the vicinal hydroxyl groups provides additional carboxyl groups which provide the sites for strontium ion chelation leading to highly porous structure. In a study by Ahmed et al, strontium ion incorporated carbonate apatite nanoparticles were developed as an insulin delivery system. They observed that, cross-linking with strontium ions increases the electrostatic interaction towards insulin molecules and prevent the initial burst release of insulin (Ahmad et al., 2015). So the high M/G ratio, methacrylate grafting and strontium ion cross-linking

plays significant role in controlled insulin delivery. The continuous delivery of biomolecule towards the wound site can avoid frequent changing of wound dressing, thus prevent the disruption of granulation tissue formation (Pawar et al., 2013). A wound dressing capable of extended delivery of biomolecule for a period of 48h would be beneficial for wound management.

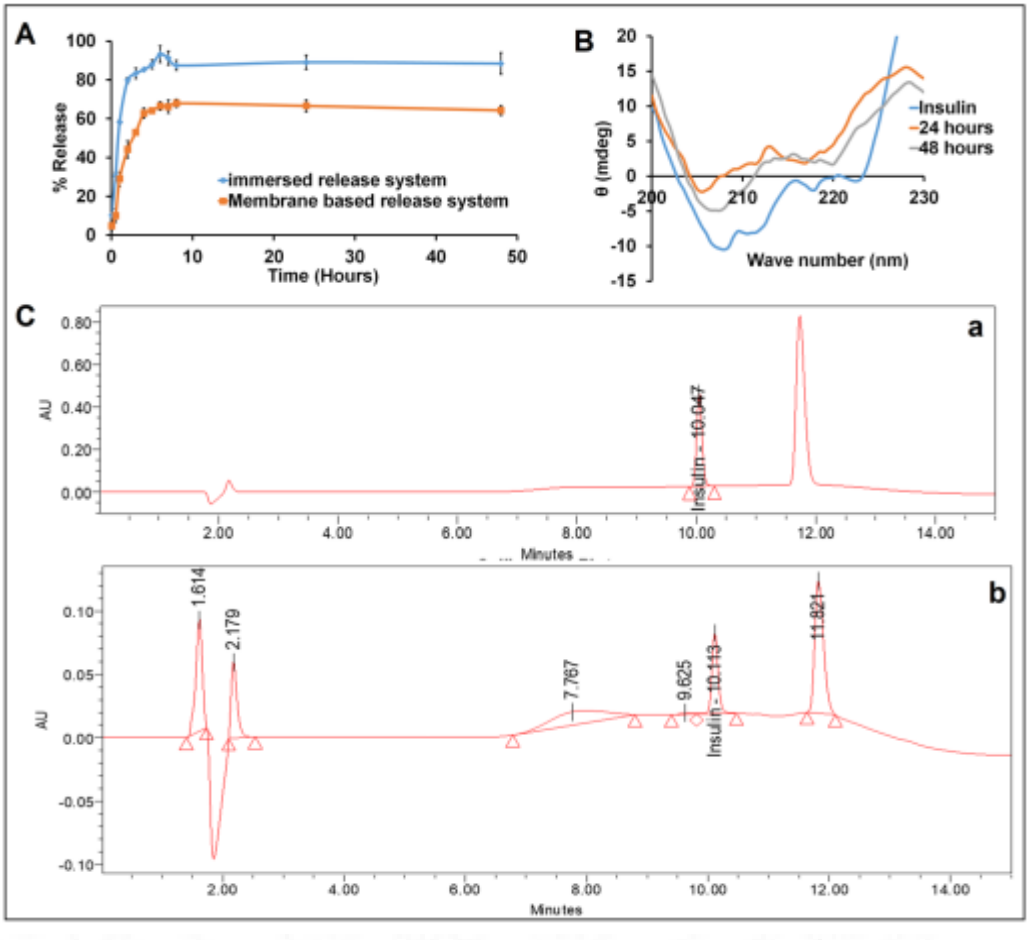

Figure 41: A) Percentage of insulin release from AGM2S3 hydrogel analyzed by immersed and membrane based systems B) Circular dichroism spectra of insulin released from AGM2S3 hydrogel after 24h and 48h release C) Quantification of insulin by HPLC a) insulin standard b) insulin released from the hydrogel at 24h.

The bioactivity of the released insulin was analysed by different methods. The insulin release in 24h was quantified to be 82% by ELISA. HPLC analysis also showed 80% release within 10 min. The retention time for released insulin was similar to that of insulin standard (figure 41C). These results suggested that, there was no degradation of insulin by matrix-biomolecule interaction. Using circular dichroism, the structural integrity of the insulin was further analyzed. The circular dichroism spectra of insulin molecule showed the double minima peaks around 208nm and 222nm. A similar structure was observed with released insulin from the AGM2S3 hydrogel after 24h, but a structural variation was observed after 48h release (figure 39B). This indicates that there was no adverse interaction between the matrix and loaded insulin up to 24h.

Insulin loaded AGM2S3 hydrogel		
Immersed release system		
Release kinetics model	Equation	R^2
Zero order	y = 3.8895x + 67.318	0.7157
First order	y = 0.0507x + 4.2032	0.6715
Higuchi Model	y = 27.191x + 28.639	0.7728
Korsemeyer Peppas model	y = 0.3748x + 1.6807	0.8609
Membrane based release system		
Release kinetics model	Equation	R^2
Zero order	y = 10.377x + 20.465	0.9345
First order	y = 0.141x + 3.5464	0.9077
Higuchi Model	y = 32.293x + 2.7589	0.9791
Korsemeyer Peppas model	y = 0.4956x + 1.5312	0.9853

Table 8: Comparison of release kinetics of insulin released from AGM2S3 hydrogel with different release kinetic models.

4.2.1.2 Simvastatin (SIM) delivery

Simvastatin (SIM) loaded AGM2S3 hydrogels showed a burst release during initial hours. Within one hour, there a 90% release occurred in immersed release

system and 83% release observed with membrane based system (figure 41 A). After reaching 100% release within 5h, a decline in the release was observed with immersed release system. The comparison of release kinetics by different models showed that both release system were not following any of the kinetics model due to the initial burst release of the drug from the matrix (table 9). A similar burst release of simvastatin was observed in as study by Yan et al, with microspheres made up of poly-L-lactide (PLLA) and alginate shell (Yan et al., 2017). They observed that simvastatin loaded within the core showed zero order release pattern *in vitro* due to the polymer erosion. The HPLC results showed similar retention time for standard and the SIM released from the hydrogel, indicating that there is no adverse matrix drug interaction (figure 42 B).

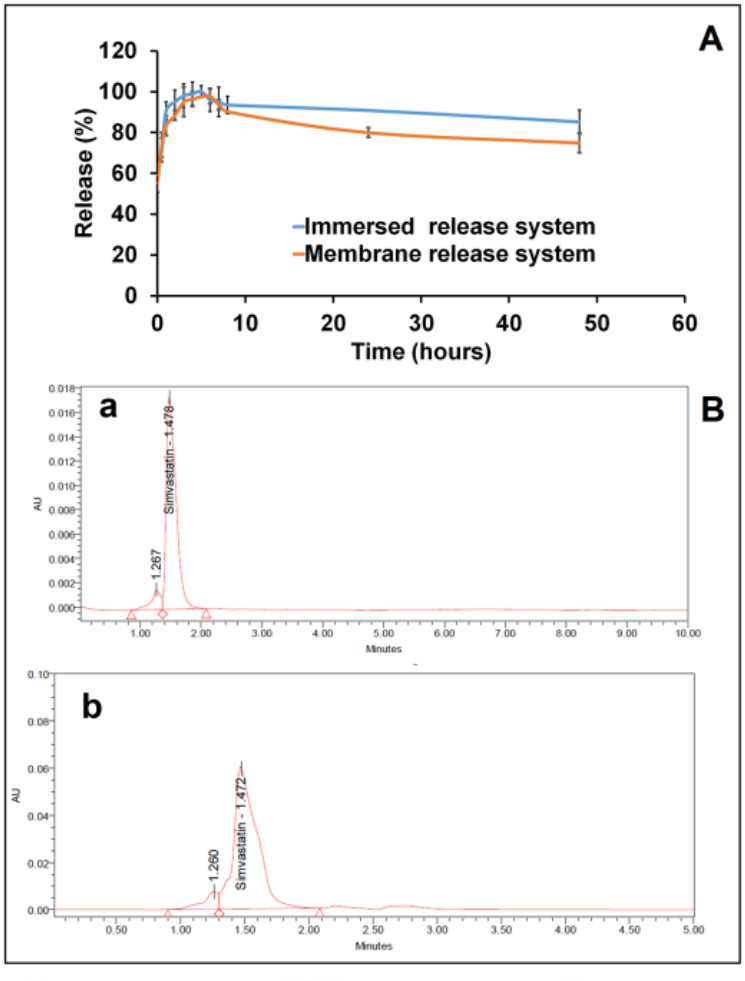

Figure 42: A) Release profile of simvastatin from AGM2S3 hydrogel analyzed by immersed and membrane based systems B) Quantification of simvastatin a) simvastatin standard b) SIM released from the hydrogel at 24h.

Simvastatin loaded AGM2S3 hydrogel		
Immersed release system		
Release kinetics model	Equation	R^2
Zero order	y = 3.7533x + 83.749	0.2955
First order	y = 0.0666x + 4.274	0.3153
Higuchi Model	y = 15.36x + 71.316	0.5264
Korsemeyer Peppas model	y = 0.1129x + 4.4872	0.4525
Membrane based release system		
Release kinetics model	Equation	R^2
Zero order	y = 3.3798x + 76.779	0.3911
First order	y = 0.0665x + 4.1868	0.3363
Higuchi Model	y = 13.258x + 66.56	0.6400
Korsemeyer Peppas model	y = 0.0898x + 4.4269	0.5673

Table 9: Comparison of release kinetics of simvastatin released from AGM2S3 hydrogel with different release kinetic models.

4.2.1.3 Delivery of Glucose oxidase – Peroxidase

Another biomolecule selected for this study was glucose oxidase-peroxidase (GO-POD). Both the enzymes were loaded separately within the hydrogel and the release profile was analyzed. A controlled release pattern was observed for both GO and POD. The GO release reached a plateau within 8h in both immersed and membrane system (figure 43 A). Both systems showed about 50% release of GO at 24h. The release pattern was obeying Higuchi model of release kinetics (table 10). The native structure of glucose oxidase was studied by circular dichroism. The native GO shows αhelices and βsheets in the far UV region. The presence of residual secondary structures was indicated by the elipticity near 200-222 nm. In this region, peptide n – $\pi*$ electronic transition occurs, which is sensitive to the conformation to the secondary structures (Zoldák et al., 2004). There was no change in the structural conformation of GO up to 8h on interaction with the hydrogel. If any conformational change occurs to the protein molecule, a positive elipticity was observed due to the formation of polyproline II conformation (Shi et al., 2002). The conformational changes in the active site of GO can be studied by the interaction of flavin molecule with the tryptophan residue within the active site. In the circular dichroism spectra of glucose oxidase, a structural alteration was observed after 24h release (figure 43 B). Due to the structural alteration, the release GO and POD were conducted up to 24h only. One of the clinical challenges in the GO delivery for clinical application is its thermal and kinetic instability in stressful conditions. So this approach of GO delivery did not

adversely affect the structural stability of the protein and thereby could retain its biocatalytic acitivty for 24 hours.

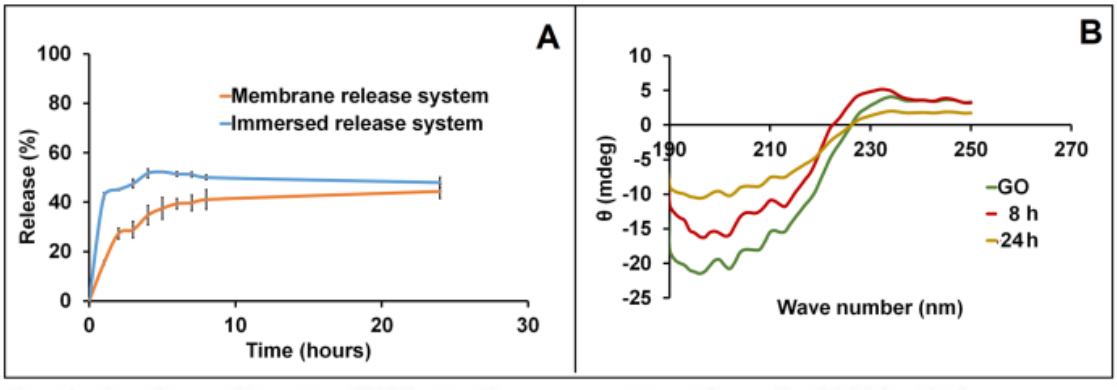

Figure 43 : A) Percentage of glucose oxidase released from AGM2S3 hydrogel analyzed by immersed and membrane based systems B) Circular dichroism spectra of GO released from AGM2S3 hydrogel after 8h and 24h release compared with native GO.

Glucose oxidase loaded AGM2S3 hydrogel		
Immersed release system		
Release kinetics model	Equation	R^2
Zero order	y = 0.9028x + 52.383	0.4699
First order	y = 0.0167x + 3.9568	0.4701
Higuchi Model	y = 0.071x + 1.7101	0.7604
Korsemeyer Peppas model	y = 0.1493x - 6.389	0.5487
Membrane based release system		
Release kinetics model	Equation	R^2
Zero order	y = 3.2805x + 28.23	0.8508
First order	y = 0.0844x + 3.3596	0.7809
Higuchi Model	y = 0.3242x + 1.4373	0.9504
Korsemeyer Peppas model	y = 0.0695x - 0.95	0.9285

Table 10: Comparison of release kinetics of glucose oxidase released from AGM2S3 hydrogel with different release kinetic models.

A higher release of POD was observed within 8h reaching up to 60% while comparing to that of GO (figure 43 A). The molecular weight of POD is 44 KDa, while

that of GO is 180 KDa. Hence the release of GO was lower compared to POD. The release pattern of POD was found to be following zero order kinetics. Zero order biomolecule release is an ideal way to improve its therapeutic effect. The concentration of the molecule can be always maintained within the therapeutic window without any side effects (X. Li et al., 2021). The constant release of POD helps to remove the reactive oxygen from the wound site and provide optimum environment for the action of GO for the conversion of glucose to D-gluconolactone and hydrogen peroxide. This reaction mechanism comprises of reductive and oxidative half reactions. In the oxidative half reaction, two electrons and protons are transferred from glucose to flavin molecule of the GO. In the reductive reaction, these electrons and protons are transferred to molecular oxygen producing hydrogen peroxide (Wohlfahrt et al., 1999). The factors such as pH, temperature and the concentration of hydrogen peroxide influence the activity of peroxidase. At higher H_2O_2 concentration, a Fenton type reaction will occur, facilitated by the formation of iron(II) oxygen complex and produce hydroxyl radicals (Ingenbosch et al., 2021). Baker et al demonstrated that peroxidase activity of horse radish peroxidase mimics the catalase activity at lower H_2O_2 concentration. In the absence of other reactants, molecular oxygen is produced by peroxidase activity from H_2O_2. They measured the effect of varying concentration of H_2O_2 on both oxygen evolution and H_2O_2 scavenging. They found that the oxygen evolution rate increased with increasing H_2O_2 concentration and got saturated at 5 mM concentration of H_2O_2. The apparent Km for H_2O_2 scavenging and molecular oxygen production was nearly 1mM H_2O_2 (Baker et al., 2000). Such pseudo catalytic activity

was observed with peroxidase during oxidative stress. In another study, Barr et al demonstrated that the generation of molecular oxygen by peroxidase was enhanced in the presence of cation radicals (Barr and Aust, 1993). So the lower H_2O_2 concentration and the presence of cation radical could be favourable for the production of molecular oxygen for wound healing to proceed.

The combined delivery of GO and POD plays significant role in controlling the local glucose level. There was 32% reduction in the glucose level within 8h which resulted in the reversion of hyperglycemic condition to the normoglycemic level (fig. 42B). The production of H_2O_2 increased during the initial hours, reached peak at 3rd hour and started declining for next 5h. The topical delivery of POD helps to reduce the H_2O_2 level below 10mM and helps in the release of molecular oxygen during the removal of H_2O_2. An oxygen deprived condition is generated by the release of GO, which unfavourable for cellular survival, the release of oxygen by the peroxidase activity could be beneficial for cellular respiration (Tao et al., 2009).

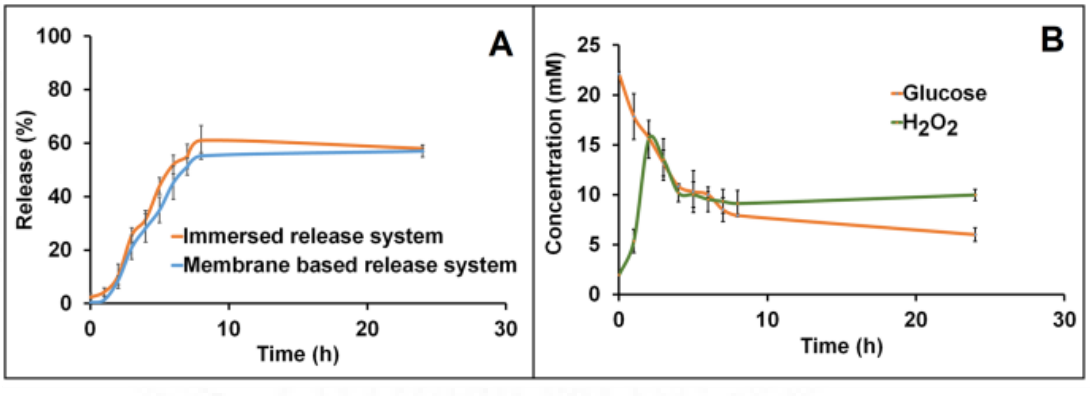

Figure 44: A) Percentage release of peroxidase from AGM2S3 hydrogel using immersed and membrane based release systems B) The change in glucose and H_2O_2 level with combined delivery of GO-POD through AGM2S3 hydrogels

Peroxidase loaded AGM2S3 hydrogel		
Immersed release system AGM2S3 POD		
Release kinetics model	Equation	R^2
Zero order	y = 7.971x - 5.1543	0.9878
First order	y = 0.4472x + 1.0032	0.7562
Higuchi Model	y = 0.0518x + 0.5508	0.7699
Korsemeyer Peppas model	y = 1.7422x + 0.3067	0.9793
Membrane based release system		
Release kinetics model	Equation	R^2
Zero order	y = 8.4813x - 2.7096	0.9743
First order	y = 0.3504x + 1.7145	0.8342
Higuchi Model	y = 1.0378x + 2.945	0.9843
Korsemeyer Peppas model	y = 1.3197x + 0.6697	0.9726

Table 11: Comparison of release kinetics of peroxidase released from AGM2S3 hydrogel with different release kinetic models.

4.2.2 Delivery of biomolecules through Alginate-g-poly (PEGMA) xerogel (AGPM2S2)

4.2.2.1 Insulin delivery

The insulin release from AGPM2S2 hydrogel was studied by immersed as well as membrane based systems (fig. 43A). With immersed system, 80% release was attained within 4h and started declining which reached up to 64% at 24h. A steady state release was observed with membrane based system and reached up to 60% within 24h. Both the systems showed a release kinetics of Korsemeyer Peppas model (table 12). The released insulin was analysed by HPLC and ELSA methods to evaluate the biological stability. The hydrogel loaded with 1IU/ml insulin showed a release of 0.76 IU/ml with ELISA and 0.514 IU/ml with HPLC methods (figure 45 C). The released insulin from AGPM2S2 hydrogel showed a reduction in its activity. To analyze the

structural variation of the molecule, CD spectrum was taken (fig. 43B). A shift in the double minima peaks around 208nm and 222nm was clearly visible in the spectra, which indicate the change in the conformation of alpha helical structure. This confirmed a matrix-biomolecule interaction. PEG molecule interact with the insulin molecule through the hydrophobic interaction and concurrently forming hydrogen bonds with the surrounding water molecules (Yang et al., 2011). The aggregation of insulin is one of the major reasons for reduced bioavailability and results in inadequate functional activity. The factors such as acidic pH, elevated temperature, interaction with hydrophobic surfaces and variation in ionic strength favors the insulin aggregation (Das et al., 2022). Nault et al reported that upon binding with hydrophobic surfaces, a conformational change is induced in insulin, resulting in α-to-β structural transition and finally leads to the formation of amyloid fibers. (Nault et al., 2013). By contact angle measurement, it was observed that the increased concentration of PEGMA monomer used for grafting induced hydrophobicity to the xerogel surface. So this could be the reason for the change in the confirmation of insulin during prolonged contact within the hydrogel.

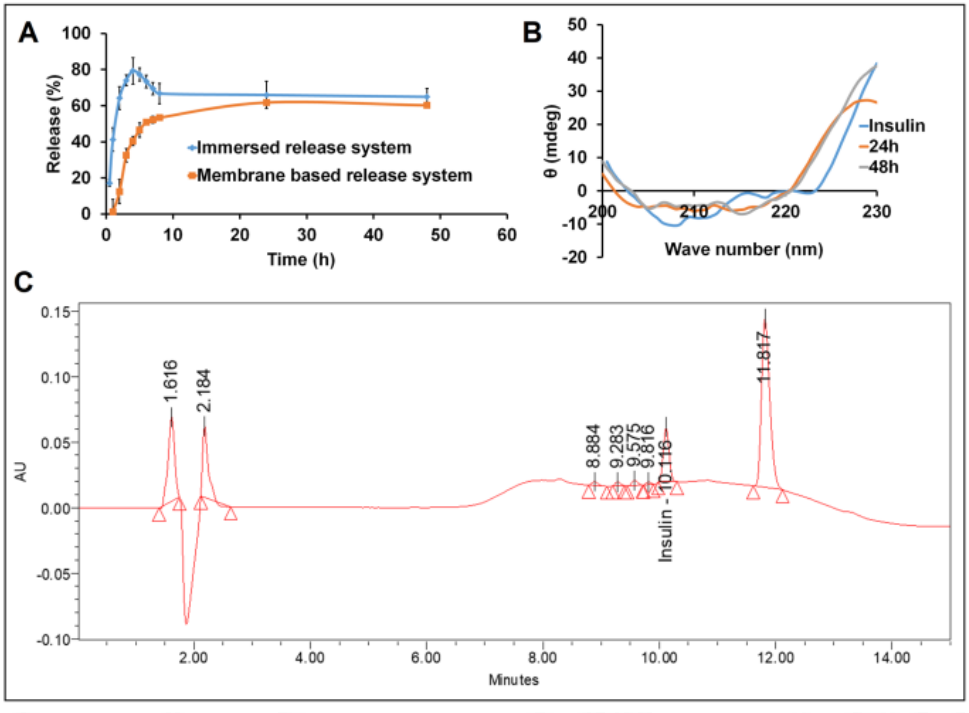

Figure 45: A) Percentage of insulin release from AGPM2S2 hydrogel analyzed by immersed and membrane based systems B) Circular dichroism spectra of insulin released from AGPM2S2 hydrogel after 24h and 48h release C) Quantification of insulin released from the hydrogel at 24h by HPLC.

Insulin loaded AGPM2S2 hydrogel		
Immersed release system		
Release kinetics model	Equation	R^2
Zero order	y = 5.0162x + 42.176	0.4244
First order	y = 0.1194x + 3.5696	0.4081
Higuchi Model	y = 0.0277x + 0.16	0.5884
Korsemeyer Peppas model	y = 1.6357x - 2.4013	0.7411
Membrane based release system		
Release kinetics model	Equation	R^2
Zero order	y = 7.4437x + 2.6845	0.8642
First order	y = 0.4157x + 1.7173	0.5578
Higuchi Model	y = 0.0277x + 0.16	0.5884
Korsemeyer Peppas model	y = 0.5175x - 0.1465	0.9291

Table 12: Comparison of release kinetics of insulin released from AGPM2S2 hydrogel with different release kinetic models.

4.2.2.2 Simvastatin delivery

Simvastatin loaded AGPM2S2 hydrogels showed an initial burst release. The immersed release system showed 90% release and membrane based system showed 80% release at 5^{th} hour (figure 46 A). After 5 h, both the systems showed a reduction in the release which maintained at that level up to 48h. The release pattern followed the Higuchi model of release kinetics (table 13). The initial burst release is due to the release of surface bound drug molecules in the buffer. Due to its small molecular weight, the release of SIM was faster during the initial period. However, upon swelling, the hydrophobic domains of the hydrogel get exposed, which facilitate the interaction of the hydrophobic drug. The entrapment of hydrophobic drugs within these domains further slows down the drug release (Leganés et al., 2022). The released SIM quantified by HPLC analysis was found to be 5.07µg/ml (figure 46 B).

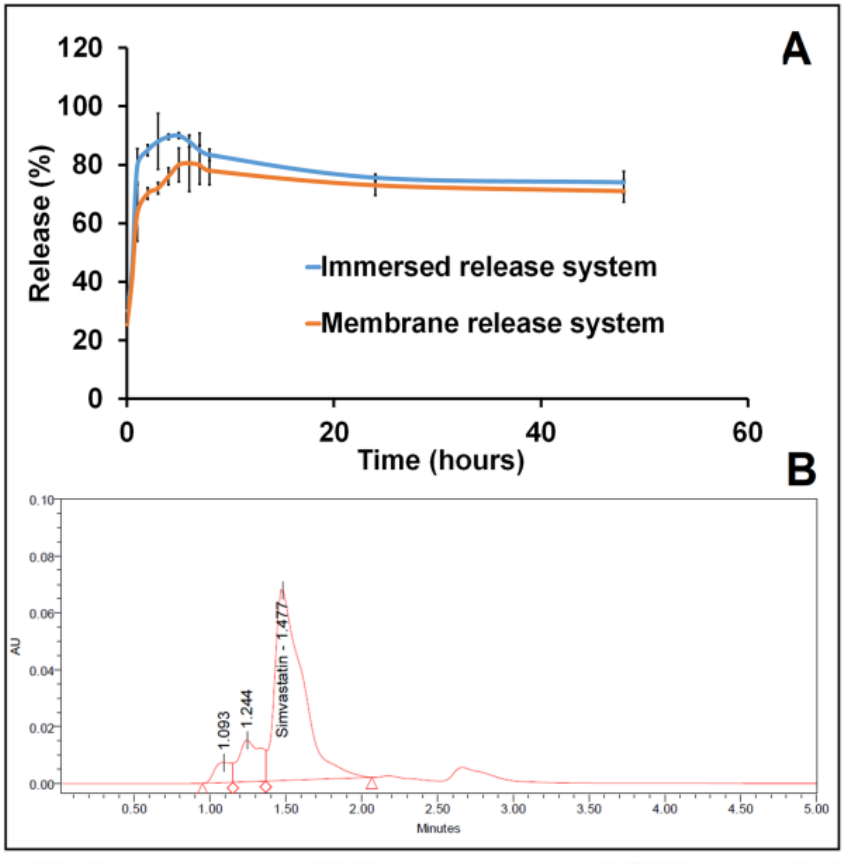

Figure 46: A) Percentage of simvastatin release from AGPM2S2 hydrogel analyzed by immersed and membrane based systems B) quantification of simvastatin released from the hydrogel at 24h by HPLC.

Simvastatin loaded AGPM2S2 hydrogel		
Immersed release system		
Release kinetics model	Equation	R^2
Zero order	y = 7.4732x + 66.26	0.6977
First order	y = 0.0967x + 4.1374	0.5848
Higuchi Model	y = 26.465x + 48.812	0.8733
Korsemeyer Peppas model	y = 0.2995x + 1.8213	0.6452
Membrane based release system		
Release kinetics model	Equation	R^2
Zero order	y = 8.418x + 60.703	0.6902
First order	y = 0.1132x + 4.0408	0.6206
Higuchi Model	y = 29.962x + 40.955	0.9062
Korsemeyer Peppas model	y = 0.2721x + 1.8471	0.8877

Table 13: Comparison of release kinetics of simvastatin released from AGPM2S2 hydrogel with different release kinetic models.

4.2.2.3 Delivery of Glucose oxidase – peroxidase

Glucose oxidase loaded AGPM2S2 hydrogels showed very poor release pattern. The maximum release observed at 5th hour for both immersed (41%) and membrane based system (33%). Then a reduction in the release was observed which reached up to 25% at 24h (figure 47 A). The reduction in release can be attributed to the interaction of glucose oxidase molecules with the matrix. The increase in hydrophobic interaction of protein with the poly (PEGMA) chains resulted in lower release pattern. The comparison with different kinetics model showed no specific pattern of release (table 14). The matrix interaction was evidenced by the CD spectra also (figure 47 B). The spectra of glucose oxidase release at 8h and 24h showed a shift compared to the native GO.

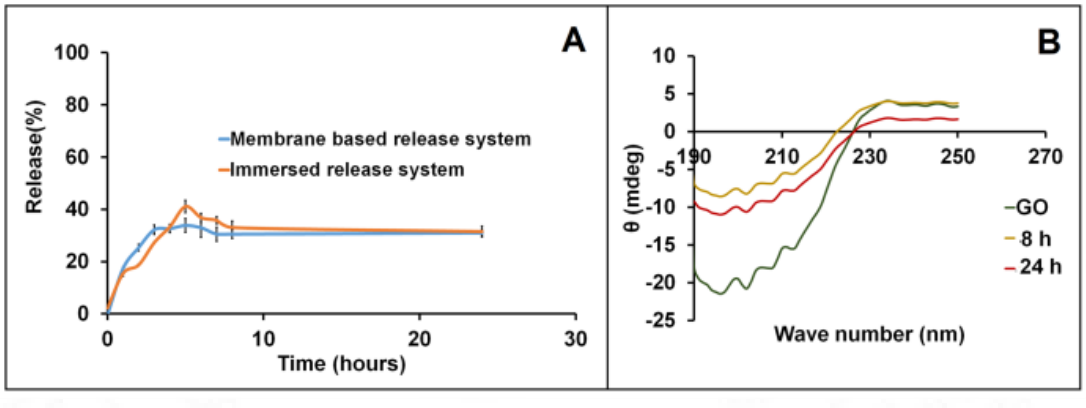

Figure 47: A) Percentage of glucose oxidase released from AGPM2S2 hydrogel analyzed by immersed and membrane based systems B) Circular dichroism spectra of GO released from AGPM2S2 hydrogel after 8h and 24h release compared with native GO.

Glucose oxidase loaded AGPM2S2 hydrogel		
Immersed release system AGPM2S2 GO		
Release kinetics model	Equation	R^2
Zero order	y = 1.4397x + 22.935	0.4080
First order	y = 0.0591x + 3.0961	0.4194
Higuchi Model	y = 0.0838x - 0.4272	0.5423
Korsemeyer Peppas model	y = 0.2654x + 1.3073	0.6978
Membrane based release system		
Release kinetics model	Equation	R^2
Zero order	y = 2.9151x + 17.078	0.6264
First order	y = 0.1151x + 2.8418	0.6542
Higuchi Model	y = 0.0593x + 0.2484	0.7242
Korsemeyer Peppas model	y = 0.4541x + 1.1977	0.8369

Table 14: Comparison of release kinetics of glucose oxidase released from AGPM2S2 hydrogel with different release kinetic models.

The release of POD from the hydrogel was higher compared to GO. The hydrogel showed 50% release of POD within 8h and continued up to 24h (figure 48 A). A zero order release kinetics was followed by both release systems (table 15). The combined delivery of GO-POD system through AGPM2S2 hydrogel could control the local glucose level and ROS level (figure 48 B). Effect of these enzymes on glucose levels and the H_2O_2 production was evaluated under in vitro conditions. There was a 40% reduction in glucose within 24h. The utilization of glucose resulted in the formation of H_2O_2, and reached peak value of 18mM within 3h. By the action of POD, the H_2O_2 level was reduced to 10mM within 24h.

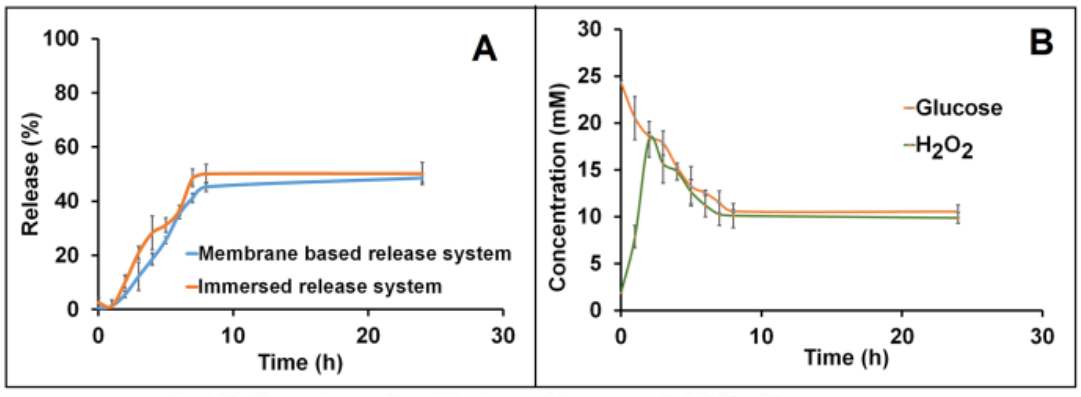

Figure 48: A) Percentage release of peroxidase from AGPM2S2 hydrogel using immersed and membrane based release systems B) The change in glucose and H_2O_2 level with combined delivery of GO-POD through AGPM2S2 hydrogels.

Peroxidase loaded AGPM2S2 hydrogel		
Immersed release system		
Release kinetics model	Equation	R^2
Zero order	y = 6.2x - 4.1944	0.9802
First order	y = 0.4561x + 0.6669	0.8487
Higuchi Model	y = 0.0376x + 1.1692	0.9653
Korsemeyer Peppas model	y = 1.713x + 0.1948	0.9873
Membrane based release system		
Release kinetics model	Equation	R^2
Zero order	y = 6.5822x - 0.802	0.9744
First order	y = 0.4226x + 1.0678	0.7119
Higuchi Model	y = 0.0362x + 1.0105	0.9836
Korsemeyer Peppas model	y = 1.669x + 0.3288	0.9158

Table 15: Comparison of release kinetics of peroxidase released from AGPM2S2 hydrogel with different release kinetic models.

4.2.3 Delivery of biomolecules through Alginate diamine-g-poly (PEGMA) xerogel (ADPM2S2)

4.2.3.1 Insulin delivery

The loaded insulin from ADPM2S2 hydrogel got released over a period of 48h. The membrane based system showed a steady state increase in insulin release and reached up to 65% within 7h and continued to 48h (figure 49 A). However, the

immersed system showed 90% release within 6h and continued the same pattern up to 48h. Both the release systems showed Korsemeyer Peppas model of release kinetics (table 16). The continuous release of insulin from the matrix was due to the absence of any adverse biomolecule-matrix interaction. This was further confirmed by the CD spectra (figure 49 B). It showed that the alpha helical structure of the insulin molecule was well retained even after 24h release. By HPLC analysis, 80% release of the loaded insulin was confirmed (figure 47 C). The reduction in the amount of PEGMA monomer used in grafting and the incorporation of diamine PEG molecule resulted in a matrix that favours the free flow of biomolecule through the gel by swelling mediated diffusion. This modification could effectively reduce the biomolecule-matrix interaction and retaining the functional activity of the loaded molecule.

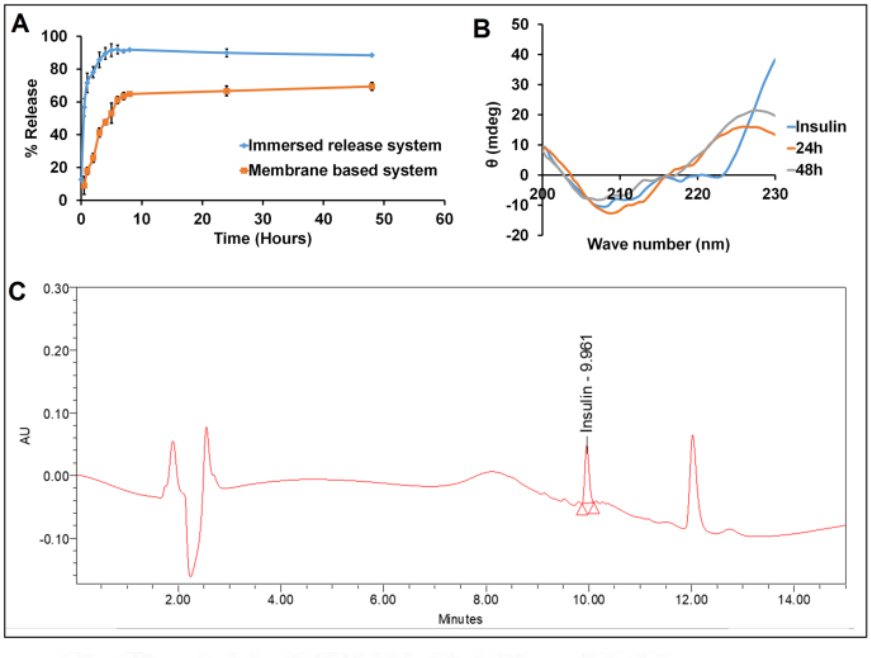

Figure 49: A) Percentage of insulin release from ADPM2S2 hydrogel analyzed by immersed and membrane based systems B) Circular dichroism spectra of insulin released from ADPM2S2 hydrogel after 24h and 48h release C) Quantification of insulin released from the hydrogel at 24h by HPLC.

Insulin loaded ADPM2S2 hydrogel		
Immersed release system		
Release kinetics model	Equation	R^2
Zero order	y = 2.689x + 74.296	0.7549
First order	y = 0.0325x + 4.3093	0.7409
Higuchi Model	y = 0.0768x - 4.5942	0.8577
Korsemeyer Peppas model	y = 0.1265x + 1.8621	0.9283
Membrane based release system		
Release kinetics model	Equation	R^2
Zero order	y = 6.2911x + 23.611	0.8927
First order	y = 0.1175x + 3.4022	0.8057
Higuchi Model	y = 0.0435x - 0.2661	0.9585
Korsemeyer Peppas model	y = 0.4485x + 1.449	0.9679

Table 16: Comparison of release kinetics of insulin released from ADPM2S2 hydrogel with different release kinetic models.

4.2.3.2 Simvastatin delivery

The ability of the hydrogel ADPM2S2 for the controlled delivery of simvastatin was analyzed at pH 7.4 (figure 50 A). Compared to other two hydrogels, initial burst release was not observed with ADPM2S2 hydrogels. With the immersed system, 98% release was observed by 8h which remained at that level up to 48h. But with membrane based system a steady state increase in release was observed which reached up to 85% by 48h. The release pattern was found follow Korsemeyer Peppas model of release kinetics (table 17). The released SIM was further quantified by HPLC (figure 50 B) and showed 91% release after 48h (loaded conc. of SIM: 6µg/ml, released conc. 5.473µg/ml). Yasasvini et al demonstrated a prolonged drug delivery by loading simvastatin-chitosan microparticles into PVA hydrogel for wound healing applications. This system showed 92% release of SIM within 7 days and exhibited considerable reduction in the wound area by both *in vitro* and *in vivo* analysis (Yasasvini et al., 2017). In another study, Park et al demonstrated the release kinetics of SIM loaded gelatin–poly (ethylene glycol)–tyramine-based hydrogels. In their

system, an initial burst release of SIM followed by sustained release was observed. They suggested that the initial burst release could be by improving the mechanical strength of the hydrogel (Park et al., 2012). Usually, for chronic wound management repeated drug administration is required at regular time intervals for a longer duration. This signifies the importance of sustained release which helps to reduce the dosing frequency and maintain the appropriate therapeutic concentration of the drug at wound site (Lipsky and Hoey, 2009).

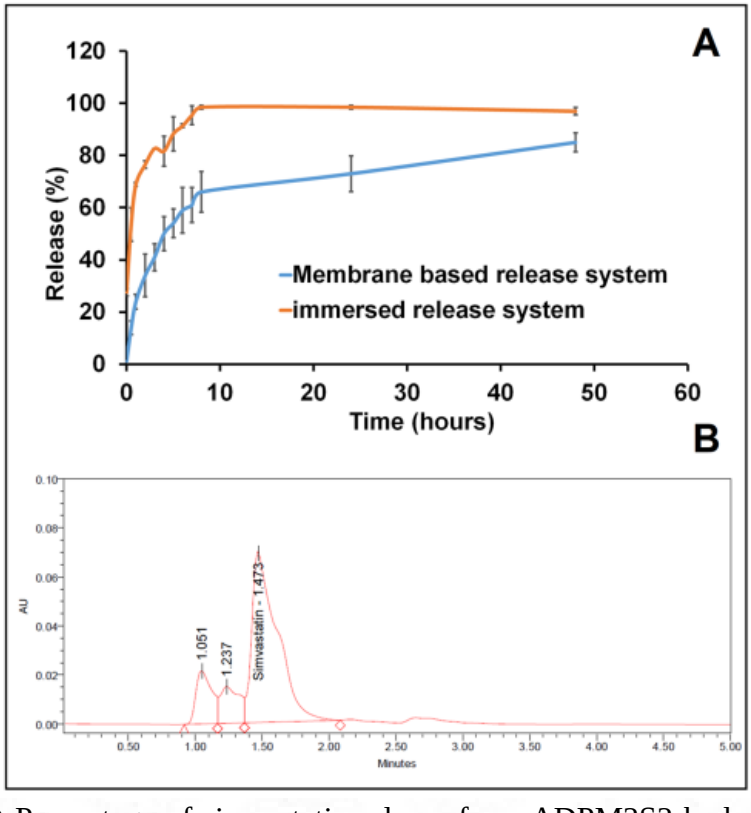

Figure 50: A) Percentage of simvastatin release from ADPM2S2 hydrogel analyzed by immersed and membrane based systems B) Quantification of simvastatin released from the hydrogel at 24h by HPLC

Simvastatin loaded ADPM2S2 hydrogel		
Immersed release system		
Release kinetics model	Equation	R^2
Zero order	y = 6.7366x + 51.84	0.7548
First order	y = 0.1063x + 3.8948	0.6050
Higuchi Model	y = 22.916x + 37.442	0.9352
Korsemeyer Peppas model	y = 0.1978x + 4.1722	0.9644
Membrane based release system		
Release kinetics model	Equation	R^2
Zero order	y = 7.4012x + 13.406	0.9161
First order	y = 0.3196x + 2.1853	0.5467
Higuchi Model	y = 22.218x + 8.9041	0.9741
Korsemeyer Peppas model	y = 0.489x + 3.1889	0.9955

Table 17: Comparison of release kinetics of simvastatin released from ADPM2S2 hydrogel with different release kinetic models.

4.2.3.3 Delivery of Glucose oxidase – peroxidase

Glucose oxidase from the loaded ADPM2S2 hydrogel showed a release of 48% within 8h and 50% by 24h with membrane based system. With immersed release system a higher release of 50% and 61% was observed at 8h and 24h respectively (figure 51 A).

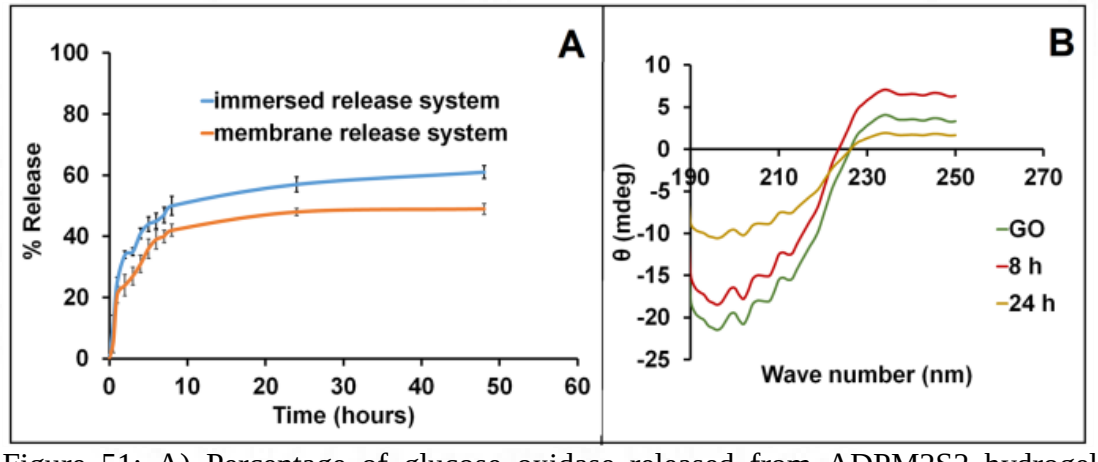

Figure 51: A) Percentage of glucose oxidase released from ADPM2S2 hydrogel analyzed by immersed and membrane based systems B) circular dichroism spectra of GO released from AGPM2S2 hydrogel after 8h and 24h release compared with native GO.

The release pattern for GO was found to be Korsemeyer Peppas model (table 18). GO molecule binds with the amino groups of the diamine PEG molecule, since it has a net negative charge at physiological pH (Deng et al., 2007). The structural integrity of GO was further confirmed by CD spectroscopy (figure 51 B). The CD spectrum of the GO released at 8h was similar to that of the native enzyme. However the spectra of the GO released after 24 hour showed a shift, which can be attributed to a change in the conformation of GO. Hence it can be inferred that the catalytic activity of GO would be effective for the initial 8h only. Thus a frequent therapeutic dosage will be needed for maintaining the appropriate dose of GO at the wound surface.

GO loaded ADPM2S2 hydrogel		
Immersed release system		
Release kinetics model	Equation	R^2
Zero order	y = 3.25x + 25.5	0.9303
First order	y = 0.0869x + 3.2801	0.8754
Higuchi Model	y = 0.0751x - 0.9751	0.9729
Korsemeyer Peppas model	y = 0.3199x + 1.4101	0.9791
Membrane based release system		
Release kinetics model	Equation	R^2
Zero order	y = 4.25x + 15.5	0.9803
First order	y = 0.1272x + 2.9297	0.9822
Higuchi Model	y = 0.0582x + 0.0231	0.9482
Korsemeyer Peppas model	y = 0.4307x + 1.2731	0.9277

Table 18: Comparison of release kinetics of glucose oxidase released from ADPM2S2 hydrogel with different release kinetic models.

Due to smaller MW compared to GO, the peroxidase release from the hydrogel was higher which showed 75% and 65% within 24h for immersed and membrane based systems respectively (figure 52 A). The release pattern of POD was found to be zero order kinetics (table19). The combined delivery of GO and POD helps in the

reversion of hyperglycemic condition towards normoglycemic level within 8h and sustained the normal glucose level for 24h (figure 52 B). The formation of H_2O_2 was controlled due to increased release of POD from the hydrogel compared to other two systems. With ADPM2S2 hydrogel, the H_2O_2 level could able to maintain below 5mM.

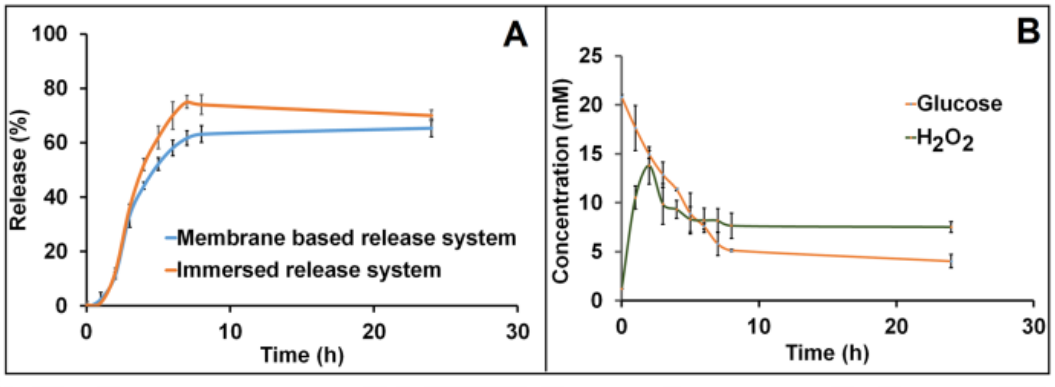

Figure 52: A) Percentage release of peroxidase from ADPM2S2 hydrogel using immersed and membrane based release systems B) The change in glucose and H_2O_2 level with combined delivery of GO-POD through ADPM2S2 hydrogels.

Immersed release system ADPM2S2 POD		
Release kinetics model	Equation	R^2
Zero order First order Higuchi Model Korsemeyer Peppas model	y = 9.0417x + 0.0835 y = 0.3928x + 1.5955 y = 0.0265x + 0.9565 y = 1.5579x + 0.5637	0.9099 0.7099 0.9610 0.9008
Membrane based release system		
Release kinetics model	Equation	R^2
Zero order First order Higuchi Model Korsemeyer Peppas model	y = 11.126x - 2.2446 y = 0.4746x + 1.2708 y = 0.0216x + 1.006 y = 1.9165x + 0.3762	0.9177 0.6651 0.9611 0.8942

Table 19: Comparison of release kinetics of peroxidase released from ADPM2S2 hydrogel with different release kinetic models.

4.3 *In vitro* wound healing with biomolecules using optimized xerogel ADPM2S2

The *in vitro* wound healing effect of the selected biomolecules such as insulin, simvastatin and glucose oxidase were studied under high glucose conditions. The cells selected for the *in vitro* analysis include fibroblast cells (L929), keratinocytes (HaCaT) and macrophages (RAW 264.7). The cells were grown in medium containing normal levels of glucose and later shifted to hyperglycemic condition to mimic the diabetic condition *in vitro*. The L929 cells were maintained in minimal essential medium with low glucose (5mM). By gradient increase in the glucose concentration in the medium, the cells were shifted to DMEM with high glucose (25mM). Thus the cells acclimatised under high glucose conditions were used for the experiments mimicking diabetic conditions. For HaCaT and RAW cells, RPMI 1640 with low glucose (11.1mM) was used as the growth medium. By sequentially increasing the glucose concentration, the cells were shifted to DMEM with high glucose (25mM), which was then used for *in vitro* studies.

4.3.1 In vitro wound healing effects of insulin-loaded ADPM2S2 hydrogel

4.3.1.1 Cytotoxicity evaluation

The viability of fibroblast cells exposed to varying concentration of insulin was analyzed by MTT assay (figure 53 A). Insulin showed cytotoxic response at a concentration >1 IU/mL and cellular proliferation with 0.1-0.5 IU/mL concentrations. Below 0.1 IU/mL, the cell viability was decreasing, so the 100 mIU/mL of insulin was taken as the optimized concentration for *in vitro* studies. The cell viability was reduced to 60% under high glucose condition, due to the increased oxidative stress within the

cells. Hyperglycemic condition disrupt the normal fibroblast physiology and derange the secretion of extracellular matrix proteins (Berlanga-Acosta et al., 2012).

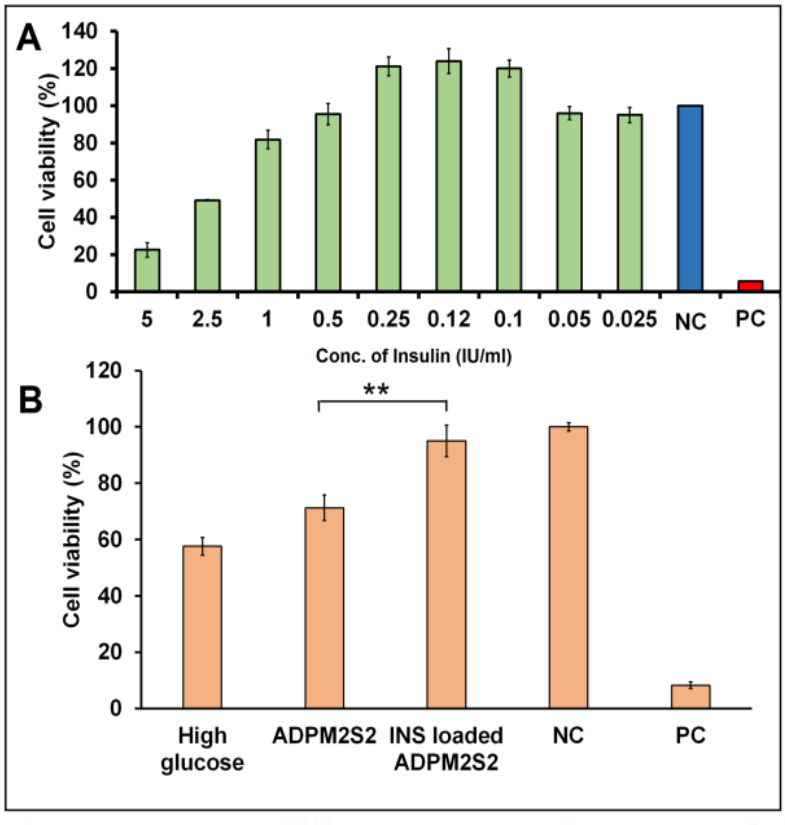

Figure 53: Cytocompatibility evaluation on L929 cells treated with A) varying concentration of insulin and B) extracts of ADPM2S2 and insulin loaded ADPM2S2 and compared with controls (**p<0.01). Growth medium as the negative control (NC) and 0.1% Triton X100 as the positive control (PC).

The cell viability was found to be increased to 71% with hydrogel treatment, which was further enhanced to 95% with the treatment of insulin loaded ADPM2S2 hydrogels (figure 53B). Fujimoto et al demonstrated that, insulin at a physiological concentration of 100mIU/mL stimulated the glucose uptake and uridine incorporation into RNA in cultured fibroblasts. The increase in the uridine incorporation by the insulin treatment was taken as an index of faster growth rate (Fujimoto and Williams, 1974). In another study, Monaco et al elucidated that the increase in fibroblast

proliferation in response to insulin was due to the activation of calcium-calmodulin-dependent kinases pathway. Insulin stimulation induce the activation of ERK and Raf-1, which results in the increased thymidine uptake (Monaco et al., 2009).

4.3.1.2 Collagen deposition

The effect of insulin on collagen deposition from L929 cells were analyzed by the Sirius red assay (figure 54). There was significant enhancement in the collagen production by insulin loaded ADPM2S2 hydrogel (175±4.5µg/mL) than ADPM2S2 hydrogel (152±7.9µg/mL) alone. The collagen production in diabetic fibroblast was reduced to 107±5.1µg/mL, while under normal glucose condition the collagen production was 145±3.1µg/mL. The release of Sr ion from the hydrogel as well as the release of loaded insulin had good impact on collagen synthesis. The influence of insulin on collagen production and maturation was evidenced by increase in hydroxyproline level (Wang and Xu, 2020). Kjellstrom et al studied the effect of insulin on collagen production in cultured skin fibroblasts derived from diabetic patients. Insulin at a concentration of 10^2 to 10^3 mU/L improved the collagen deposition. Insulin favors the incorporation of proline residues during collagen synthesis. The increase in insulin concentration beyond 10^3 mU/L didn't stimulate the collagen deposition (Kjellström and Malmquist, 1984). In another study Goldstein et al., demonstrated that the insulin stimulated collagen production through IGF-1 (insulin like growth factor-1) receptors. Insulin at a concentration of 20ng/mL increased the collagen production by 58% and showed the upregulation of mRNA levels for αl(I) and αl(III) collagen chains in lung fibroblasts (Goldstein et al., 1989). So the insulin treatment can influence the tissue repair and promote ECM formation

especially in diabetic wounds which is in agreement with the results obtained from our studies.

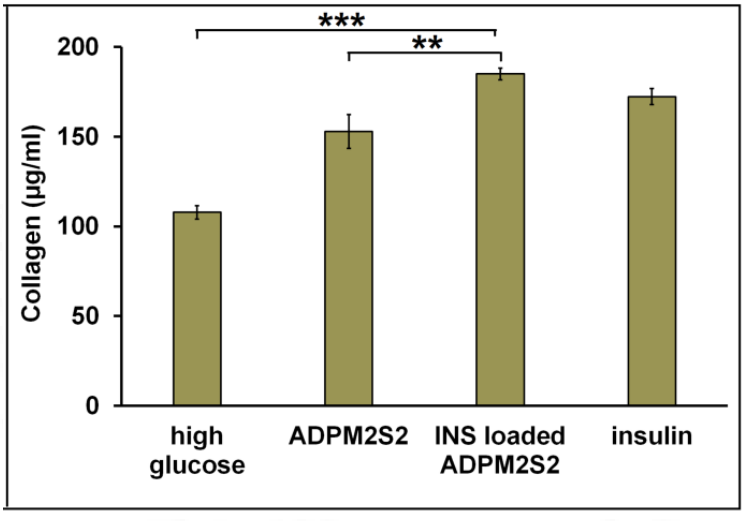

Figure 54: Deposition of collagen from L929 cells treated with insulin loaded ADPM2S2 and ADPM2S2 hydrogel alone in comparison with insulin (100 mIU/mL) and control cells grown under high glucose condition (**p<0.01, ***p<0.001).

4.3.1.3 Scratch wound assay

The effect of insulin on *in vitro* wound healing was analyzed by the classical scratch wound assay on fibroblast as well as keratinocytes (figure 55 I-II). The fibroblast cells treated with insulin loaded ADPM2S2 hydrogel showed a wound closure of 52±2.8% compared to 33±1.4% for ADPM2S2 alone within 4h.

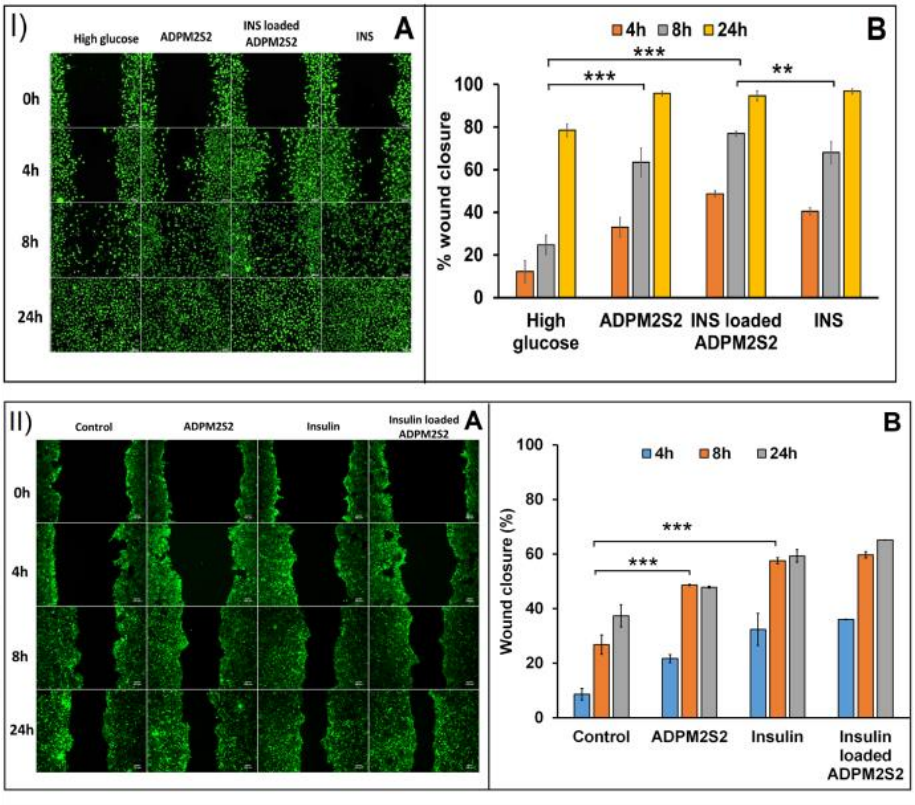

Figure 55: Scratch wound assay with percentage wound closure performed on I) L929 cells and II) HaCaT cells treated with ADPM2S2 loaded with and without insulin and compared with controls (** $p<0.01$, ***$p<0.001$).

But the wound closure was low in the case of control cells gown under hyperglycemic condition which was only 12±4.1% within 4h. After 8h, the percentage of wound closure was 63±4.1% and 79±4.2% for ADPM2S2 and insulin loaded ADPM2S2 respectively, whereas it was 24±5.2% for the cell grown under hyperglycemic conditions. Similarly, insulin loaded material had good wound healing effect on keratinocytes also. Under high glucose condition, HaCaT cells showed a wound closure of 22±3.4% within 8h. Upon treatment with ADPM2S2 hydrogel, the %wound closure increased to 48±2.6% within 8h. The application of insulin further improved the wound closure to 58±2.8%. These results suggest that insulin have

influence on cell migration and proliferation. The insulin induced keratinocyte migration and differentiation are mediated through insulin receptor dependent PI3K-Akt-Rac1 pathway. The molecular mechanism of insulin triggered keratinocyte functions following the topical delivery were studied by Liu et al on skin excisional wounds. Insulin at a critical concentration ranging from 10^{-7}M to 10^{-5}M significantly enhanced the keratinocyte migration within 24h by *in vitro* analysis. To eliminate the possibility of proliferation, cells were treated with mytomycin C (5 μg/mL) and identified that the processes of cell proliferation and migration were independently regulated by the hormone insulin. For keratinocyte proliferation, integrin α3β1 and laminin 332 (LN332) plays a critical role, and their expression particularly at the migrating edge was also improved with insulin treatment. Keratin10 one of the markers for keratin differentiation was also expressed in basal keratinocytes and these results indicate the effect of insulin in promoting wound closure (Liu et al., 2009).

4.3.1.4 Cell migration-Actin staining

The effect of insulin on cell migration was assessed by staining the actin filaments in fibroblast cells (figure 56). The cellular morphology and the actin filament distributions were disturbed under hyperglycemic condition. The cells treated with the material alone showed good actin filament orientation due to the effect of released Sr ions from the hydrogel. The actin staining was quantified as the corrected total cell fluorescence (CTCF) using ImageJ software and the data of the test groups and controls were compared. With insulin loaded hydrogels, a significant improvement in the corrected total cell fluorescence (CTCF) was observed which indicates the effect of insulin on actin filament organization. Several reports suggest that the subcellular

actin filament organization within the fibroblast cells is influenced by insulin. Increase in actin polymerization was indicated by the reduction in subcellular concentration of free G-actin molecules. The mechanism by which insulin modulate the actin filament polymerization is through tyrosine kinase activity (Vedeler et al., 1991). Insulin induced actin filament remodeling enables the translocation of GLUT4 to the cell surface for glucose transportation in skeletal muscle cells (Bisht and Dey, 2008).

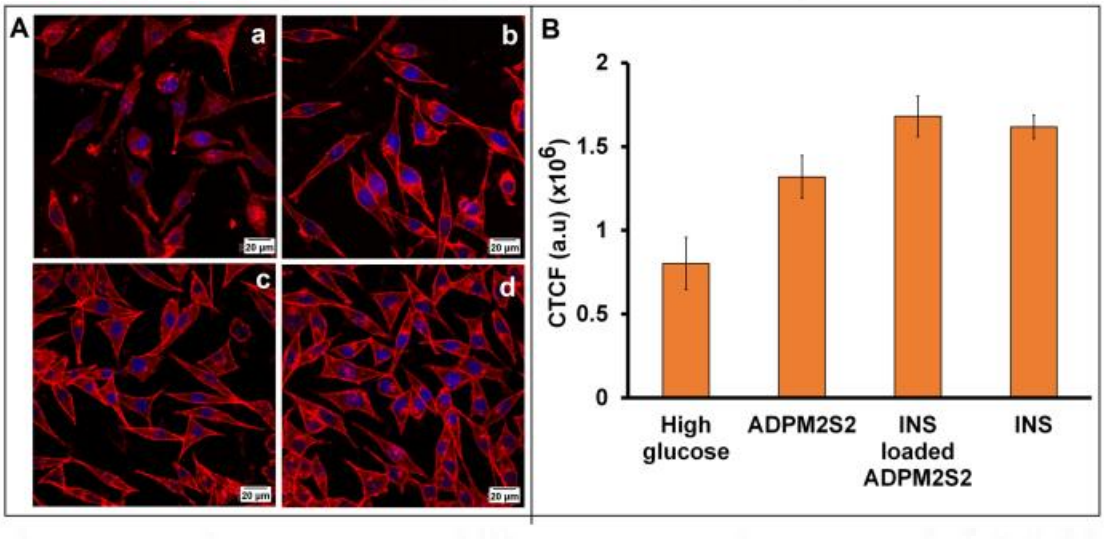

Figure 56: A) Actin filament organization in L929 cells treated with a) high glucose b) extract of ADPM2S2 hydrogel c) insulin (100mIU/ml) and d) extract of insulin loaded ADPM2S2 hydrogel and B) the corrected total cell fluorescence analyzed by ImageJ software.

4.3.1.5 Expression of Phospho Akt

The Akt/mTOR (serine threonine kinase (Akt) and mammalian target of rapamycin (mTOR)) signaling pathway plays a significant role in the wound repair and the dysfunction of this pathway results in the impaired wound healing in diabetes. Usually, growth factors act as the upstream regulators of this pathway. They phosphorylate the Akt molecule by activating PI3K, which in turn activate mTOR proteins. The activated mTOR molecule stimulate the protein synthesis required for

cell proliferation, migration, angiogenesis and collagen deposition (Jere et al., 2019). The effect of insulin in the expression of phospho Akt was analyzed under high glucose conditions (figure 57). As shown in the figure, there was reduction in the p-Akt expressing cells under hyperglycemic condition (25mM). A reduction in the expression of p-Akt in the endothelial cells was demonstrated by Varma et al under high glucose condition at 20mM and 40mM concentrations. This PI3k-Akt signaling defects leads to the macrovascular complications during diabetes, so the therapeutic restoration of the activity may have clinical significance (Varma et al., 2005). With insulin treatment, the number of p-Akt expressing cells was increased. Lima et al demonstrated that the topical application of insulin containing cream over the diabetic wound could enhance the healing process by modulating the AKT (serine threonine kinase) and ERK (extracellular signal-regulated kinase) pathways. The phosphorylated Akt molecule can regulate cell survival and protein synthesis by modulating the phosphorylation of different proteins involved in the signaling cascade. The activation of Akt is important for the release of VEGF for vascular maturation and angiogenesis. Insulin participate in the activation of IR/SHC/ERK pathway, which also play significant role in wound healing by catalyzing the phosphorylation of transcription factors for cellular proliferation and differentiation (Lima et al., 2012). In comparison to other growth factors, insulin is far more affordable and widely accessible. Here in this work, the results demonstrate the potential of insulin towards wound healing applications. Hence it can be inferred that a wound healing material through which

insulin can be delivered, could be an effective and affordable means for better wound care in diabetes patients.

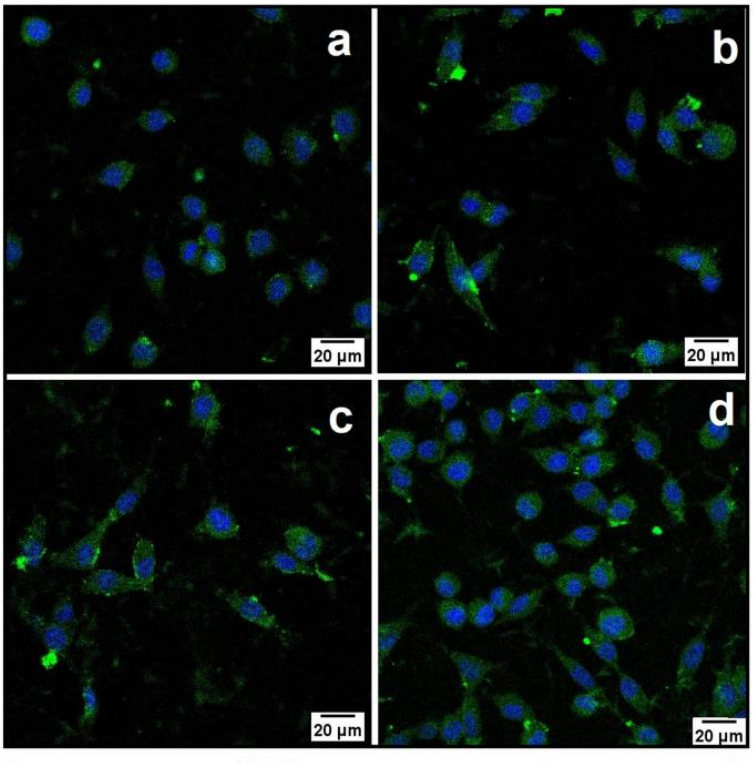

Figure 57: The expression of phospho Akt in L929 cells treated with a) high glucose media (25mM), b) the extracts of ADPM2S2 hydrogel c) insulin (100mIU/ml) and d) insulin loaded ADPM2S2 hydrogel.

4.3.1.6 Annexin-PI assay for cellular apoptosis

The increased cellular apoptosis is another concern in delayed wound healing in diabetic wounds. The flow cytometry studies with L929 cells under high glucose condition showed increase in late apoptotic cell population up to 65%. The early and late apoptotic cell population for ADPM2S2 treated group was 23% and 27%, while that of insulin loaded ADPM2S2 group was 20% and 17% respectively. And the percentage of live cells after treatment with ADPM2S2 and insulin loaded ADPM2S2 were 52% and 63% respectively. Insulin treatment could effectively reduce the late

apoptotic cells compared to high glucose controls. Different signalling pathways get altered during diabetes, including downstream Bcl2 associated death promoter (BAD) signalling. This leads to the decreased cell proliferation and increased apoptosis under high glucose conditions. The increase in oxidative stress created by hyperglycemia causes the deposition of advanced glycation end products and oxidative altered proteins. Emanuelli et al. elucidated that these structurally altered protein deposition inhibit fibroblast proliferation and collagen expression. This leads to the stimulation of stress-activated kinase p38 and mitogen-activated protein kinase (MAPK), which in turn down-regulate extracellular signal regulated kinase 1 and 2 (ERK1/2) and AKT/PKB. Such dysregulated signalling results in increased apoptosis of cells.

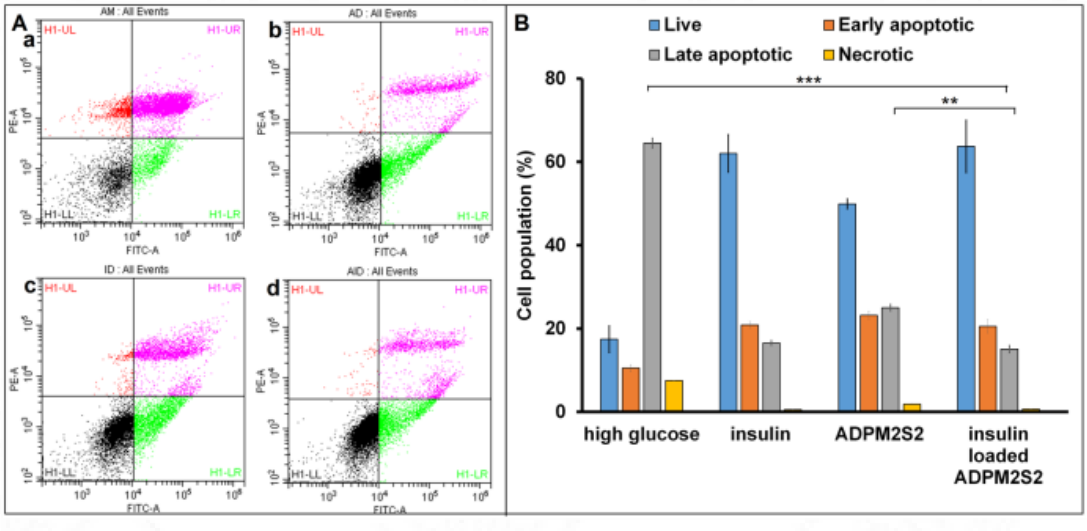

Figure 58: A) Flow cytometry analysis on L929 cells for the identification of cellular apoptosis treated with a) control (high glucose 25mM), b) ADPM2S2 hydrogel c) insulin (100mIU/ml) and d) insulin loaded ADPM2S2 hydrogel B) the percentage of cell population with various treatment (** $p<0.01$, ***$p<0.001$).

The oxidative stress lead to the development of senescent cells, DNA damage and cell cycle arrest in chronic wound bed (Emanuelli et al., 2016). Hyperglycemia alter the hypoxia-inducible factor-1α (HIF-1α) signalling, the main controller of the

oxygen hemostasis (Frykberg and Banks, 2015). The decreased oxygen supply to the wound surface further increases the apoptosis. Jing et al, elucidated that HIF-1α induction is mediated through the AKT/mTOR pathway, so the therapeutic approaches aimed to enhance this signalling cascade could be beneficial for diabetic wound management (Jing et al., 2015). Topical insulin thus improves the wound healing by regulating the oxidative stress.

4.3.1.7 Gene expression studies

The effect of insulin in wound healing was analysed by the *in vitro* gene expression studies. The genes of interest were COL1A1, keratin16, GLUT1, TNFα, IL-6, CD86, TGFβ1, IL-10 and CD163. The gene expression of COL1A1 and TGF β1 was analysed in L929 cells, keratin16 and GLUT1 expression in HaCaT cells and IL-6, TNFα, IL-10, C86 and CD163 in RAW 264.7 cells. The cells grown under normal glucose condition was treated as control. There was 1.6 fold increase in the expression of COL1A1 with insulin loaded ADPM2S2 compared to 0.8 fold by ADPM2S2 hydrogel alone. Keratin 16 expression was increased by 1.7 fold with insulin treatment, similar result was obtained with scratch wound assay. The GLUT1 (glucose transporter 1) expression within fibroblast cells was increased with insulin treatment, which help to regulate the local glucose concentration at the wound bed.

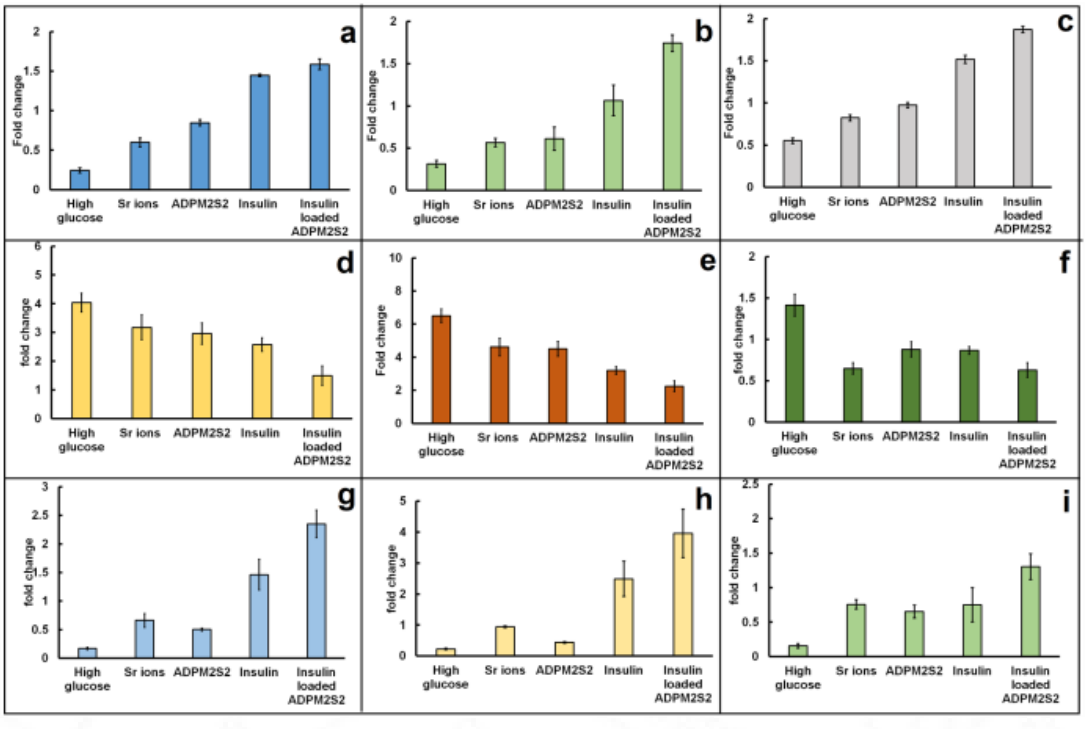

Figure 59: Gene expression of profile of different gene involved in wound healing with the treatment of insulin loaded ADPM2S2 hydrogel a) COL1A1 b) keratin16 c) GLUT1 d) TNFα e) IL-6 f) CD86 g) TGFβ1 h) IL-10 and i) CD163. The cell source for the genes are as follows, COL1A1 and TGF-β1 expression from L929, keratin 16 and GLUT1 expression from HaCaT and IL-6, TNFα, IL-10, C86 and CD163 from RAW 264.7 cells.

The proinflammatory cytokines such as TNFα and IL-6 expression was increased with cells treated under high glucose condition. A 4 fold increase in the TNFα level under high glucose condition was reduced to 1.3 fold by treating with insulin loaded ADPM2S2 hydrogel. Similarly, a 6.1 fold increase in IL-6 expression was reduced to 2.2 fold with insulin loaded hydrogel treatment. A reduction in the expression of CD86, the surface marker of pro-inflammatory M1 macrophage with insulin treatment indicates the role of insulin in regulating the inflammatory response. Tessaro et al. studied the effect of insulin treatment on macrophages of diabetic male C57BL/6 mice, stimulated by LPS (100 ng/mL). They observed that insulin could

effectively reduce the secretion of LPS-induced TNF-α, IL-6 and IL-1β in tissue specific macrophages. Insulin regulate the inflammatory response in macrophages through the modulation of PI3-kinase and ERK 1/2 pathways (Tessaro et al., 2017).

The upregulation of TGFβ1 plays a significant role in collagen deposition and extra cellular matrix formation. Insulin loaded ADPM2S2 hydrogel showed 2.3 fold increase in TGFβ1 expression. The increased expression of TGFβ1 enhanced the collagen production with insulin treatment, as seen from the Sirius red assay. Insulin also have a significant role in macrophage polarization, by upregulating the CD163 expression and down regulating the CD86 expression. This facilitates the recruitment of the M2 phenotype towards the wound bed. Topical application of insulin induces the early recruitment of neutrophils and increases the IL-10 level. Insulin also facilitate the chemotaxis and the phagocytosis of the macrophages and regulate the monocyte chemo-attractant protein-1 (MCP-1) expression for the secretion of the inflammatory mediators towards the wound site (Chen et al., 2012).

4.3.2 Effect of simvastatin on wound healing

4.3.2.1 Cytotoxicity evaluation

The cytotoxic level of simvastatin (SIM) was analysed on L929 cells by MTT assay (figure 60) and observed that it can be safely used up to 100µM concentration. Since a high- cell viability of 96% was observed with 60µM SIM, it was selected as the optimized concentration for *in vitro* analysis. Further, cell viability of SIM loaded ADPM2S2 was analysed and showed >80% viability. Oktarina et al demonstrated that SIM has antioxidant action at low doses, which helps to reduce the amount of ROS in

fibroblast cells under high glucose environment and thereby enhances cell survival and proliferation. SIM also showed a protective effect on skin fibroblasts after UV irradiation (Oktarina and Iqbal, 2022).

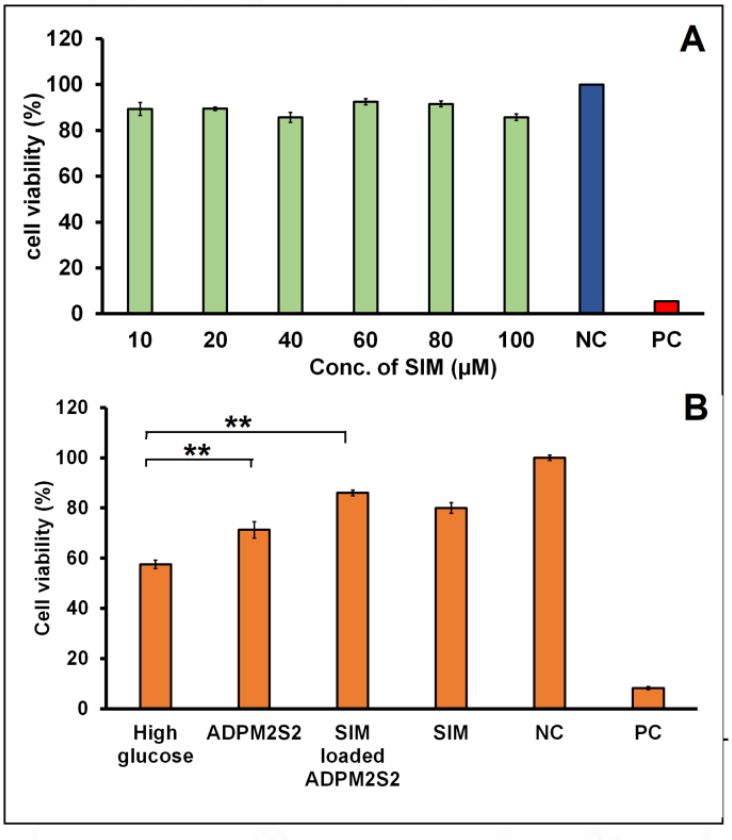

Figure 60: Cytocompatibility evaluation on L929 cells treated with A) varying concentration of SIM and B) extracts of ADPM2S2 and SIM loaded ADPM2S2 in comparison with the controls (**p<0.01).

4.3.2.2 Collagen deposition

The collagen production from fibroblast cells under high glucose condition was analyzed by the Sirius red assay (figure 61). Under normoglycemic condition, the collagen production was 145±3.1µg/ml, while under hyperglycemic condition the collagen production was only 107±5.1 µg/ml. While comparing the collagen production with treatment of hydrogel and SIM alone, no significant improvement was

observed. But with SIM loaded ADPM2S2 hydrogel, collagen production was enhanced to 156±4.6µg/ml. Fibroblast proliferation slows down and undergoes structural changes in diabetic wounds. This leads to a reduction in the synthesis of ECM proteins like collagen, resulting in impaired wound healing process (Black et al., 2003). Strontium ions play a significant role in collagen synthesis and matrix formation. The ADPM2S2 hydrogel showed 40% release (3mM) of Sr ions within 48h. This released Sr ions enhanced the collagen deposition from L929 cells.

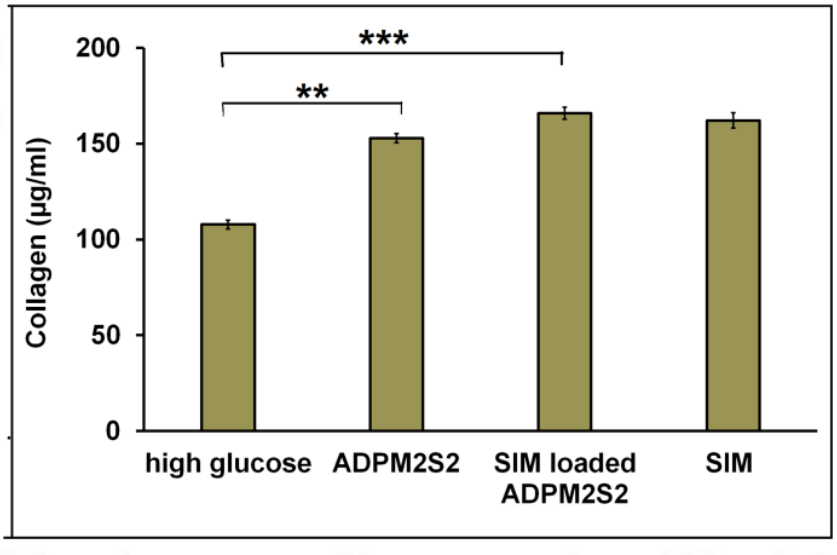

Figure 61: Deposition of collagen from L929 cells treated with SIM loaded ADPM2S2 and ADPM2S2 hydrogel alone in comparison with SIM (60µM) and control cells grown under high glucose condition (**p<0.01, ***p<0.001).

A similar result was observed by Wang et al, where 3 to5 mM concentration of strontium ions could stimulate the mRNA expression of type II collagen and IGF-1, which promote extracellular matrix synthesis. The expression of MMP-13 got suppressed with increase in concentration of Sr ions, which in turn inhibit the degradation of collagen (Wang et al., 2013). Simvastatin molecule has positive impact

on the expression of prolyl-4-hydroxylase (P4H) α1, which is one of the key enzymes in collagen synthesis. This enzyme catalyzes the conversion of proline to hydroxyl proline in X-Pro-Gly triplets during post translational modification of collagen (Zhang et al., 2013). Khoshneviszadeh et al demonstrated an increase in fibroblast proliferation and collagen bundle synthesis by the topical application of SIM on full thickness skin wounds in rat models (Khoshneviszadeh et al., 2014).

4.3.2.3 Cell migration-Actin staining

The effect of SIM on cellular migration was assessed by staining of actin filaments in fibroblast cells (figure 62). Hyperglycemic condition induces physiological changes within the fibroblast cells leading to reduced expression of α-smooth muscle expression. The alteration in the cell morphology and actin filament distribution was observed with cells under high glucose condition. The treatment with ADPM2S2 hydrogel showed good actin filament orientation. This is due to the release of strontium ions from the matrix. As reported earlier the analysis of crystalline structure of actin revealed that strontium ions are one of the integral component of the actin monomer, which plays a significant role in the actin polymerization (Strzelecka-Gołaszewska, 2001). Strontium ions bound to the secondary structure of actin molecules; with monomer A of actin, Sr ions interact with Asp222, Glu224 and Glu316 via water molecules, while with monomer B, coordinated through carbonyl oxygen of Val30 and connected to Asp56 and Glu93 via a water molecule (Klenchin et al., 2006). Thus the localized delivery of Sr ions has a good impact on actin filament organization in diabetic conditions.

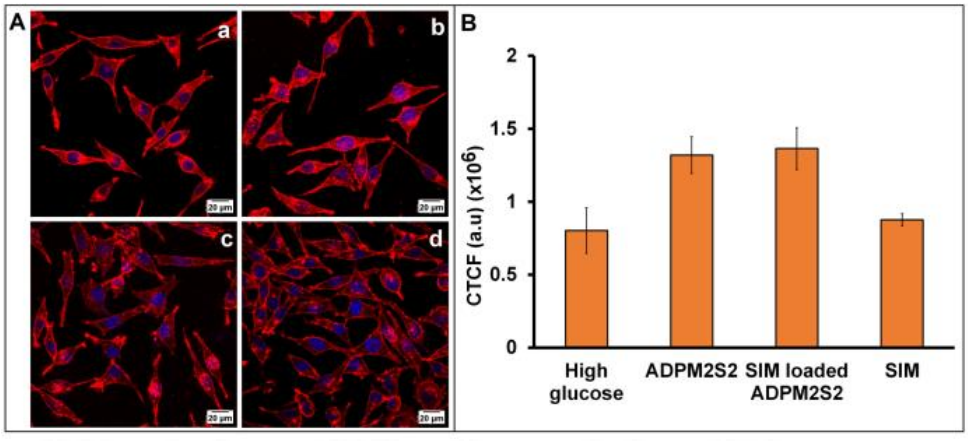

Figure 62: A) Migration of fibroblast cells analysed by actin filament staining a) high glucose control b) cells treated with the extract of ADPM2S2 hydrogel c) cells treated with the extract of SIM loaded ADPM2S2 hydrogel and cells treated with SIM (60µm). B) The corrected total cell fluorescence of different groups analysed by Image J software.

The quantification of the corrected cell fluorescence showed that there was no significant improvement in the actin filament organization with SIM treated groups compared to control cells under high glucose conditions. This is in agreement with previously reported studies in which no significant improvement in the actin filament organization was observed with SIM treatment (Chubinskiy-Nadezhdin et al., 2017). Similarly no significant difference in the actin filament formation was observed with ADPM2S2 treated and SIM loaded ADPM2S2 groups.

4.3.2.4 Scratch wound assay

The effect of SIM on *in vitro* wound healing was analyzed by the classical scratch wound assay on fibroblast as well as keratinocytes (figure 62). The fibroblast cells cultured under hyperglycemic condition showed a wound closure of 12±4.1% within 4h. Wounds treated with SIM loaded ADPM2S2 hydrogel showed 48±2.6%

wound closure compared to 33±1.4% for ADPM2S2 alone within 4h. After 8h, the percentage of wound closure was 53±1.1% and 67±4.2% for ADPM2S2 and SIM loaded ADPM2S2 respectively. Similarly, SIM loaded material also had good wound healing effect on keratinocytes. Under high glucose condition, HaCaT cells showed a wound closure of 22±3.4% within 8h. Upon treatment with ADPM2S2 hydrogel, the %wound closure was increased to 35±2.6% within 8h. The application of SIM further improved the wound closure to 45±3.8%. These results suggest that SIM have influence on cell migration and proliferation. The enhanced wound healing with SIM-loaded ADPM2S2 highlights the significance of synergistic interaction of strontium ions with SIM. Ramhormozi et al studied the effect of topically delivered SIM in modulating the Akt/mTOR pathway. The activation of this pathway augments the epithelial cell proliferation and migration as well as collagen synthesis. They studied the effect of bone marrow derived mesenchymal stem cells along with SIM in second degree burn wound models and observed the elevated expression of Akt and mTOR genes, resulted in the accelerated wound healing process (Ramhormozi et al., 2021).

Khoshneviszadeh et al demonstrated the *in vivo* wound healing effects of SIM loaded carboxymethylcellulose gels. The topical application of 2% SIM on 1cm^2 full thickness wounds on rat models showed complete re-epithelialization within 12 days with no sign of any inflammatory response compared to controls (Khoshneviszadeh et al., 2014). In another study by Yasasvini et al, the wound healing effects of polyvinyl alcohol hydrogel incorporated with SIM loaded chitosan microparticles was demonstrated. They observed that there was significant reduction in wound area with

hydrogel loaded with low dose of SIM compared to high-dose hydrogels (Yasasvini et al., 2017). The simultaneous delivery of SIM and Sr ions was demonstrated by Li et al through a multifunctional biomaterial based on hydroxy apatite microspheres. The particles released 4.56 ± 0.36% of SIM and 2.51 ± 0.03% of Sr ions simultaneously within 24h and the release was sustained for 35 days. The microspheres which simultaneously release SIM and Sr ions could be used as a drug-loading platform for constructing biomaterials with osteogenic and angiogenic abilities (G. Li et al., 2021). SIM also modulate the healing process by reducing the oxidative stress, promoting lymph angiogenesis and immunomodulatory effect (Raposio et al., 2016). So the therapeutic approach of simultaneous delivery of SIM and Sr ions could be effective for diabetic wound management.

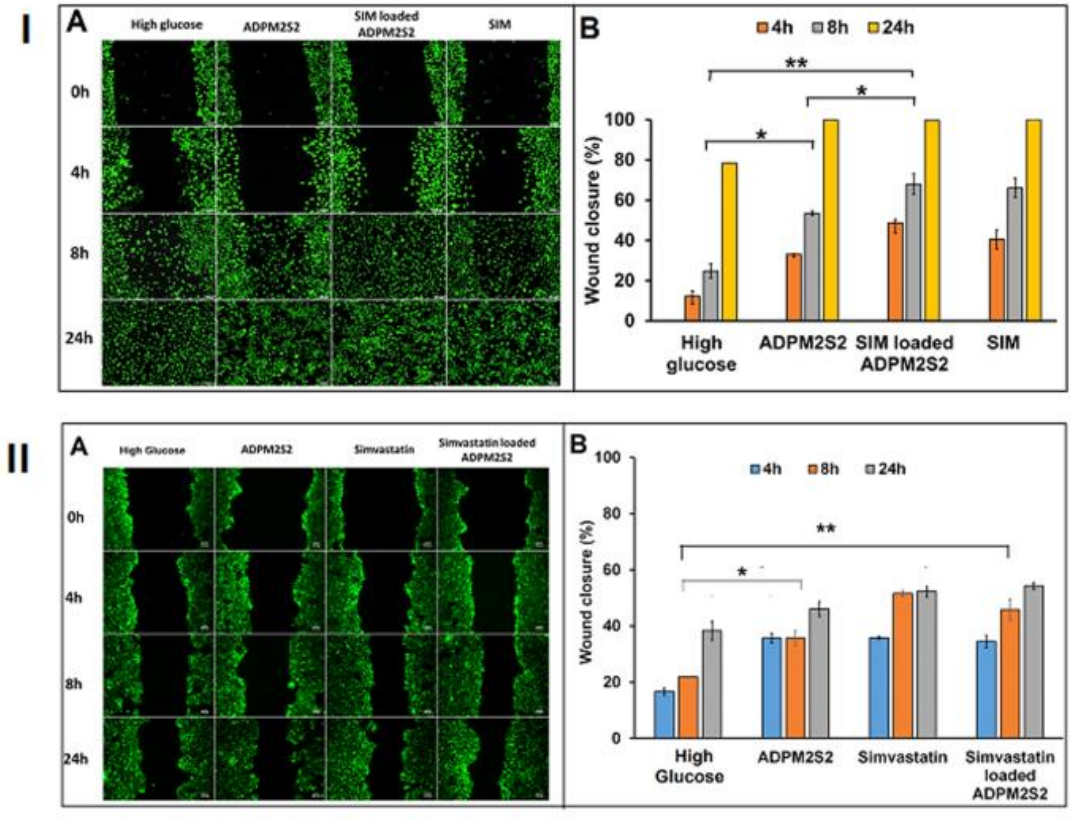

Figure 63: Scratch wound assay with percentage wound closure performed on I) L929 cells and II) HaCaT cells treated with ADPM2S2 loaded with and without SIM and compared with controls (** $p<0.01$, ***$p<0.001$).

4.3.2.5 Anti-inflammatory activity

The anti-inflammatory activity of SIM-loaded ADPM2S2 hydrogels were analysed by the quantifying the TNF-α produced from the macrophages (figure 64). The TNF-α produced by the LPS stimulated macrophages was found to be 265±1.8pg/ml within 24h. The treatment of the cells with SIM showed a significant reduction in TNF-α level up to 168±4.8pg/ml. The TNF-α level of the cells treated with ADPM2S2 alone and SIM loaded ADPM2S2 was 240±3.3pg/ml and 149±6.8pg/ml respectively. These results suggest that the material alone has an anti-inflammatory activity of 19±2.4% which can be attributed to the release of Sr ions

from the hydrogels. Thus strontium ions possess anti-inflammatory activity and induce the conversion of macrophages towards M2 phenotype.

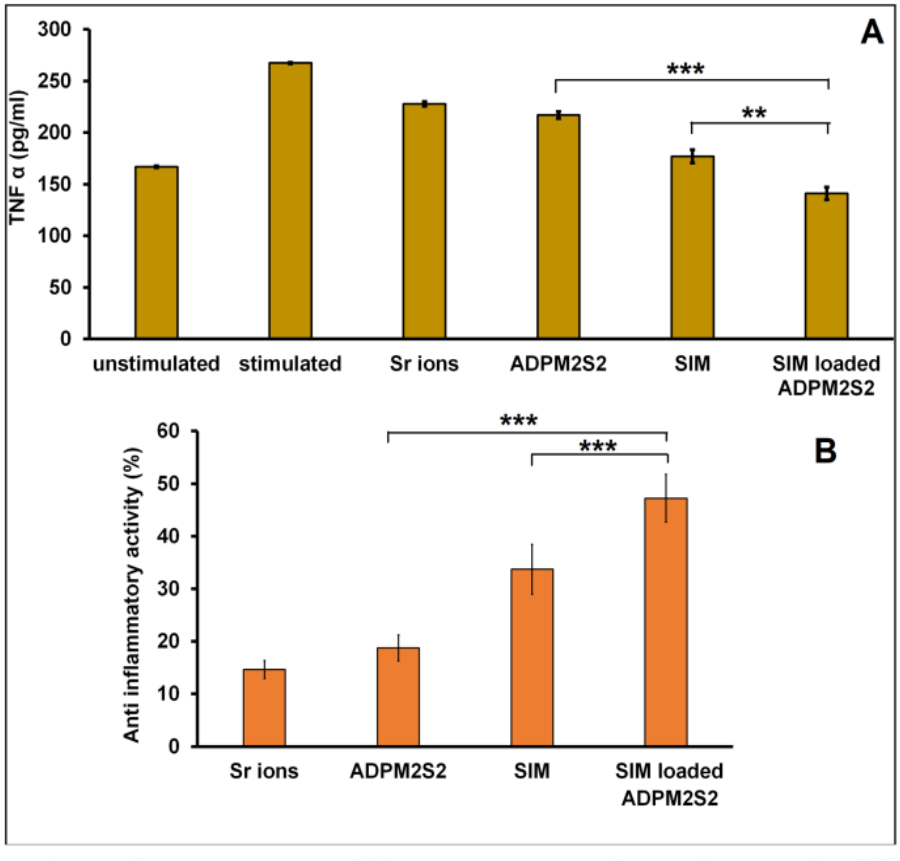

Figure 64: A) The quantification of TNF-α level by ELISA in LPS stimulated macrophages B) the percentage of anti-inflammatory activity shown by different test groups (**p<0.01,***p<0.001).

You et al demonstrated that strontium functionalized biomaterials play significant role in immunomodulation by upregulating the expression of anti-inflammatory cytokines and growth factors associated with tissue regeneration (You et al., 2022). The anti-inflammatory activity was increased up to 44±4.5% with the SIM loaded hydrogel. The prolonged inflammatory phase in chronic wounds are characterized by the elevated TNF-α levels, which leads to enhanced proteolysis and

reduced extracellular matrix deposition (Ashcroft et al., 2012). The increased pro-inflammatory cytokines alter the cellular activities such proliferation, migration, macrophage polarization and vascularization (Xu et al., 2013). In diabetes, the higher glucose level produces oxidative stress, leading to the elevated pro-inflammatory cytokines, which in turn leads to the prolonged inflammatory phase. So any therapeutic approach which targets towards reducing the TNF-α level could be effective for diabetic wound management (Ponugoti et al., 2012). Tuomisto et al demonstrated that the treatment with SIM can block the TNF-α induced NF- κB transcriptional activity and IκB degradation and produce strong anti-inflammatory activity (Tuomisto et al., 2008). Under hyperinflammatory conditions, SIM at a concentration of 25μM showed protective effect on endothelial progenitor cells (EPC), resulting in the significant reduction in the TNF-α mediated apoptosis (Henrich et al., 2007). Simvastatin treatment promote the up-regulation of silent information regulator type-1 (SIRT1) protein, which prevent the TNF-α induced apoptosis in EPC and promote endothelial proliferation (Du et al., 2014). In another study, Buabeid et al demonstrated that SIM loaded nano composite of silver nanoparticles prevents the granuloma formation during chronic inflammation and supress the TNF-α and IL-1ß expression through the transcription factor NF-kB (Buabeid et al., 2022). Some studies showed that statin drugs have significant impact on the restoration of microcirculation of the sciatic nerve during diabetic neuropathy (Gulcan et al., 2007).

4.3.2.5 Flow cytometry analysis

The effect of SIM in macrophage polarization was evaluated by the flow cytometry analysis (figure 65). To differentiate the M1 and M2 macrophages, CD86 and CD163 surface markers were used respectively. As shown in the figure, the control cells grown under high glucose condition showed increase in M1 population. With SIM treatment, a shift towards M2 population was observed. The M2 phenotype increased from 8.8% of SIM alone treated group to 10.3% with SIM loaded ADPM2S2 hydrogel treatment. The increase in M2 phenotype in SIM loaded ADPM2S2 group is due to the synergistic action of SIM and Sr ions.

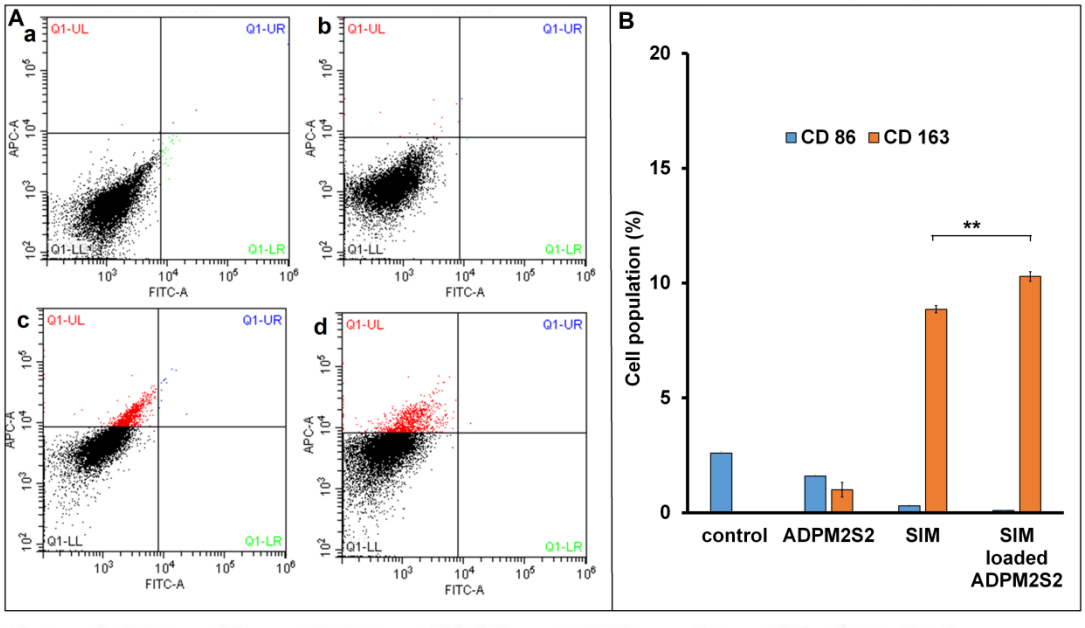

Figure 65: A) Flow cytometry analysis for determining the macrophage polarization with a) high glucose control b) ADPM2S2 hydrogel c) SIM (60µM) and d) SIM loaded ADPM2S2 hydrogel and B) the percentage of M1 and M2 macrophage cell population (**p<0.01).

The prolonged inflammatory phase in diabetic wounds is due to the persistent M1 phenotype at the wound area. The high glucose condition trigger the pro-

inflammatory signaling, leading to the impaired transition of M1 to M2 phenotype. So a wound dressing which is effective in the transition of M1 to M2 phenotype is an attractive approach for the treatment of diabetic wounds (Louiselle et al., 2021).

4.3.2.6 Gene expression studies

The synergistic effect of simultaneous delivery of SIM and Sr ions in wound healing was analyzed by the *in vitro* gene expression studies (figure 66). The COL1A1 gene was upregulated by1.3 fold in SIM treated groups compared to material alone. A similar result was obtained with the Sirius red assay for collagen deposition. The effect of SIM treatment on cell proliferation and migration was observed by the increased expression of keratin 16, which was also evidenced by the scratch wound assay. GLUT1 is another important gene which plays significant role in diabetic wound healing, by regulating the local glucose concentration. A reduced expression of GLUT1 was observed with cells grown under high glucose condition. The GLUT1 expression was increased by 0.8 fold and 1.1 fold with the treatment of hydrogel alone and loaded with SIM respectively. The gene expression of pro-inflammatory cytokines such as IL6 and TNFα were decreased with SIM and Sr ion treatment. A 4.2 fold increase in the expression of TNFα under hyperglycemic condition was reduced to 1.3 fold with SIM loaded hydrogel treatment. A similar result was obtained by the quantification of TNFα by ELISA. The upregulation of IL 10, which is one of an anti-inflammatory cytokine, was observed with SIM loaded ADPM2S2 hydrogel due to the combined effect of SIM and Sr ions. The anti-inflammatory activity was mediated through the recruitment of M2 macrophages towards the wound site. Simvastatin

treatment showed increased expression of CD163 and reduction in CD86 expression. The expression of CD86 was reduced from 1.4 fold with cells under high glucose condition to 0.5 fold with SIM loaded hydrogel. Similarly, CD163 expression was improved to 2.2 fold with the treatment of SIM loaded hydrogel. A similar result was obtained with flow cytometry analysis. This indicated that SIM plays a critical role in the macrophage polarization from M1 to M2 phenotype.

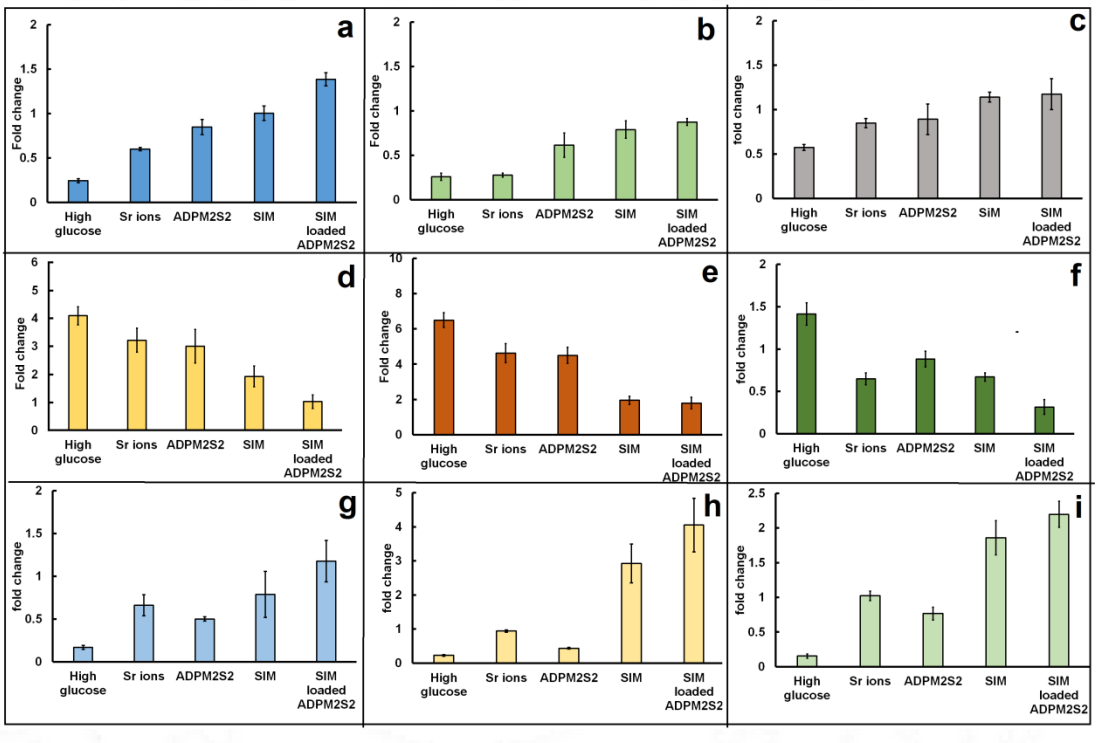

Figure 66: Gene expression of profile of different gene involved in wound healing with the treatment of simvastatin loaded ADPM2S2 hydrogel a) COL1A1 b) keratin16 c) GLUT1 d) TNFα e) IL-6 f) CD86 g) TGFβ1 h) IL-10 and i) CD163. The cell source for the genes are as follows, COL1A1 and TGF-β1 expression from L929, keratin 16 and GLUT1 expression from HaCaT and IL-6, TNFα, C86 and CD163 from RAW 264.7 cells.

TGFβ1 is another important gene that plays important role in the collagen deposition and fibronectin synthesis. It is reported that all forms of TGFβ is found to

be absent in chronic wound bed resulting in the fibroblast abnormalities and reduced cell proliferation and migration (Liarte et al., 2020). The TGFβ1 gene was expressed 3.3 fold and 4.2 fold with SIM treatment and SIM loaded ADPM2S2 hydrogel respectively. So these *in vitro* results showed that the localized delivery of SIM combined with Sr ions could be effective in promoting wound healing process. The systemic administration of SIM is suggested by the clinicians to treat the prolonged inflammation with diabetic ulcers. But the high dosage will cause myotoxic and hepatotoxic consequences. So the local administration of SIM is more effective than systemic administration (Zhao et al., 2020).

4.3.3 In vitro wound healing effects of glucose oxidase peroxidase-loaded ADPM2S2 hydrogel

4.3.3.1 Cytotoxicity evaluation

The viability of L929 cells in presence of varying concentrations of glucose oxidase was analysed (figure 67). Glucose oxidase at a concentration of ≤150mIU/mL showed more than 80% cell viability. So 150mIU/mL of GO was taken as the optimized concentration for *in vitro* studies. Cell viability of GO-POD loaded ADPM2S2 system was analysed by MTT assay on fibroblast cells. Under high glucose condition only 60% cells were viable, which increased to 70% with the treatment of ADPM2S2 hydrogel alone. The release of GO-POD from the hydrogel improved the cellular viability up to 83% compared to 66% viability with cells treated with GO alone loaded hydrogels. A cytotoxic response was observed with GO alone loaded systems, due to the generation of hydrogen peroxide and subsequently reactive oxygen species. The incorporation of POD helps to neutralize hydrogen peroxide and thereby scavenge

the ROS produced locally and protects the cells from toxic effects of ROS. The reduction in the H_2O_2 level as well as increase in the molecular oxygen favour cellular respiration. Since wound healing is an energy demanding process, adequate amount of oxygen is necessary for the release of energy for neovascularization, antimicrobial action and collagen synthesis (Gordillo and Sen, 2003).

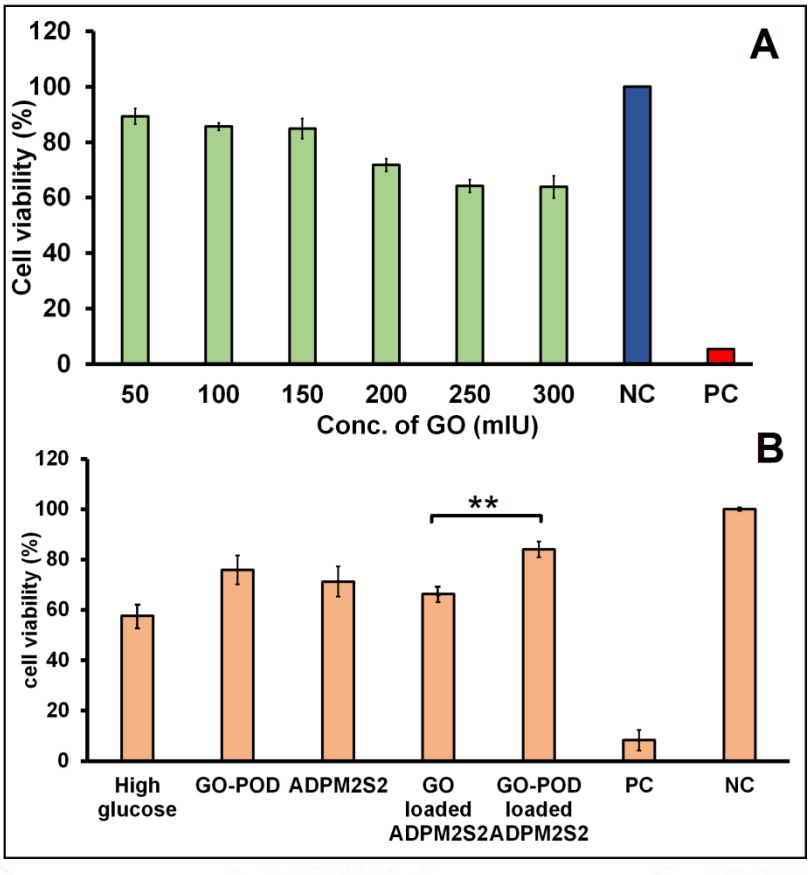

Figure 67: Cytocompatibility evaluation on L929 cells treated with A) varying concentration of GO (50 to 300 mIU/mL) and B) extracts of ADPM2S2, GO loaded ADPM2S2 and GO-POD loaded ADPM2S2 compared with controls (**p<0.01).

Under hyperglycemic condition, cells may undergo phenotypic changes, resulting in impaired cell proliferation and differentiation. Spravchikov observed that epidermal human keratinocytes shifted their morphology from small organized cells

under normal glucose condition towards large flattened cells under high glucose condition (Spravchikov et al., 2001). Keratinocytes cultured under high glucose conditions also showed a reduction in replicative life span with reduced DNA synthesis and protein production (Terashi et al., 2005). The down regulation of p38/MAPK pathway leads to the inhibition of keratinocyte migration under high glucose condition (Li et al., 2019). The enhanced nitration of annexin A2 protein caused by high glucose stress also make fibroblasts to exhibit impaired cell migration and inhibits bFGF signalling (Xuan et al., 2014).

4.3.3.2 Collagen deposition

The effects of the enzymes GO-POD on collagen deposition was analysed by treating L929 cells grown under high glucose conditions with the extracts from the hydrogels loaded with GO alone and GO-POD (figure 68). The collagen production was reduced to 107±4.2µg/mL under high glucose condition compared to cells grown under normal condition. A significant improvement in the collagen production was observed with the treatment of GO-POD loaded ADPM2S2 hydrogel as well as ADPM2S2 hydrogel alone. Cells treated with the extract of ADPM2S2 showed a deposition of 159±3.6µg/mL, while that of GO-POD loaded system was 166±5.1 µg/mL. The deposition of collagen was reduced with GO alone loaded systems to 140±3.7µg/mL compared to ADPM2S2 and its GO-POD loaded systems. The incorporation of POD effectively reduces the H_2O_2 level and favour the collagen deposition.

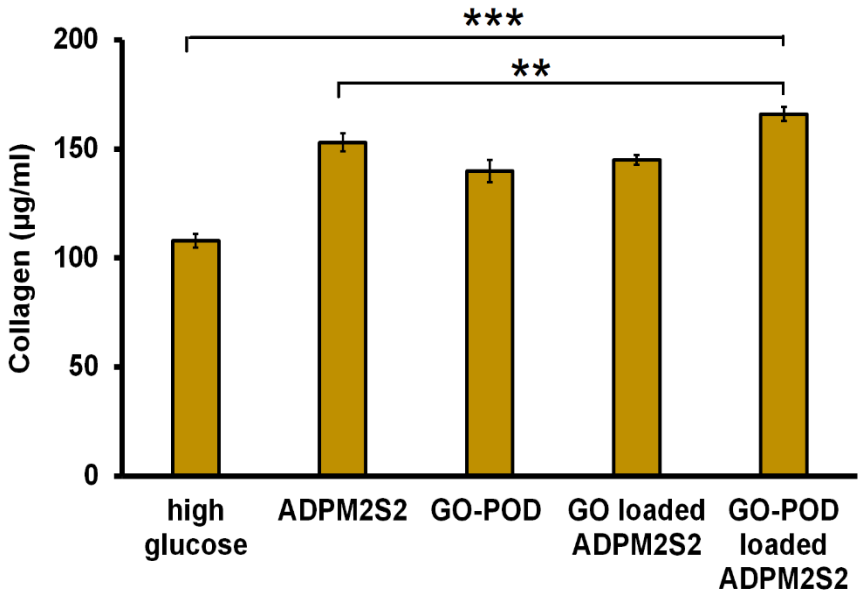

Figure 68: Deposition of collagen from L929 cells treated with GO and GO-POD loaded ADPM2S2 and ADPM2S2 hydrogel alone and compared with GO-POD (GO: 150mIU/mL and POD: 15 IU/mL) and control cells treated under high glucose condition (**p<0.01, ***p<0.001).

Wilgus et al reported that the elevated H_2O_2 increased the expression of transforming growth factor, resulting in fibroblast proliferation, which in turn interfere with the scar-less wound healing in murine foetal model (Wilgus et al., 2005). So it is ideal to maintain optimum level H_2O_2 at the wound surface. The peroxidase enzyme helps to maintain the local H_2O_2 level and to regulate the collagen extracellular matrix biosynthesis. DeNichilo et al reported that peroxidases have pro-fibrogenic capacity to stimulate the fibroblast migration and promote the secretion of collagenous proteins for ECM formation (DeNichilo et al., 2015). The post translational modifications in prolyl-4-hydroxylases are regulated by peroxidases in a dose dependent manner. So the GO-POD loaded ADPM2S2 hydrogels can be effectively used to regulate high glucose level, which in turn improve the wound healing process.

4.3.3.3 Scratch wound assay

The scratch wound assay was performed on both fibroblast cells and keratinocytes (figure 69). The percentage of wound closure with fibroblast cells under hyperglycemic condition was 20 ± 3.6% by 8h. Treatment with ADPM2S2 hydrogels showed a wound closure of 57% within 8h. No significant increase in wound closure was observed with GO-POD loaded ADPM2S2 hydrogels (61%) compared to hydrogel alone at 8h. The percentage of wound closure with keratinocytes under hyperglycemic condition was 17% by 8h and 33% by 24h. The keratinocytes treated with ADPM2S2 hydrogel showed a wound closure of 35% in 8h and 42% within 24h. A similar result was observed with GO-POD loaded ADPM2S2 hydrogels, the wound closure was 36% and 44% for 8h and 24h respectively. But a significant improvement in wound closure was observed with GO-POD loaded system compared to cells treated under high glucose conditions. The results showed that the controlled delivery of GO-POD has positive impact on wound healing process.

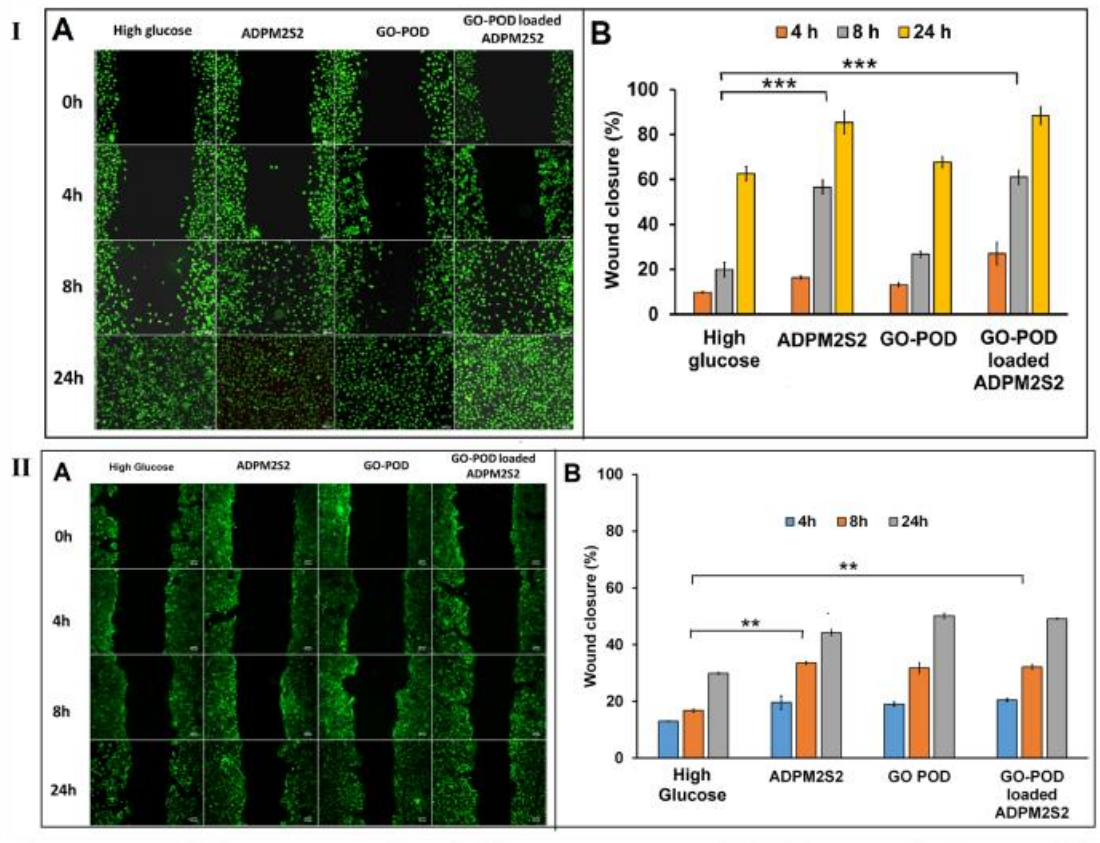

Figure 69: Scratch wound assay with percentage wound closure performed on I) L929 cells and II) HaCaT cells treated with ADPM2S2 loaded with and without GO-POD in comparison with controls (** $p<0.01$, ***$p<0.001$).

The combined delivery of GO-POD could effectively regulate the reactive oxygen species produced as a consequence of hyperglycaemic condition. The effect of high glucose on fibroblast migration was studied by Xuan et al., and suggested that high glucose inhibits the basic fibroblast growth factor (bFGF) signalling and there by delays cell migration (Xuan et al., 2014). The effect of GO incorporated collagen matrices on diabetic wound healing was studied by Arul et al and they observed improved cell proliferation and granulation tissue formation. *In vivo* studies on diabetic rat models showed fully matured granulation tissue with well aligned collagen

fibers and histopathological evaluation showed clearly differentiated keratinocytes with more collagen fibers in the extracellular matrix for GO treated groups (Arul et al., 2012).

4.3.3.4 Cell migration-Actin staining

The actin filament organization towards wound area plays a significant role in wound healing process. The molecules that regulate the actin filament dynamics can alter the rate of wound closure (Kopecki and Cowin, 2016). However under high glucose condition, altered cell migratory behaviour was observed. As shown in figure 70, the cells grown in high glucose media showed altered actin filament structure. High glucose leads to increased oxidative stress within the cells, which causes loss of polarity, impaired protrusion and adhesion of cells. Cells treated with hydrogel alone and the GO-POD loaded systems showed improved actin filament orientation compared to cells grown in high glucose medium and the cells treated directly with GO-POD. The quantitative analysis of the fluorescence intensity using ImageJ software also showed significant improvement in actin filament orientation with GO-POD loaded hydrogel treatment. But the cells treated directly with GO-POD showed alteration in the cell morphology and actin filament staining. This can be attributed to the increased oxidative stress created on the cells by the direct application of GO-POD. The concentration of H_2O_2 might affect the actin orientation and viability of the cells. The differential sensitivity of fibroblast and keratinocytes towards varying concentration of H_2O_2 was analysed by Loo et al and observed that keratinocytes were resistant up to 700μM concentration of H_2O_2, while fibroblast showed cytotoxic effect

with H_2O_2 concentration at 500µM or above (Loo and Halliwell, 2012). In order to control the H_2O_2 concentration, a controlled release of GO-POD is necessary, which enables the proper actin filament orientation under hyperglycemic condition. The deleterious effect of high glucose can be nullified by the sustained delivery of GO-POD towards the wound microenvironment.

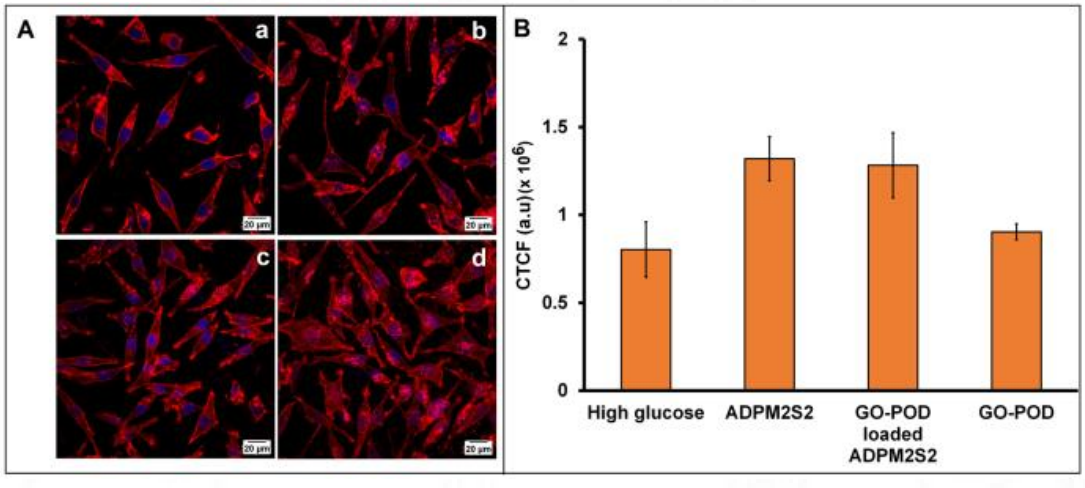

Figure 70: A) Migration of fibroblast cells analysed by actin filament staining a) high glucose control b) cells treated with the extract of ADPM2S2 hydrogel c) cells treated with the extract of GO-POD loaded ADPM2S2 hydrogel and cells treated with GO-POD (GO:150mIU, POD:15IU) B) The corrected total cell fluorescence of different groups analysed by Image J software.

4.3.3.5 Reactive oxygen species production

The formation of reactive oxygen species was analysed by DCFDA assay in fibroblast cells. As shown in the figure 71, under hyperglycemic condition more fluorescent cells were observed due to the production of ROS within the cells. Hyperglycemic condition can induce cellular damage due to the formation of reactive oxygen species. Similar results were observed with the direct treatment of H_2O_2 as well as GO on to the cells. Hydrogels loaded with GO alone also produced ROS

positive cells. This is attributed to the formation of hydrogen peroxide due to the breakdown of glucose to D glucono lactone and hydrogen peroxide by the action GO. In the case of direct treatment of GO-POD to the cells also there was ROS generation, however it was lesser in comparison with GO alone. However a significant reduction in ROS production was observed with the combined delivery of GO-POD through the hydrogels which is due to the conversion of hydrogen peroxide to water by the peroxidase enzyme. The ECM proteins gets modified or degraded by the reactive oxygen species and also impairs the functions of fibroblasts and keratinocytes (Dunnill et al., 2017). Reactive oxygen species in excess can interact with the other biological molecules through oxidation-reduction mechanisms. The excessive ROS can activate the pro-apoptotic pathway and induce the cell death (Zhu et al., 2017).

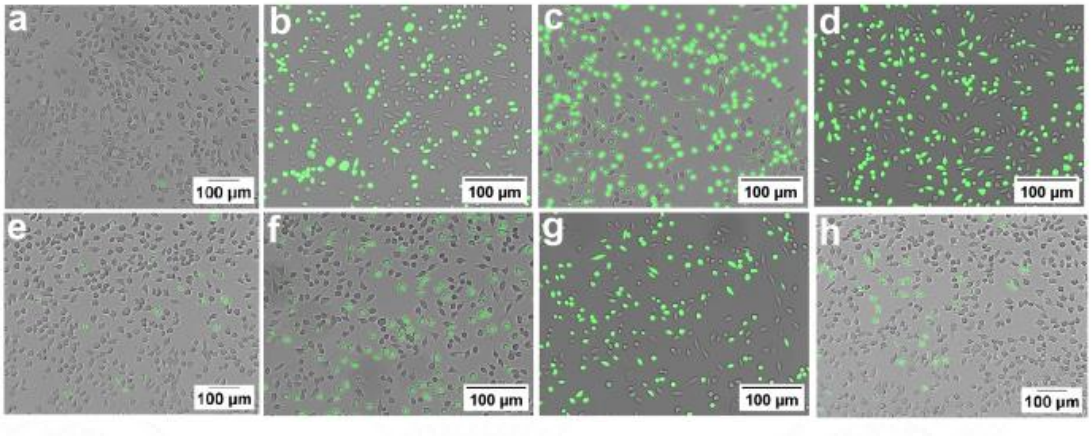

Figure 71: Reactive oxygen species by DCFDA assay on fibroblast cells a) control-low glucose b) control-high glucose c) H_2O_2 d) GO (150mIU) e) extract of ADPM2S2 hydrogel f) GO-POD (150mIU/mL, 15 IU/mL), g) extract of GO loaded ADPM2S2 hydrogel h) extract of GO-POD loaded ADPM2S2 hydrogel.

Excess amounts of ROS possess toxic effect, however an optimum level of ROS is necessary for the normal cell functioning and homeostasis. The redox reaction

initiated by H_2O_2 plays a significant role in various basic cellular processes such as proliferation, secretion and migration (Dumas and Knaus, 2021). Klyubin et al demonstrated that H_2O_2 at a concentration of 10µM can act as a chemo-attractant for inflammatory cells. Hydrogen peroxide can convert into a chemo-attractant molecule without interacting with the plasma precursor. Hence it was suggested that H_2O_2 could play an important role in cell-cell communication similar to secondary messengers (Klyubin et al., 1996). In another study, Niethammer et al the role of H_2O_2 in zebra fish larvae during the early events of wound healing was identified. They observed that H_2O_2 plays a significant role in the wound-to-leucocyte signalling around the wound margin to support the reparative process (Niethammer et al., 2009). The oxidative stress level of H_2O_2 was identified by Tur et al by studying the effect of varying concentration of the same on mice excisional wound models. They observed that H_2O_2 concentration of 10mM showed improved angiogenesis and reparative response in vivo (Tur et al., 1995). In our study, the GO-POD loaded ADPM2S2 hydrogel could effectively maintain the H_2O_2 level below 10mM, which could be optimum for promoting wound healing process.

4.3.3.6 Gene expression studies

The effect of the 24h extracts from GO-POD loaded ADPM2S2 hydrogels in the expression of various genes involved in wound healing was analysed by RT PCR. The up regulation of genes such as keratin16, GLUT1 and TGFβ1 were observed with cells grown under hyperglycemic conditions when treated with the 24h extracts of GO-POD. Under hyperglycemic condition, GLUT1 expression was reduced due to the

increased oxidative stress created by the reactive oxygen species. The GLUT1 expression was upregulated to 1.5 fold with GO-POD loaded ADPM2S2 hydrogel compared to 0.6 fold with cells grown under high glucose condition. The GO-POD system could effectively reduce the glucose concentration as well as ROS level, thereby enhance the expression of GLUT1(Andrisse et al., 2014, p. 1). There was no significant improvement in COL1A1 expression with GO-POD treatment when compared to cells treated with hydrogel alone. No anti-inflammatory activity was also shown by GO-POD system. The level of pro-inflammatory cytokines such as TNFα and IL-6 was not reduced significantly with GO-POD loaded hydrogels compared to hydrogel alone treatment. There was no improvement in macrophage polarization towards M2 phenotype observed with GO-POD system compared to treatment with hydrogel alone.

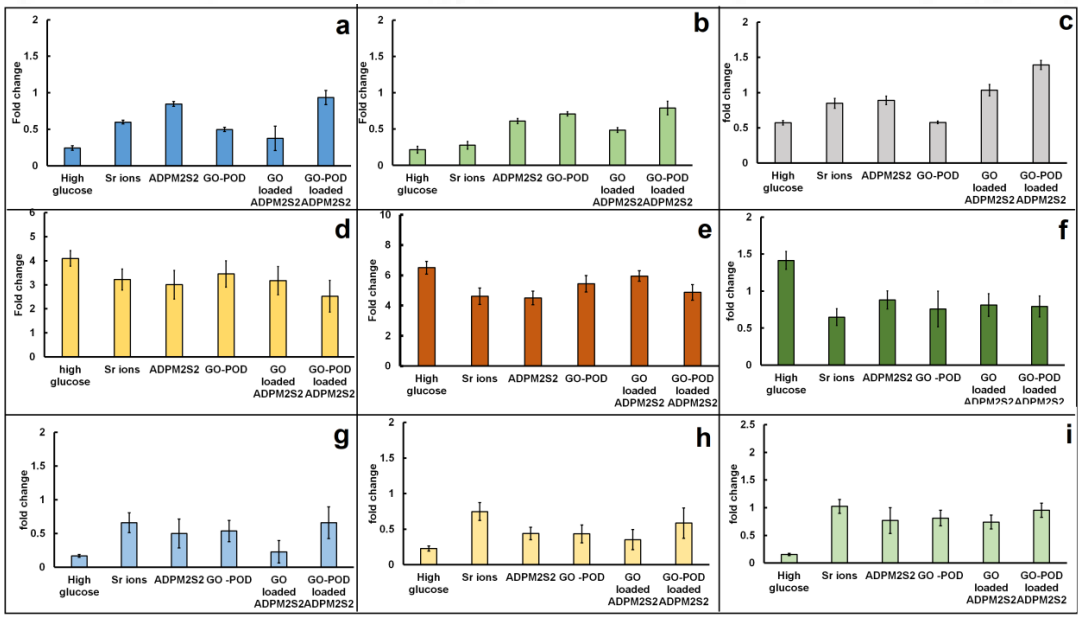

Figure 72: Gene expression of profile of different gene involved in wound healing with the treatment of GO-POD loaded ADPM2S2 hydrogel a) COL1A1 b) keratin16 c) GLUT1 d) TNFα e) IL-6 f) CD86 g) TGFβ1 h) IL-10 and i) CD163.

By *in vitro* studies, it was observed that GO-POD delivery towards diabetic wounds had significant role in regulating the local glucose as well as ROS levels. The major wound healing stages such as collagen deposition, wound closure and anti-inflammatory activity were not improved significantly compared to the delivery of other biomolecules by in vitro analysis. Another important aspect of topical delivery of GO-POD system is the production of molecular oxygen at the wound surface. In this study, it was not able to determine the dissolved oxygen by *in vitro* analysis. The release of oxygen is already established by a commercial product based on glucose oxidase namely Oxyzyme ^{TM} (Archimed ^{TM}, UK). It is an enzyme activated hydrogel wound dressing an oxidase enzyme and a halide. The oxidase enzyme converts the atmospheric oxygen into H_2O_2, which in turn gets converted into oxygen by the iodide component. In diabetic wounds, the blood circulation is often compromised, which restricts the flow of oxygen towards the wound site. So the hyperbaric oxygen therapy or topical oxygen therapy are usually recommended by the clinicians. Such systemic oxygen therapy will not be effective for diabetic wounds in terms of cost and practicability (Brimson and Nigam, 2013). So therapeutic wound dressing which control the local glucose concentration and maintain oxygen level in the wound bed could be a promising approach for diabetic wound management.

4.4 Evaluation of *in-vivo* wound healing efficacy of insulin-loaded ADPM2S2 hydrogel

The wound healing effect of topically delivered insulin through ADPM2S2 hydrogel was analyzed in diabetic rat models. Full thickness wounds were created on streptozotocin induced diabetic Sprague Dawley rats and the rate of wound healing

was analyzed at different time points such as 7, 14 and 21 days. The test groups used in this study includes the treatment with hydrogel alone, insulin-loaded hydrogel (200mIU/mL insulin loaded within 4cm^2 xerogel), insulin alone (200mIU/mL) and commercial alginate wound dressing. The diabetic rats with untreated wounds were kept as the control. For this study, 90 rats were induced with streptozotocin and from which 60 rats showing stable hyperglycemic condition were selected (n=4). The period needed for the complete wound healing in diabetic control group was 21 days. The prolonged inflammation, impaired vascular flow and poor tissue oxygenation impairs wound healing in diabetes. The macroscopic images of wound healing in different groups (figure 73) showed the formation of delicate crust in all groups within 7 to 12 days. As the healing progressed, the crust became thickened and began to detach. The slough formation was observed within the control wounds as well as wounds directly treated with insulin, which contains the non-viable necrotic tissue often white or yellow in color. The changing of wound dressing on alternative days helps to remove the slough and promote the renewal of epidermal cells. An early slough appearance is thought to indicate a quicker tissue reaction, which would result in the formation of a repaired epidermal layer earlier. The diabetic control groups showed the fibrous tissue (scab) formation and localized tissue destruction even after day 16.

4.4.1 Planimetry

The percentage of wound closure was analysed by planimetry (figure 74). The wound margins were traced on a paper and change in the wound area was calculated using Image J software. The photographic images were also taken from an equal

distance using a photographic stand. The wounds in diabetic control rats showed 50% wound closure within 7 days, 80% by 14 days and within 21 days 87% closure was attained. While comparing commercial alginate wound dressing and ADPM2S2 hydrogel, a higher wound closure of 92% was observed with in-house alginate hydrogel compared to commercial alginate wound care material (85%) at day14. Similarly, a significant improvement in the wound closure was observed in wounds treated with insulin loaded ADPM2S2, rather than direct application of insulin to the wound surface. At day 7, the % wound closure for insulin alone and insulin loaded ADPM2S2 hydrogels were 57% and 65% respectively. Within 14 days, 85% wound closure was observed with direct insulin application, while 95% of the wound closed with the treatment of insulin loaded ADPM2S2 hydrogel.

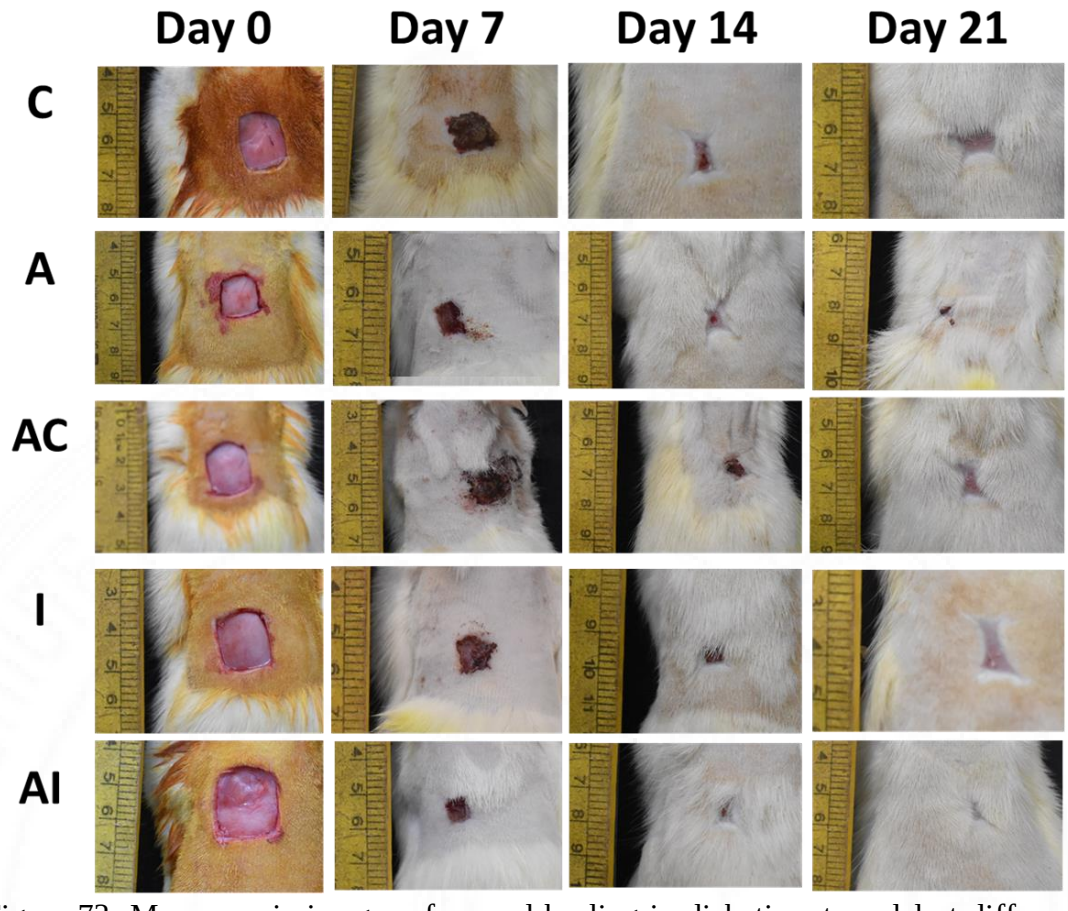

Figure 73: Macroscopic images of wound healing in diabetic rat model at different time points (day 0, day 7, day 14 and day 21) C: control, A : wound treated with ADPM2S2 xerogel, AC: Commercial alginate based wound dressing (P1), I : wounds treated with insulin, AI: wounds treated with insulin loaded ADPM2S2.

Abdelkader et al studied the cutaneous wound healing effect of topically delivered insulin which was loaded within nanoparticle and embedded in poly(vinyl alcohol)-borate hydrogel in diabetic rat. Histological images of the insulin treated diabetic wounds showed reduced inflammatory response, increased angiogenesis, formation of granulation tissue and collagen deposition. Treating diabetic wound with free insulin didn't show any improvement in healing process and resulted in irregular epidermal morphology (Abdelkader et al., 2018). A similar result was observed in our study. The results showed that the direct application of insulin on the wound surface

was not effective in promoting healing process. The effective concentration of insulin was not available in the wound bed as it was not retained and also lost due to the movement of rats within the cage. So the wound healing pattern of insulin treated test groups was similar to that of diabetic controls.

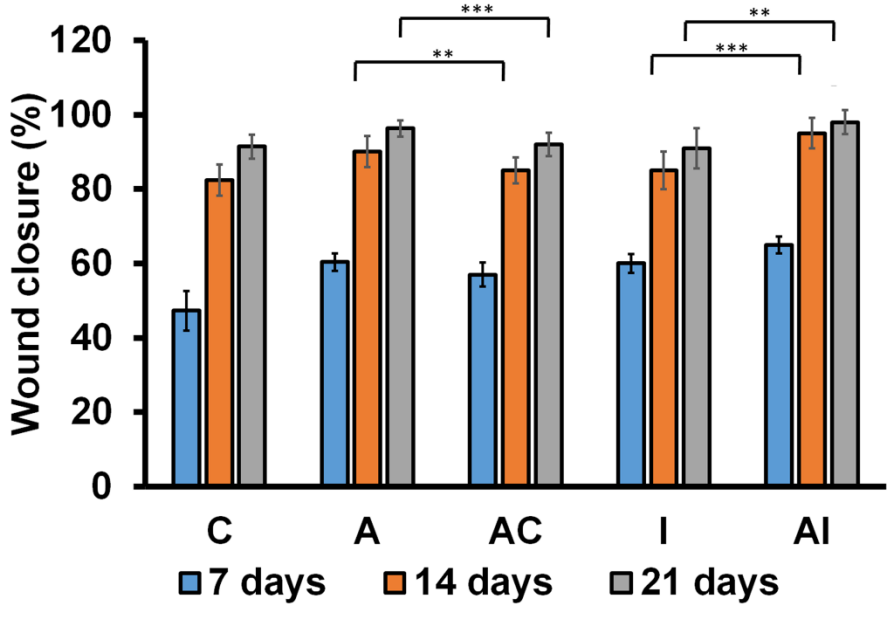

Figure 74: Percentage of wound closure calculated by planimetry analysis. C: control, A: wound treated with ADPM2S2 xerogel, AC: Commercial alginate based wound dressing (P1), I: wounds treated with insulin, AI: wounds treated with insulin loaded ADPM2S2 (**p<0.01, ***p<0.001).

4.4.2 Haematoxylin and Eosin staining

For histopathologic evaluations, H&E staining was performed and the percentage of re-epithelialization was calculated from the images using Image J software (figure 75, 76). The re-epithelialization was faster in wounds treated with insulin loaded ADPM2S2 hydrogel compared to other test groups. The percentage of re-epithelialization was 58% and 80% at 7^{th} and 14^{th} day respectively for insulin loaded

ADPM2S2 hydrogel. Wounds treated with insulin alone showed only 64% of re-epithelialization at 14th day. A significant improvement in the wound closure was observed with the controlled delivery of insulin towards the wound site.

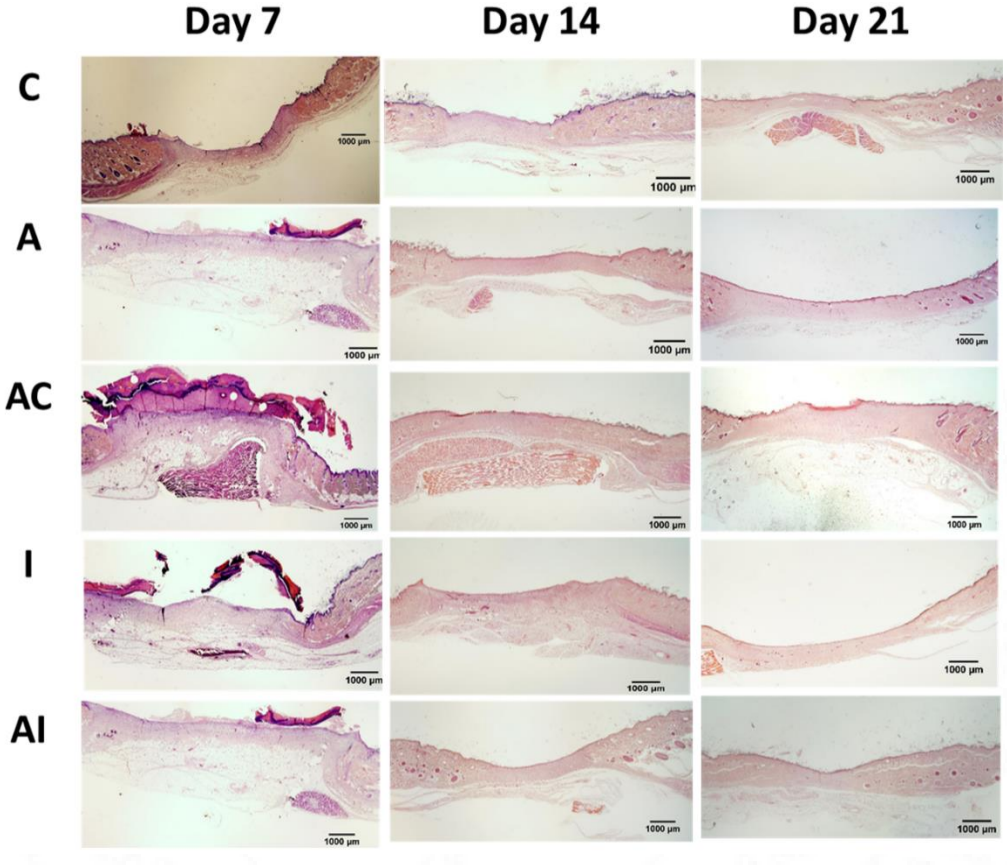

Figure 75: Representative photomicrographs of sections stained with hematoxylin and eosin (H&E) at different time points where C: control, A: wound treated with ADPM2S2 xerogel, AC: Commercial alginate based wound dressing (P1), I: wounds treated with insulin, AI: wounds treated with insulin loaded ADPM2S2.

The re-epithelialization was not complete in wounds treated with commercial alginate dressing. At 14th day, the % re-epithelialization was 58% and 71% for commercial material and ADPM2S2 hydrogel respectively. By *in vitro* analysis, it was observed that commercial alginate dressings had cytotoxic effect after 24h of contact

on the cell surface. Hence it can be inferred that the deposition of alginate fibres over the wound surface impeded the healing process in commercial alginate dressing treated wounds. The healing quality of the wound is represented by the granulation tissue. It is reported that the thickness of the granulation tissue gets reduced in diabetic wounds (Yang et al., 2020). In a study reported by Li et al., topical application of insulin loaded pH-sensitive hydrogel on diabetic rat wounds resulted in enhanced granulation tissue formation, collagen production and re-epithelialisation. The control groups showed necrotic tissues, foreign bodies and poor granulation tissue at the wound site on both 4^{th} and 12^{th} day of healing (Z. Li et al., 2021). The topical application of insulin showed significant improvement in burn wound healing also, by increasing the coverage area and thickness of granulation tissue by activating the PI3K-Akt Rac1 pathway (Dhall et al., 2015).

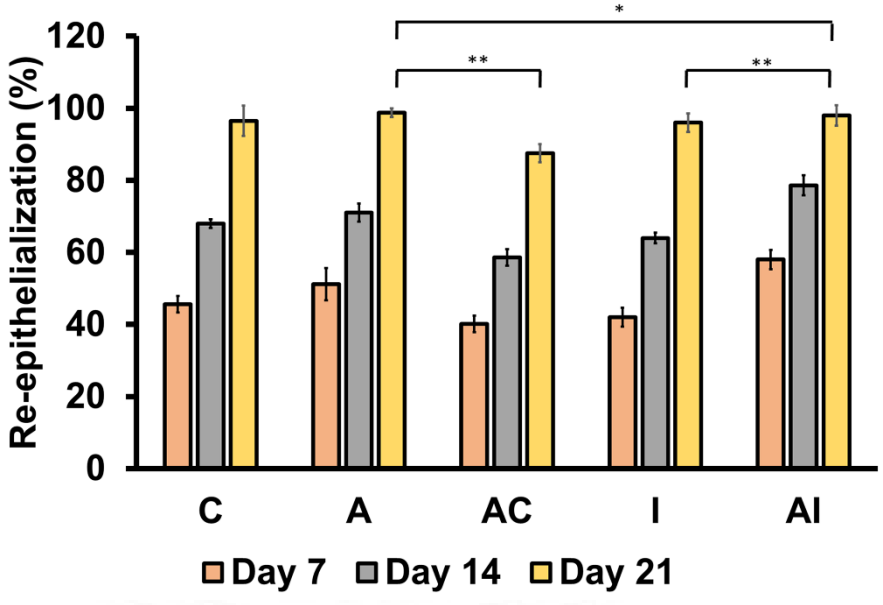

Figure 76: Percentage of re –epithelialization analyzed by ImageJ software C: control, A: wound treated with ADPM2S2 xerogel, AC: Commercial alginate based wound

dressing (P1), I: wounds treated with insulin, AI: wounds treated with insulin loaded ADPM2S2 (*$p<0.05$, **$p<0.01$).

Topical insulin application controls the inflammation at the wound surface. Topically applied insulin decreases the infiltration of neutrophils by inhibiting MIP-2 (Macrophage inflammation protein-2) expression (AbdelKader, 2016). Insulin shows anti-inflammatory activity by promoting macrophage polarization towards M2 phenotype. The topical application of insulin could effectively control the hyperglycemic condition locally and reduce the M1 phenotype. Insulin also favours the activation of phosphatidylinositol-3 kinase (PI3K)/Akt/Ras-related signalling or peroxisome proliferator-activated receptor-gamma (PPAR-γ) signalling which aid in the switching of M1 to M2 macrophage polarization. So the prolonged inflammation phase in the diabetic wound could be effectively controlled by the topical application of insulin (Louiselle et al., 2021).

4.4.3 Immunohistochemistry

The serine threonine kinase Akt, also known as protein kinase B (PKB) is a crucial component of the insulin signalling pathway that connects to activated cytokine and growth factor receptors. The phosphorylation of Akt at its activation loop (Thr308) and C-terminal tail (Ser473), occurs by the enzymatic activation of phosphatidylinositol-dependent kinase (PDK)-1 and the mammalian target of rapamycin (mTOR)/rapamycin-insensitive partner of mTOR. Akt molecule exist as three highly conserved forms such as Akt1, Akt2 and Akt3. During acute wound repair process, increased expression of phosphorylated Akt1 molecules are observed with the wound margin keratinocytes (Goren et al., 2009). During wound healing process, a

marked increase in the Akt phosphorylation at Ser473 and Thr308 were observed. The reduced Akt expression was noticed in diabetic wounds due to the impaired Akt/mTOR pathway (Huang et al., 2015). Similarly, in our study also we observed a reduction in phospho Akt expressing cells in diabetic controls (figure 77). With topical insulin treatment increased expression of phospho Akt was observed. More number of phospho Akt expressing cells was observed with ADPM2S2 hydrogel loaded with insulin compared to material alone at day 14. Binding of insulin to the insulin receptors induces cell signalling through the activation of receptor tyrosine kinase, which in turn activate other kinases downstream in the PI3K signalling cascade. This help to promote cellular proliferation, migration and glucose metabolism by activating pAkt and p-mTOR molecules (Peterson and Chandler, 2022).

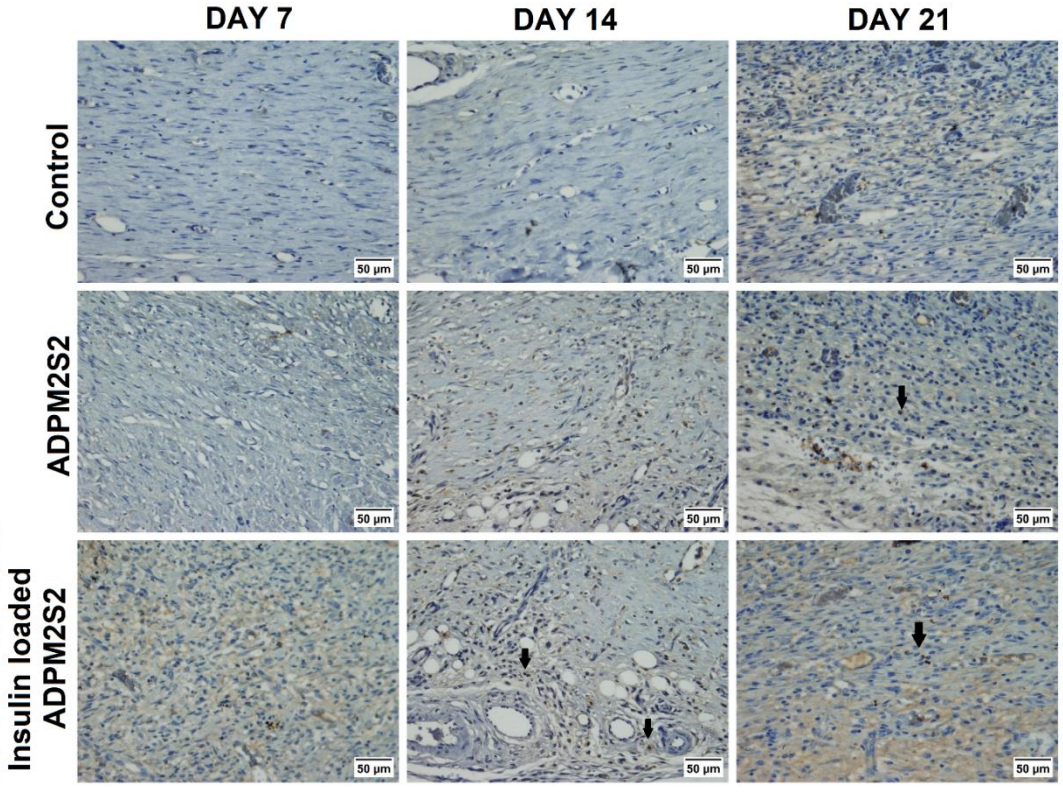

Figure 77: The expression of phospho Akt analysed by immunohistochemistry at different time points (day 7, day 14 and day 21) for wounds treated with ADPM2S2 hydrogel and insulin loaded ADPM2S2 hydrogel and compared with diabetic control.

Treatment with insulin enhances VEGF production in keratinocytes via Akt1 at the posttranscriptional level from a constitutive VEGF-encoding mRNA pool via a downstream phosphorylation 4E-BP1 (Goren et al., 2009). Evart et al., demonstrated that the activation of insulin signalling in diabetic rat led to a strong induction of the Akt/mTOR cascade. Immunohistochemistry results showed an increase in the expression of phospho Akt under high insulin concentration. (Evert et al., 2012). In another study, Peterson et al, illustrated the effect of exogenous insulin therapy in diabetic keratopathy. The exogenous insulin promoted the corneal cell proliferation by activating PI3K/Akt pathway in diabetic condition. So insulin can be used as an adjunctive therapy for diabetic corneal wound healing (Peterson and Chandler, 2022).

As a potent anti-inflammatory agent, insulin also aids in cell survival through metabolic and biosynthetic processes. The glucose metabolism activates TNFα and fatty acid production stimulates NFk-β. Through this signalling, insulin aids in the anti-inflammatory activity and promote the production of protein. Additionally, the expression of mTOR, MMPs, and eNOS can be increased as a result of insulin activating the Akt pathway, which leads to the growth of new blood vessels. Anti-inflammatory activity also mediated through the encouragement of M1 to M2 macrophage transition. So the localized delivery of biomolecules having anti-inflammatory activity could be highly helpful in the diabetic wound management (Kaur and Choudhury, 2020).

The current research is focusing on development of advanced wound care products with improved wound healing potential rather than the conventional wound healing techniques. It will be extremely beneficial for society and the economy to develop low-cost, safe wound healing techniques (Sun et al., 2021). The topical delivery of insulin could be a promising strategy as an alternative to conventional therapies. *In vitro* and *in vivo* preliminary safety and efficacy assessments showed that the topical insulin improves wound healing without causing side effects (Sun et al., 2021). The effect of topical application of insulin cream on wound healing was analysed in male Wistar diabetic rats. The wounds treated with 0.5U/100g of insulin showed faster wound healing with higher protein levels such as nitric oxide synthase (NOS) and vascular endothelial growth factor (VEGF) than the injured tissue of normal rats. The increased expression of insulin receptor substrate (IRS), protein

kinase B (AKT), and extracellular signal–regulated kinases (ERK) were also evidenced (Lima et al., 2012).

Different randomized clinical trials have been conducted to evaluate the wound healing effect of insulin through topical application. Insulin can be delivered as local injection, spray or cream or through a delivery system. To analyse the wound healing activity of topically delivered insulin, Wang et al reviewed 15 animal studies and 10 clinical trials performed by different research groups. They identified that topically delivered insulin could favour wound closure by regulating pathways which includes promoting cellular migration, reducing inflammation, enhancing re-epithelialization and neovascularization (Wang and Xu, 2020). In 1976, Van Ort and Gerber evaluated the wound healing effect of insulin in patients with decubitus ulcer. They included six patients in their pilot study and given 10U insulin twice daily for 5 days. There was significant improvement in the rate of wound healing with treatment group compared to controls by 15^{th} day (Van Ort and Gerber, 1976). In another study, Rezvani et al studied the effect of topical application of insulin in 45 patients with chronic extremity wounds. The healing rate was higher for treatment group compared to control without any signs of hypoglycaemia (Rezvani et al., 2009). Similarly Zhang et al., injected insulin into the base of the ulcer in patients with diabetic foot (n=18) and observed enhanced formation of granulation tissues and new blood vessels. A higher number of patients (n=110) with diabetic foot ulcer received insulin impregnated dressing and showed significant reduction in wound size within 2 weeks (Zhang and Lv, 2016). In our study, the *in vivo* results showed rapid wound closure and granulation tissue

formation with wounds treated with insulin loaded hydrogel. A significant reduction in the wound area was observed within 14 days. As observed in the *in vitro* results, insulin had a positive impact on collagen production and regulation of inflammatory response. By *in vitro* gene expression studies, a reduction in the pro-inflammatory cytokines and enhanced macrophage polarization towards M2 phenotype were observed with insulin loaded ADPM2S2 hydrogel loaded groups.

The structure of insulin is highly vulnerable to the harsh wound microenvironment. So the protective delivery of insulin is highly suggested. Li et al encapsulated insulin within micro particles and incorporated into silk fibroin sponges and showed an extended release up to 30days without changing its molecular structure (X. Li et al., 2017). Insulin loaded chitosan nanoparticles embedded within hydrogel was synthesized by Riberio et al., showed improved cell proliferation and angiogenesis in diabetic rat models (Ribeiro et al., 2020). Dawoud et al, performed the localized delivery of insulin using liposomal chitosan gel. The controlled delivery of insulin reduced the erythema of ulcer without altering glucose level and improved the healing rate (Dawoud et al., 2019). Insulin delivery systems made up of nanocarriers such as micelles, liposomes, nanoparticles or matrix assisted delivery using synthetic or biological materials protects insulin against degradation.

Growth factor incorporated wound care materials are available in the market. Growth factors are generally unstable biomolecules that are sensitive to changes in temperature, light, or ionic strength, which can result in denaturation and decreased biological activity. Although being one of the most affordable growth factors, insulin's

topical therapeutic usage has been linked to a short half-life *in vivo* because of proteases in the wound bed. In order to retain the three-dimensional protein structure of insulin, proteolysis need to be prevented by various techniques. Although several studies have been done over the years demonstrating the potential advantages of insulin-loaded systems for wound healing, there are currently no products on the market. So this necessitates the need for more research to learn more about the security and efficacy of these topical delivery methods. However, a number of commercially accessible treatments have arisen that employ growth factors to promote wound healing; as a result, insulin may go a similar route. The studies on the effect of topical delivery of insulin using animal models and randomized clinical trials reported that insulin possesses a great potential in the therapy of both acute and chronic wounds. The mechanism of action of insulin on wounds is expected to be better understood with more in-depth study, and insulin will likely be employed extensively in clinical wound healing treatments.

CHAPTER 5

SUMMARY AND CONCLUSIONS

Diabetic wounds are the most common type of chronic wounds, caused by un-controlled diabetes mellitus. DFU are associated with increased rate of lower limb amputation which results in 50% mortality within 5 years. Despite increasing prevalence and mortalities, the effective treatment for diabetic wounds remains limited. The current treatment strategies are very expensive and are not affordable by the patients. The biomaterial based approaches which include advanced wound care materials, matrix based localized delivery of therapeutic molecules etc could be a cost effective and safe treatment strategy for diabetic wound management. The topical delivery of biomolecules helps to modulate the healing phases and accelerate the healing process by various mechanisms. But the unfavorable wound micro-environment during wound chronicity reduces the efficacy of the biomolecules. So the approaches to modulate the wound micro-environment and make it favorable for the biomolecules to act is highly in demand and hence there is an urgent need for developing advanced wound care materials. To address this gap area, we developed alginate based wound care biomaterials with an aim for diabetic wound management.

Alginate is one of the key players in the wound care market. But its limited mechanical strength and increased rate of dissolution makes it unsuitable for chronic wound management as well as biomolecule delivery. The main limitation associated with current alginate dressings is that the remnants of alginate fibres remain in the wound bed after the dressing has been removed and need saline irrigation for its

clearance. This is found to cause foreign body reaction, leading to severe inflammatory reactions. Besides, though biomolecule delivery using ionically cross-linked alginate hydrogels are reported, the sustained release of biomolecules is not ensured due to the exchange of divalent cations with the wound fluid, resulting in alginate hydrogel instability. To overcome this issue, we developed dual cross-linked alginate hydrogel. Alginate was grafted with methacrylate monomers by free radical polymerization reaction and chemically cross-linked with methylene bisacrylamide. To further improve the mechanical stability of the hydrogels, ionic cross-linking with strontium ions was done and the hydrogels were subjected to lyophilization to produce corresponding xerogels. Three xerogel were synthesized namely, alginate-g-poly (methacrylic acid) (AGMS), alginate-g-poly (PEGMA) (AGPMS) and alginate diamine PEG-g-poly (PEGMA) (ADPMS) xerogels. Different batches of xerogels were synthesized by varying strontium ion cross-linking from 50mM to 200mM. The developed xerogels were opaque in nature which gets converted into transparent hydrogel upon contact with water and the mechanical stability was found to be maintained in the hydrogel form. Based on their water absorption capacity, water vapor transmission rate (WVTR), porosity and dissolution rate, the optimized xerogels were selected. The hydrogels were stable at different pH such as 5.8, 6.8, 7.4 and 8.0. As the wound become chronic, more amount of wound exudate will be produced, so a stable swelling pattern at pH 6.8, 7.4 and 8.0 are very critical. The WVTR of the xerogels was ranging from 1500- 1800 $g/m^2/24h$ and the xerogels showed a porosity of 75 -90%. The % dissolution of the hydrogels was 20 – 30% within 72h at pH 7.4,

among which higher weight loss was observed with alginate-g-poly (methacrylic acid) xerogels. Based on these results, AGM2S3, AGPM2S2 and ADPM2S2 were selected as the optimized xerogels.

The optimized xerogels were characterized by different physico-chemical characterization techniques and it is summarized in the table 20. The grafting with methacrylate monomers and chemical cross-linking with bisacrylamide was confirmed with FTIR and NMR analysis. The AGM2S3 xerogels showed higher adhesiveness in normal rat skin compared to other xerogels. The tensile strength and modulus were also higher for AGM2S3 xerogels due to the limited chain mobility and rigidity of the polymer chains. The SEM analysis revealed that the xerogel was highly porous and the pore walls were thin and found to be fragile in nature. A higher amount of strontium ions was involved in the ionic cross-linking, but only <10% was released within 48h, suggesting a strong binding of strontium ions within the xerogel. The quantification of strontium ions by ICP analysis as well as XPS confirmed the higher concentration of strontium on the surface of AGM2S3 xerogel, which contribute to the increased hemostatic activity (80%) within 5 min.

Parameters	**AGM2S3**	**AGPM2S2**	**ADPM2S2**
MW before crosslinking (Da)	1.87×10^5	2.17×10^5	2.39×10^5
% swelling (48 h)			
pH 5.8	2800 ±108	1810±62	1483±96
pH 6.8	3704 ±80	1920±88	1663± 47
pH 7.4	2941±92	1735±74	1504± 62
pH 8.0	2789±85	1678±65	1540±78

WVTR (37°C) ($g/m^2/24h$)	1879±75	1395±74	1490±76
Porosity (%)	90.5±7.1	78±5.4	74±6.8
Pore size by SEM (µm)	76 ± 23	80±37	76±24
% weight loss (pH 7.4)	22.4±3.2	20.2±1.3	17.8±2.7
Adhesiveness (N/cm) Normal skin Wounded skin	 0.9 ± 0.14 0.61± 0.06	 0.58 ± 0.01 0.62± 0.12	 0.55 ± 0.07 0.54 ± 0.08
Tensile strength (kPa) Xerogel Hydrogel	 520 ± 50 60 ± 5.4	 433 ± 60 148±17	 435 ± 39 48 ± 7
Contact angle (°)	66.3±2.28	94±3.2	67.2±1.2
Amount of Sr ions involved in crosslinking (mM)	58±4.6	12±3.2	15±2.7
Quantification of Sr by XPS	1 %	0.2%	0.3%
Binding energy (eV)	134	132.8	135.2
ICP Analysis	Na : 0.060 % Sr : 0.635 %	Na : 0.011 % Sr : 0.514 %	Na : 0.0038 % Sr : 0.552 %
Strontium ion release 48 h	6.11±2.1%	35.1±2.1%	40.9±1.2%
Hemostatic activity (5 min)	82%	46%	59%
Collagenase inhibitory activity (%)	27	36±2.3	39±2.1
Wound closure by scratch wound assay on HaCaT cells (4h)	20±3.3%	30±2.7	34±2.5

Table 20: Comparison chart of different physico-chemical and biological properties of AGM2S3, AGPM2S2 and ADPM2S2 xerogels.

While analyzing the physical properties of the AGPM2S2 xerogels, the material showed higher tensile strength in wet condition compared other hydrogels. This was due to the incorporation of flexible poly (PEGMA) chains. But grafting with poly (PEGMA) reduced the hydrophilic nature, as evidenced by the higher contact angle. The SEM images showed well-formed pores with some deposition over the surface. The quantification of Sr ions showed that only 12% got involved in cross-linking, of which about 35% released within 48h. The increased release of strontium ion from the other two hydrogels compared to AGM2S3 contributes to the higher percentage of collagenase inhibitory activity and wound closure by scratch wound assay. But cytotoxicity studies by test on extract and direct contact assay showed reduced cell viability with AGPM2S2 hydrogel after 48h. This was due to the increased concentration of poly (PEGMA) used for xerogel synthesis. To overcome this issue, alginate chains were first conjugated with diamine PEG molecule. This helped to reduce the concentration of PEGMA used for grafting. The conjugation with diamine PEG reduced the gelation time and obtained non-adherent xerogels. The percentage weight loss was lower compared to other xerogels and the pores were well formed without any debri over the surface. Since the concentration of PEGMA was reduced compared to the AGPM2S2 xerogel, the hydrophilic nature of the ADPM2S2 xerogel was higher than AGPM2S2. The strontium ion release from ADPM2S2 was found to be higher reaching up to 40% within 48h, resulting in higher percentage of wound closure and collagenase activity compared to other two materials.

The in-house developed xerogels were compared with the commercial alginate dressing materials. The commercial materials were highly unstable at pH 7.4 and 8.0 and got disintegrated into fibers. Both the products showed >80% weight loss by 72h. The direct contact assay showed cytotoxic effect on L929 cells due to the deposition of alginate fibers. So comparing with the commercial alginate based dressings, the developed xerogels possess excellent properties as a wound care material.

The efficacy of the materials for biomolecule delivery was further analyzed. The biomolecules selected for the study includes insulin, simvastatin and glucose oxidase- peroxidase. The biomolecules were loaded by diffusion filling method and its release kinetics was analyzed. A comparative analysis is given in table 21. The AGM2S3 hydrogels showed continous release of insulin up to 48h, but structural variation was observed at 48h release. The bioactivity of insulin was confirmed with ELISA and HPLC analysis. So this material could be used for insulin delivery up to 24h without any adverse interaction with the matrix. Simvastatin loaded AGM2S3 hydrogels showed a burst release, 100% release occurred within 5h followed by a decline in the release. Due to the bulk release, this matrix is not suitable for SIM delivery. While analyzing the efficacy of the matrix for GO-POD release, a controlled release pattern was observed. In the circular dichroism spectra of glucose oxidase, a structural alteration was visible after 24h release. So AGM2S3 can be used as a matrix for GO-POD release up to 8h retaining its biocatalytic activity.

Delivery of biomolecules	AGM2S3	AGPM2S2	ADPM2S2
Insulin loaded hydrogels			
Release kinetics model (Membrane system, pH 7.4, 48h)	Korsemeyer Peppas kinetics	Korsemeyer Peppas kinetics	Korsemeyer Peppas kinetics
Release quantified by HPLC	90 %	80 %	92 %
Release quantified by ELISA	96 %	84 %	95 %
CD spectra	Structural variation at 48h	Structural variation at 24h and 48h.	No structural variation up to 48h
Simvastatin loaded hydrogels			
Release kinetics model (Membrane system, pH 7.4, 48h)	Korsemeyer Peppas kinetics	Higuchi model	Korsemeyer Peppas kinetics
Release quantified by HPLC	91 %	84 %	92 %
GO-POD loaded hydrogels			
Release kinetics model (Membrane system, pH 7.4, 48h)	Higuchi model	Korsemeyer Peppas kinetics	Korsemeyer Peppas kinetics
CD spectra	Structural variation at 24h	Structural variation at 8h and 24h.	Structural variation at 24h
Release kinetics model (Membrane system, pH 7.4, 48h)	Korsemeyer Peppas kinetics	Korsemeyer Peppas kinetics	Korsemeyer Peppas kinetics
Conc. of glucose remaining in the high glucose media (25mM) after 8h.of enzymatic activity	7 mM	10 mM	3 mM
Amount of H_2O_2 formed after 8h of enzymatic activity	10 mM	12 mM	7 mM

Table 21: Comparison of efficacy of the hydrogels for biomolecule delivery

The insulin release from AGPM2S2 hydrogel showed a steady state release pattern up to 48h. The CD spectra of released insulin showed structural alteration compared to native insulin. This suggests strong interaction of the insulin with the matrix, which reduces the activity of the insulin. Simvastatin loaded AGPM2S2 hydrogels showed an initial burst release up to 5h and further slowed down due to the entrapment of the drug with the hydrophobic domains of the hydrogels. The GO-POD loaded hydrogels showed release up to 24h. But structural alteration of the glucose oxidase after 8h was observed due to the matrix interaction. So this system could not be effective for the release of GO-POD for a longer period.

The efficacy of ADPM2S2 for the controlled delivery of the selected biomolecules was analyzed. The release of insulin was observed up to 48h without any structural alterations. The HPLC and ELISA analysis revealed that the bioactivity of the released insulin remained intact even after 48h. Simvastatin loaded ADPM2S2 hydrogels showed release up to 48h compared to other hydrogels. So this matrix could be effective for the topical delivery of SIM for prolonged period. The release of GO-POD through ADPM2S2 hydrogel showed controlled release without any structural variation to GO up to 8h. The GO-POD matrix could effectively control the local glucose and H_2O_2 concentration. While comparing the release profile of the selected biomolecules, the ADPM2S2 hydrogels was found to be the best among the three materials. This hydrogel enables the effective delivery of the molecules without affecting its activity. Biomolecules loaded within ADPM2S2 hydrogels were further studied for *in vitro* wound healing activities.

The role of biomolecules in different aspects of healing was assessed by *in vitro* analysis under hyperglycemic conditions. The selected biomolecules were loaded within ADPM2S2 hydrogel analyzed and compared the effects on *in vitro* wound closure, collagen deposition, cellular migration and the expression of various genes involved in wound healing. Insulin (100mIU) was loaded onto ADPM2S2 hydrogel and the effect of the released insulin on wound closure was evaluated which was found to have enhanced healing effect compared to hydrogel alone as well as direct application of insulin. The subcellular actin filament organization within the fibroblast cells were influenced by insulin, thereby promotes the cellular migration. The immunocytochemistry analysis showed an increase in the expression of phospho Akt by insulin treatment, suggesting the activation of the Akt/mTOR pathway involved in wound healing process. The increased cellular apoptosis is another concern in delayed wound healing in diabetic wounds. Insulin treatment could effectively reduce the late apoptotic cells compared to high glucose controls. The treatment with insulin showed an up-regulation of the genes involved in the wound healing process such as COL1A1, keratin16, GLUT1, TGFβ1, IL-10 and CD163 and down regulated the expression of TNFα, IL-6, and CD163. This indicates that insulin has significant role in collagen production, keratinocyte migration, anti-inflammatory activity as well as macrophage polarization towards M2 phenotype.

The *in vitro* wound healing effect of simvastatin (SIM) loaded ADPM2S2 hydrogels were further analysed under high glucose conditions. The optimized concentration of SIM was 60µM. Simvastatin loaded ADPM2S2 hydrogels showed a

significant improvement in the collagen production from fibroblast cells, compared to cells treated with simvastatin alone. The synergistic action of SIM with Sr ions showed an increase in the percentage of wound closure by scratch wound assay. But there was no significant improvement in the actin filament organization on treatment with SIM compared to control cells grown under high glucose condition. The anti-inflammatory activity of SIM-loaded ADPM2S2 hydrogels were analysed by the quantification of the TNF-α produced from LPS stimulated macrophages. The anti-inflammatory activity of the hydrogel alone was 20%, which was increased to 47% by the synergistic action of Sr ions and SIM released from the hydrogel. The up-regulation of anti-inflammatory cytokines as well as polarization towards M2 macrophage phenotype also confirmed the role of SIM in regulating inflammatory response.

To analyze the wound healing effects of glucose oxidase – peroxidase (GO – POD), the optimized amount used was 150mIU with GO and 1.5 IU with that of POD. Under hyperglycemic condition, the deposition of collagen was reduced with the treatment of GO alone loaded hydrogel due to the increased production of H_2O_2. The incorporation of POD effectively reduced the H_2O_2 level and favoured the collagen deposition. The scratch wound assay showed that the controlled delivery of GO-POD has positive impact on *in vitro* wound healing process. The improvement in the actin filament orientation was observed with the combined delivery of GO-POD, due to the reduction in the high glucose level as well as reactive oxygen species. The hydrogels loaded with GO-POD showed up-regulation of the genes such as keratin16, GLUT1 and TGF β1, with no improvement in anti-inflammatory activity. While comparing

these i*n vitro* results, insulin loaded system showed good *in vitro* wound closure, collagen deposition and cellular migration, so it was selected for the *in vivo* wound healing efficacy evaluation.

In vivo wound healing effect of insulin loaded ADPM2S2 hydrogels was analysed in diabetic rat model. Full thickness wounds were created on streptozotocin induced diabetic Sprague Dawley rats and the rate of wound healing was analyzed at different time points such as 7, 14 and 21 days. The wounds in diabetic control rats showed 50% closure within 7 days, which increased up to 80% by 14 days and within 21 days 87% closure has been attained. While comparing commercial alginate wound dressing and ADPM2S2 hydrogel, a higher wound closure of 92% was observed with in-house alginate hydrogel compared to commercial alginate wound care material (85%) at day14. Similarly, a significant improvement in the wound closure was observed in wounds treated with insulin loaded ADPM2S2, rather than direct application of insulin to the wound surface. The re-epithelialization was faster in wounds treated with insulin loaded ADPM2S2 hydrogel compared to other test groups. Immunohistochemistry evaluation showed a reduction in phospho Akt expressing cells in diabetic controls. With topical insulin treatment, the expression of phospho Akt got increased. More number of phospho Akt expressing cells were observed with ADPM2S2 hydrogel loaded with insulin compared to material alone at day 14.

Key points

- Alginate based wound care materials were successfully developed and the xerogels were named as alginate-g-poly(methacrylic acid) (AGMS), alginate-g-poly(PEGMA) (AGPMS) and alginate diamine-g-poly(PEGMA) (ADPMS).
- The synthesis of alginate based xerogels was performed by grafting with different methacrylate monomers by free radical polymerization, followed by dual crosslinking reaction with methylene bisacrylamide and strontium ions.
- After various physico-chemical characterizations, AGM2S3, AGPM2S2 and ADPM2S2 were selected as the optimized materials from different formulations. While comparing with the commercial alginate based wound care materials, the in-house alginate based xerogels showed good swelling and reduced dissolution.
- The efficacy of the hydrogels for controlled delivery of biomolecules was evaluated. The biomolecules selected for the studies were insulin, simvastatin and GO-POD.
- ADPM2S2 hydrogels showed controlled release for all the selected biomolecules and more importantly the biological activity of biomolecules remained intact.
- The *in vitro* studies on various skin cells were performed with ADPM2S2 loaded with different biomolecules under high glucose conditions. Among which insulin shows good cellular migration and collagen deposition.
- Insulin loaded ADPM2S2 hydrogels was then selected for *in vivo* evaluation.
- Wound healing experiments were performed on diabetic rat models by creating full thickness wound (2 x2 cm). A significant improvement in wound closure was observed with insulin loaded ADPM2S2 compared to the insulin alone treatment.
- ADPM2S2 xerogel showed significant improvement in wound closure within 14 days compared to commercial alginate wound dressings.

From these observations, it is concluded that the insulin loaded ADPM2S2 xerogels could be a promising therapeutic strategy for diabetic wound management.

Future perspectives

Wound healing efficacy of topical delivery of insulin using animal models and randomized clinical trials is of great interest globally, which reports that insulin possesses great wound healing potential. But wound healing studies using appropriate chronic wound models are not yet performed. So the therapeutic effects of the xerogel loaded with biomolecules in chronic wound models need to be assessed. Further, the wound healing effect of the insulin loaded hydrogel need to be extrapolated into large animal models. The angiogenic potential of the hydrogel was not explored in this study, which need to be addressed. The management of cavity wounds is very difficult, since the healing is not proper within the cavities. Hence another future aspect is to evaluate the potential of these xerogels in healing of such cavity wounds.

CHAPTER 6

BIBLIOGRAPHY

1. Abd El-Alim, S.H., Salama, A., Darwish, A.B., 2020. Provesicular elastic carriers of Simvastatin for enhanced wound healing activity: An in-vitro/in-vivo study. Int J Pharm 585, 119470. https://doi.org/10.1016/j.ijpharm.2020.119470
2. AbdelKader, A., 2016. The Role of Insulin in Wound Healing Process: Mechanism of Action and Pharmaceutical Applications, in: Journal of Analytical & Pharmaceutical Research. https://doi.org/10.15406/japlr.2016.02.00007
3. Abdelkader, D.H., Tambuwala, M.M., Mitchell, C.A., Osman, M.A., El-Gizawy, S.A., Faheem, A.M., El-Tanani, M., McCarron, P.A., 2018. Enhanced cutaneous wound healing in rats following topical delivery of insulin-loaded nanoparticles embedded in poly(vinyl alcohol)-borate hydrogels. Drug Deliv Transl Res 8, 1053–1065. https://doi.org/10.1007/s13346-018-0554-0
4. Aderibigbe, B.A., Buyana, B., 2018. Alginate in Wound Dressings. Pharmaceutics 10, 42. https://doi.org/10.3390/pharmaceutics10020042
5. Ahmad, A., Othman, I., Md Zain, A.Z., Chowdhury, E.H., 2015. Controlled release of insulin in blood from strontium-substituted carbonate apatite complexes. Curr Drug Deliv 12, 210–222. https://doi.org/10.2174/1567201811666140708104031
6. Ahmed, A., Getti, G., Boateng, J., 2021. Medicated multi-targeted alginate-based dressings for potential treatment of mixed bacterial-fungal infections in diabetic foot ulcers. International Journal of Pharmaceutics 606, 120903. https://doi.org/10.1016/j.ijpharm.2021.120903
7. Akyol, M., Polat, Z.A., Özçelik, S., Kaya, Ö., 2013. The effects of strontium chloride on viability of mouse connective tissue fibroblast cells. Cumhuriyet Medical Journal 35, 33–38.
8. Al-Jabri, A.A.Q.S.S.H.A.A., 2021. The Therapeutic Potential of Bioactive Polysaccharides in Tissue Repairing and Wound Healing -. Systematic Reviews in Pharmacy 12, 470–479.
9. Alsharif, S.B., Wali, R., Vanyo, S.T., Andreana, S., Chen, K., Sheth, B., Swihart, M.T., Dziak, R., Visser, M.B., 2023. Strontium-loaded hydrogel scaffolds to promote gingival fibroblast function. Journal of Biomedical Materials Research Part A 111, 6–14. https://doi.org/10.1002/jbm.a.37439

10. Andrisse, S., Koehler, R.M., Chen, J.E., Patel, G.D., Vallurupalli, V.R., Ratliff, B.A., Warren, D.E., Fisher, J.S., 2014. Role of GLUT1 in regulation of reactive oxygen species. Redox Biology 2, 764–771. https://doi.org/10.1016/j.redox.2014.03.004

11. Arul, V., Masilamoni, J.G., Jesudason, E.P., Jaji, P.J., Inayathullah, M., Dicky John, D.G., Vignesh, S., Jayakumar, R., 2012. Glucose oxidase incorporated collagen matrices for dermal wound repair in diabetic rat models: a biochemical study. J Biomater Appl 26, 917–938. https://doi.org/10.1177/0885328210390402

12. Asai, J., Takenaka, H., Hirakawa, S., Sakabe, J., Hagura, A., Kishimoto, S., Maruyama, K., Kajiya, K., Kinoshita, S., Tokura, Y., Katoh, N., 2012. Topical simvastatin accelerates wound healing in diabetes by enhancing angiogenesis and lymphangiogenesis. Am J Pathol 181, 2217–2224. https://doi.org/10.1016/j.ajpath.2012.08.023

13. Ashcroft, G.S., Jeong, M.-J., Ashworth, J.J., Hardman, M., Jin, W., Moutsopoulos, N., Wild, T., McCartney-Francis, N., Sim, D., McGrady, G., Song, X.-Y., Wahl, S.M., 2012. Tumor necrosis factor-alpha (TNF-α) is a therapeutic target for impaired cutaneous wound healing. Wound Repair Regen 20, 38–49. https://doi.org/10.1111/j.1524-475X.2011.00748.x

14. Attia, E.A.S., Belal, D.M.I., El Samahy, M.H., El Hamamsy, M.H., 2014. A pilot trial using topical regular crystalline insulin vs. aqueous zinc solution for uncomplicated cutaneous wound healing: Impact on quality of life. Wound Repair Regen 22, 52–57. https://doi.org/10.1111/wrr.12122

15. Aumiller, W.D., Dollahite, H.A., 2015. Pathogenesis and management of diabetic foot ulcers. Journal of the American Academy of PAs 28, 28–34. https://doi.org/10.1097/01.JAA.0000464276.44117.b1

16. Baker, C.J., Deahl, K., Domek, J., Orlandi, E.W., 2000. Scavenging of H2O2 and Production of Oxygen by Horseradish Peroxidase. Archives of Biochemistry and Biophysics 382, 232–237. https://doi.org/10.1006/abbi.2000.2013

17. Balaji, S., LeSaint, M., Bhattacharya, S.S., Moles, C., Dhamija, Y., Kidd, M., Le, L.D., King, A., Shaaban, A., Crombleholme, T.M., Bollyky, P., Keswani, S.G., 2014. Adenoviral Mediated Gene Transfer of IGF-1 Enhances Wound Healing and Induces Angiogenesis. J Surg Res 190, 367–377. https://doi.org/10.1016/j.jss.2014.02.051

18. Barbu, A., Neamtu, B., Zăhan, M., Iancu, G.M., Bacila, C., Mireșan, V., 2021. Current Trends in Advanced Alginate-Based Wound Dressings for Chronic Wounds. J Pers Med 11, 890. https://doi.org/10.3390/jpm11090890

19. Barr, D.P., Aust, S.D., 1993. On the mechanism of peroxidase-catalyzed oxygen production. Arch Biochem Biophys 303, 377–382. https://doi.org/10.1006/abbi.1993.1298

20. Berger, J., Reist, M., Mayer, J.M., Felt, O., Peppas, N.A., Gurny, R., 2004. Structure and interactions in covalently and ionically crosslinked chitosan hydrogels for biomedical applications. Eur J Pharm Biopharm 57, 19–34. https://doi.org/10.1016/s0939-6411(03)00161-9

21. Berlanga-Acosta, J., Schultz, G.S., López-Mola, E., Guillen-Nieto, G., García-Siverio, M., Herrera-Martínez, L., 2012. Glucose Toxic Effects on Granulation Tissue Productive Cells: The Diabetics' Impaired Healing. BioMed Research International 2013, e256043. https://doi.org/10.1155/2013/256043

22. Best, L.C., Bone, E.A., Russell, R.G.G., 1981. Strontium ions stimulate phosphoinositide metabolism in human blood platelets. FEBS Letters 134, 88–90. https://doi.org/10.1016/0014-5793(81)80557-1

23. Bisht, B., Dey, C.S., 2008. Focal Adhesion Kinase contributes to insulin-induced actin reorganization into a mesh harboring Glucose transporter-4 in insulin resistant skeletal muscle cells. BMC Cell Biology 9, 48. https://doi.org/10.1186/1471-2121-9-48

24. Black, E., Vibe-Petersen, J., Jorgensen, L.N., Madsen, S.M., Agren, M.S., Holstein, P.E., Perrild, H., Gottrup, F., 2003. Decrease of collagen deposition in wound repair in type 1 diabetes independent of glycemic control. Arch Surg 138, 34–40. https://doi.org/10.1001/archsurg.138.1.34

25. Boucly, A., Rochet, F., Arnoux, Q., Gallet, J.-J., Bournel, F., Tissot, H., Marry, V., Dubois, E., Michot, L., 2018. Soft X-ray Heterogeneous Radiolysis of Pyridine in the Presence of Hydrated Strontium-Hydroxyhectorite and its Monitoring by Near-Ambient Pressure Photoelectron Spectroscopy. Sci Rep 8, 6164. https://doi.org/10.1038/s41598-018-24329-8

26. Bouhadir, K.H., Alsberg, E., Mooney, D.J., 2001. Hydrogels for combination delivery of antineoplastic agents. Biomaterials 22, 2625–2633. https://doi.org/10.1016/s0142-9612(01)00003-5

27. Braux, J., Velard, F., Guillaume, C., Bouthors, S., Jallot, E., Nedelec, J.-M., Laurent-Maquin, D., Laquerrière, P., 2011. A new insight into the dissociating effect of strontium on bone resorption and formation. Acta Biomater 7, 2593–2603. https://doi.org/10.1016/j.actbio.2011.02.013

28. Brimson, C. h., Nigam, Y., 2013. The role of oxygen-associated therapies for the healing of chronic wounds, particularly in patients with diabetes. Journal of the

European Academy of Dermatology and Venereology 27, 411–418. https://doi.org/10.1111/j.1468-3083.2012.04650.x

29. Brus, J., Urbanova, M., Czernek, J., Pavelkova, M., Kubova, K., Vyslouzil, J., Abbrent, S., Konefal, R., Horský, J., Vetchy, D., Vysloužil, J., Kulich, P., 2017. Structure and Dynamics of Alginate Gels Cross-Linked by Polyvalent Ions Probed via Solid State NMR Spectroscopy. Biomacromolecules 18, 2478–2488. https://doi.org/10.1021/acs.biomac.7b00627

30. Buabeid, M., Arafa, E.-S.A., Yaseen, H.S., Umar, M.I., Murtaza, G., 2022. Anti-inflammatory effect of simvastatin by impeding TNF-α and interleukin-1ß pathways: antiangiogenic activity of simvastatin and simvastatin-loaded silver nanoparticles. Artificial Cells, Nanomedicine, and Biotechnology 50, 208–217. https://doi.org/10.1080/21691401.2022.2098306

31. Catanzano, O., Straccia, M.C., Miro, A., Ungaro, F., Romano, I., Mazzarella, G., Santagata, G., Quaglia, F., Laurienzo, P., Malinconico, M., 2015. Spray-by-spray in situ cross-linking alginate hydrogels delivering a tea tree oil microemulsion. Eur J Pharm Sci 66, 20–28. https://doi.org/10.1016/j.ejps.2014.09.018

32. Chen, X., Liu, Y., Zhang, X., 2012. Topical insulin application improves healing by regulating the wound inflammatory response. Wound Repair Regen 20, 425–434. https://doi.org/10.1111/j.1524-475X.2012.00792.x

33. Cheng, Y., Qin, J., Huang, Y., Wang, T., 2022. The antimicrobial effects of PLGA microspheres containing the antimicrobial peptide OP-145 on clinically isolated pathogens in bone infections. Sci Rep 12, 14541. https://doi.org/10.1038/s41598-022-18690-y

34. Chereddy, K.K., Vandermeulen, G., Préat, V., 2016. PLGA based drug delivery systems: Promising carriers for wound healing activity. Wound Repair Regen 24, 223–236. https://doi.org/10.1111/wrr.12404

35. Chou, A.I., Nicoll, S.B., 2009. Characterization of photocrosslinked alginate hydrogels for nucleus pulposus cell encapsulation. Journal of Biomedical Materials Research Part A 91A, 187–194. https://doi.org/10.1002/jbm.a.32191

36. Chubinskiy-Nadezhdin, V.I., Negulyaev, Y.A., Morachevskaya, E.A., 2017. Simvastatin induced actin cytoskeleton disassembly in normal and transformed fibroblasts without affecting lipid raft integrity. Cell Biology International 41, 1020–1029. https://doi.org/10.1002/cbin.10812

37. Coger, V., Million, N., Rehbock, C., Sures, B., Nachev, M., Barcikowski, S., Wistuba, N., Strauß, S., Vogt, P.M., 2019. Tissue Concentrations of Zinc, Iron, Copper, and Magnesium During the Phases of Full Thickness Wound Healing in a

Rodent Model. Biol Trace Elem Res 191, 167–176. https://doi.org/10.1007/s12011-018-1600-y

38. Cox, N., Rapatskiy, L., Su, J.-H., Pantazis, D.A., Sugiura, M., Kulik, L., Dorlet, P., Rutherford, A.W., Neese, F., Boussac, A., Lubitz, W., Messinger, J., 2011. Effect of Ca2+/Sr2+ Substitution on the Electronic Structure of the Oxygen-Evolving Complex of Photosystem II: A Combined Multifrequency EPR, 55Mn-ENDOR, and DFT Study of the S2 State. J. Am. Chem. Soc. 133, 3635–3648. https://doi.org/10.1021/ja110145v

39. Cozzi, D., Desideri, P.G., Lepri, L., 1969. The mechanism of ion exchange with algenic acid. Journal of Chromatography A 40, 130–137. https://doi.org/10.1016/S0021-9673(01)96628-2

40. Das, A., Shah, M., Saraogi, I., 2022. Molecular Aspects of Insulin Aggregation and Various Therapeutic Interventions. ACS Bio Med Chem Au 2, 205–221. https://doi.org/10.1021/acsbiomedchemau.1c00054

41. Davidovich-Pinhas, M., Bianco-Peled, H., 2010. A quantitative analysis of alginate swelling. Carbohydrate Polymers 79, 1020–1027. https://doi.org/10.1016/j.carbpol.2009.10.036

42. Dawoud, M.H.S., Yassin, G.E., Ghorab, D.M., Morsi, N.M., 2019. Insulin Mucoadhesive Liposomal Gel for Wound Healing: a Formulation with Sustained Release and Extended Stability Using Quality by Design Approach. AAPS PharmSciTech 20, 158. https://doi.org/10.1208/s12249-019-1363-6

43. Deng, L., Liu, Y., Yang, G., Shang, L., Wen, D., Wang, F., Xu, Z., Dong, S., 2007. Molecular "Wiring" Glucose Oxidase in Supramolecular Architecture. Biomacromolecules 8, 2063–2071. https://doi.org/10.1021/bm061049l

44. DeNichilo, M.O., Panagopoulos, V., Rayner, T.E., Borowicz, R.A., Greenwood, J.E., Evdokiou, A., 2015. Peroxidase enzymes regulate collagen extracellular matrix biosynthesis. Am J Pathol 185, 1372–1384. https://doi.org/10.1016/j.ajpath.2015.01.013

45. Dhall, S., Silva, J.P., Liu, Y., Hrynyk, M., Garcia, M., Chan, A., Lyubovitsky, J., Neufeld, R.J., Martins-Green, M., 2015. Release of insulin from PLGA-alginate dressing stimulates regenerative healing of burn wounds in rats. Clin Sci (Lond) 129, 1115–1129. https://doi.org/10.1042/CS20150393

46. Dias, J.R., Ribeiro, N., Baptista-Silva, S., Costa-Pinto, A.R., Alves, N., Oliveira, A.L., 2020. In situ Enabling Approaches for Tissue Regeneration: Current Challenges and New Developments. Frontiers in Bioengineering and Biotechnology 8.

47. Djavid, G.E., Tabaie, S.M., Tajali, S.B., Totounchi, M., Farhoud, A., Fateh, M., Ghafghazi, M., Koosha, M., Taghizadeh, S., 2020. Application of a collagen matrix dressing on a neuropathic diabetic foot ulcer: a randomised control trial. J Wound Care 29, S13–S18. https://doi.org/10.12968/jowc.2020.29.Sup3.S13

48. Donati, I., Mørch, Y.A., Strand, B.L., Skjåk-Braek, G., Paoletti, S., 2009. Effect of elongation of alternating sequences on swelling behavior and large deformation properties of natural alginate gels. J Phys Chem B 113, 12916–12922. https://doi.org/10.1021/jp905488u

49. Driver, V.R., Fabbi, M., Lavery, L.A., Gibbons, G., 2010. The costs of diabetic foot: The economic case for the limb salvage team. Journal of Vascular Surgery, Strategies to Prevent and Heal Diabetic Foot Ulcers: Building a Partnership for Amputation Prevention 52, 17S-22S. https://doi.org/10.1016/j.jvs.2010.06.003

50. Du, G., Song, Y., Zhang, T., Ma, L., Bian, N., Chen, X., Feng, J., Chang, Q., Li, Z., 2014. Simvastatin attenuates TNF-α-induced apoptosis in endothelial progenitor cells via the upregulation of SIRT1. International Journal of Molecular Medicine 34, 177–182. https://doi.org/10.3892/ijmm.2014.1740

51. Dumas, A., Knaus, U.G., 2021. Raising the 'Good' Oxidants for Immune Protection. Front Immunol 12, 698042. https://doi.org/10.3389/fimmu.2021.698042

52. Dunnill, C., Patton, T., Brennan, J., Barrett, J., Dryden, M., Cooke, J., Leaper, D., Georgopoulos, N.T., 2017. Reactive oxygen species (ROS) and wound healing: the functional role of ROS and emerging ROS-modulating technologies for augmentation of the healing process. Int Wound J 14, 89–96. https://doi.org/10.1111/iwj.12557

53. El-Wakil, N.A., Hassan, E.A., Hassan, M.L., Abd El-Salam, S.S., 2019. Bacterial cellulose/phytochemical's extracts biocomposites for potential active wound dressings. Environ Sci Pollut Res Int 26, 26529–26541. https://doi.org/10.1007/s11356-019-05776-w

54. Emaldi, I., Hamzehlou, S., Sanchez-Dolado, J., Leiza, J.R., 2017. Kinetics of the Aqueous-Phase Copolymerization of MAA and PEGMA Macromonomer: Influence of Monomer Concentration and Side Chain Length of PEGMA. Processes 5, 19. https://doi.org/10.3390/pr5020019

55. Emanuelli, T., Burgeiro, A., Carvalho, E., 2016. Effects of insulin on the skin: possible healing benefits for diabetic foot ulcers. Arch Dermatol Res 308, 677–694. https://doi.org/10.1007/s00403-016-1686-z

56. Erik H. Mürer, 1981. Strontium and Platelet Function | SpringerLink 465–478.

57. Evert, M., Calvisi, D.F., Evert, K., De Murtas, V., Gasparetti, G., Mattu, S., Destefanis, G., Ladu, S., Zimmermann, A., Delogu, S., Thiel, S., Thiele, A., Ribback, S., Dombrowski, F., 2012. V-AKT murine thymoma viral oncogene homolog/mammalian target of rapamycin activation induces a module of metabolic changes contributing to growth in insulin-induced hepatocarcinogenesis. Hepatology 55, 1473–1484. https://doi.org/10.1002/hep.25600

58. Fahimirad, S., Abtahi, H., Satei, P., Ghaznavi-Rad, E., Moslehi, M., Ganji, A., 2021. Wound healing performance of PCL/chitosan based electrospun nanofiber electrosprayed with curcumin loaded chitosan nanoparticles. Carbohydr Polym 259, 117640. https://doi.org/10.1016/j.carbpol.2021.117640

59. Fitzmaurice, G.J., McWilliams, B., Nölke, L., Redmond, J.M., McGuinness, J.G., O'Donnell, M.E., 2014. Do Statins Have a Role in the Promotion of Postoperative Wound Healing in Cardiac Surgical Patients? The Annals of Thoracic Surgery 98, 756–764. https://doi.org/10.1016/j.athoracsur.2014.02.089

60. Foster, N.B., 1925. DIABETIC COMA. Journal of the American Medical Association 84, 719–722. https://doi.org/10.1001/jama.1925.02660360001001

61. Frykberg, R.G., Banks, J., 2015. Challenges in the Treatment of Chronic Wounds. Advances in Wound Care 4, 560–582. https://doi.org/10.1089/wound.2015.0635

62. Fujimoto, W.Y., Williams, R.H., 1974. Insulin action on the cultured human fibroblast. Glucose uptake, protein synthesis, RNA synthesis. Diabetes 23, 443–448. https://doi.org/10.2337/diab.23.5.443

63. Furukawa, F., Huff, J.C., Lyons, M.B., Weston, W.L., Norris, D.A., 1988. Characterization and practical benefits of keratinocytes cultured in strontium-containing serum-free medium. J Invest Dermatol 90, 690–696. https://doi.org/10.1111/1523-1747.ep12560908

64. Goldstein, R., POLIKS, C.F., PILCH, P.F., SMITH, B.D., FINE, A., 1989. Stimulation of Collagen Formation by Insulin and Insulin-Like Growth Factor I in Cultures of Human Lung Fibroblasts*. Endocrinology 124, 964–970. https://doi.org/10.1210/endo-124-2-964

65. Gonzalez, A.C. de O., Costa, T.F., Andrade, Z. de A., Medrado, A.R.A.P., 2016. Wound healing - A literature review. An. Bras. Dermatol. 91, 614–620. https://doi.org/10.1590/abd1806-4841.20164741

66. Gordillo, G.M., Sen, C.K., 2003. Revisiting the essential role of oxygen in wound healing. Am J Surg 186, 259–263. https://doi.org/10.1016/s0002-9610(03)00211-3

67. Goren, I., Müller, E., Schiefelbein, D., Gutwein, P., Seitz, O., Pfeilschifter, J., Frank, S., 2009. Akt1 Controls Insulin-Driven VEGF Biosynthesis from Keratinocytes: Implications for Normal and Diabetes-Impaired Skin Repair in Mice. Journal of Investigative Dermatology 129, 752–764. https://doi.org/10.1038/jid.2008.230

68. Graham, C., 2005. The role of silver in wound healing. Br J Nurs 14, S22, S24, S26 passim. https://doi.org/10.12968/bjon.2005.14.Sup5.19954

69. Greenhalgh, D.G., 1996. The Role of Growth Factors in Wound Healing. Journal of Trauma and Acute Care Surgery 41, 159.

70. Gulcan, E., Gulcan, A., Erbilen, E., Toker, S., 2007. Statins may be useful in diabetic foot ulceration treatment and prevention. Med Hypotheses 69, 1313–1315. https://doi.org/10.1016/j.mehy.2007.03.022

71. Guo, S., Ren, Y., Chang, R., He, Y., Zhang, D., Guan, F., Yao, M., 2022. Injectable Self-Healing Adhesive Chitosan Hydrogel with Antioxidative, Antibacterial, and Hemostatic Activities for Rapid Hemostasis and Skin Wound Healing. ACS Appl. Mater. Interfaces 14, 34455–34469. https://doi.org/10.1021/acsami.2c08870

72. Guo, W., Hu, N., 2007. Interaction of myoglobin with poly(methacrylic acid) at different pH in their layer-by-layer assembly films: an electrochemical study. Biophys Chem 129, 163–171. https://doi.org/10.1016/j.bpc.2007.05.015

73. Han, W., Zhou, B., Yang, K., Xiong, X., Luan, S., Wang, Y., Xu, Z., Lei, P., Luo, Z., Gao, J., Zhan, Y., Chen, G., Liang, L., Wang, R., Li, S., Xu, H., 2020. Biofilm-inspired adhesive and antibacterial hydrogel with tough tissue integration performance for sealing hemostasis and wound healing. Bioactive Materials 5, 768–778. https://doi.org/10.1016/j.bioactmat.2020.05.008

74. Haug, A., Larsen, B., Smidsrød, O., 1974. Uronic acid sequence in alginate from different sources. Carbohydrate Research 32, 217–225. https://doi.org/10.1016/S0008-6215(00)82100-X

75. Haug, A., Smidsrød, O., 1967. Strontium–Calcium Selectivity of Alginates. Nature 215, 757–757. https://doi.org/10.1038/215757a0

76. He, X., Ding, Y., Xie, W., Sun, R., Hunt, N.C., Song, J., Sun, X., Peng, C., Zeng, Q., Tan, Y., Liu, Y., 2019. Rubidium-Containing Calcium Alginate Hydrogel for Antibacterial and Diabetic Skin Wound Healing Applications. ACS Biomater. Sci. Eng. 5, 4726–4738. https://doi.org/10.1021/acsbiomaterials.9b00547

77. Hegde, V., Uthappa, U.T., Altalhi, T., Jung, H.-Y., Han, S.S., Kurkuri, M.D., 2022. Alginate based polymeric systems for drug delivery, antibacterial/microbial, and

wound dressing applications. Materials Today Communications 33, 104813. https://doi.org/10.1016/j.mtcomm.2022.104813

78. Henrich, D., Seebach, C., Wilhelm, K., Marzi, I., 2007. High dosage of simvastatin reduces TNF-alpha-induced apoptosis of endothelial progenitor cells but fails to prevent apoptosis induced by IL-1beta in vitro. J Surg Res 142, 13–19. https://doi.org/10.1016/j.jss.2006.04.011

79. Herman, T.F., Bordoni, B., 2021. Wound Classification, in: StatPearls. StatPearls Publishing, Treasure Island (FL).

80. Holte, O., Tønnesen, H.H., Karlsen, J., 2006. Measurement of diffusion through calcium alginate gel matrices. Pharmazie 61, 30–34.

81. Hrynyk, M., Martins-Green, M., Barron, A.E., Neufeld, R.J., 2010. Sustained prolonged topical delivery of bioactive human insulin for potential treatment of cutaneous wounds. Int J Pharm 398, 146–154. https://doi.org/10.1016/j.ijpharm.2010.07.052

82. Hrynyk, M., Martins-Green, M., Barron, A.E., Neufeld, R.J., 2012. Alginate-PEG sponge architecture and role in the design of insulin release dressings. Biomacromolecules 13, 1478–1485. https://doi.org/10.1021/bm300186k

83. Huang, H., Cui, W., Qiu, W., Zhu, M., Zhao, R., Zeng, D., Dong, C., Wang, X., Guo, W., Xing, W., Li, X., Li, L., Tan, Y., Wu, X., Chen, L., Fu, X., Luo, D., Xu, X., 2015. Impaired wound healing results from the dysfunction of the Akt/mTOR pathway in diabetic rats. J Dermatol Sci 79, 241–251. https://doi.org/10.1016/j.jdermsci.2015.06.002

84. Huang, Z., Li, S., Kou, Y., Huang, L., Yu, T., Hu, A., 2019. Risk factors for the recurrence of diabetic foot ulcers among diabetic patients: a meta-analysis. Int Wound J 16, 1373–1382. https://doi.org/10.1111/iwj.13200

85. Huijberts, M.S.P., Schaper, N.C., Schalkwijk, C.G., 2008. Advanced glycation end products and diabetic foot disease. Diabetes Metab Res Rev 24 Suppl 1, S19-24. https://doi.org/10.1002/dmrr.861

86. Ilmi, Z.N., Wulandari, P.A.C., Husen, S.A., Winarni, D., Alamsjah, M.A., Awang, K., Vastano, M., Pellis, A., Macquarrie, D., Pudjiastuti, P., 2020. Characterization of Alginate from Sargassum duplicatum and the Antioxidant Effect of Alginate–Okra Fruit Extracts Combination for Wound Healing on Diabetic Mice. Applied Sciences 10, 6082. https://doi.org/10.3390/app10176082

87. Ingenbosch, K.N., Quint, S., Dyllick-Brenzinger, M., Wunschik, D.S., Kiebist, J., Süss, P., Liebelt, U., Zuhse, R., Menyes, U., Scheibner, K., Mayer, C., Opwis, K.,

Gutmann, J.S., Hoffmann-Jacobsen, K., 2021. Singlet-Oxygen Generation by Peroxidases and Peroxygenases for Chemoenzymatic Synthesis. ChemBioChem 22, 398–407. https://doi.org/10.1002/cbic.202000326

88. ISO 10993-5, 2009. ISO 10993-5:2009 [WWW Document]. ISO. URL https://www.iso.org/cms/render/live/en/sites/isoorg/contents/data/standard/03/64/36406.html (accessed 11.4.20).

89. Järbrink, K., Ni, G., Sönnergren, H., Schmidtchen, A., Pang, C., Bajpai, R., Car, J., 2016. Prevalence and incidence of chronic wounds and related complications: a protocol for a systematic review. Systematic Reviews 5, 152. https://doi.org/10.1186/s13643-016-0329-y

90. Jeffcoate, W.J., Vileikyte, L., Boyko, E.J., Armstrong, D.G., Boulton, A.J.M., 2018. Current Challenges and Opportunities in the Prevention and Management of Diabetic Foot Ulcers. Diabetes Care 41, 645–652. https://doi.org/10.2337/dc17-1836

91. Jere, S.W., Houreld, N.N., Abrahamse, H., 2019. Role of the PI3K/AKT (mTOR and GSK3β) signalling pathway and photobiomodulation in diabetic wound healing. Cytokine & Growth Factor Reviews 50, 52–59. https://doi.org/10.1016/j.cytogfr.2019.03.001

92. Jing, L., Li, S., Li, Q., 2015. Akt/hypoxia-inducible factor-1α signaling deficiency compromises skin wound healing in a type 1 diabetes mouse model. Exp Ther Med 9, 2141–2146. https://doi.org/10.3892/etm.2015.2394

93. Karakasyan, C., Renard, D., Davy, J., Mathos, J., Marquis, M., Lack, S., 2015. Microfluidics-assisted generation of stimuli-responsive hydrogels based on alginates incorporated with thermo-responsive and amphiphilic polymers as novel biomaterials. Colloids and Surfaces B: Biointerfaces.

94. Kast, H., Funke, W., 1979. Crosslinking mechanism in radical polymerization of tetrafunctional monomers. Die Makromolekulare Chemie 180, 1335–1338. https://doi.org/10.1002/macp.1979.021800519

95. Kaur, P., Choudhury, D., 2020. Modulation of Inflammatory Dynamics by Insulin to Promote Wound Recovery of Diabetic Ulcers, Wound Healing. IntechOpen. https://doi.org/10.5772/intechopen.92096

96. Kaur, P., Sharma, A.K., Nag, D., Das, A., Datta, S., Ganguli, A., Goel, V., Rajput, S., Chakrabarti, G., Basu, B., Choudhury, D., 2019. Novel nano-insulin formulation modulates cytokine secretion and remodeling to accelerate diabetic wound healing. Nanomedicine: Nanotechnology, Biology and Medicine 15, 47–57. https://doi.org/10.1016/j.nano.2018.08.013

97. Khansa, I., Schoenbrunner, A.R., Kraft, C.T., Janis, J.E., 2019. Silver in Wound Care—Friend or Foe?: A Comprehensive Review. Plast Reconstr Surg Glob Open 7, e2390. https://doi.org/10.1097/GOX.0000000000002390

98. Khasana M, Mudasir M, Kuncaka A et al. Enhancement of the sensitivity and selectivity of the voltammetric sensor for uric acid using molecularly imprinted polymer. Indones. 10(3), 295–300 (2010).

99. Khoshneviszadeh, M., Ashkani-Esfahani, S., Namazi, M.R., Noorafshan, A., Geramizadeh, B., Miri, R., 2014. Topical Simvastatin Enhances Tissue Regeneration in Full-Thickness Skin Wounds in Rat Models. Iran J Pharm Res 13, 263–269.

100. Kim, B., La Flamme, K., Peppas, N.A., 2003. Dynamic swelling behavior of pH-sensitive anionic hydrogels used for protein delivery. Journal of Applied Polymer Science 89, 1606–1613. https://doi.org/10.1002/app.12337

101. Kim, S.H., Heo, E.J., Lee, S.W., 2009. The effect of topically applied recombinant human growth hormone on wound healing in pigs. Wounds 21, 158–163.

102. Kjellström, T., Malmquist, J., 1984. Insulin effects on collagen and protein production in cultured human skin fibroblasts from diabetic and non-diabetic subjects. Horm Metab Res 16, 168–171. https://doi.org/10.1055/s-2007-1014734

103. Klenchin, V.A., Khaitlina, S.Y., Rayment, I., 2006. Crystal structure of polymerization-competent actin. J Mol Biol 362, 140–150. https://doi.org/10.1016/j.jmb.2006.07.001

104. Klyubin, I.V., Kirpichnikova, K.M., Gamaley, I.A., 1996. Hydrogen peroxide-induced chemotaxis of mouse peritoneal neutrophils. Eur J Cell Biol 70, 347–351.

105. Kolarsick, P.A.J., Kolarsick, M.A., Goodwin, C., 2011. Anatomy and Physiology of the Skin. Journal of the Dermatology Nurses' Association 3, 203. https://doi.org/10.1097/JDN.0b013e3182274a98

106. Kopecki, Z., Cowin, A.J., 2016. The Role of Actin Remodelling Proteins in Wound Healing and Tissue Regeneration, Wound Healing - New insights into Ancient Challenges. IntechOpen. https://doi.org/10.5772/64673

107. Kornblatt, A.P., Nicoletti, V.G., Travaglia, A., 2016. The neglected role of copper ions in wound healing. Journal of Inorganic Biochemistry 161, 1–8. https://doi.org/10.1016/j.jinorgbio.2016.02.012

108. Krischak, G.D., Augat, P., Claes, L., Kinzl, L., Beck, A., 2007. The effects of non-steroidal anti-inflammatory drug application on incisional wound healing in rats. J Wound Care 16, 76–78. https://doi.org/10.12968/jowc.2007.16.2.27001

109. Laurienzo, P., Malinconico, M., Motta, A., Vicinanza, A., 2005. Synthesis and characterization of a novel alginate–poly(ethylene glycol) graft copolymer. Carbohydrate Polymers 62, 274–282. https://doi.org/10.1016/j.carbpol.2005.08.005

110. Leal, D., Matsuhiro, B., Rossi, M., Caruso, F., 2008. FT-IR spectra of alginic acid block fractions in three species of brown seaweeds. Carbohydr. Res. 343, 308–316. https://doi.org/10.1016/j.carres.2007.10.016

111. Lee, K.Y., Mooney, D.J., 2012. Alginate: Properties and biomedical applications. Progress in Polymer Science 37, 106–126. https://doi.org/10.1016/j.progpolymsci.2011.06.003

112. Leganés, J., Rodríguez, A.M., Arranz, M.A., Castillo-Sarmiento, C.A., Ballesteros-Yáñez, I., Migallón, A.S., Merino, S., Vázquez, E., 2022. Magnetically responsive hydrophobic pockets for on–off drug release. Materials Today Chemistry 23, 100702. https://doi.org/10.1016/j.mtchem.2021.100702

113. Li, G., Huang, J., Wei, J., Liu, C., Zuo, Y., Li, J., Li, Y., 2021. Fabrication of strontium and simvastatin loaded hydroxyapatite microspheres by one-step approach. Materials Letters 300, 130234. https://doi.org/10.1016/j.matlet.2021.130234

114. Li, L., Zhang, Junhui, Zhang, Q., Zhang, D., Xiang, F., Jia, J., Wei, P., Zhang, Jiaping, Hu, J., Huang, Y., 2019. High Glucose Suppresses Keratinocyte Migration Through the Inhibition of p38 MAPK/Autophagy Pathway. Front. Physiol. 10, 24. https://doi.org/10.3389/fphys.2019.00024

115. Li, S., Li, L., Guo, C., Qin, H., Yu, X., 2017. A promising wound dressing material with excellent cytocompatibility and proangiogenesis action for wound healing: Strontium loaded Silk fibroin/Sodium alginate (SF/SA) blend films. Int J Biol Macromol 104, 969–978. https://doi.org/10.1016/j.ijbiomac.2017.07.020

116. Li, X., Li, Q., Zhao, C., 2021. Zero-Order Controlled Release of Water-Soluble Drugs Using a Marker Pen Platform. ACS Omega 6, 13774–13778. https://doi.org/10.1021/acsomega.1c01141

117. Li, X., Liu, Y., Zhang, J., You, R., Qu, J., Li, M., 2017. Functionalized silk fibroin dressing with topical bioactive insulin release for accelerated chronic wound healing. Materials Science and Engineering: C 72, 394–404. https://doi.org/10.1016/j.msec.2016.11.085

118. Li, Y., Ju, S., Li, X., Li, W., Zhou, S., Wang, G., Cai, Y., Dong, Z., 2023. Characterization of the microenvironment of diabetic foot ulcers and potential drug identification based on scRNA-seq. Frontiers in Endocrinology 13.

119. Li, Z., Chen, S., Wu, B., Liu, Z., Cheng, L., Bao, Y., Ma, Y., Chen, L., Tong, X., Dai, F., 2020. Multifunctional Dual Ionic-Covalent Membranes for Wound Healing. ACS Biomater. Sci. Eng. 6, 6949–6960. https://doi.org/10.1021/acsbiomaterials.0c01512

120. Li, Z., Zhao, Y., Liu, He, Ren, M., Wang, Z., Wang, X., Liu, Hou, Feng, Y., Lin, Q., Wang, C., Wang, J., 2021. pH-responsive hydrogel loaded with insulin as a bioactive dressing for enhancing diabetic wound healing. Materials & Design 210, 110104. https://doi.org/10.1016/j.matdes.2021.110104

121. Liarte, S., Bernabé-García, Á., Nicolás, F.J., 2020. Role of TGF-β in Skin Chronic Wounds: A Keratinocyte Perspective. Cells 9, 306. https://doi.org/10.3390/cells9020306

122. Lima, M.H.M., Caricilli, A.M., de Abreu, L.L., Araújo, E.P., Pelegrinelli, F.F., Thirone, A.C.P., Tsukumo, D.M., Pessoa, A.F.M., dos Santos, M.F., de Moraes, M.A., Carvalheira, J.B.C., Velloso, L.A., Saad, M.J.A., 2012. Topical insulin accelerates wound healing in diabetes by enhancing the AKT and ERK pathways: a double-blind placebo-controlled clinical trial. PLoS One 7, e36974. https://doi.org/10.1371/journal.pone.0036974

123. Lipsky, B.A., Hoey, C., 2009. Topical antimicrobial therapy for treating chronic wounds. Clin Infect Dis 49, 1541–1549. https://doi.org/10.1086/644732

124. Litwiniuk, K., Speyrer, S., Gauto, Grzela, 2016. Hyaluronic Acid in Inflammation and Tissue Regeneration. Wounds : a compendium of clinical research and practice 28.

125. Liu, G., Li, Y., Yang, L., Wei, Y., Wang, X., Wang, Z., Tao, L., 2017. Cytotoxicity study of polyethylene glycol derivatives. RSC Adv. 7, 18252–18259. https://doi.org/10.1039/C7RA00861A

126. Liu, G., Zhou, H., Wu, H., Chen, R., Guo, S., 2016. Preparation of alginate hydrogels through solution extrusion and the release behavior of different drugs. J Biomater Sci Polym Ed 27, 1808–1823. https://doi.org/10.1080/09205063.2016.1237452

127. Liu, X., Xu, H., Zhang, M., Yu, D.-G., 2021. Electrospun Medicated Nanofibers for Wound Healing: Review. Membranes 11, 770. https://doi.org/10.3390/membranes11100770

128. Liu, Y., Petreaca, M., Yao, M., Martins-Green, M., 2009. Cell and molecular mechanisms of keratinocyte function stimulated by insulin during wound healing. BMC Cell Biol 10, 1. https://doi.org/10.1186/1471-2121-10-1

129. Loo, A.E.K., Halliwell, B., 2012. Effects of hydrogen peroxide in a keratinocyte-fibroblast co-culture model of wound healing. Biochem Biophys Res Commun 423, 253–258. https://doi.org/10.1016/j.bbrc.2012.05.100

130. Louiselle, A.E., Niemiec, S.M., Zgheib, C., Liechty, K.W., 2021. Macrophage polarization and diabetic wound healing. Translational Research 236, 109–116. https://doi.org/10.1016/j.trsl.2021.05.006

131. Lu, W., Bao, D., Ta, F., Liu, D., Zhang, D., Zhang, Z., Fan, Z., 2020. Multifunctional Alginate Hydrogel Protects and Heals Skin Defects in Complex Clinical Situations. ACS Omega 5, 17152–17159. https://doi.org/10.1021/acsomega.0c01108

132. M P Filippov, R.K., 1974. Determination of composition of alginates by infrared spectroscopic method. Chem. Zvesti 6, 817–819.

133. MacIntosh, F.C., 1941. A colorimetric method for the standardization of heparin preparations. Biochemical Journal 35, 776–782. https://doi.org/10.1042/bj0350776

134. Madau, M., Le Cerf, D., Dulong, V., Picton, L., 2021. Hyaluronic Acid Functionalization with Jeffamine® M2005: A Comparison of the Thermo-Responsiveness Properties of the Hydrogel Obtained through Two Different Synthesis Routes. Gels 7, 88. https://doi.org/10.3390/gels7030088

135. Maia, F.R., Fonseca, K.B., Rodrigues, G., Granja, P.L., Barrias, C.C., 2014. Matrix-driven formation of mesenchymal stem cell-extracellular matrix microtissues on soft alginate hydrogels. Acta Biomater 10, 3197–3208. https://doi.org/10.1016/j.actbio.2014.02.049

136. Maiti, S., Singha, K., Ray, S., Dey, P., Sa, B., 2009. Adipic acid dihydrazide treated partially oxidized alginate beads for sustained oral delivery of flurbiprofen. Pharm Dev Technol 14, 461–470. https://doi.org/10.1080/10837450802712658

137. Mao, Y., Pan, M., Yang, H., Lin, X., Yang, L., 2020. Injectable hydrogel wound dressing based on strontium ion cross-linked starch. Front. Mater. Sci. 14, 232–241. https://doi.org/10.1007/s11706-020-0508-6

138. Martínez-Jiménez, M.A., Aguilar-García, J., Valdés-Rodríguez, R., Metlich-Medlich, M.A., Dietsch, L.J.P., Gaitán-Gaona, F.I., Kolosovas-Machuca, E.S., González, F.J., Sánchez-Aguilar, J.M., 2013. Local use of insulin in wounds of

diabetic patients: higher temperature, fibrosis, and angiogenesis. Plast Reconstr Surg 132, 1015e–1019e. https://doi.org/10.1097/PRS.0b013e3182a806f0

139. Martinsen, A., Storrø, I., Skjårk-Bræk, G., 1992. Alginate as immobilization material: III. Diffusional properties. Biotechnology and Bioengineering 39, 186–194. https://doi.org/10.1002/bit.260390210

140. Mathew-Steiner, S.S., Roy, S., Sen, C.K., 2021. Collagen in Wound Healing. Bioengineering 8. https://doi.org/10.3390/bioengineering8050063

141. Medikabazaar, 2022. Wound Dressings: Types of dressings and advances in the wound care industry. Medikabazaar - News, Trends, and Information. URL https://www.medikabazaar.com/blog/medical-consumables/wound-dressings-types-of-dressings-and-advances-in-the-wound-care-industry/ (accessed 2.10.23).

142. Mohandas, A., PT, S.K., Raja, B., Lakshmanan, V.-K., Jayakumar, R., 2015. Exploration of alginate hydrogel/nano zinc oxide composite bandages for infected wounds. Int J Nanomedicine 10, 53–66. https://doi.org/10.2147/IJN.S79981

143. Mollah, M.Z.I., Zahid, H.M., Mahal, Z., Faruque, M.R.I., Khandaker, M.U., 2021. The Usages and Potential Uses of Alginate for Healthcare Applications. Frontiers in Molecular Biosciences 8.

144. Monaco, S., Illario, M., Rusciano, M.R., Gragnaniello, G., Di Spigna, G., Leggiero, E., Pastore, L., Fenzi, G., Rossi, G., Vitale, M., 2009. Insulin stimulates fibroblast proliferation through calcium-calmodulin-dependent kinase II. Cell Cycle 8, 2024–2030. https://doi.org/10.4161/cc.8.13.8813

145. Montanucci, P., Terenzi, S., Santi, C., Pennoni, I., Bini, V., Pescara, T., Basta, G., Calafiore, R., 2015. Insights in Behavior of Variably Formulated Alginate-Based Microcapsules for Cell Transplantation. BioMed Research International 2015, 1–11. https://doi.org/10.1155/2015/965804

146. Morales-González, M., Díaz, L.E., Dominguez-Paz, C., Valero, M.F., 2022. Insights into the Design of Polyurethane Dressings Suitable for the Stages of Skin Wound-Healing: A Systematic Review. Polymers 14, 2990. https://doi.org/10.3390/polym14152990

147. Mørch, Ý.A., Donati, I., Strand, B.L., Skjåk-Bræk, G., 2006. Effect of Ca^{2+}, Ba^{2+}, and Sr^{2+} on Alginate Microbeads. Biomacromolecules 7, 1471–1480. https://doi.org/10.1021/bm060010d

148. Morgan, D., 1997. Alginate Dressings: Part 1: Historical Aspects. Journal of Tissue Viability 7, 4–9. https://doi.org/10.1016/S0965-206X(97)80014-9

149. Mukai, K., Nakajima, Y., Asano, K., Nakatani, T., 2019. Topical estrogen application to wounds promotes delayed cutaneous wound healing in 80-week-old female mice. PLOS ONE 14, e0225880. https://doi.org/10.1371/journal.pone.0225880

150. Nasseri, S., Sharifi, M., 2022. Therapeutic Potential of Antimicrobial Peptides for Wound Healing. Int J Pept Res Ther 28, 38. https://doi.org/10.1007/s10989-021-10350-5

151. Nault, L., Guo, P., Jain, B., Bréchet, Y., Bruckert, F., Weidenhaupt, M., 2013. Human insulin adsorption kinetics, conformational changes and amyloidal aggregate formation on hydrophobic surfaces. Acta Biomaterialia 9, 5070–5079. https://doi.org/10.1016/j.actbio.2012.09.025

152. Neves, M.I., Moroni, L., Barrias, C.C., 2020. Modulating Alginate Hydrogels for Improved Biological Performance as Cellular 3D Microenvironments. Frontiers in Bioengineering and Biotechnology 8.

153. Niethammer, P., Grabher, C., Look, A.T., Mitchison, T.J., 2009. A tissue-scale gradient of hydrogen peroxide mediates rapid wound detection in zebrafish. Nature 459, 996–999. https://doi.org/10.1038/nature08119

154. Nourian Dehkordi, A., Mirahmadi Babaheydari, F., Chehelgerdi, M., Raeisi Dehkordi, S., 2019. Skin tissue engineering: wound healing based on stem-cell-based therapeutic strategies. Stem Cell Research & Therapy 10, 111. https://doi.org/10.1186/s13287-019-1212-2

155. Oktarina, D.A.M., Iqbal, R.M., 2022. Protective effects of simvastatin against ultraviolet B-induced photoaging of human dermal fibroblasts. Iranian Journal of Dermatology 25, 34–40. https://doi.org/10.22034/ijd.2021.270743.1330

156. Oliva, N., Almquist, B.D., 2020. Spatiotemporal delivery of bioactive molecules for wound healing using stimuli-responsive biomaterials. Advanced Drug Delivery Reviews 161–162, 22–41. https://doi.org/10.1016/j.addr.2020.07.021

157. Ontario Health (Quality), 2021. Skin Substitutes for Adults With Diabetic Foot Ulcers and Venous Leg Ulcers: A Health Technology Assessment. Ont Health Technol Assess Ser 21, 1–165.

158. Onyekwelu I, Yakkanti R, Protzer L, Pinkston CM, Tucker C, Seligson D. Surgical Wound Classification and Surgical Site Infections in the Orthopaedic Patient. J Am Acad Orthop Surg Glob Res Rev. 2017 Jun 13;1(3):e022. doi: 10.5435/JAAOSGlobal-D-17-00022.

159. Ouyang, L., Dan, Y., Shao, Z., Yang, S., Yang, C., Liu, G., Duan, D., 2019. MMP-sensitive PEG hydrogel modified with RGD promotes bFGF, VEGF and EPC-mediated angiogenesis. Exp Ther Med 18, 2933–2941. https://doi.org/10.3892/etm.2019.7885

160. Park, Y.S., David, A.E., Park, K.M., Lin, C.-Y., Than, K.D., Lee, K., Park, J.B., Jo, I., Park, K.D., Yang, V.C., 2012. Controlled Release of Simvastatin from In situ Forming Hydrogel Triggers Bone Formation in MC3T3-E1 Cells. AAPS J 15, 367–376. https://doi.org/10.1208/s12248-012-9442-6

161. Parnell, L.K.S., Ciufi, B., Gokoo, C.F., 2005. Preliminary use of a hydrogel containing enzymes in the treatment of stage II and stage III pressure ulcers. Ostomy Wound Manage 51, 50–60.

162. Patel, S., Srivastava, S., Singh, M.R., Singh, D., 2019. Mechanistic insight into diabetic wounds: Pathogenesis, molecular targets and treatment strategies to pace wound healing. Biomedicine & Pharmacotherapy 112, 108615. https://doi.org/10.1016/j.biopha.2019.108615

163. Patil, N.S., Dordick, J.S., Rethwisch, D.G., 1996. Macroporous poly(sucrose acrylate) hydrogel for controlled release of macromolecules. Biomaterials 17, 2343–2350. https://doi.org/10.1016/S0142-9612(96)00089-0

164. Pawar, H.V., Tetteh, J., Boateng, J.S., 2013. Preparation, optimisation and characterisation of novel wound healing film dressings loaded with streptomycin and diclofenac. Colloids Surf B Biointerfaces 102, 102–110. https://doi.org/10.1016/j.colsurfb.2012.08.014

165. Percival, N.J., 2002. Classification of Wounds and their Management. Surgery (Oxford), Basic Surgical Techniques / Wound Healing / Theatre Problems 20, 114–117. https://doi.org/10.1383/surg.20.5.114.14626

166. Perez-Favila, A., Martinez-Fierro, M.L., Rodriguez-Lazalde, J.G., Cid-Baez, M.A., Zamudio-Osuna, M. de J., Martinez-Blanco, M. del R., Mollinedo-Montaño, F.E., Rodriguez-Sanchez, I.P., Castañeda-Miranda, R., Garza-Veloz, I., 2019. Current Therapeutic Strategies in Diabetic Foot Ulcers. Medicina 55, 714. https://doi.org/10.3390/medicina55110714

167. Peterson, C., Chandler, H.L., 2022. Insulin facilitates corneal wound healing in the diabetic environment through the RTK-PI3K/Akt/mTOR axis in vitro. Molecular and Cellular Endocrinology 548, 111611. https://doi.org/10.1016/j.mce.2022.111611

168. Pilehvar-Soltanahmadi, Y., Dadashpour, M., Mohajeri, A., Fattahi, A., Sheervalilou, R., Zarghami, N., 2018. An Overview on Application of Natural

Substances Incorporated with Electrospun Nanofibrous Scaffolds to Development of Innovative Wound Dressings. Mini Rev Med Chem 18, 414–427. https://doi.org/10.2174/1389557517666170308112147

169. Place, E.S., Rojo, L., Gentleman, E., Sardinha, J.P., Stevens, M.M., 2011. Strontium- and zinc-alginate hydrogels for bone tissue engineering. Tissue Eng Part A 17, 2713–2722. https://doi.org/10.1089/ten.TEA.2011.0059

170. Pollard, F.H., Martin, J.V., 1956. The spectrophotometric determination of the alkaline-earth metals with murexide, eriochrome black T and with o-cresolphthalein complexone. Analyst 81, 348–353. https://doi.org/10.1039/AN9568100348

171. Ponugoti, B., Dong, G., Graves, D.T., 2012. Role of forkhead transcription factors in diabetes-induced oxidative stress. Exp Diabetes Res 2012, 939751. https://doi.org/10.1155/2012/939751

172. Pop, M.A., Almquist, B.D., 2017. Biomaterials: A potential pathway to healing chronic wounds? Exp Dermatol 26, 760–763. https://doi.org/10.1111/exd.13290

173. Praeger, F.C., Stanulis-Praeger, B.M., Gilchrest, B.A., 1987. Use of strontium to separate calcium-dependent pathways for proliferation and differentiation in human keratinocytes. J Cell Physiol 132, 81–89. https://doi.org/10.1002/jcp.1041320111

174. Putnis, S., Khan, W.S., Wong, J.M.-L., 2014. Negative Pressure Wound Therapy – A Review of its Uses in Orthopaedic Trauma. Open Orthop J 8, 142–147. https://doi.org/10.2174/1874325001408010142

175. Queen, D., Gaylor, J.D.S., Evans, J.H., Courtney, J.M., Reid, W.H., 1987. The preclinical evaluation of the water vapour transmission rate through burn wound dressings. Biomaterials 8, 367–371. https://doi.org/10.1016/0142-9612(87)90007-X

176. Queen, D., Orsted, H., Sanada, H., Sussman, G., 2004. A dressing history. Int Wound J 1, 59–77. https://doi.org/10.1111/j.1742-4801.2004.0009.x

177. Ramhormozi, P., Ansari, J.M., Simorgh, S., Asgari, H.R., Najafi, M., Barati, M., Babakhani, A., Nobakht, M., 2021. Simvastatin accelerates the healing process of burn wound in Wistar rats through Akt/mTOR signaling pathway. Annals of Anatomy - Anatomischer Anzeiger 236, 151652. https://doi.org/10.1016/j.aanat.2020.151652

178. Raposio, E., Libondi, G., Bertozzi, N., Grignaffini, E., Grieco, M.P., 2016. Effects of Topic Simvastatin for the Treatment of Chronic Vascular Cutaneous

Ulcers: A Pilot Study. J Am Coll Clin Wound Spec 7, 13–18. https://doi.org/10.1016/j.jccw.2016.06.001

179. Rego, A.C.M. do, Araújo Filho, I., Damasceno, B.P.G.L., Egito, E.S.T., Silveira, I.A. da, Brandão-Neto, J., Medeiros, A.C., 2007. Simvastatin improves the healing of infected skin wounds of rats. Acta Cirúrgica Brasileira 22, 57–63. https://doi.org/10.1590/S0102-86502007000700012

180. Rezvani Ghomi, E., Khalili, S., Nouri Khorasani, S., Esmaeely Neisiany, R., Ramakrishna, S., 2019. Wound dressings: Current advances and future directions. Journal of Applied Polymer Science 136, 47738. https://doi.org/10.1002/app.47738

181. Rezvani, O., Shabbak, E., Aslani, A., Bidar, R., Jafari, M., Safarnezhad, S., 2009. A randomized, double-blind, placebo-controlled trial to determine the effects of topical insulin on wound healing. Ostomy Wound Manage 55, 22–28.

182. Rezvanian, M., Ng, S.-F., Alavi, T., Ahmad, W., 2021. In-vivo evaluation of Alginate-Pectin hydrogel film loaded with Simvastatin for diabetic wound healing in Streptozotocin-induced diabetic rats. Int J Biol Macromol 171, 308–319. https://doi.org/10.1016/j.ijbiomac.2020.12.221

183. Ribeiro, M.C., Correa, V.L.R., Silva, F.K.L. da, Casas, A.A., Chagas, A. de L. das, Oliveira, L.P. de, Miguel, M.P., Diniz, D.G.A., Amaral, A.C., Menezes, L.B. de, 2020. Wound healing treatment using insulin within polymeric nanoparticles in the diabetes animal model. Eur J Pharm Sci 150, 105330. https://doi.org/10.1016/j.ejps.2020.105330

184. Rittié, L., Kang, S., Voorhees, J.J., Fisher, G.J., 2008. Induction of collagen by estradiol: difference between sun-protected and photodamaged human skin in vivo. Arch Dermatol 144, 1129–1140. https://doi.org/10.1001/archderm.144.9.1129

185. Saidak, Z., Marie, P.J., 2012. Strontium signaling: molecular mechanisms and therapeutic implications in osteoporosis. Pharmacol Ther 136, 216–226. https://doi.org/10.1016/j.pharmthera.2012.07.009

186. Santema, T.B., Lenselink, E.A., Balm, R., Ubbink, D.T., 2015. Comparing the Meggitt-Wagner and the University of Texas wound classification systems for diabetic foot ulcers: inter-observer analyses. Int Wound J 13, 1137–1141. https://doi.org/10.1111/iwj.12429

187. Savin, C.-L., Popa, M., Delaite, C., Costuleanu, M., Costin, D., Peptu, C.A., 2019. Chitosan grafted-poly(ethylene glycol) methacrylate nanoparticles as carrier

for controlled release of bevacizumab. Materials Science and Engineering: C 98, 843–860. https://doi.org/10.1016/j.msec.2019.01.036

188. Schweiger, R.G., 1962. Acetylation of Alginic Acid. I. Preparation and Viscosities of Algin Acetates. J. Org. Chem. 27, 1786–1789. https://doi.org/10.1021/jo01052a072

189. Shah, S.A., Sohail, M., Khan, S.A., Kousar, M., 2021. Improved drug delivery and accelerated diabetic wound healing by chondroitin sulfate grafted alginate-based thermoreversible hydrogels. Materials Science and Engineering: C 126, 112169. https://doi.org/10.1016/j.msec.2021.112169

190. Sharifi, M., Jang, C.W., Abrams, C.F., Palmese, G.R., 2014. Toughened epoxy polymers via rearrangement of network topology. J. Mater. Chem. A 2, 16071–16082. https://doi.org/10.1039/C4TA03051F

191. Sharma, R., Sharma, S.K., Mudgal, S.K., Jelly, P., Thakur, K., 2021. Efficacy of hyperbaric oxygen therapy for diabetic foot ulcer, a systematic review and meta-analysis of controlled clinical trials. Sci Rep 11, 2189. https://doi.org/10.1038/s41598-021-81886-1

192. Shi, C., Wang, C., Liu, H., Li, Q., Li, R., Zhang, Y., Liu, Y., Shao, Y., Wang, J., 2020. Selection of Appropriate Wound Dressing for Various Wounds. Frontiers in Bioengineering and Biotechnology 8, 182. https://doi.org/10.3389/fbioe.2020.00182

193. Shi, M., Du, Z., Qi, Y., Li, W., Hu, H., Lin, X., Wang, S., Tang, Z., Zhou, M., 2022. Wound microenvironment-responsive glucose consumption and hydrogen peroxide generation synergistic with azithromycin for diabetic wounds healing. Theranostics 12, 2658–2673. https://doi.org/10.7150/thno.64244

194. Shi, Z., Woody, R.W., Kallenbach, N.R., 2002. Is polyproline II a major backbone conformation in unfolded proteins? Adv Protein Chem 62, 163–240. https://doi.org/10.1016/s0065-3233(02)62008-x

195. Simões, D., Miguel, S.P., Ribeiro, M.P., Coutinho, P., Mendonça, A.G., Correia, I.J., 2018. Recent advances on antimicrobial wound dressing: A review. Eur J Pharm Biopharm 127, 130–141. https://doi.org/10.1016/j.ejpb.2018.02.022

196. Singh, D., Singh, M.R., 2012. Development of antibiotic and debriding enzyme-loaded PLGA microspheres entrapped in PVA-gelatin hydrogel for complete wound management. Artificial Cells, Blood Substitutes, and Biotechnology 40, 345–353. https://doi.org/10.3109/10731199.2012.675337

197. Spravchikov, N., Sizyakov, G., Gartsbein, M., Accili, D., Tennenbaum, T., Wertheimer, E., 2001. Glucose effects on skin keratinocytes: implications for diabetes skin complications. Diabetes 50, 1627–1635. https://doi.org/10.2337/diabetes.50.7.1627

198. Stadler, V., Kirmse, R., Beyer, M., Breitling, F., Ludwig, T., Bischoff, F.R., 2008. PEGMA/MMA copolymer graftings: generation, protein resistance, and a hydrophobic domain. Langmuir 24, 8151–8157. https://doi.org/10.1021/la800772m

199. Stephen, S., Agnihotri, M., Kaur, S., 2016. A Randomized, Controlled Trial to Assess the Effect of Topical Insulin Versus Normal Saline in Pressure Ulcer Healing. Ostomy Wound Manage 62, 16–23.

200. Strzelecka-Gołaszewska, H., 2001. Divalent Cations, Nucleotides, and Actin Structure, in: dos Remedios, C.G., Thomas, D.D. (Eds.), Molecular Interactions of Actin: Actin Structure and Actin-Binding Proteins, Results and Problems in Cell Differentiation. Springer, Berlin, Heidelberg, pp. 23–41. https://doi.org/10.1007/978-3-540-46560-7_3

201. Subramaniam, T., Fauzi, M.B., Lokanathan, Y., Law, J.X., 2021. The Role of Calcium in Wound Healing. Int J Mol Sci 22, 6486. https://doi.org/10.3390/ijms22126486

202. Sun, S., Zhang, L., Liu, J., Li, H., 2021. Insulin Topical Application for Wound Healing in Nondiabetic Patients. Computational and Mathematical Methods in Medicine 2021, e9785466. https://doi.org/10.1155/2021/9785466

203. Tai, C., Bouissil, S., Gantumur, E., Carranza, M.S., Yoshii, A., Sakai, S., Pierre, G., Michaud, P., Delattre, C., 2019. Use of Anionic Polysaccharides in the Development of 3D Bioprinting Technology. Applied Sciences 9, 2596. https://doi.org/10.3390/app9132596

204. Tanihara, M., Suzuki, Y., Yamamoto, E., Noguchi, A., Mizushima, Y., 2001. Sustained release of basic fibroblast growth factor and angiogenesis in a novel covalently crosslinked gel of heparin and alginate. J Biomed Mater Res 56, 216–221. https://doi.org/10.1002/1097-4636(200108)56:2<216::aid-jbm1086>3.0.co;2-n

205. Tao, Z., Raffel, R.A., Souid, A.-K., Goodisman, J., 2009. Kinetic Studies on Enzyme-Catalyzed Reactions: Oxidation of Glucose, Decomposition of Hydrogen Peroxide and Their Combination. Biophys J 96, 2977–2988. https://doi.org/10.1016/j.bpj.2008.11.071

206. Tennenberg, S.D., Finkenauer, R., Dwivedi, A., 1999. Absence of Lipopolysaccharide-Induced Inhibition of Neutrophil Apoptosis in Patients With Diabetes. Archives of Surgery 134, 1229–1234. https://doi.org/10.1001/archsurg.134.11.1229

207. Terashi, H., Izumi, K., Deveci, M., Rhodes, L.M., Marcelo, C.L., 2005. High glucose inhibits human epidermal keratinocyte proliferation for cellular studies on diabetes mellitus. Int Wound Journal 2, 298–304. https://doi.org/10.1111/j.1742-4801.2005.00148.x

208. Tessaro, F.H.G., Ayala, T.S., Nolasco, E.L., Bella, L.M., Martins, J.O., 2017. Insulin Influences LPS-Induced TNF-α and IL-6 Release Through Distinct Pathways in Mouse Macrophages from Different Compartments. CPB 42, 2093–2104. https://doi.org/10.1159/000479904

209. Thalhimer, W., 1923. INSULIN TREATMENT OF POSTOPERATIVE (NONDIABETIC) ACIDOSIS. Journal of the American Medical Association 81, 383–385. https://doi.org/10.1001/jama.1923.02650050037013

210. Thapa, R.K., Diep, D.B., Tønnesen, H.H., 2020. Topical antimicrobial peptide formulations for wound healing: Current developments and future prospects. Acta Biomater 103, 52–67. https://doi.org/10.1016/j.actbio.2019.12.025

211. Toda, K.-I., Grinnell, F., 1987. Activation of Human Keratinocyte Fibronectin Receptor Function in Relation to Other Ligand-Receptor Interactions. Journal of Investigative Dermatology 88, 412–417. https://doi.org/10.1111/1523-1747.ep12469745

212. Tottoli, E.M., Dorati, R., Genta, I., Chiesa, E., Pisani, S., Conti, B., 2020. Skin Wound Healing Process and New Emerging Technologies for Skin Wound Care and Regeneration. Pharmaceutics 12, 735. https://doi.org/10.3390/pharmaceutics12080735

213. Tuomisto, T.T., Lumivuori, H., Kansanen, E., Häkkinen, S.-K., Turunen, M.P., van Thienen, J.V., Horrevoets, A.J., Levonen, A.-L., Ylä-Herttuala, S., 2008. Simvastatin has an anti-inflammatory effect on macrophages via upregulation of an atheroprotective transcription factor, Kruppel-like factor 2. Cardiovascular Research 78, 175–184. https://doi.org/10.1093/cvr/cvn007

214. Tur, E., Bolton, L., Constantine, B.E., 1995. Topical hydrogen peroxide treatment of ischemic ulcers in the guinea pig: blood recruitment in multiple skin sites. J Am Acad Dermatol 33, 217–221. https://doi.org/10.1016/0190-9622(95)90238-4

215. Van Ort, S.R., Gerber, R.M., 1976. Topical application of insulin in the treatment of decubitus ulcers: a pilot study. Nurs Res 25, 9–12.

216. Varaprasad, K., Nùñez, D., Ide, W., Jayaramudu, T., Sadiku, E.R., 2020. Development of high alginate comprised hydrogels for removal of Pb(II) ions. Journal of Molecular Liquids 298, 112087. https://doi.org/10.1016/j.molliq.2019.112087

217. Varma, S., Lal, B.K., Zheng, R., Breslin, J.W., Saito, S., Pappas, P.J., Hobson, R.W., Durán, W.N., 2005. Hyperglycemia alters PI3k and Akt signaling and leads to endothelial cell proliferative dysfunction. Am J Physiol Heart Circ Physiol 289, H1744–H1751. https://doi.org/10.1152/ajpheart.01088.2004

218. Vedeler, A., Pryme, I.F., Hesketh, J.E., 1991. Insulin induces changes in the subcellular distribution of actin and 5′-nucleotidase. Mol Cell Biochem 108, 67–74. https://doi.org/10.1007/BF00239543

219. Wagner, D., 2011. The Role of T Cells in Type 1 Diabetes, Type 1 Diabetes - Pathogenesis, Genetics and Immunotherapy. IntechOpen. https://doi.org/10.5772/22040

220. Wallace, H.A., Basehore, B.M., Zito, P.M., 2021. Wound Healing Phases, in: StatPearls. StatPearls Publishing, Treasure Island (FL).

221. Walther, M., Vestweber, P.K., Kühn, S., Rieger, U., Schäfer, J., Münch, C., Vogel-Kindgen, S., Planz, V., Windbergs, M., 2023. Bioactive Insulin-Loaded Electrospun Wound Dressings for Localized Drug Delivery and Stimulation of Protein Expression Associated with Wound Healing. Mol Pharm 20, 241–254. https://doi.org/10.1021/acs.molpharmaceut.2c00610

222. Wang, J., Xu, J., 2020. Effects of Topical Insulin on Wound Healing: A Review of Animal and Human Evidences. Diabetes Metab Syndr Obes 13, 719–727. https://doi.org/10.2147/DMSO.S237294

223. Wang, J., Zhu, X., Liu, L., Shi, X., Yin, L., Zhang, Y., Li, X., Wang, Z., Liu, G., 2013. Effects of strontium on collagen content and expression of related genes in rat chondrocytes cultured in vitro. Biol Trace Elem Res 153, 212–219. https://doi.org/10.1007/s12011-013-9640-9

224. Wang, M., Yang, Y., Yuan, K., Yang, S., Tang, T., 2021. Dual-functional hybrid quaternized chitosan/Mg/alginate dressing with antibacterial and angiogenic potential for diabetic wound healing. Journal of Orthopaedic Translation 30, 6–15. https://doi.org/10.1016/j.jot.2021.07.006

225. Wang, T., Zheng, Y., Shi, Y., Zhao, L., 2019. pH-responsive calcium alginate hydrogel laden with protamine nanoparticles and hyaluronan oligosaccharide promotes diabetic wound healing by enhancing angiogenesis and antibacterial activity. Drug Deliv Transl Res 9, 227–239. https://doi.org/10.1007/s13346-018-00609-8

226. Wang, X., Hao, T., Qu, J., Wang, C., Chen, H., 2015. Synthesis of Thermal Polymerizable Alginate-GMA Hydrogel for Cell Encapsulation. Journal of Nanomaterials 2015, e970619. https://doi.org/10.1155/2015/970619

227. Wells, L.A., Sheardown, H., 2007. Extended release of high pI proteins from alginate microspheres via a novel encapsulation technique. Eur J Pharm Biopharm 65, 329–335. https://doi.org/10.1016/j.ejpb.2006.10.018

228. Whitney, J.D., 2005. Overview: Acute and Chronic Wounds. Nursing Clinics of North America, Wound Care 40, 191–205. https://doi.org/10.1016/j.cnur.2004.09.002

229. Whittam, A.J., Maan, Z.N., Duscher, D., Wong, V.W., Barrera, J.A., Januszyk, M., Gurtner, G.C., 2016. Challenges and Opportunities in Drug Delivery for Wound Healing. Adv Wound Care (New Rochelle) 5, 79–88. https://doi.org/10.1089/wound.2014.0600

230. Widgerow, A.D., 2012. Deconstructing the stalled wound. Wounds 24, 58–66.

231. Wilgus, T.A., Bergdall, V.K., Dipietro, L.A., Oberyszyn, T.M., 2005. Hydrogen peroxide disrupts scarless fetal wound repair. Wound Repair and Regeneration 13, 513–519. https://doi.org/10.1111/j.1067-1927.2005.00072.x

232. Wilkinson, H.N., Hardman, M.J., 2020. Wound healing: cellular mechanisms and pathological outcomes. Open Biology 10, 200223. https://doi.org/10.1098/rsob.200223

233. Wohlfahrt, G., Witt, S., Hendle, J., Schomburg, D., Kalisz, H.M., Hecht, H.J., 1999. 1.8 and 1.9 A resolution structures of the Penicillium amagasakiense and Aspergillus niger glucose oxidases as a basis for modelling substrate complexes. Acta Crystallogr D Biol Crystallogr 55, 969–977. https://doi.org/10.1107/s0907444999003431

234. Wu, Y., Joseph, S., Aluru, N.R., 2009. Effect of Cross-Linking on the Diffusion of Water, Ions, and Small Molecules in Hydrogels. J. Phys. Chem. B 113, 3512–3520. https://doi.org/10.1021/jp808145x

235. Xu, F., Zhang, C., Graves, D.T., 2013. Abnormal Cell Responses and Role of TNF-α in Impaired Diabetic Wound Healing. Biomed Res Int 2013, 754802. https://doi.org/10.1155/2013/754802

236. Xu, Z., Liang, B., Tian, J., Wu, J., 2021. Anti-inflammation biomaterial platforms for chronic wound healing. Biomater. Sci. 9, 4388–4409. https://doi.org/10.1039/D1BM00637A

237. Xuan, Y.H., Huang, B.B., Tian, H.S., Chi, L.S., Duan, Y.M., Wang, X., Zhu, Z.X., Cai, W.H., Zhu, Y.T., Wei, T.M., Ye, H.B., Cong, W.T., Jin, L.T., 2014. High-Glucose Inhibits Human Fibroblast Cell Migration in Wound Healing via Repression of bFGF-Regulating JNK Phosphorylation. PLOS ONE 9, e108182. https://doi.org/10.1371/journal.pone.0108182

238. Yamagiwa, K., Kozawa, T., Ohkawa, A., 1995. Effects of Alginate Composition and Gelling Conditions on Diffusional and Mechanical Properties of Calcium-Alginate Gel Beads. Journal of Chemical Engineering of Japan 28, 462–467. https://doi.org/10.1252/jcej.28.462

239. Yan, M., Ni, J., Shen, H., Song, D., Ding, M., Huang, J., 2017. Local controlled release of simvastatin and PDGF from core/shell microspheres promotes bone regeneration in vivo. RSC Adv. 7, 19621–19629. https://doi.org/10.1039/C7RA01503H

240. Yang, C., Lu, D., Liu, Z., 2011. How PEGylation enhances the stability and potency of insulin: a molecular dynamics simulation. Biochemistry 50, 2585–2593. https://doi.org/10.1021/bi101926u

241. Yang, P., Wang, D., Shi, Y., Li, M., Gao, M., Yu, T., Liu, D., Zhang, J., Wang, J., Zhang, X., Liu, Y., 2020. Insulin-Containing Wound Dressing Promotes Diabetic Wound Healing Through Stabilizing HIF-1α. Frontiers in Bioengineering and Biotechnology 8, 1431. https://doi.org/10.3389/fbioe.2020.592833

242. Yasasvini, S., Anusa, R., VedhaHari, B., Prabhu, P., RamyaDevi, D., 2017. Topical hydrogel matrix loaded with Simvastatin microparticles for enhanced wound healing activity. Materials Science and Engineering: C 72, 160–167. https://doi.org/10.1016/j.msec.2016.11.038

243. You, J., Zhang, Y., Zhou, Y., 2022. Strontium Functionalized in Biomaterials for Bone Tissue Engineering: A Prominent Role in Osteoimmunomodulation. Frontiers in Bioengineering and Biotechnology 10.

244. Yu, H., Liu, Y., Yang, X., He, J., Zhang, F., Zhong, Q., Guo, X., 2021. Strontium ranelate promotes chondrogenesis through inhibition of the Wnt/-

catenin pathway. Stem Cell Res Ther 12, 296. https://doi.org/10.1186/s13287-021-02372-z

245. Yu, W., Jiang, Y.-Y., Sun, T.-W., Qi, C., Zhao, H., Chen, F., Shi, Z., Zhu, Y.-J., Chen, D., He, Y., 2016. Design of a novel wound dressing consisting of alginate hydrogel and simvastatin-incorporated mesoporous hydroxyapatite microspheres for cutaneous wound healing. RSC Adv. 6, 104375–104387. https://doi.org/10.1039/C6RA20892D

246. Zhang, J., Wang, H., Shi, J., Wang, Y., Lai, K., Yang, X., Chen, X., Yang, G., 2016. Combination of simvastatin, calcium silicate/gypsum, and gelatin and bone regeneration in rabbit calvarial defects. Scientific Reports 6, 23422. https://doi.org/10.1038/srep23422

247. Zhang, K., Meng, X., Kong, J., Liu, F.-F., Yang, J.-M., Gao, F., Zhang, Y., Zhang, C., 2013. Simvastatin increases Prolyl-4-Hydroxylase α1 expression in atherosclerotic plaque and ox-LDL-stimulated human aortic smooth muscle cells via p38 MAPK and ERK1/2 signaling. Journal of Molecular and Cellular Cardiology 65, 43–50. https://doi.org/10.1016/j.yjmcc.2013.09.010

248. Zhang, L., Ma, Y., Pan, X., Chen, S., Zhuang, H., Wang, S., 2018. A composite hydrogel of chitosan/heparin/poly (γ-glutamic acid) loaded with superoxide dismutase for wound healing. Carbohydrate Polymers 180, 168–174. https://doi.org/10.1016/j.carbpol.2017.10.036

249. Zhang, Q., Dong, J., Yu, Z., 2020. Pleiotropic use of Statins as non-lipid-lowering drugs. Int J Biol Sci 16, 2704–2711. https://doi.org/10.7150/ijbs.42965

250. Zhang, S., Ge, G., Qin, Y., Li, W., Dong, J., Mei, J., Ma, R., Zhang, X., Bai, J., Zhu, C., Zhang, W., Geng, D., 2023. Recent advances in responsive hydrogels for diabetic wound healing. Materials Today Bio 18, 100508. https://doi.org/10.1016/j.mtbio.2022.100508

251. Zhang, Z., Lv, L., 2016. Effect of local insulin injection on wound vascularization in patients with diabetic foot ulcer. Exp Ther Med 11, 397–402. https://doi.org/10.3892/etm.2015.2917

252. Zhang, Z., Zhang, W., Xu, Y., Liu, D., 2022. Efficacy of hyperbaric oxygen therapy for diabetic foot ulcers: An updated systematic review and meta-analysis. Asian Journal of Surgery 45, 68–78. https://doi.org/10.1016/j.asjsur.2021.07.047

253. Zhao, B., Li, X., Xu, H., Jiang, Y., Wang, D., Liu, R., 2020. <p>Influence of Simvastatin-Strontium-Hydroxyapatite Coated Implant Formed by Micro-Arc Oxidation and Immersion Method on Osteointegration in Osteoporotic

Rabbits</p> [WWW Document]. International Journal of Nanomedicine. https://doi.org/10.2147/IJN.S244815

254. Zhao, F., Lei, B., Li, X., Mo, Y., Wang, R., Chen, D., Chen, X., 2018. Promoting in vivo early angiogenesis with sub-micrometer strontium-contained bioactive microspheres through modulating macrophage phenotypes. Biomaterials 178, 36–47. https://doi.org/10.1016/j.biomaterials.2018.06.004

255. Zhou, X., Wang, H., Zhang, J., Li, X., Wu, Y., Wei, Y., Ji, S., Kong, D., Zhao, Q., 2017. Functional poly(ε-caprolactone)/chitosan dressings with nitric oxide-releasing property improve wound healing. Acta Biomaterialia 54, 128–137. https://doi.org/10.1016/j.actbio.2017.03.011

256. Zhu, G., Wang, Q., Lu, S., Niu, Y., 2017. Hydrogen Peroxide: A Potential Wound Therapeutic Target. MPP 26, 301–308. https://doi.org/10.1159/000475501

257. Zied, S., Elie, A.-J., Luc, P., Didier, L.C., 2012. Anionic Polysaccharide Hydrogels with Charges Provided by the Polysaccharide or the Crosslinking Agent. Drug Delivery Letters 2, 240–250.

258. Zoldák, G., Zubrik, A., Musatov, A., Stupák, M., Sedlák, E., 2004. Irreversible thermal denaturation of glucose oxidase from Aspergillus niger is the transition to the denatured state with residual structure. J Biol Chem 279, 47601–47609. https://doi.org/10.1074/jbc.M406883200

ANNEXURES

1. List of publications from Thesis

Research articles

1. Rajalekshmy G.P. and Rekha M.R., Strontium ion cross-linked alginate-g-poly (PEGMA) xerogels for wound healing applications: *in vitro* studies, *Carbohydrate Polymers*, Vol: 251, 2021, 117119. https://doi.org/10.1016/j.carbpol.2020.117119. (Impact factor: **10.72**).
2. Rajalekshmy G.P. and Rekha M.R. "Synthesis and evaluation of an alginate-methacrylate xerogel for insulin delivery towards wound healing applications." *Therapeutic Delivery*. 2021; 12(3):215-234. doi: 10.4155/tde-2020-0128. (Impact factor: **2.44**).
3. Rajalekshmy G.P. and Rekha M. R. Wound Healing Effects of Glucose Oxidase-Peroxidase Incorporated Alginate Diamine PEG-g-Poly (PEGMA) Xerogels under High Glucose Conditions: An in Vitro Evaluation. *Materialia*, *23*, 2022. 101464. https://doi.org/10.1016/j.mtla.2022.101464. (Impact score: **5.6**).

2. Curriculum vitae

Educational Qualifications

M. Sc. Medical Laboratory Technology (Biochemistry),
Kerala University of Health Sciences (2015)

B. Sc. Medical Laboratory Technology, Kerala University (2013)

Achievements

- CSIR Junior Research Fellowship in June 2016 (Rank – 17)
- ICMR Junior Research Fellowship in June 2016
- First Rank In MSc MLT Biochemistry examination in 2015
- First Rank In BSc MLT Examination in 2013
- DBT scholarship, Dept. of Biotechnology, India in 2008

Awards

- **Certificate of Merit for Best paper publication** on 39th Annual Convocation on 6th May 2023 from Sree Chitra Tirunal Institute for Medical Sciences and Technology, Trivandrum.
- Won the title of **'Outstanding Researcher Award'** in Biomaterial Science in Asian Research Award in 2023 (ASTRA 2023) Organized by World Research Council and Time of Research, in Asia Science, Technology & Research Congress 2023, Trichy, Tamilnadu, India.

Presentations in Conferences

Poster presentations:

1. Biomet 2018, 24-28 July 2018, organized by Centre for Biomaterials, cellular & Molecular Theranostics (CBCMT), VIT University, Vellore. Rajalekshmy G.P and Rekha M.R., "Physico-chemical Characterization of Alginate based wound care material for chronic wound management."
2. Two day conference in Defining Ethics and Welfare in Preclinical research (DEW 2022) on 14-15 November 2022. Organized by SCTIMST, Trivandrum.

Rajalekshmy G P and Rekha M R. “The implementation of 3Rs in cutaneous wound healing models”.

3. International Union of Materials Research Society International conference in Asia (IUMRS-ICA) on 19-23 December 2022. Organized by MRSI, IIT Jodhpur. Rajalekshmy G P and Rekha M R. “Modified alginate based xerogel mediated topical insulin delivery for diabetic wound healing”.

Oral presentations:

1. 6th International Conference on Natural Polymers, 7-9 December 2018, Organized by International & Inter University Centre for Nanoscience & Nanotechnology (IIUCNN). Rajalekshmy G.P. and Rekha M R. “Topical Delivery of insulin using Alginate-g-poly(methacrylic acid) xerogels for wound healing applications”.
2. Annual Technical Committee meeting (ATM), Material Research Society of India (MRSI), 23rd March 2019, NIIST, Trivandrum. Rajalekshmy G.P. and Rekha M.R. “Functionalized alginate-g-poly(PEGMA) xerogels for insulin delivery towards wound healing applications”.
3. One day symposium Dept of Biochemistry, SCTIMST on 2nd August 2019. Rajalekshmy G.P and Rekha M R. “The effect of topical use of insulin on chronic wound healing”.
4. 1st Online conference on Blends, Composites, Bio composites and nanocomposites (ICNC 2020) on 9-11th October 2020, organized by School of Energy Materials (SEM), Mahatma Gandhi University, Kottayam. Rajalekshmy G P and Rekha M R “Wound healing effect of strontium ion cross-linked alginate-g-poly(PEGMA) xerogels : an in vitro analysis”.
5. 11th World Biomaterial Congress Virtual 2020 conference, Glasgow (WBC 2020) held from 11 -15th December. Rajalekshmy G.P. and Rekha M.R. “Strontium crosslinked alginate-g-poly(PEGMA) xerogels for diabetic wound healing : An in vitro analysis”.
6. International symposium on Advanced Materials (ISAM 2021), Material Research Society of India (MRSI), 26-27 March 2021 (Online). Rajalekshmy

G.P. and Rekha M.R. “Topical delivery of simvastatin and strontium ions using Alginate Diamine PEG-g-poly(PEGMA) xerogels for diabetic wound healing”.

7. 34th Kerala science congress 2022, on 27-29 January 2022, Thiruvananthapuram, Organized by KSCSTE NATPAC. Rajalekshmy G P, Rekha M R “Glucose – oxidase peroxidase incorporated Alginate Diamine PEG-g-poly(PEGMA) xerogels for Diabetic wound healing.”
8. International Conference on Polymeric Materials in Medicine (ICPMM 2022), Virtual Conference on 25- 26 February 2022. Organized by SPSI, Trivandrum Chapter, SCTIMST. Rajalekshmy G.P. and Rekha M.R.“Modified Alginate based xerogels for Diabetic wound healing: A comparative study.”
9. National Seminar on Recent Approaches in Biochemical research on 23 -24 June 2022. Organized by Dept. of Biochemistry and Advanced Centre for Tissue engineering. Rajalekshmy G.P. and Rekha M.R. “Localized delivery of simvastatin through Alginate diamine PEG-poly(PEGMA) xerogels for chronic wound management: A molecular Approach.”

APPENDICES

Appendix A: Ethical Committee Approval

SREE CHITRA TIRUNAL INSTITUTE FOR MEDICAL SCIENCES AND TECHNOLOGY.
BIOMEDICAL TECHNOLOGY WING.

INSTITUTIONAL ANIMAL ETHICS COMMITTEE

SCT/ABS/IAEC-112/06 Date: 03/03/2022

To,
Dr. Rekha MR,
Division of Biosurface Technology.

The Institutional Animal Ethics Committee reviewed and discussed application to conduct the following proposal on 21.02.2022 in IAEC meeting held at Sree Chitra Tirunal Institute for Medical Sciences and Technology, Thiruvananthapuram.

B Form No - **SCT/IAEC-435/JANUARY/2022/112**: Efficacy evaluation of alginate based wound care biomaterial for diabetic wound management.

No. of Animals requested: Rat, Sprague Dawley: 90nos

The following members of the Institutional Animal Ethics Committee were present at the 112nd meeting held on 21.02.2022 at 10.00am.

Member Name	*Designation*	*Affiliation with the institution*
Dr. TV Anilkumar	Scientist from different discipline(Chairperson)	Yes
Dr. Harikrishnan V S	Veterinarian, Member secretary	Yes
Dr. K R Chandramohan Nair	Main Nominee	No
Dr. P.R. Umashankar	Scientist in charge of animal house facility	Yes
Dr. Guruvayoorappan C	Socially aware nominee	No
Dr. Srinivas G	Biological scientist	Yes
Dr.Murali Krishna P	Scientist from outside the Institute	No

IAEC Decision

Approved

Approval date: 21/02/2022
Expiry date: 31/08/2022

Dr.Harikrishnan V S,
Secretary-IAEC,
Tel No: 04712520227/243
Email: iaec@sctimst.ac.in

Appendix B: Publications

Review article

Rajalekshmy Girishkumar Padmakumari, Caroline Diana Sherly, Rekha Mannemcherril Ramesan. Therapeutic delivery of nucleic acids for skin wound healing. ***Therapeutic Delivery*** 2022; 13(6):339-358. doi: 10.4155/tde-2022-0003. (Impact factor: **2.44**).

Book chapters

- Rajalekshmy G.P., Lekshmi Devi L., Jasmin Joseph and Rekha M.R "An overview on potential biomedical applications of polysaccharides in the Book "Functional Polysaccharides for Biomedical Applications", 2019, P No. 33-94. Elsevier. ISBN: 978-0-08-102555-0.
- G.P. Rajalekshmy, Rajan Annie Mariya, and M.R. Rekha. Pullulan-based nanomaterials in drug delivery applications, 2021, P.No.383-404. Published in the book entitled "Biopolymer-Based Nanomaterials in Drug Delivery and Biomedical Applications". Elsevier. ISBN: 978-0-12-820874-8.
- Rajalekshmy G.P., Rekha M.R. Trends in Bioactive Biomaterials in Tissue Engineering and Regenerative Medicine. Biomaterials in Tissue Engineering and Regenerative Medicine. 2021, 271-303. Springer. ISBN: 978-981-16-0001-2.
- Rajalekshmy G.P., Rekha M.R. and Harikrishnan V.S. Biomaterial mediated therapeutic delivery for wound healing: Approaches, pre-clinical evaluation and current status. Book: Engineered Biomaterials- Progress and Prospects (accepted).

Appendix C: Plagiarism check report

Ouriginal by Turnitin

Document Information

Analyzed document	Thesis for Plagiarism check.docx (D160288243)
Submitted	2023-03-07 02:03:00
Submitted by	Rekha M.R.
Submitter email	rekhamr@sctimst.ac.in
Similarity	2%
Analysis address	rekhamr.sctims@analysis.urkund.com

Sources included in the report

W	URL: https://www.mdpi.com/2073-4409/11/15/2439 Fetched: 2023-01-09 08:46:46	1
W	URL: https://www.frontiersin.org/articles/10.3389/fbioe.2016.00082/full Fetched: 2019-10-10 10:49:34	1
W	URL: https://www.ncbi.nlm.nih.gov/pmc/articles/PMC6027439/ Fetched: 2019-10-03 07:39:31	2
W	URL: https://www.ncbi.nlm.nih.gov/pmc/articles/PMC8471591/ Fetched: 2021-11-13 07:46:28	1
SA	**Sree Chitra Tirunal Institute, Thiruvananthapuram / Manuscript_Book Chapter.docx** Document Manuscript_Book Chapter.docx (D140973366) Submitted by: rekhamr@sctimst.ac.in Receiver: rekhamr.sctims@analysis.urkund.com	3
SA	**project thesis.docx** Document project thesis.docx (D77801700)	1
W	URL: https://www.ncbi.nlm.nih.gov/pmc/articles/PMC8488380/ Fetched: 2021-11-01 13:18:26	1
W	URL: https://jbioleng.biomedcentral.com/articles/10.1186/s13036-020-0227-7 Fetched: 2020-05-08 13:08:51	2
SA	**Sree Chitra Tirunal Institute, Thiruvananthapuram / Manuscript_AGPMS.docx** Document Manuscript_AGPMS.docx (D65922004) Submitted by: rekhamr@sctimst.ac.in Receiver: rekhamr.sctims@analysis.urkund.com	1
SA	**Sree Chitra Tirunal Institute, Thiruvananthapuram / Manuscript GG-g-PEGMA_V6.docx** Document Manuscript GG-g-PEGMA_V6.docx (D146124817) Submitted by: rekhamr@sctimst.ac.in Receiver: rekhamr.sctims@analysis.urkund.com	20

Ouriginal by Turnitin

SA	**Sree Chitra Tirunal Institute, Thiruvananthapuram / Manuscript_P.docx** Document Manuscript_P.docx (D146214398) Submitted by: rekhamr@sctimst.ac.in Receiver: rekhamr.sctims@analysis.urkund.com	2
SA	**Development and Characterization of Lupeol and PDGF Loaded Novel Delivery System for Treatment of Wounds in Diabetics (Satish Patel).pdf** Document Development and Characterization of Lupeol and PDGF Loaded Novel Delivery System for Treatment of Wounds in Diabetics (Satish Patel).pdf (D40591060)	2
SA	**GOPIKA.S.pdf** Document GOPIKA.S.pdf (D140306984)	2

Entire Document